國立中央大學天文研究所
鹿林天文台年報

2010

No.8

國立中央大學天文研究所 編

目錄

研究報告

A&A 523, A84 (2010)
DOI: 10.1051/0004-6361/201015172

Astronomy & Astrophysics

A multi-site campaign to detect the transit of the second planet in HAT-P-13★ (Research Note)

Gy. M. Szabó[1,2,3], L. L. Kiss[1,4], J. M. Benkő[1], Gy. Mező[1], J. Nuspl[1], Zs. Regály[1], K. Sárneczky[1], A. E. Simon[1,2], G. Leto[5], R. Zanmar Sanchez[5], C.-C. Ngeow[6], Zs. Kővári[1], and R. Szabó[1]

[1] Konkoly Observatory of the Hungarian Academy of Sciences, PO Box 67, 1525 Budapest, Hungary
e-mail: [szgy;kiss]@konkoly.hu
[2] Department of Experimental Physics and Astronomical Observatory, University of Szeged, 6720 Szeged, Hungary
[3] Hungarian Eötvös Fellow, Department of Astronomy, University of Texas at Austin, 1 University Station, Austin, TX 78712, USA
[4] Sydney Institute for Astronomy, School of Physics A28, University of Sydney, NSW 2006, Australia
[5] INAF - Osservatorio Astrofisico di Catania, via Santa Sofia 78, 95123 Catania, Italy
[6] Graduate Institute of Astronomy, National Central University, No. 300, Jhongda Rd, Jhongli City, Taoyuan County 32001, Taiwan

Received 8 June 2010 / Accepted 23 September 2010

ABSTRACT

Aims. A possible transit of HAT-P-13c had been predicted to occur on 2010 April 28. Here we report on the results of our multi-site campaign organised to detect the event.

Methods. CCD photometric observations were carried out at five observatories in five countries. We reached 30% time coverage in a 5-day interval centered on the suspected transit of HAT-P-13c. Two transits of HAT-P-13b were also observed.

Results. No transit of HAT-P-13c was detected during the campaign. By a numerical experiment with 10^5 model systems, we conclude that HAT-P-13c is not a transiting exoplanet with a significance level from 65% to 72%, depending on the planet parameters and the prior assumptions. We present two times of transit of HAT-P-13b ocurring at BJD 2 455 141.5522 ± 0.0010 and BJD 2 455 249.4508 ± 0.0020. The TTV of HAT-P-13b is consistent with zero within 0.001 days. The refined orbital period of HAT-P-13b is 2.916293 ± 0.000010 days.

Key words. planetary systems – stars: individual: HAT-P-13

1. Introduction

Multiple planetary systems analogous to our Solar System play a key role in understanding planet formation and evolution. If planets in multiple systems display transits as well (e.g. Kepler-9, Holman et al. 2010), a very detailed analysis becomes possible, resulting in a set of dynamical parameters and even the internal density distribution of the planets (Batyigin et al. 2009). As write, three multiple systems with a transiting component have been discovered. The CoRoT-7 system has two orbiting super-Earths, one showing transits (Léger et al. 2009; Queloz et al. 2009); HAT-P-7 hosts a hot Jupiter in a polar or retrograde orbit and a long-period companion that may either be a planet or a star (Pál et al. 2008; Winn et al. 2009). But the most prominent example of such systems is HAT-P-13 (Bakos et al. 2009; Winn et al. 2010). The central star of this system is a G4 dwarf of 1.22 $M_\odot$ mass and 1.56 $R_\odot$ radius. HAT-P-13b is a 0.85 M_J hot Jupiter on a 2.9 day orbit that has almost been circularized. HAT-P-13c has a minimum mass of $M \sin i = 15.2$ M_J in a 428-day orbit with an eccentricity of 0.69. Winn et al. (2010) predicted a possible transit for the second planet, which, if confirmed, would make HAT-P-13 an extremely special system.

In multiple planetary systems, the most important question is whether the orbital planes are aligned. If this is the case for HAT-P-13 b and c, the exact mass of companion c can be derived. The Δi mutual inclination may be derived from the transit timing variations (TTV), of HAT-P-13b (Bakos et al. 2009). A more stringent constraint on coplanarity would be delivered if HAT-P-13c also transits. In this case, the coplanarity is highly probable, and the radius and the orbit of planet c can be measured. If the apsides are also aligned, tidal dynamics can reveal planet b's internal structure, which is a fascinating opportunity to extract unique information on an exoplanet (Batygin et al. 2009; Fabricky 2009).

It has been unknown whether HAT-P-13c transits. The dynamical models of Mardling (2010) suggest that the HAT-P-13 system is likely to be close to prograde coplanar or have a mutual inclination between 130° and 135°. She interpreted the system geometry as a result of early chaotic interactions. A hypothetical d companion was invoked at the early stages of evolution that should have escaped later and could explain the vivid scattering history. Her argument for coplanarity is that lower masses are favored for dynamical reasons, although c's high inclination itself favours a large mutual inclination. Winn et al. (2010) points to the observed small stellar obliquity $\psi_{*,b}$ as indirect evidence of orbital alignment: in Mardling's model, after planet d has escaped, $\psi_{*,b}$ oscillates about a mean value of Δi. Thus,

★ Photometric data are only available in electronic form at the CDS via anonymous ftp to cdsarc.u-strasbg.fr (130.79.128.5) or via http://cdsarc.u-strasbg.fr/viz-bin/qcat?J/A+A/523/A84

Table 1. Summary of instruments involved in HAT-P-13 observations.

Code	Telescope	CCD	FoV	Resolution
K60	Konkoly 0.6 Schmidt, Piszkéstető, Hungary	1526 × 1024 KAF	25′× 17′	1.0″/pixel
K100	Konkoly 1.0 RCC, Piszkéstető, Hungary	1340 × 1300 PI VersArray 1300b NTE	7′× 7′	0.32″/pixel
SLN	INAF-OACt 0.91, Fracastoro, Italy	1100 × 1100 KAF1001E	13′× 13′	0.77 ″/pixel
TEN	0.8 RCC Tenagra II, Arizona, USA	1024 × 1024	14.8′× 14.8′	0.81 ″/pixel
LNO	Langkawi 0.5 RCC, Malaysia	1024 × 1024 SBIG 1001E CCD	20′× 20′	1.2 ″/pixel
SLT	Lulin 0.4 RCC, Taiwan	3056 × 3056 Apogee U9000	50.7′× 50.7′	0.99″/pixel

Table 2. Observations during the HAT-P-13c campaign.

Date	K60	TEN	SLT	LNO	SLN
2010–04–22	20:23–22:23 (80)				
04–25	18:40–23:33 (190)	03:01–05:17 (101)	12:17–15:03 (108)		
04–26	18:43–21:27 (134)	04:44–07:01 (100)		14:28–14:56 (34)	
04–27		03:10–05:26 (85)			20:46–23:56 (162)
04–28	18:41–22:53 (139)	05:30–06:52 (61)		13:34–14:55 (23)	20:37–00:08 (116)
04–29	18:45–23:15 (349)	04:55–06:49 (84)		13:42–15:32 (58)	20:53–23:58 (128)
04–30	18:43–23:17 (342)	04:55–06:55 (51)			
05–01	19:21–20:32 (66)	05:39–06:17 (45)	11:48–14:16 (55)	12:42–14:45 (60)	
05–03	19:25–22:50 (252)				

Notes. Telescope codes: K60: Konkoly 60 cm Schmidt, TEN: Tenagra, SLT: Lulin, LNO: Langkawi, SLN: INAF-OACt. Observation windows and the number of photometry points are indicated.

observing small value for $\psi_{*,b}$ at any time, such as now, is unlikely unless Δi is small.

The refined orbital elements suggested that the transit – if it happened – should have occurred around 2010 April 28, 17 UT, (JD 2 455 315.2) with 1.9 days *FWHM* of transit probability and a maximal duration of 14.9 h (Winn 2010). We started monitoring of HAT-P-13 for further transits in November 2009 and organised an international campaign in the 2 weeks surrounding the expected transit of HAT-P-13c.

2. Observations and data reduction

The seasonal visibility of HAT-P-13 is quite unfavorable in April. Hence the longest possible run at mid-northern latitudes may last 3–4 h after twilight with observations ending at high ($X > 2$) airmass. Our data were collected at 5 observing sites with 6 telescopes, and, due to the weather conditions, 30% time coverage was reached. The telescope parameters and the log of the observations is shown in Tables 1 and 2, respectively.

The observing strategy was the same in most observatories: a sequence of RRRVVV was repeated continuously, while Tenagra Observatory measured the first half of the light curve in *R*, and the second half in *V*. The integration time was adjusted throught the night to compensate for the air mass variation in an effort to take advantage of the full dynamic range of the camera. The average exposure times were about 65 s and 35 s in the *V* and *R* bands, respectively. Each night several bias, dark, and sky flat images were taken for calibration.

Before the multisite campaign, we observed HAT-P-13 on 8 additional nights. Two nights (2009 November 05/06 and 2010 February 21/22) included a transit of HAT-P-13b, the remainder were acquired as out-of-transit observations. In these observations, the K100 telescope was also involved. No transit signal exceeding a depth of 0.005 (3-sigma level) was observed during the following out-of-transit observation runs: 2009–11–05/06, 23:03–03:45 UT (1 RCC), 2010–01–11/12, 01:41–04:29 (1 RCC), 2010–01–14/15, 21:41–23:19 (0.6 Schmidt), 2010–01–16/17, 22:20–03:39 (0.6 Schmidt), 2010–02–21/22, 18:32–02:19 (0.6 Schmidt), 2010–03–18/19, 19:08–00:03 (0.6 Schmidt), 2010–03–18/19, 20:08-23:37 (1 RCC) 2010–03–19/20, 21:38–00:11 (0.6 Schmidt), 2010–03–28/29, 18:30–00:16 (0.6 Schmidt).

Transits of HAT-P-13b were analyzed with an automated image processing and aperture photometry pipeline developed in the GNU-R[1] environment. The flat image was constructed as the median of the normalized flat frames (i.e., each of the acquired images were divided by the mean of their pixel values), and similar procedures were performed for darks and biases. After the standard calibrations, star identification was performed. Comparison stars were selected iteratively to attain the highest signal-to-noise ratio in the light curve. Finally, 3 comparison stars were used in all images (2MASS J08392449+4723225, 2 MASS J08392164+4720500, and 2MASS J08391779+4722238) to ensure the consistency of the entire dataset. The $J - K$ colors of the comparison stars are 0.419, 0.384, and 0.337, quite close to $J - K = 0.353$ of HAT-P-13.

The data were corrected for systematics with the well-known parameter decorrelation technique (e.g. Robinson et al. 1995), in our case applying the specific implementation of the External Parameter Decorrelation (EPD) in constant mode (Bakos et al. 2010). The observed external parameters were the PSF of stellar profiles and the local photometry of the flat-field image at the same X, Y positions as the stars observed. The variation in stellar profile is a known error source which has been involved in most standard reduction pipelines of exoplanet photometry. Taking residuals of flat field correction as error source into account, dividing with the flat field under/overestimates the

[1] http://www.r-project.org

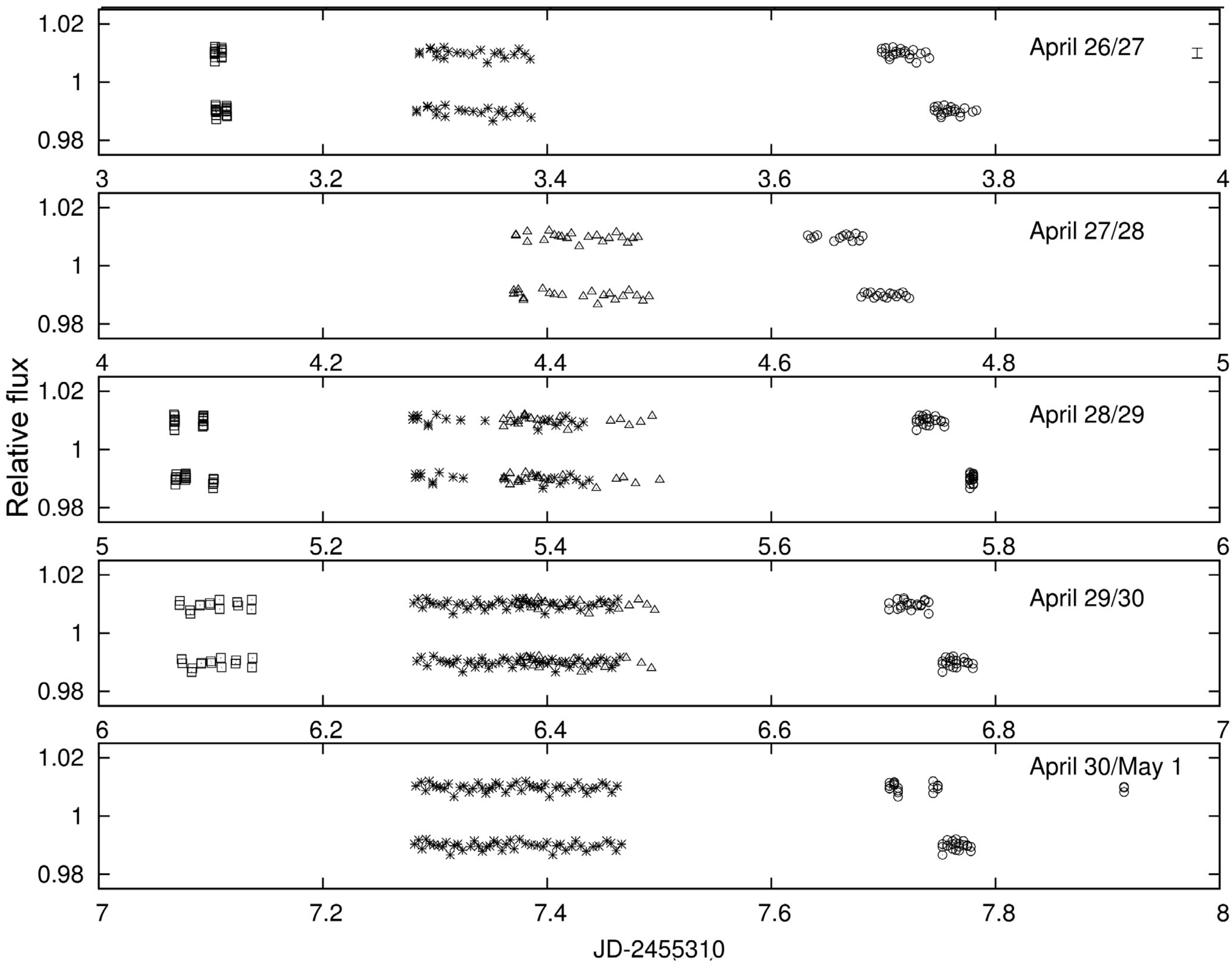

Fig. 1. Observations of HAT-P-13 during April 26–30. Observations have been shifted by +0.01 (V points) and −0.01 (R points) as indicated. Different symbols correspond to the different observatories: square: Langkawi, stars: Konkoly, triangles: INAF-OACt, circle: Tenagra. The typical standard deviation is 0.0013 in R and 0.0014 in V. A ±0.0015 error bar is indicated in the upper right corner of the top panel.

necessary correction by a factor of a few 0.1%. We found that most of the artificial patterns of the light curves is due to systematic residuals of flat field correction and could be eliminated effectively in this way. In the end, 6585 raw photometric points were extracted. We omitted points out of the 5–95% quantile interval of the measured fluxes and averaged the surviving points by 3. This resulted in 1952 data points submitted to further analysis.

3. Results

3.1. Significance analysis of the null detection

In Fig. 1, we plot sample light curves from the multisite campaign. The panels show the combined light curves from April 26, 27, 28, 29, and 30. Neither signs of ingress or egress nor significant deviations from the average brightness were observed. These features strongly imply that all observations are out of transit, and HAT-P-13c is likely to be a non-transiting exoplanet.

What is the significance of this conclusion? The time coverage of our data is 30%. Thus the first answer could be that a transit could happen anytime 70% of the time, i.e. when observations were not performed, and this null result is essentially insignificant. But this conclusion is incorrect and in fact, our observations rule out the majority of transiting orbits for HAT-P-13c.

We performed a numerical experiment to quantitatively measure the significance. A set of 10^5 exoplanets were simulated on a similar orbit to HAT-P-13 (a 428 day period around an 1.22 $R_\odot$, 1.56 $R_\odot$ star). The radius of the planet was assumed to be 1.2 R_J, which is the typical size of the most massive known exoplanets. With this choice, the density of HAT-P-13c is 8.7 times that of the Jupiter. The orbital eccentricity of the model was $e = 0.691$, the argument of periastron was $\omega = 176.7°$, coefficients for quadratic limb darkening were $\gamma_1 = 0.3060$, $\gamma_2 = 0.3229$ (planet and orbit parameters from Bakos et al. 2009). To include grazing transits, the value of the impact parameter b was allowed to be >1 and was drawn from uniform distibution between 0 and 1.08. The transit time followed a uniform distribution in the April 26.5 UT and April 30.5 UT interval. In some possible planet configurations, it is probable that data of a given run could have included only the bottom of the transit. This should be visible as a slight offset from the remaining runs, but this cannot be detected because of non-photometric conditions. What we are sure about is that ingress and egress phases were not detected within

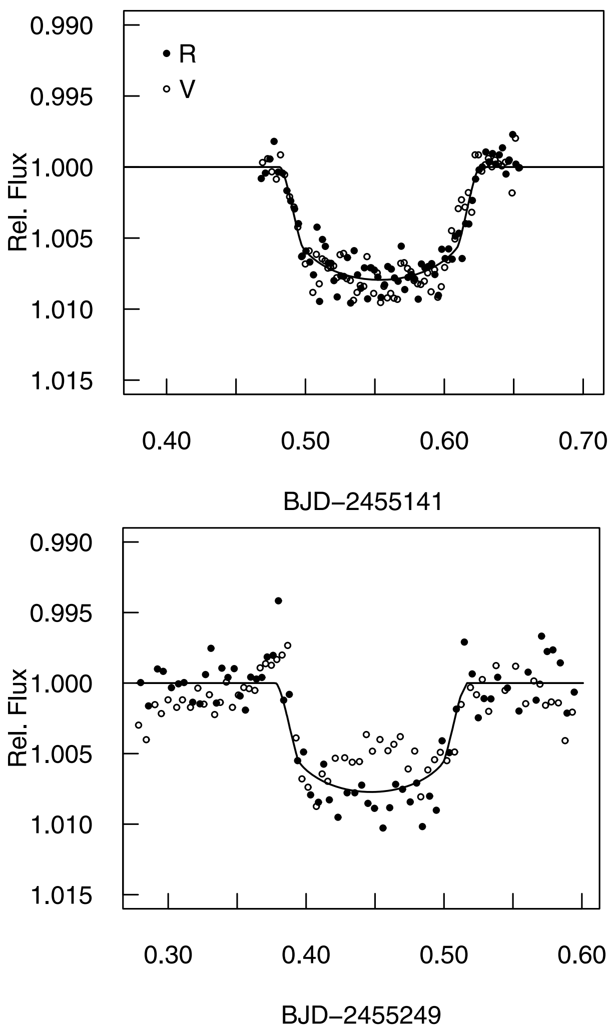

Fig. 2. Model fit to the transit on November 05/06, 2009 (*upper panel*) and February 21/22, 2010 (*lower panel*). *V* and *R* band data are plotted with open and soild dots, respectively.

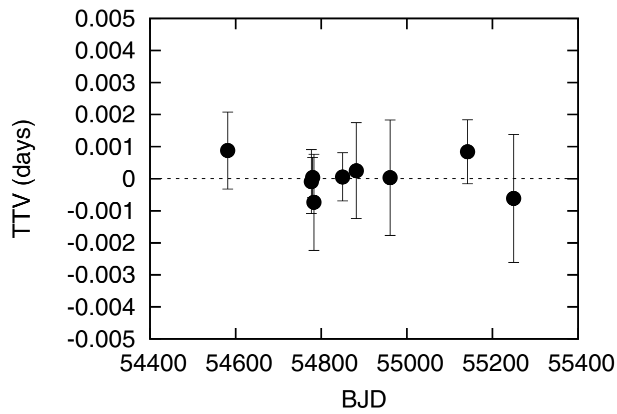

Fig. 3. Transit timing variation of HAT-P-13b.

our time coverage. This information also tightly constrains the possible orbits in the transit time–impact parameter space.

Model transit light curves were sampled at the times of observation points (all data in Table 2), sorted to observation runs, and the average intensity level was individually subtracted. We added bootstrap noise to the individual points (the measured light curve errors were randomly added to the simulated values with subtitution). A χ^2 test was then applied to check whether the simulations are inconsistent with zero at the 99% significance level. In this way, we identified these configurations of HATP-P-13c that should have been observed in our measurements (we call these observable configurations in the following). Because our observations are consistent with zero variation, observable configurations are explicitly excluded by our data.

We inferred that 72% of the 10^5 model transit configurations should have been observable. Therefore the hypothesis that HAT-P-13c is a transiting exoplanet can be rejected with 72% confidence. By allowing the mean transit times to be distributed normally around April 28 17 UT with 1.9 day standard deviation, the level of significance turns out to be 70%. The level of significance does not vary significantly in the range of orbits allowed by the parameter uncertainties in Bakos et al (2009), because the errors are rather small (3% in e and 0.3% in ω). We reduced the model light curves in amplitude to define the size limit where the detection efficiency begins to decrease significantly. The resulting significance was 65% when the amplitude was reduced by 0.45. The planet size corresponding to this signal amplitude is 1.04 $R_{\rm J}$, which is our detection limit. The conclusion is that roughly three quaters of all possible transiting configurations are excluded by our observations.

This result does not mean that HAT-P-13c cannot orbit on an aligned orbit with HAT-P-13b. HAT-P-13c is quite far from the central star, hence the star's apparent diameter is 0.6 degrees as seen from the planet. Thus, transiting configurations require the orbit to be in a thin region, very close to our line of sight. There is a huge set of possible configurations in which HAT-P-13c is in an orbit close to that of planet b, without displaying any transits. In this case, the TTV of HAT-P-13b can help us determine the orientation of HAT-P-13c's orbital plane (Bakos et al. 2009).

3.2. Transit timing variations of HAT-P-13b

Before the suspected transit of HAT-P-13c, two transits of HAT-P-13b had been observed to help refine the period and search for TTV. Data from 2009-11-05/06 (measured with the K100 telescope, Table 1) and 2010 February 21/22 (K60 telescope) are plotted in Fig. 2. In November (upper panel in Fig. 2), the sky was photometric during the transit, but it was foggy in the evening and from 40 min after the egress phase. In February 2010, cirri were present that significantly affected the *V* band data, but the *R* light curve was well reconstructed with constant EPD (see lower panel in Fig. 2).

Times of minima were determined by fitting a model light curve, similarly to the method described in Szabó et al. (2010). For the November 2009 transit, both *V* and *R* data were included in the fitting, while we used only the *R* curve for the February 2010 transit. (However, even including the more noisy *V* curve does not change the mid-transit time by more than 0.0004 days.)

To reduce the degrees of freedom in the fit, the shape of the model was not adjusted; we used previously published parameters (Winn et al. 2010). The model light curve was calculated with our transit simulator (Simon et al. 2009, 2010). The model was shifted in time to minimise the rms scatter in the measurements. We determined new transit times of: BJD 2 455 141.5522 ± 0.001 and 2 455 249.4508 ± 0.002. Seven transit times were published by Bakos et al. (2009), which were included in the TTV analysis. After combining all data, we inferred the period of HAT-P-13b to be 2.916293 ± 0.000010 days, while the determined TTV diagram is plotted in Fig. 3. All points are consistent with zero within the error bars. It has to be noted that HAT-P-13b must exhibit some TTV, because of the perturbations by HAT-P-13c. HAT-P-13c causes 8.5 s light-time effect (LITE) and perturbations in the orbit of HAT-P-13b. On short (≈1 yr) timescales, the LITE is dominant. However, the expected LITE is smaller than the ambiguity of our transit times by a factor of 5, and therefore there is no chance of a positive detection at this level of accuracy.

4. Summary

The main results of this study can be summarised as:

- A multisite campaign was organised to observe HAT-P-13 around the expected transit of HAT-P-13c. Two transits of HAT-P-13b were also observed.
- HAT-P-13c was not observed to transit. We have concluded that HAT-P-13c is not a transiting planet with 72% significance.
- Our revised measurement of the period of HAT-P-13b is 2.916293 ± 0.000010 days. Our measured TTV is consistent with zero variation.

Acknowledgements. This project has been supported by the Hungarian OTKA Grants K76816 and MB08C 81013, and the "Lendület" Young Researchers' Program of the Hungarian Academy of Sciences. Gy.M.Sz. was supported by the "Bolyai" Research Fellowship of the Hungarian Academy of Sciences. The 91 cm telescope of the Serra La Nave station is supported by INAF Osservatorio Astrofisico di Catania, Italy. We acknowledge assistance of the queue observers, Karzaman Ahmad from LNO and Hsiang-Yao Hsiao from Lulin Observatory. ZsK acknowledges the support of the Hungarian OTKA grants K68626 and K81421.

References

Bakos, G. Á, Howard, A. W., Noyes, R. W., et al. 2009, ApJ, 707, 446
Bakos, G. Á, Torres, G. Pál, A., et al. 2010, ApJ, 710, 1724
Batygin, K., Bodenheimer, P., & Laughlin, G. 2009, ApJ, 704, L49
Fabrycky, D. C. 2009, Transiting Planets, ed. E. Pont, D. Sasselov, & M. J. Holman (Cambridge, MA: Cambridge Univ. Press), 173
Holman, M. J., et al. 2010, Science Express, DOI: 10.1126/science.1195778
Léger, A., Rouan, D., Schneider, J., et al., 2009, A&A, 506, 287
Mardling, R. A. 2010, MNRAS, 407, 1048
Pál, A., Bakos, G. Á., Torres, G., et al. 2008, ApJ, 680, 1450
Queloz, D., Bouchy, F., Moutou, C., et al. 2009, A&A, 506, 303
Robinson, L. B., Wei, M. Z., Borucki, W. J., et al. 1995, PASP, 107, 1094
Simon, A. E., Szabó, Gy. M., Szatmáry, K., et al., 2009, EM&P, 105, 385
Simon, A. E., Szabó, Gy. M., Szatmáry, K., & Kiss, L. L. 2010, MNRAS, 406, 2038
Szabó, Gy. M., Haja, O., Szatmary, K., Pal, A., & Kiss, L. L. 2010, IBVS, 5919
Winn, J. N., Johnson, J. A., Albrecht, S., et al. 2009, ApJ, 703, L99
Winn, J. N., Johnson, J. A., Howard, A. W., et al. 2010, ApJ, 718, 575

Astron. Nachr. / AN **999**, No. 88, 789 – 793 (2010) / **DOI** ***please set DOI!***

Ground-based observations of *Kepler* asteroseismic targets*

K. Uytterhoeven[1,], R. Szabó[2], J. Southworth[3], S. Randall[4], R. Østensen[5], J. Molenda-Żakowicz[6], M. Marconi[7], D.W. Kurtz[8], L. Kiss[2,9], J. Gutiérrez-Soto[10], S. Frandsen[11], P. De Cat[12], H. Bruntt[13], M. Briquet[5], X.B. Zhang[14], J.H. Telting[15], M. Stęślicki[6], V. Ripepi[7], A. Pigulski[6], M. Paparó[2], R. Oreiro[5], C. Ngeow[16], E. Niemczura[6], J. Nemec[17], A. Narwid[6], P. Mathias[18], S. Martín-Ruíz[10], H. Lehmann[19], G. Kopacki[6], C. Karoff[20,11], J. Jackiewicz[21], M. Ireland[9], D. Huber[9], A.A. Henden[22], G. Handler[23], A. Grigahcène[24], E.M. Green[25], R. Garrido[10], L. Fox Machado[26], J. Debosscher[5], O.L. Creevey[27], G. Catanzaro[28], Z. Bognár[2], K. Biazzo[29], S. Bernabei[30]**

[1] Lab. AIM, CEA/DSM-CNRS-Université Paris Diderot; CEA, IRFU, SAp, Saclay, 91191, Gif-sur-Yvette, France
[2] Konkoly Observatory of the Hungarian Academy of Sciences, 1121 Budapest, Hungary
[3] Department of Physics, University of Warwick, Coventry CV4 7AL, UK
[4] European Southern Observatory, Karl-Schwarzschild-Str. 2, 85748 Garching bei Mnchen, Germany
[5] Instituut voor Sterrenkunde, KULeuven, Celestijnenlaan 200D, 3001 Leuven, Belgium
[6] Instytut Astronomiczny, Uniwersytet Wrocławski, Kopernika 11, 51-622 Wrocław, Poland
[7] INAF - Osservatorio Astronomico di Capodimonte, Via Moiariello 16, 80131 Napoli, Italy
[8] Jeremiah Horrocks Institute of Astrophysics, University of Central Lancashire, Preston PR1 2HE, UK
[9] Sydney Institute for Astrophysics, School of Physics, University of Sydney, Australia
[10] Instituto de Astrofísica de Andalucía (CSIC), Apartado 3004, 18080 Granada, Spain
[11] Department of Physics and Astronomy, Aarhus University, 8000 Aarhus C, Denmark
[12] Royal Observatory of Belgium, Ringlaan 3, 1180 Brussel, Belgium
[13] LESIA, Observatoire de Paris-Meudon, 92195 Meudon, France
[14] National Astronomical Observatories, Chinese Academy of Sciences, Beijing 100012, China
[15] Nordic Optical Telescope, Santa Cruz de La Palma, Spain
[16] National Central University, No. 300, Jhongda Rd, Jhongli City, Taoyuan County 32001, Taiwan
[17] Department of Physics & Astronomy, Camosun College, Victoria, British Columbia, Canada
[18] Lab. d'Astrophysique de Toulouse-Tarbes, Université de Toulouse, CNRS, 57 avenue d'Azereix, 65000 Tarbes, France
[19] Thüringer Landessternwarte, 07778 Tautenburg, Germany
[20] School of Physics and Astronomy, University of Birmingham, Edgbaston, Birmingham B15 2TT, UK
[21] Department of Astronomy, New Mexico State University, Las Cruces, NM 88001, USA
[22] American Association of Variable Star Observers, 49 Bay State Road, Cambridge, MA 02138, USA
[23] Institut für Astronomie, Türkenschanzstr. 17, 1180 Wien, Austria
[24] Centro de Astrofísica, Faculdade de Ciências, Universidade do Porto, Rua das Estrelas, 4150-762 Porto, Portugal
[25] Steward Observatory, University of Arizona, 933 North Cherry Avenue, Tucson, AZ 85721, USA
[26] Observatorio Astronómico Nacional, Instituto de Astronomía, UNAM, Ensenada B.C., Apdo. Postal 877, México
[27] Instituto de Astrofísica de Canarias, 38200 La Laguna, Tenerife, Spain; Departamento de Astrofísica, Universidad de La Laguna, 38205 La Laguna, Tenerife, Spain
[28] INAF - Osservatorio Astrofisico di Catania, Via S. Sofia 78, 95123 Catania, Italy
[29] INAF - Osservatorio Astrofisico di Arcetri, Largo Enrico Fermi 5, 50125 Firenze, Italy
[30] INAF - Osservatorio Astronomico di Bologna, Via Ranzani 1, 40127 Bologna, Italy

Received 01 April 2010, accepted —
Published online later

Key words stars: fundamental parameters, stars: oscillations

We present the ground-based activities within the different working groups of the *Kepler* Asteroseismic Science Consortium (KASC). The activities aim at the systematic characterization of the 5000+ KASC targets and at the collection of ground-based follow-up time-series data of selected promising *Kepler* pulsators. So far, 36 different instruments at 31 telescopes on 23 different observatories in 12 countries are in use and a total of more than 530 observing nights has been awarded.

* Based on observations made with the Isaac Newton Telescope and William Herschel Telescope operated by the Isaac Newton Group, with the Nordic Optical Telescope, operated jointly by Denmark, Finland, Iceland, Norway, and Sweden, with the Italian Telescopio Nazionale Galileo (TNG) operated by the Fundación Galileo Galilei of the INAF (Istituto Nazionale di Astrofisica), and with the Mercator telescope, operated by the Flemish

1 Introduction

The *Kepler* Asteroseismic Science Consortium, KASC[1], unites hundreds of asteroseismologists from institutes all over the world in different topical Working Groups, with the aim of performing seismic studies of all types of pulsating stars across the Hertzsprung-Russell diagram, based on *Kepler* time-series space photometry. The ground-based observational Working Groups (GBOsWG) take care of the organisation of ground-based observations in support of the *Kepler* space data. Additional ground-based multi-colour and spectral information are indispensable for a successful seismic modelling (see, e.g., Uytterhoeven et al. 2008a, 2009; Uytterhoeven 2009). The need for ground-based support data is motivated by two objectives: 1) the characterization of all *Kepler* targets in terms of fundamental stellar parameters, 2) the identification of mode parameters from multi-colour and spectral time-series observations for selected pulsators.

The KASC GBOsWG is making great efforts in organising and planning telescope time on various instruments around the world to meet these objectives and to ensure an optimal seismic exploitation of the *Kepler* data. So far, 36 different instruments at 31 telescopes on 23 different observatories in 12 countries are involved and a total of more than 530 observing nights has been awarded.

2 Characterization of 5000+ KASC targets

The *Kepler* space data do not provide information on basic stellar parameters such as effective temperature ($T_{\rm eff}$), gravity ($\log g$), metallicity, and the projected rotational velocity ($v \sin i$), which are important to classify the targets and are crucial for successful asteroseismic modelling. Hence, spectral and multi-colour information are needed to complement the space data. A first effort to compile a catalogue of stellar parameters, derived from Sloan photometry, has been undertaken in the form of the *Kepler* Input Catalogue (KIC, Latham et al. 2005). However, the accuracy of values of $\rm T_{eff}$ and $\log$g in KIC is generally too low for seismic modelling. Hence, additional ground-based efforts are required. The aim of the KASC GBOsWG is to obtain for each of the 5000+ KASC asteroseismic targets a spectrum with a sufficient resolution to derive $T_{\rm eff}$, $\log g$, micro-turbulence, $v \sin i$ and metallicity (Sousa et al. 2008; Frasca et al. 2006; Bruntt 2009; Niemczura et al. 2009), and multi-colour information to derive reddening, metallicity, and absolute magnitude (Rogers 1995; Kupka & Bruntt 2001).

The systematic characterization of 5000+ targets requires a huge observational effort and involves a long-term project, spread out over several instruments. So far, within the KASC GBOsWG, more than 278 nights have been awarded for the characterization project with 26 different instruments on 17 observatories. More time has been and will be applied for.

The first effort to characterize asteroseismic *Kepler* targets dates back to 2004. Since then, a project is running to characterize KASC solar-like stars (Molenda-Żakowicz et al. 2007, 2008, 2009b). Nowadays, several observational projects, focussed either on a specific pulsation class or on several classes simultaneously, are ongoing to systematically observe all KASC targets. In Table 1 we present an overview of the *awarded* observing time for target characterization. Additional information on the observations is given in Uytterhoeven et al. (2010). In addition to the spectroscopic and multi-colour observations, an interferometric project is ongoing with PAVO@CHARA at Mt Wilson Observatory (USA) to measure angular diameters for some of the brighest Kepler targets. Results on the physical parameter determination of a selection of δ Sct, γ Dor and hybrid targets are recently presented in Catanzaro et al. (2010).

More observing time has been applied for. Spectropolarimetric observations are planned to investigate magnetic signatures in selected Cepheids, RR Lyr, δ Sct, and Be stars with ESPaDOnS@CFHT, Mauna Kea (USA) (P.I. JN, JG-S). An ambitious proposal to observe 95% of all KASC asteroseismic targets with the multi-fiber, multi-object spectrograph LAMOST@4m telescope at Xinglong observatory (CN) has been submitted (P.I. PDC).

3 Time-series observations of selected promising *Kepler* pulsators

Important key ingredients for an asteroseismic study are precise pulsation frequencies, accurately identified pulsation modes, and strong constraints on atmospheric parameters. Accurate values of the pulsation frequencies will be provided for by the *Kepler* photometry, while accurate atmospheric parameters will be derived from the ground-based data obtained in the framework of the project outlined in the previous section.

For solar-like oscillators, mode identification relies on the regularity of the frequency pattern in the power spectrum (e.g. Mathur et al. 2010). This method is not directly applicable to larger amplitude pulsators, for which a combination of non-linear effects, rotation, and convection selects the observed modes in a way that is not yet fully understood (e.g. Townsend 2009; Miglio et al. 2008; Suárez et al.

Community, all on the island of La Palma at the Spanish Observatorio del Roque de los Muchachos of the Instituto de Astrofísica de Canarias. Based on observations made with the IAC-80 operated on the island of Tenerife by the Instituto de Astrofísica de Canarias at the Spanish Observatorio del Teide. Also based on observations taken at the observatories of Sierra Nevada, San Pedro Mártir, Vienna, Xinglong, Apache Point, Lulin, Tautenburg, McDonald, Skinakas, Pic du Midi, Mauna Kea, Steward Observatory, Mt. Wilson, Białków Observatory of the Wrocław University, Piszkéstető Mountain Station, and Observatoire de Haute Provence. Based on spectra taken at the Loiano (INAF-OA Bologna), Serra La Nave (INAF - OA Catania) and Asiago (INAF - OA Padova) Observatories. Also based on observations collected at the Centro Astronómico Hispano Alemán (CAHA) at Calar Alto, operated jointly by the Max-Planck-Institut für Astronomie and the Instituto de Astrofísica de Andalucía (CSIC). We acknowledge with thanks the variable star observations from the AAVSO International Database contributed by observers worldwide and used in this research.

** e-mail: katrien.uytterhoeven@cea.fr

[1] http://astro.phys.au.dk/KASC

Table 1 Overview of the awarded observing time for target characterization. Information is given on the observatory, the telescope and instrument, the number of awarded nights (N) or hours (h), the type of targets, and the principal investigator (P.I.) of the proposal. Proposals aimed at the characterization of several pulsators (γ Dor, δ Sct, β Cep, Be, solar-like, roAp, and Slowly Pulsating B (SPB) stars, and stars in clusters) are labelled "combined". Spectra that were obtained through a filler programme at the beginning or the end of the night, are indicated as "filler".

Observatory	Telescope	N	Target	P.I.
Sierra Nevada (E)	0.90m photometer	8N	combined	SM-R
San Pedro Martir (MX)	1.5m photometer	5N	combined	LFM
	2.12m spectrograph	2N	combined	LFM
Teide (E)	IAC80 CAMELOT	14N	combined	KU
Piszkéstető (H)	1.0mRRC CCD	7N	combined	MP/ZB
Calar Alto (E)	2.2m BUSCA	5N	combined	KU
La Palma (E)	INT WFC	5N	combined	KU
	NOT FIES	3N	combined	KU
	Mercator HERMES	7N	combined	MB
Loiano (I)	1.52m BFOSC	4N	combined	VR
Catania (I)	0.9m FRESCO	7N	combined	VR
McDonald (USA)	2.7m cs23	8N	combined	PDC
Tautenburg (D)	2m Coudé	14N	combined	HL
Sierra Nevada (E)	0.9m photometer	2N	Be stars	JG-S
	1.52m ALBIREO	2+10N	Be stars	JG-S
Skinakas (GR)	1.3m spectrograph	4N	Be stars	JG-S
La Palma (E)	NOT Alfosc	1N	Be stars	JG-S
Catania (I)	0.9m FRESCO	3N	δ Sct stars	GC
Loiano (I)	1.52m BFOSC	3N	δ Sct stars	VR
		10N	δ Sct stars	GC
Asiago (I)	1.82m AFOSC	3N	δ Sct stars	VR
La Palma (E)	TNG SARG	2h	δ Sct stars	VR
Catania (I)	0.9m FRESCO	15+15+25+12+25N	solar-like stars	JM-Ż
	0.9m CCD	10N	solar-like stars	JM-Ż
La Palma (E)	TNG SARG	12N	solar-like stars	GC
	NOT FIES	2+1.5N	solar-like stars	CK
Mauna Kea (USA)	CFHT ESPaDOnS	10h	solar-like stars	HB
Pic du Midi (F)	TBL NARVAL	20h+20h	solar-like stars	HB
Mt Wilson (USA)	CHARA PAVO	>3N	solar-like stars	DH, MI
Steward (USA)	BOK B&C spectrograph	10N	compact stars	EMG
La Palma (E)	WHT ISIS	4.5N	compact stars	RØ
	INT IDS	5+4N	compact stars	RO
	NOT FIES	filler	compact stars	JHT
La Palma (E)	NOT FIES	6N+7N	K giants, roAp stars	SF
Mauna Kea (USA)	CFHT ESPaDOnS	2h	giants in NGC 6811	HB
La Palma (E)	Mercator HERMES	∼45h	binaries with pulsating components	JD
Tautenburg (D)	2m Coudé	filler	SPB, β Cep stars	HL
Haute Provence (F)	1.92m SOPHIE	filler	γ Dor stars	PM

2005; Degroote et al. 2010). For these targets, the identification of modes observed by *Kepler* requires ground-based multi-colour and spectral time-series analysis (e.g. Briquet et al. 2009; Poretti et al. 2009; Uytterhoeven et al. 2008b; Rodríguez et al. 2006).

Multi-epoch spectroscopy is also important in the case of (eclipsing) spectroscopic binaries with a pulsating component, because by using spectra one can directly derive the component masses (Tango et al. 2006; Vučkovic et al. 2007; Creevey et al. 2009; Desmet et al. 2010), and it is possible to disentangle the binary components (Harmanec et al. 2004) and study the line-profile variability of the components in full detail (Uytterhoeven et al. 2005).

To date, within the KASC GBOsWG, a total of at least 256 nights has been awarded with 15 different instruments on 13 observatories for specific time-series projects. Additional telescope time has been applied for. An overview of the *awarded* observing time is given in Table 2. We refer again to Uytterhoeven et al. (2010) for a description of the observations. The projects involve RR Lyr stars and Cepheids, Slowly Pulsating B stars, β Cep stars, hybrid γ Dor/δ Sct candidates, and pulsators in clusters. The latter concerns a large photometric multi-site campaign on the clusters NGC 6866, carried out in 2009, and NGC 6811, scheduled for 2010. The cluster NGC 6866 is known to host at least three δ Sct and two γ Dor candidates (Molenda-Żakowicz et al. 2009a), and there are 12 known δ Sct stars in NGC 6811 (Luo et al. 2009).

4 Future plans

The ground-based counterpart of *Kepler* is crucial for the successful execution of seismic studies. The GBOsWG will continue to organise ground-based observations to comple-

Table 2 Overview of the awarded time for the collection of multi-colour or spectral time-series of selected promising asteroseismic *Kepler* targets. Information is given on the observatory, the telescope and instrument, the number of awarded nights (N), the type of targets, and the principal investigator (P.I.) of the proposal.

Observatory	Telescope	N	Targets	P.I.
Sierra Nevada (E)	1.5m CCD	15N	NGC 6866	RG
Vienna (A)	0.8m CCD	14N	NGC 6866	GH
Piszkéstető (H)	0.9m CCD	14N	NGC 6866	RS
Xinglong (CN)	0.85m CCD	14N	NGC 6866	XZ
Białków (PL)	0.6m CCD	8+14N	NGC 6866	JM-Ż
Catania (I)	0.9m CCD	8N	NGC 6866	KB
Sierra Nevada (E)	1.5m CCD	15N	NGC 6811	RG
Vienna (A)	0.8m CCD	14N	NGC 6811	GH
Piszkéstető (H)	0.9m CCD	14N	NGC 6811	RS
Xinglong (CN)	0.85m CCD	14N	NGC 6811	XZ
Białków (PL)	0.6m CCD	10N	NGC 6811	JM-Ż
Loiano (I)	1.52m CCD	10N	NGC 6811	HB
Catania (I)	0.9m CCD	10N	NGC 6811	JM-Ż
Teide (E)	IAC-80 CAMELOT	14N	NGC 6811	OC
Apache Point (USA)	NMSU 1.0m	14N	NGC 6811	JJ
Lulin (TW)	0.4m SLT	18N	RR Lyr, Cepheids	NCC
Lulin (TW)	1.0m LOT	3N	RR Lyr, Cepheids	NCC
AAVSONet	0.2-0.6m telescopes	>1N	RR Lyr, Cepheids	AH
Sierra Nevada (E)	0.9m photometer	14N	hybrid γ Dor/δ Sct stars	AG/SM-R
McDonald (USA)	2.2m B&C spectrograph	7N	SPB, γ Dor stars	PDC
La Palma (E)	Mercator HERMES	11N	SPB, β Cep stars	HL

ment the *Kepler* light curves. So far, the observational and organisational efforts have been very successful with more than 530 observing nights already awarded. Additional observing time with dedicated multi-colour and spectroscopic instruments will be applied for in the coming observing semesters. The ground-based support of *Kepler* is putting a heavy pressure on ground-based telescopes in the Northern hemisphere, especially on the ones equipped with a (high-R) spectrograph. Therefore, assistance and help from the community is very welcome. We encourage everyone who has access to (further) telescopes and wants to help with observations, data reduction or data analysis, to join the project. This very important task of supporting *Kepler* from the ground revives the use of small/mid-sized telescopes, which is a significant benefit for all the national observatories involved.

Acknowledgements. MB is Postdoctoral Fellow of the Fund for Scientific Research, Flanders. This work was supported by MNiSW grant N203 014 31/2650 and by the National Office for Research and Technology through the Hungarian Space Office Grant No. URK09350 and the ‘Lendület’ program of the Hungarian Academy of Sciences.

References

Briquet, M., Uytterhoeven, K., Morel, T., et al., 2009, A&A 506: 269B
Bruntt, H. 2009, A&A 506, 235
Catanzaro, G., Ripepi, V., Bernabei, S. et al.: 2010, MNRAS, submitted
Creevey, O., Uytterhoeven, K., Martín-Ruiz, S., et al.: 2009, A&A 507, 901
Degroote, P., Aerts, C., Baglin, A., et al.: 2010, Nature 464, 259
Desmet, M., Frémat, Y., Baudin, F., et al.: 2010, MNRAS 401, 418
Frasca, A., Guillout, P., Marilli, E., et al.: 2006, A&A 454, 301
Harmanec, P., Uytterhoeven, K., Aerts, C., 2004, A&A 422, 1013
Kupka, F., Bruntt, H.: 2001, in ’First COROT/MONS/MOST Ground Support Workshop’, ed. C. Sterken (Brussels: Vrije Univ.), 39
Latham, D.W., Brown, T.M., Monet, D.G., Everett, M., Esquerdo, G. A., Hergenrother, C. W.: 2005, AAS 37, 1340
Luo, Y.P., Zhang, X.B., Luo, C.Q., Deng, L.C., Luo, Z.Q., 2009, New Astronomy 14, 584
Mathur, S., Garcia, R.A., Regulo, C., et al. 2010, A&A 511, A46
Miglio, A., Montalban, J., Noels, A., Eggenberger, P.: 2008, MNRAS 386, 1487
Molenda-Żakowicz, J., Frasca, A., Latham, D.W., Jerzykiewicz, M.: 2007, AcA 57, 301
Molenda-Żakowicz, J., Frasca, A., Latham, D.W.: 2008, AcA 58, 419
Molenda-Żakowicz, J., Kopacki, G., Steślicki, M., Narwid, A., 2009a, AcA 59, 193
Molenda-Żakowicz, J., Jerzykiewicz, M., Frasca, A: 2009b, AcA 59, 213
Niemczura, E., Rodler, F., Müller, A.: 2009, CoAst 158, 146
Poretti, E., Michel, E., Garrido, R., et al.: 2009, A&A 506, 85
Rodríguez, E., Amado, P.J., Suárez, J.C., et al.: 2006, A&A 450, 715
Rogers, N. Y.: 1995, Commun. Asteroseismology, 78, 1
Sousa, S.G., Santos, N.C., Mayor, M., et al.: 2008, A&A 487, 373
Suárez, J.C., Bruntt, H., Buzasi, D.: 2005, A&A 438, 633
Tango, W. J., Davis, J., Ireland, et al.: 2006, MNRAS, 370, 884
Townsend, R.: 2009, AIP Conf. Proc. 1170, 355
Uytterhoeven, K., Briquet, M., Aerts, C., Telting, J. H., Harmanec, P., Lefever, K., Cuypers, J.: 2005, A&A 432, 955
Uytterhoeven, K., Poretti, E., Rainer, M., et al.: 2008a, Journal of Physics, Conf. Ser. 118, 2077
Uytterhoeven, K., Mathias, P., Poretti, E., et al.: 2008b, A&A 489, 2213
Uytterhoeven, K.: 2009, CoAst 158, 156

Uytterhoeven, K., Poretti, E., Mathias, P., et al.: 2009, AIP Conf. Proc. 1170, 327
Uytterhoeven, K., Briquet, M., Bruntt, H., et al.: 2010, AN, submitted (this volume)
Vučkovic, M., Aerts, C., Østensen, R., et al.: 2007, A&A 471, 605

The Astrophysical Journal Letters, 724:L16–L21, 2010 November 20 doi:10.1088/2041-8205/724/1/L16

ULTRA-BRIGHT OPTICAL TRANSIENTS ARE LINKED WITH TYPE Ic SUPERNOVAE

A. Pastorello[1], S. J. Smartt[1], M. T. Botticella[1], K. Maguire[1], M. Fraser[1], K. Smith[1], R. Kotak[1], L. Magill[1], S. Valenti[1], D. R. Young[1], S. Gezari[2,14], F. Bresolin[3], R. Kudritzki[3], D. A. Howell[4], A. Rest[5], N. Metcalfe[6], S. Mattila[1,7,8], E. Kankare[1,7,9], K. Y. Huang[10], Y. Urata[11], W. S. Burgett[3], K. C. Chambers[3], T. Dombeck[3], H. Flewelling[3], T. Grav[2], J. N. Heasley[3], K. W. Hodapp[3], N. Kaiser[3], G. A. Luppino[3], R. H. Lupton[12], E. A. Magnier[3], D. G. Monet[13], J. S. Morgan[3], P. M. Onaka[3], P. A. Price[3], P. H. Rhoads[3], W. A. Siegmund[3], C. W. Stubbs[5], W. E. Sweeney[3], J. L. Tonry[3], R. J. Wainscoat[3], M. F. Waterson[3], C. Waters[3], and C. G. Wynn-Williams[3]

[1] Astrophysics Research Centre, School of Mathematics and Physics, Queen's University Belfast, Belfast BT7 1NN, UK; a.pastorello@qub.ac.uk
[2] Department of Physics and Astronomy, Johns Hopkins University, 3400 North Charles Street, Baltimore, MD 21218, USA
[3] Institute for Astronomy, University of Hawaii at Manoa, Honolulu, HI 96822, USA
[4] Las Cumbres Observatory Global Telescope Network and the Department of Physics, University of California, Santa Barbara, CA 93117, USA
[5] Department of Physics, Harvard University, Cambridge, MA 02138, USA
[6] Department of Physics, University of Durham, South Road, Durham DH1 3LE, UK
[7] Tuorla Observatory, Department of Physics and Astronomy, University of Turku, Piikkiö, FI 21500, Finland
[8] Stockholm Observatory, Department of Astronomy, AlbaNova University Center, SE 106 91 Stockholm, Sweden
[9] Nordic Optical Telescope, Apartado 474, E-38700 Santa Cruz de La Palma, Spain
[10] Academia Sinica Institute of Astronomy and Astrophysics, Taipei 106, Taiwan
[11] Institute of Astronomy, National Central University, Chung-Li 32054, Taiwan
[12] Department of Astrophysical Sciences, Princeton University, Princeton, NJ 08544, USA
[13] US Naval Observatory, Flagstaff Station, Flagstaff, AZ 86001, USA
Received 2010 August 16; accepted 2010 September 9; published 2010 October 25

ABSTRACT

Recent searches by unbiased, wide-field surveys have uncovered a group of extremely luminous optical transients. The initial discoveries of SN 2005ap by the Texas Supernova Search and SCP-06F6 in a deep Hubble pencil beam survey were followed by the Palomar Transient Factory confirmation of host redshifts for other similar transients. The transients share the common properties of high optical luminosities (peak magnitudes ~ -21 to -23), blue colors, and a lack of H or He spectral features. The physical mechanism that produces the luminosity is uncertain, with suggestions ranging from jet-driven explosion to pulsational pair instability. Here, we report the most detailed photometric and spectral coverage of an ultra-bright transient (SN 2010gx) detected in the Pan-STARRS 1 sky survey. In common with other transients in this family, early-time spectra show a blue continuum and prominent broad absorption lines of O II. However, about 25 days after discovery, the spectra developed type Ic supernova features, showing the characteristic broad Fe II and Si II absorption lines. Detailed, post-maximum follow-up may show that all SN 2005ap and SCP-06F6 type transients are linked to supernovae Ic. This poses problems in understanding the physics of the explosions: there is no indication from late-time photometry that the luminosity is powered by ^{56}Ni, the broad light curves suggest very large ejected masses, and the slow spectral evolution is quite different from typical Ic timescales. The nature of the progenitor stars and the origin of the luminosity are intriguing and open questions.

Key words: supernovae: general – supernovae: individual (SN 2010gx, SCP-06F6, SN 2005ap)

Online-only material: color figures

1. INTRODUCTION

The discovery of unusual optical transients is a goal of modern surveys. Focused supernova searches (e.g., the Texas Supernova Search) or all-sky surveys, such as the Panoramic Survey Telescope & Rapid Response System (Pan-STARRS), the Catalina Real-time Transient Survey (CRTS), the Palomar Transient Factory (PTF), and Skymapper are expected to discover a large number of new types of stellar explosions in the next years. The preliminary results are remarkable, and newly discovered transients are revolutionizing our knowledge of stellar explosions. Ultra-bright supernovae (SNe) associated with faint and, presumably, metal-poor host galaxies are the most spectacular recent discoveries (Quimby et al. 2007; Gezari et al. 2009; Miller et al. 2009; Gal-Yam et al. 2009; Young et al. 2010).

The field has moved quickly, prompted by the unusual transient SCP-06F6, discovered in the *Hubble Space Telescope* Cluster Supernova Survey (Barbary et al. 2009). Its light curve was symmetric, with a ∼100 day rise time in the observed frame. The spectrum showed broad absorption features and the transient was associated with no obvious host galaxy (although a weak source, 1″.5 from the transient, was marginally detected at magnitude $z \sim 25.8$).[15] Without robust constraints on the absolute magnitude for this transient, even the discrimination between Galactic and extra-galactic origin was uncertain. Possible scenarios proposed by Barbary et al. (2009) for SCP-06F6 were an outburst of a Galactic C-rich white dwarf (WD), a broad absorption lines quasar or a micro-lensing event, but none of them was fully convincing. Assuming that the broad features in the spectra of SCP-06F6 were the C_2 Swan bands, Gänsicke et al. (2009) tentatively fixed the redshift at $z = 0.14$, implying an absolute peak magnitude of about −18, suggesting an SN-like explosion of a C-rich Wolf-Rayet (WR) star. A tidal disruption of a C-rich star by a black hole (Rosswog et al. 2009; Soker

[14] *Hubble* Fellow.

[15] Unless specified, magnitudes are in the AB system.

et al. 2009), a Galactic WD-asteroid merger, and a type Ia SN in a dense, C-rich wind produced by a companion star (Soker et al. 2009) were also proposed as alternative explanations.

A few events have recently been discovered sharing observed properties with SCP-06F6. Data for a total sample of six objects have been presented by Quimby et al. (2010b). One of them was SN 2005ap, an enigmatic object originally presented in Quimby et al. (2007) and classified as a peculiar, overluminous SN IIL. Through the detection of narrow interstellar Mg II lines, Quimby et al. (2010b) have definitely proved that these transients are not located in the Galaxy or in the Local Group, but are relatively distant objects, with redshifts between 0.26 and 1.19. Consequently, they are extremely luminous, with u-band absolute magnitudes spanning between −22 and −23. On the basis of the lack of any evidence of a slope consistent with ^{56}Co decay in the late-time light curve of both SCP-06F6 and SN 2005ap, Quimby et al. (2010b) favored either a pulsational pair-instability outburst scenario, or core-collapse SNe powered by rapidly rotating young magnetars.

Unfortunately, follow-up observations collected so far for these transients and the information available for properly studying and modeling their data have been incomplete. The discovery of a relatively nearby object of this class caught early and followed in detail, has provided us with a new opportunity to study the energy output and spectral evolution of one of nature's brightest explosions.

2. THE DISCOVERY OF SN 2010GX

The CRTS team (Drake et al. 2009) first announced the discovery of an optical transient (CSS100313:112547-084941) at R.A. = 11:25:46.71 and decl. = −08:49:41.4, on images obtained on 2010 March 13 (magnitude 18.5; Mahabal et al. 2010). Its optical spectrum showed a blue, featureless continuum, and the initial redshift determination ($z = 0.17$) was later corrected by the same authors to $z = 0.23$ (Mahabal & Drake 2010).

On the following day, Quimby et al. (2010a) reported the independent discovery by the PTF survey (Rau et al. 2009; Law et al. 2009) of the same variable source (labeled as PTF10cwr) at several epochs between March 5 and 16, while no object was seen on March 4.27 UT to a limiting magnitude of 20.4. Optical spectra on March 18.27 UT showed that PTF10cwr was a luminous SN similar to the ultra-bright SN 2005ap (Quimby et al. 2007). The spectrum showed broad features attributed to O II (Quimby et al. 2010a). The presence of narrow lines attributed to a host galaxy allowed them to estimate the redshift to $z = 0.23$.

In the course of the Pan-STARRS 1 Telescope (PS1) 3π survey, we recovered the transient (PS1-1000037, hereafter SN 2010gx) between March 12 and 17 showing that its luminosity was still rising (Pastorello et al. 2010). Pastorello et al. (2010) noted the presence of a faint host galaxy in archive Sloan Digital Sky Survey (SDSS) images (SDSS J112546.72-084942.0) with magnitudes $g = 22.7$, $g-r = 0.3$ and confirmed the Quimby et al. (2010a) redshift estimate of $z = 0.23$. At this redshift, the g-band absolute magnitude of the host galaxy is about −18, similar to that of the LMC.

3. OBSERVATIONS

3.1. Photometry

We carried out an extensive *ugriz* photometric follow-up campaign of SN 2010gx using the telescopes listed in Table 1.

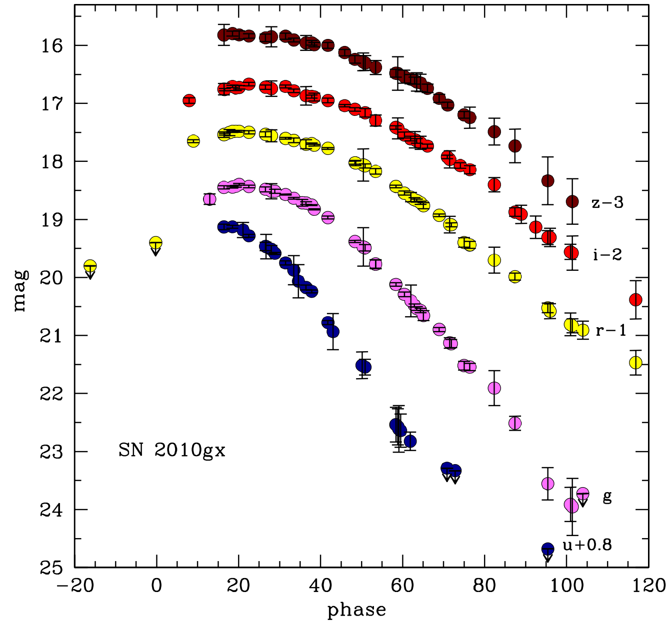

Figure 1. Observed *ugriz* light curves of SN 2010gx. The phase is from JD = 2,455,260, used as an indicative explosion epoch. Detection limits from Mahabal et al. (2010) and Quimby et al. (2010a) are included.

(A color version of this figure is available in the online journal.)

The observed light curves, calibrated using 10 SDSS stars in the field of the transient, are shown in Figure 1. The transient was discovered in the rising phase, and its light curves are asymmetric. The pre-discovery limit of March 4 (Quimby et al. 2010a) indicates that SN 2010gx experienced a fast rise to maximum, followed by a slower magnitude decline. A similar asymmetry was also observed in the light curve of SN 2005ap (Quimby et al. 2007). The photometric evolution of SN 2010gx is somewhat different from the bell-like shape observed in the slow-evolving light curve of SCP-06F6 (Barbary et al. 2009). Assuming negligible host galaxy reddening (Galactic reddening of $E(B-V) = 0.04$ mag; Schlegel et al. 1998) and accounting for redshift effects,[16] an absolute rest-frame peak magnitude of $M_B \approx -21.2$ (Vega system) is determined for SN 2010gx. In Figure 2, we compare the rest-frame, B-band absolute light curve of SN 2010gx with those of a few ultra-bright events and classical type Ib/c SNe, including broad-lined energetic SNe Ic. The epoch of the B-band maximum for SN 2010gx was computed with a low-order polynomial fit to the light curve and found to be at JD = 2455283 ± 2. The absolute peak magnitude of SN 2010gx is slightly fainter than that of SN 2005ap,[17] while no direct comparison is possible with the peculiar SN 2007bi (observed well past-maximum in the B band; Young et al. 2010) and SCP-06F6 (Barbary et al. 2009, for which a reliable rest-frame absolute light curve was computed only for the u band). However, SN 2010gx appears to be 2.5–5 mag brighter than SNe Ib/c reported in Figure 2, and its overall evolution is much slower than that of normal Ib/c events, although faster than that experienced by SN 2007bi.

A major difference between the light curves of SNe Ib/c and SN 2010gx is the apparent lack of a radioactive tail, in analogy to that observed in the case of other objects of the

[16] Time dilation and K-correction (computed using our SN 2010gx spectra), with the latter producing Johnson B band from observed SDSS r band.

[17] Note that only unfiltered photometry is available for SN 2005ap, calibrated using USNO-B1.0 $R2$ magnitudes (Quimby et al. 2007).

Table 1
Observed (Non-*K*-corrected) Photometry of SN 2010gx (AB mag) Plus Associated Errors

Date	JD	Phase[a]	*u*	*g*	*r*	*i*	*z*	Telescope
2010 Mar 12	2455267.95	−12.2				18.95 (0.05)		PS1
2010 Mar 13	2455268.99	−11.4			18.65 (0.03)			PS1
2010 Mar 17	2455272.96	−8.2		18.65 (0.09)				PS1
2010 Mar 20	2455276.42	−5.3	18.33 (0.05)	18.45 (0.03)	18.54 (0.05)	18.76 (0.10)	18.82 (0.18)	LT
2010 Mar 21	2455276.61	−5.2			18.53 (0.02)	18.76 (0.02)		NOT
2010 Mar 22	2455277.77	−4.3			18.50 (0.05)			GS
2010 Mar 22–23	2455278.50	−3.7	18.33 (0.02)	18.44 (0.02)	18.48 (0.02)	18.71 (0.02)	18.80 (0.04)	LT
2010 Mar 23	2455279.31	−3.0		18.43 (0.02)	18.48 (0.02)	18.73 (0.05)		LOT
2010 Mar 24	2455280.14	−2.3		18.40 (0.02)	18.48 (0.02)	18.72 (0.03)	18.82 (0.07)	LOT
2010 Mar 25	2455281.07	−1.6	18.38 (0.13)					UVOT
2010 Mar 27	2455282.52	−0.4	18.48 (0.03)	18.43 (0.02)	18.50 (0.03)	18.67 (0.03)	18.84 (0.04)	LT
2010 Mar 31	2455286.58	2.9	18.66 (0.07)	18.48 (0.04)	18.53 (0.05)	18.72 (0.04)	18.87 (0.07)	LT
2010 Mar 31	2455286.70	3.0	18.67 (0.21)					UVOT
2010 Apr 1	2455287.99	4.1	18.72 (0.07)	18.51 (0.13)	18.56 (0.10)	18.75 (0.13)	18.85 (0.17)	FTN
2010 Apr 2	2455288.85	4.8	18.78 (0.02)	18.52 (0.04)				FTN
2010 Apr 4	2455291.45	6.9	18.95 (0.04)	18.57 (0.01)	18.60 (0.02)	18.71 (0.02)	18.84 (0.05)	LT
2010 Apr 6	2455293.48	8.5	19.08 (0.25)	18.64 (0.02)	18.64 (0.04)	18.78 (0.03)	18.91 (0.03)	LT
2010 Apr 8	2455294.59	9.4	19.26 (0.29)					UVOT
2010 Apr 9	2455295.53	10.2		18.71 (0.06)				GS
2010 Apr 9	2455296.46	10.9	19.37 (0.04)	18.72 (0.02)	18.70 (0.08)	18.87 (0.16)	18.96 (0.13)	LT
2010 Apr 11	2455297.84	12.1	19.44 (0.02)	18.75 (0.01)	18.69 (0.01)	18.88 (0.03)	18.96 (0.04)	FTN
2010 Apr 11	2455298.48	12.6		18.82 (0.01)	18.72 (0.01)	18.89 (0.07)	18.99 (0.04)	LT
2010 Apr 15	2455301.80	15.3	19.98 (0.04)	18.97 (0.03)	18.78 (0.02)	18.95 (0.04)	19.00 (0.05)	FTN
2010 Apr 16	2455303.04	16.3	20.13 (0.31)					UVOT
2010 Apr 19	2455305.88	18.6				19.04 (0.02)	19.12 (0.06)	FTN
2010 Apr 21	2455308.38	20.6		19.38 (0.02)	19.02 (0.03)	19.10 (0.03)	19.24 (0.07)	LT
2010 Apr 22	2455308.58	20.8			19.03 (0.05)			GS
2010 Apr 23	2455310.13	22.1	20.71 (0.23)					UVOT
2010 Apr 23	2455310.40	22.3		19.48 (0.33)	19.06 (0.28)		19.28 (0.15)	LT
2010 Apr 24	2455310.84	22.6	20.75 (0.14)	19.49 (0.05)	19.08 (0.04)			FTN
2010 Apr 24	2455310.88	22.7				19.16 (0.08)	19.30 (0.13)	FTN
2010 Apr 26	2455313.42	24.7		19.77 (0.07)				LT
2010 Apr 26	2455313.44	24.7		19.77 (0.08)	19.17 (0.05)	19.30 (0.10)	19.38 (0.12)	LT
2010 May 1	2455318.39	28.8	21.74 (0.30)	20.12 (0.03)	19.43 (0.02)	19.41 (0.03)	19.48 (0.07)	LT
2010 May 2	2455318.84	29.1	21.77 (0.31)			19.43 (0.18)	19.49 (0.29)	FTN
2010 May 2	2455319.09	29.3	21.81 (0.40)					UVOT
2010 May 3	2455319.54	29.7	21.84 (0.29)					LT
2010 May 3	2455320.43	30.4		20.29 (0.04)	19.55 (0.04)	19.54 (0.05)	19.54 (0.11)	LT
2010 May 5	2455321.88	31.6	22.02 (0.16)					FTN
2010 May 5	2455321.94	31.7				19.61 (0.04)	19.58 (0.08)	FTS
2010 May 5	2455322.03	31.7		20.40 (0.27)	19.62 (0.08)			FTS
2010 May 6	2455322.88	32.4		20.48 (0.03)	19.66 (0.04)			FTS
2010 May 6	2455322.94	32.5					19.61 (0.06)	FTS
2010 May 6	2455323.02	32.5				19.63 (0.14)		FTS
2010 May 6	2455323.48	32.9		20.54 (0.03)	19.68 (0.03)	19.65 (0.04)	19.63 (0.16)	LT
2010 May 7	2455324.38	33.6		20.57 (0.04)	19.71 (0.03)	19.68 (0.11)	19.65 (0.15)	LT
2010 May 8	2455325.11	34.2		20.66 (0.08)	19.76 (0.05)			FTS
2010 May 9	2455326.09	35.0				19.74 (0.03)	19.74 (0.07)	FTS
2010 May 12	2455328.95	37.4		20.90 (0.04)	19.93 (0.02)		19.91 (0.07)	FTS
2010 May 14	2455330.84	38.9	>22.49					FTN
2010 May 14	2455330.90	38.9				19.92 (0.03)		FTS
2010 May 14	2455331.01	39.0					20.03 (0.05)	FTS
2010 May 14–15	2455331.50	39.4		21.13 (0.09)	20.09 (0.14)	19.97 (0.15)		LT
2010 May 15	2455331.88	39.7		21.14 (0.07)	20.09 (0.03)			FTS
2010 May 16	2455332.82	40.5	>22.53					FTN
2010 May 17	2455334.09	41.5				20.07 (0.05)		FTS
2010 May 18	2455335.02	42.3		21.52 (0.08)	20.40 (0.08)		20.20 (0.06)	FTS
2010 May 19	2455336.40	43.4		21.54 (0.06)	20.44 (0.06)	20.14 (0.07)	20.25 (0.18)	LT
2010 May 25	2455342.39	48.3		21.91 (0.30)	20.70 (0.22)	20.40 (0.12)	20.49 (0.23)	LT
2010 May 30	2455347.42	52.4		22.51 (0.12)	20.99 (0.06)	20.87 (0.07)	20.73 (0.29)	LT
2010 Jun 1	2455348.95	53.6				20.91 (0.16)		FTS
2010 Jun 4	2455352.47	56.5				21.13 (0.19)		GS
2010 Jun 8	2455355.43	58.9	>23.88	23.55 (0.28)	21.52 (0.09)	21.31 (0.12)	21.33 (0.41)	WHT
2010 Jun 8	2455355.98	59.3			21.58 (0.13)	21.31 (0.16)		FTS
2010 Jun 13	2455360.97	63.4		23.91 (0.30)	21.81 (0.20)	21.56 (0.13)		FTS

Table 1
(Continued)

Date	JD	Phase[a]	u	g	r	i	z	Telescope
2010 Jun 13	2455361.42	63.8		23.95 (0.49)	21.83 (0.12)	21.58 (0.29)	21.69 (0.39)	LT
2010 Jun 16	2455363.98	65.8		>23.73	21.91 (0.16)			FTS
2010 Jun 29	2455376.88	76.3			22.47 (0.21)	22.38 (0.33)		FTS

Notes. UVOT-*u Swift*, and R and I NOT data have been converted to SDSS magnitudes. Column 2 reports the phases with respect to the *B*-band maximum. PS1 = 1.8 m Pan-STARRS1; GS = 8.1 m Gemini South +GMOS; LT = 2.0 m Liverpool Telescope +RatCam; NOT = 2.56 m Nordic Optical Telescope +ALFOSC; LOT = 1.0 m Lulin Telescope; UVOT = *Swift* +UVOT; FTN = 2.0 m Faulkes Telescope North +MEROPE; FTS = 2.0 m Faulkes Telescope South +MEROPE; WHT = 4.2 m William Herschel Telescope +ACAM.
[a] Corrected for time dilation.

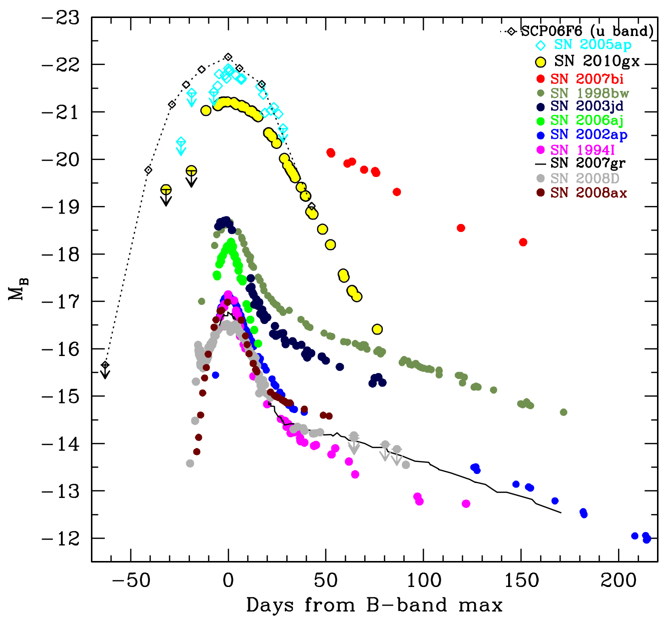

Figure 2. *B*-band absolute light curves of SN 2010gx (Vega system) and a number of ultra-bright events and canonical stripped-envelope SNe, including the type Ic SNe 1994I (Richmond et al. 1996, and references therein), 2002ap (Pandey et al. 2002; Foley et al. 2003; Yoshii et al. 2003; Tomita et al. 2006), 2006aj (Campana et al. 2006; Cobb et al. 2006; Mirabal et al. 2006; Pian et al. 2006; Sollerman et al. 2006), 2003jd (Valenti et al. 2008a), and 1998bw (Galama et al. 1998; McKenzie & Schaefer 1999; Sollerman et al. 2000; Patat et al. 2001); the type Ib SNe 2007gr (Valenti et al. 2008b; Hunter et al. 2009) and 2008D (Mazzali et al. 2008; Soderberg et al. 2008; Modjaz et al. 2009); the type IIb SN 2008ax (Pastorello et al. 2008). *B*-band light curves for the luminous SNe 2005ap, 2010gx, and 2007bi are obtained correcting the observed broadband photometry for time dilation and differences in effective rest-frame band (*K*-correction). The high redshift of SCP-06F6 ($z = 1.189$) did not allow us to compute a realistic *B*-band absolute light curve, so we estimated the *u*-band light curve (Vega system) from the i_{775}-band photometry of Barbary et al. (2009). *K*-corrections for the luminous objects were computed using the spectra published by Barbary et al. (2009), Quimby et al. (2007), Young et al. (2010), and this Letter.

(A color version of this figure is available in the online journal.)

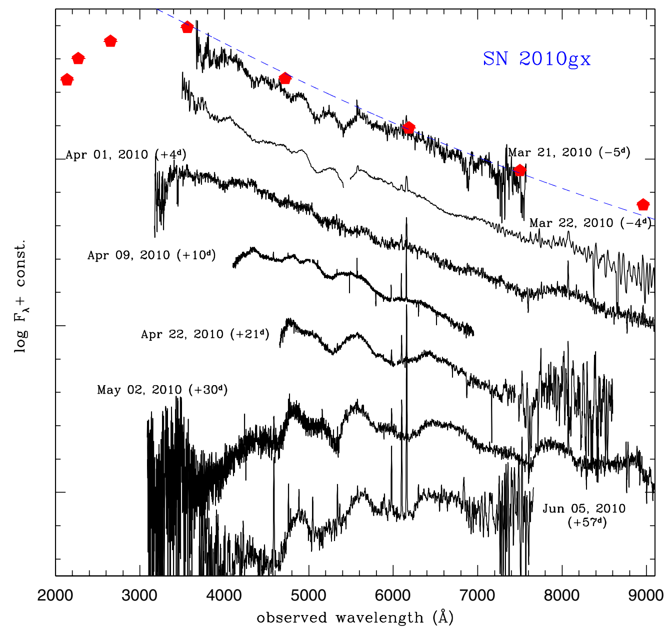

Figure 3. Spectral evolution of SN 2010gx. All spectra are in the observed frame. The phases in parentheses are relative to the *B*-band maximum. The red pentagons represent the observed spectral energy distribution calculated using *Swift*-UVOT (PI: Quimby) and Liverpool Telescope photometry obtained between March 19 and March 20. Early UVOT magnitudes (Vega system) are: $uw2 = 18.69 \pm 0.07$ (JD = 2,455,276.18), $um2 = 18.21 \pm 0.08$ (JD = 2,455,274.64), and $uw1 = 17.71 \pm 0.06$ (JD = 2,455,274.65). The deviation of the ultra-violet contribution from a hot blackbody continuum ($T_{bb} = 15{,}000$ K, dotted blue line) is probably due to line blanketing in that region.

(A color version of this figure is available in the online journal.)

Quimby et al. sample. However, with the data collected so far, we cannot exclude the possibility that the light curve flattens onto a radioactive tail at later epochs. In that case, the expected amount of ^{56}Ni ejected by SN 2010gx would be comparable (or only marginally higher, e.g., $\lesssim 1\ M_\odot$) to that of type Ib/c SNe.

3.2. Spectroscopy

A sequence of spectra of SN 2010gx was obtained with the 2.56 m Nordic Optical Telescope and the 4.2 m William Herschel Telescope (La Palma, Canary Islands), and the 8.1 m Gemini South Telescope (Cerro Pachón, Chile). Pre-maximum spectra obtained on March 21 and 22 show a very blue continuum (with a blackbody temperature $T_{bb} = 15{,}000 \pm 1700$ K) with broad absorption features below ∼5700 Å (Figure 3). Weak, narrow emission lines (Hα, Hβ, and the [O III] doublet at 4959,5007 Å) of the host galaxy are also visible, confirming the identification of the broad features as O II, also identified by Quimby et al. (2010b) in the spectra of SN 2005ap (Figure 4, top).

A spectrum obtained on April 1 (+4 days) is still blue ($T_{bb} \simeq 13{,}000 \pm 1200$ K) but is almost featureless. A significant evolution of the spectra of SN 2010gx then occurred at 10–20 days after peak. At these epochs the spectra show very broad P-Cygni absorptions of Ca II, Fe II, and Si II, very similar to those observed in spectra of young SNe Ic (Filippenko 1997). The subsequent spectrum, obtained on May 2 (+30 days), is markedly more similar to those of SNe Ic soon after maximum light. Finally, a further spectrum was obtained on June 5 (+57 days) and showed only a mild evolution in the spectral features.

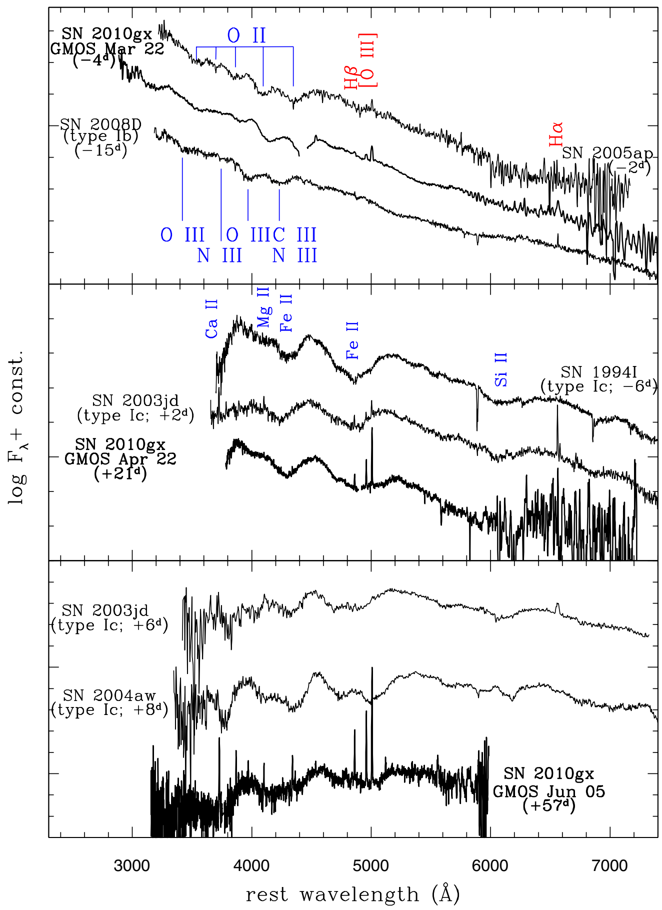

Figure 4. Top: comparison of early-time spectra of SNe 2010gx and 2005ap (Quimby et al. 2007) with one of the type Ib SN 2008D associated with the X-ray transient (XRT) 080109 (obtained +1.84 days from XRT 080109; Modjaz et al. 2009). All spectra show similar absorption bumps between 3500 Å and 4500 Å, although slightly shifted in the three spectra. These have been tentatively identified as O II features (Quimby et al. 2010b) and blends of O III/N III/C III (Modjaz et al. 2009). Middle: comparison of the April 22 spectrum of SN 2010gx with spectra of the Ic SN 1994I (Baron et al. 1996) and the moderately broad-lined SN 2003jd (Valenti et al. 2008a) around maximum. Now the spectrum of SN 2010gx is dominated by broad absorptions at about 3700 Å (Ca II H and K), 4300 Å (Mg II, blended with Fe II), 4900 Å (Fe II, plus possibly Mg I), and 6100 Å (Si II). Bottom: comparison of the June 5 spectrum of SN 2010gx with later spectra of the type Ic SNe 2003jd (Valenti et al. 2008a) and 2004aw (Taubenberger et al. 2006). The phases labeled in figure are from the *B*-band maximum.

(A color version of this figure is available in the online journal.)

The spectral evolution of SN 2010gx from an SCP-06F6-like event to a type Ic SN provides an unexpected clue for understanding the evolutionary path of this class of transients. In order to produce O II features (together with the Si III, C II, and Mg II lines observed in spectra of other objects of this family, see Quimby et al. 2010a, and Figure 4, top), high photospheric temperatures are necessary. Interestingly, Modjaz et al. (2009) noted a short-life "W" feature in a very early spectrum of the type Ib SN 2008D. That feature, visible in a spectrum taken 1.84 days after the X-ray flash 080109 associated with the SN, disappeared 1 day later. Modjaz et al. (2009) noted striking similarity with the early-time spectrum of SN 2005ap and (following Quimby et al. 2007) tentatively identified such short-life features as a combination of O III, N III, and C III lines. However, the "W" feature in SN 2008D is slightly blueshifted compared to the analogous feature visible in the early spectra of SNe 2005ap and 2010gx. Therefore, fleeting lines due to ionized intermediate-mass elements could be common in very early spectra of some type Ib/c SNe. However, these lines are visible for several weeks after the explosion in SCP-06F6-like objects, which is likely due to higher densities and temperatures of the ejecta which persist for longer than in canonical SNe Ib/c.

As the SN expands, the ejecta become cooler and other broad lines appear (Ca II, Mg II, Fe II, and Si II). These features are commonly visible in Ib/c spectra around maximum (Filippenko 1997). In Figure 4 (middle), a later spectrum of SN 2010gx (+21 days) is compared with a pre-maximum spectrum of the normal type Ic SN 1994I (Baron et al. 1996) and a slightly post-maximum spectrum of the broad-line Ic SN 2003jd (Valenti et al. 2008a). The striking similarity among these three spectra is a confirmation that SN 2010gx (and possibly all SCP-06F6-like objects) should be considered spectroscopically as SNe Ic, although with rather extreme photometric properties (Section 3.1). The similarity with normal stripped-envelope SNe is even more evident in the comparison of the last spectrum of SN 2010gx (June 5) with spectra of the type Ic SNe 2003jd (Valenti et al. 2008a) and 2004aw (Taubenberger et al. 2006) obtained about 1 week after their *B*-band peaks.

4. THE NATURE OF ULTRA-BRIGHT EVENTS

SN 2010gx provides important clues to understand the nature of ultra-bright events. Its spectro-photometric similarities with this family is well established: high luminosity, slow-evolving light curves, similar spectral properties, and faint host galaxies. The spectral evolution of SN 2010gx now links this family of transients to the more common type Ib/c SNe, and by implication the progenitor stars. The overall spectral evolution is indeed similar to that of SNe Ib/c, although SN 2010gx spectroscopically evolved on a much longer timescale. The observed parameters of SN 2010gx present several problems in interpreting the explosion. Its impressive luminosity at maximum and slower evolution could simply be interpreted as implying large photospheric radii ($L \sim R^2 T^4$) and large ejecta masses ($\tau \sim (\kappa M/v)^{1/2}$; for radiative diffusion from a sphere). The energy source for SNe Ib/c is the decay of radioactive isotopes, but the 80 day long post-peak decline of SN 2010gx (Figure 2) is too steep to be due to ^{56}Co decay. It is plausible that a radioactive tail could be detected at later phases, if the light curve flattens to the luminosity of the type Ic SN 1998bw. But this would imply $\lesssim 1\ M_\odot$ of ^{56}Co decaying into ^{56}Fe to power the tail luminosity, and such a moderate mass of ^{56}Ni cannot account for the high bolometric luminosity at peak, which is $\sim$(3–4)$\times 10^{44}$ erg s^{-1}. Assuming that the bolometric luminosity from the earliest PTF detection to our earliest multi-band observation was constant, the energy radiated by SN 2010gx during the first 100 days is $\sim 6 \times 10^{51}$ erg.

The peak luminosity of SN 2010gx is quite similar to that of SN 2007bi, but the light curve and spectral evolution are completely different (Gal-Yam et al. 2009; Young et al. 2010). The slow decay time and appearance of strong [Fe II] lines in SN 2007bi suggested a kinetic energy of few $\times 10^{53}$ erg, very massive ejecta, and 3–6 $M_\odot$ of ^{56}Ni synthesized. Gal-Yam et al. (2009) postulated that this was the explosion of a 100 $M_\odot$ core in a pair-instability SN. While this possibility was also noted by Young et al. (2010), the gravitational collapse of the C+O core of a massive star ($M_{\rm ZAMS}$ = 50–100 $M_\odot$) is a viable mechanism (as recently calculated by Moriya et al. 2010). Whatever the explosion scenario, a large amount of ^{56}Ni is necessary. However, SN 2010gx is markedly different in its properties, particularly the more rapid decay in its light curve indicates that the pair-instability scenario and a large ^{56}Ni production are unlikely to be the explanation.

The apparent lack of any evidence of light curve flattening to a radioactive tail led Quimby et al. (2010b) to favor the pulsational pair-instability eruption scenario over a genuine SN explosion for SN 2005ap, SCP-06F6, and other PTF SNe. In the pulsational pair-instability model, the luminosity is generated by the collision of shells of material ejected at different times by the pulsations. Little or no ^{56}Ni powers the light curve for long periods. The outbursts are expected to be energetic, reaching very high peak luminosities and creating hot ($T_{\rm eff} \approx 25{,}000$ K), optically thick photospheres (Woosley et al. 2007). All of this is consistent with the parameters observed in ultra-bright SNe, and our well sampled light curve of SN 2010gx is not too different from those calculated by Woosley et al. (2007). However, these models are for supergiant progenitors with large, extended H-rich envelopes. The energy released in the pulsations is predicted to be $(0.005–2)\times10^{51}$ erg, in most cases below 10^{51} erg. This is enough to eject the loosely bound envelope of an extended supergiant, but weather or not this mechanism could eject a substantial part of a more compact WR star (Dessart et al. 2010) remains to be calculated in detail. Additionally, we do not see any sign of interaction between dense gas shells in the form of narrow circumstellar lines. While the pulsational pair-instability model is appealing as it can produce the high luminosity, it needs further consideration to determine if it is physically viable for H-free progenitor stars.

Another possibility, also discussed in Quimby et al. (2010b), is that ultra-bright SNe are powered by the spin down of newly born magnetars (Kasen & Bildsten 2010; Woosley 2010). A magnetar with a moderate magnetic field ($B \approx 10^{14}$ G) and spinning periods of 2–20 ms can produce peak luminosities similar to that observed in SN 2010gx ($\sim$(3–4)$\times10^{44}$ erg s^{-1}). In addition, magnetar-powered SN models do not need large ^{56}Ni and total ejected masses (Kasen & Bildsten 2010; Woosley 2010) and can show Ic SN features (Woosley 2010). However our extensive light curve coverage of SN 2010gx shows a faster decline than the model light curves, and our estimated photospheric temperatures are a factor 2–4 higher than model predictions.

The observational evidence presented in this Letter links SN 2010gx (and probably the entire family of transients described by Quimby et al. 2010b) with SNe Ic. The very luminous and broad light curve implies much larger ejecta masses than inferred even for the broad-lined SNe Ic ($\sim$8–15 $M_\odot$; Valenti et al. 2008a). The close similarity in the spectra implies that the progenitor was a massive WR star, but the energy source powering the remarkable luminosity is uncertain. In fact, we have an SN-like transient which does not comfortably match any of the known SN scenarios, i.e., core-collapse and ^{56}Ni-powered explosion, pair-instability, pulsational pair-instability nor magnetar-powered event.

The key diagnostics in the future will be late-time photometric monitoring after solar conjunction and very early detection of new events. The presence of a late-time light curve tail with a slope roughly consistent with the ^{56}Co decay could support a real SN explosion, and the early rise time can help to determine the progenitor radius and possibly signs of interaction between colliding shells. The recent suggestion that the most massive stars in the LMC may be up to 320 $M_\odot$ (Crowther et al. 2010) could lead to more diverse SN progenitor populations than is currently appreciated (Smartt 2009).

The PS1 Surveys have been made possible through contributions of the Institute for Astronomy at the University of Hawaii in Manoa, the Pan-STARRS Project Office, the Max-Planck Society and its participating institutes, the Max Planck Institute for Astronomy, Heidelberg and the Max Planck Institute for Extraterrestrial Physics, Garching, The Johns Hopkins University, the University of Durham, the University of Edinburgh, the Queens University Belfast, the Harvard- Smithsonian Center for Astrophysics, and the Los Cumbres Observatory Global Telescope Network, Incorporated. This work was conducted as part of a EURYI scheme award.

REFERENCES

Barbary, K., et al. 2009, ApJ, 690, 1358
Baron, E., Hauschildt, P. H., Branch, D., Kirshner, R. P., & Filippenko, A. V. 1996, MNRAS, 279, 799
Campana, S., et al. 2006, Nature, 442, 1008
Cobb, B. E., Bailyn, C. D., van Dokkum, P. G., & Natarajan, P. 2006, ApJ, 645, L113
Crowther, P. A., Schnurr, O., Hirschi, R., Yusof, N., Parker, R. J., Goodwin, S. P., & Abu Kassim, H. 2010, MNRAS, 408, 731
Dessart, L., Livne, E., & Waldman, R. 2010, MNRAS, 405, 2113
Drake, A. J., et al. 2009, ApJ, 696, 870
Filippenko, A. V. 1997, ARA&A, 35, 309
Foley, R., et al. 2003, PASP, 115, 1220
Galama, T. J., et al. 1998, Nature, 395, 670
Gal-Yam, A., et al. 2009, Nature, 462, 624
Gänsicke, B. T., Levan, A. J., Marsh, T. R., & Wheatley, P. J. 2009, ApJ, 697, L129
Gezari, S., et al. 2009, ApJ, 690, 1313
Hunter, D. J., et al. 2009, A&A, 508, 371
Kasen, D., & Bildsten, L. 2010, ApJ, 717, 245
Law, N. M., et al. 2009, PASP, 121, 1395
Mahabal, A. A., & Drake, A. J. 2010, ATel, 2508, 1
Mahabal, A. A., et al. 2010, ATel, 2490, 1
Mazzali, P. A., et al. 2008, Science, 321, 1185
McKenzie, E. H., & Schaefer, B. E. 1999, PASP, 111, 964
Miller, A. A., et al. 2009, ApJ, 690, 1303
Mirabal, N., Halpern, J. P., An, D., Thorstensen, J. R., & Terndrup, D. M. 2006, ApJ, 643, L99
Modjaz, M., et al. 2009, ApJ, 702, 226
Moriya, T., Tominaga, N., Tanaka, M., Maeda, K., & Nomoto, K. 2010, ApJ, 717, L83
Pandey, S. B., Anupama, G. C., Sagar, R., Bhattacharya, D., Sahu, D. K., & Pandey, J. C. 2002, MNRAS, 340, 375
Pastorello, A., et al. 2008, MNRAS, 389, 955
Pastorello, A., et al. 2010, ATel, 2504, 1
Patat, F., et al. 2001, ApJ, 555, 900
Pian, E., et al. 2006, Nature, 442, 1011
Quimby, R. M., Aldering, G., Wheeler, J. C., Höflich, P., Akerlof, C. W., & Rykoff, E. S. 2007, ApJ, 668, L99
Quimby, R. M., Kulkarni, S. R., Ofek, E., Kasliwal, M. M., Levitan, D., Gal-Yam, A., & Cenko, S. B. 2010a, ATel, 2492, 1
Quimby, R. M., et al. 2010b, Nature, submitted (arXiv:0910.0059)
Rau, A., et al. 2009, PASP, 121, 1334
Richmond, M. W., et al. 1996, AJ, 111, 327
Rosswog, S., Ramirez-Ruiz, E., & Hix, W. R. 2009, ApJ, 695, 404
Schlegel, D. J., Finkbeiner, D. P., & Davis, M. 1998, ApJ, 500, 525
Smartt, S. J. 2009, ARA&A, 47, 63
Soderberg, A. M., et al. 2008, Nature, 453, 469
Soker, N., Frankowski, A., & Kashi, A. 2009, New Astron., 15, 189
Sollerman, J., Kozma, C., Fransson, C., Leibundgut, B., Lundqvist, P., Ryde, F., & Woudt, P. 2000, ApJ, 537, L127
Sollerman, J., et al. 2006, A&A, 454, 503
Taubenberger, S., et al. 2006, MNRAS, 371, 1459
Tomita, H., et al. 2006, ApJ, 644, 400
Valenti, S., et al. 2008a, MNRAS, 383, 1485
Valenti, S., et al. 2008b, ApJ, 673, L155
Woosley, S. E. 2010, ApJ, 719, L204
Woosley, S. E., Blinnikov, S., & Heger, A. 2007, Nature, 450, 390
Yoshii, Y., et al. 2003, ApJ, 592, 467
Young, D. R., et al. 2010, A&A, 512, 70

LETTERS

A change in the optical polarization associated with a γ-ray flare in the blazar 3C 279

The Fermi-LAT Collaboration and members of the 3C 279 multi-band campaign*

It is widely accepted that strong and variable radiation detected over all accessible energy bands in a number of active galaxies arises from a relativistic, Doppler-boosted jet pointing close to our line of sight[1]. The size of the emitting zone and the location of this region relative to the central supermassive black hole are, however, poorly known, with estimates ranging from light-hours to a light-year or more. Here we report the coincidence of a gamma (γ)-ray flare with a dramatic change of optical polarization angle. This provides evidence for co-spatiality of optical and γ-ray emission regions and indicates a highly ordered jet magnetic field. The results also require a non-axisymmetric structure of the emission zone, implying a curved trajectory for the emitting material within the jet, with the dissipation region located at a considerable distance from the black hole, at about 10^5 gravitational radii.

The flat spectrum radio quasar 3C 279 was the first bright γ-ray blazar reported by the EGRET instrument aboard the Compton Gamma-Ray Observatory to show strong and rapidly variable γ-ray emission[2–4]; recently, it has also been detected at photon energies above 100 GeV by the MAGIC ground-based Cherenkov telescope[5]. This blazar, at redshift $z = 0.536$, harbours a black hole with mass[6,7] $M \approx (3\text{–}8) \times 10^8 M_\odot$ (where $M_\odot$ is the mass of the Sun); for specificity, we adopt $6 \times 10^8 M_\odot$. It shows superluminal expansion best described as the jet material propagating with the bulk Lorentz factor $\Gamma_{jet} = 16 \pm 3$ at a small angle ($\theta \approx 2^\circ$) to our line of sight[8]. The high degree of the optical polarization provides evidence for the presence of a well ordered magnetic field in the emission zone[9]. This may either reflect the global topology of the large-scale magnetic field, or may result from the compression of chaotic magnetic fields in shocks and shear regions along the outflow[10].

The best coverage of the broad-band flux variability of 3C 279 was obtained after the start of routine scientific operation of the Large Area Telescope (LAT)[11] onboard the recently launched Fermi Gamma-ray Space Telescope (4 August 2008 = 54682 Modified Julian Day, or MJD). In Fig. 1 we plot the flux history in the γ-ray band above 200 MeV, as well as in the X-ray, optical, infrared and radio bands, together with polarization information in the optical band. Of all the observed bands, the γ-ray band shows the most violent variations, with a change by an order of magnitude in flux during the observation. It also dominates the electromagnetic output of 3C 279, with an apparent γ-ray luminosity of as much as $\sim 10^{48}$ erg s^{-1} (see Fig. 2 and refs 3 and 4). After being quiescent for the first 100 days or so, the γ-ray flux starts to increase at about 54780 MJD, but without any significant spectral changes: the γ-ray photon index is relatively constant during the entire observed period. The high γ-flux state persists for about 120 days and is associated with erratic flaring, accompanied by bright and variable optical emission.

Towards the end of the high-flux state there is a sharp γ-ray flare at 54880 MJD with a doubling timescale as short as one day. This sharp γ-ray flare coincides with a significant drop in the degree of optical polarization, from $\sim$30% down to a few per cent, lasting for $\Delta t \approx 20$ days. Subsequently, both γ-ray and optical fluxes gradually decrease together and reach the quiescent level, followed by a temporary recovery of the high degree of polarization. This event is associated with a dramatic change of the electric vector position angle (EVPA) of the polarization, in contrast to being relatively constant before the event at $\sim 50^\circ$ (parallel to the jet direction observed by Very Long Baseline Interferometry observations in radio bands; see ref. 8 for example). Because the EVPA has $\pm 180^\circ \times n$ (where $n = 1, 2\ldots$) ambiguity, we selected values on the assumption that the EVPA would change smoothly, such that it would follow the overall trend. The polarization angle increases slightly at 54880 MJD—coincident with the γ-ray flare—then decreases by 208° at a rate of $\sim 12^\circ$ per day, and returns to a level nearly exactly 180° from the original level, closely resembling the behaviour of optical polarization measured in BL Lacertae[12], but at a rate four times slower. This clearly indicates that the sharp γ-ray flare is unambiguously correlated with the dramatic change of optical polarization due to a single, coherent event, rather than a superposition of multiple but causally unrelated, shorter duration events.

Concurrent X-ray observations indicate a relatively steady X-ray flux during the high γ-ray flux state (although with modest amplitude variations roughly mirroring the γ-ray time series; A. Marscher, personal communication), but reveal a significant, symmetrical flare about 60 days after the second γ-ray peak—at 54950 MJD—with a duration of $\sim$20 days, similar to the duration of the γ-ray flare. It suggests that the X-ray photons are produced at a distance from the black hole comparable to the distance of the optical/γ-ray photons. Importantly, this X-ray flare is accompanied only by a modest increase of optical activity and not by a prominent optical or γ-ray flare. The X-ray spectrum during the isolated flare remains much harder than the optical spectrum (see Fig. 2), and therefore cannot be attributed to a temporary extension of the high-energy tail of the synchrotron emission, but instead, may be generated by inverse-Compton scattering of low-energy electrons. However, the similarity of the profiles of the γ-ray and X-ray flares argues against the latter being just a version of the former that is delayed owing to particle cooling, for example. Therefore, the X-ray flare must be produced independently by another mechanism involving primarily lower-energy electrons.

During the entire multiwavelength campaign reported here, the radio and millimetre fluxes are less variable than fluxes in other bands. In particular, they stay nearly constant in the periods of the two prominent γ-ray flares and the isolated X-ray flare, and no associated or delayed radio flare was observed. This suggests that the blazar activity in 3C 279 takes place where the synchrotron radiation at these wavelengths is not yet fully optically thin, constraining the transverse size R_{blazar} of the blazar emission zone[13]:

$$R_{blazar} < 5 \times 10^{16} \left(\nu F_\nu / 2 \times 10^{-11} \text{erg cm}^{-2}\,\text{s}^{-1}\right)^{1/2}$$
$$(B'/0.3\ \text{G})^{1/4} \left(\nu/10^{11.5}\text{Hz}\right)^{-7/4} \left(\Gamma_{jet}/15\right)^{-1/4} \text{cm}$$

*Lists of participants and their affiliations appear at the end of the paper.

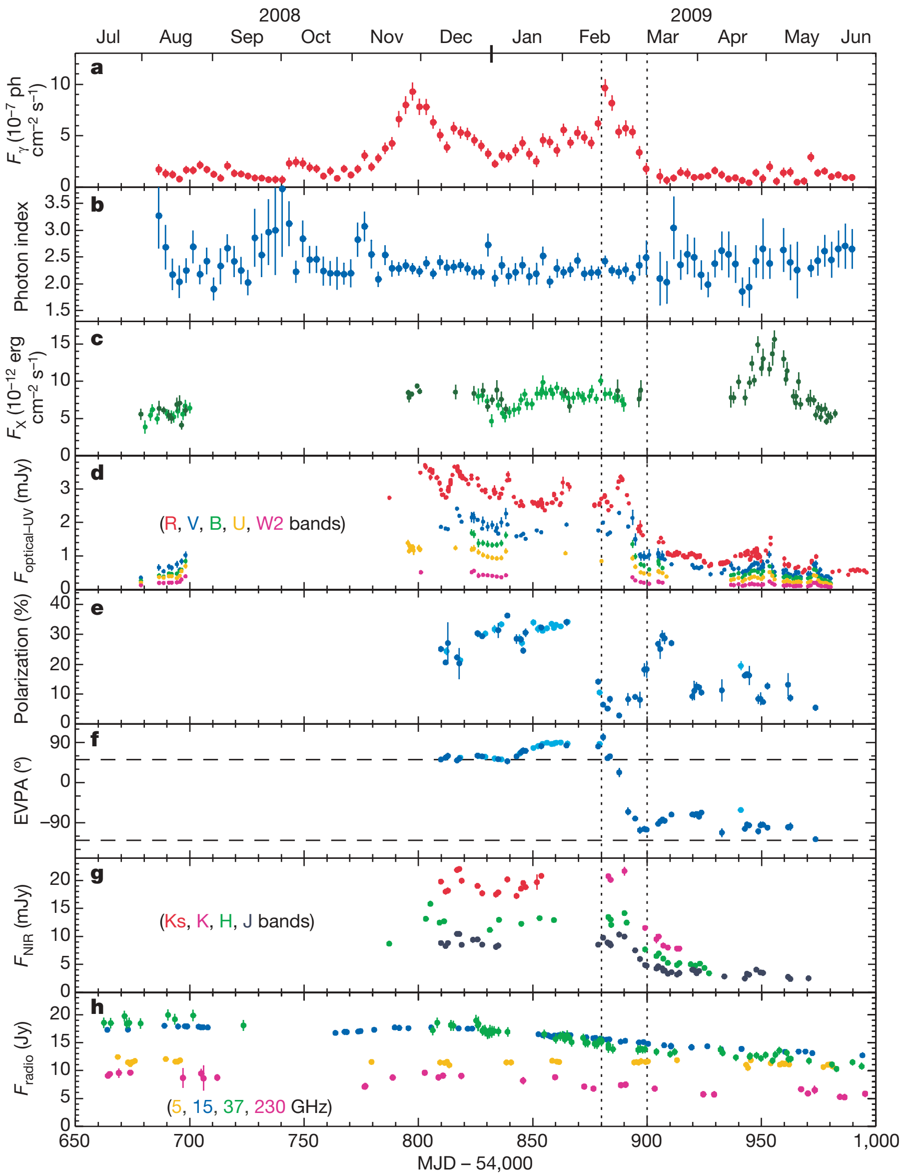

Figure 1 | History of flux in various bands, γ-ray photon index, and optical polarization of 3C 279. Light curves at the indicated wave bands covering a year since the Modified Julian Day (MJD) of 54650 (corresponding to 3 July 2008). The two dashed vertical lines indicate 54880 and 54900 MJD. Error bars at each point represent a ± 1 s.d. statistical uncertainty. **a, b,** Gamma-ray flux F_γ and photon index Γ above 200 MeV averaged over 3-day intervals as measured by Fermi-LAT from photons that passed the 'diffuse' event selection. The source fluxes are calculated using 'P6_V3_DIFFUSE' for the instrumental response function and a simple power-law spectral model: $dF/dE \propto E^{-\Gamma}$. The detailed data analysis procedures are analogous to those in ref. 22. **c,** X-ray integrated flux F_X between 2 and 10 keV, calculated by fitting the data with the simple power-law model taking into account a Galactic absorption. Light-green points are from the observations with the Proportional Counter Array (PCA) onboard the Rossi X-ray Timing Explorer (RXTE) and dark-green points are measurements by Swift-XRT. **d,** Optical and ultraviolet (UV) fluxes in several bands. *R*-band data were taken by ground-based telescopes from the GASP-WEBT collaboration[23]. *V*-band data were taken by a ground-based telescope (Kanata-TRISPEC[24]) and Swift-UVOT. Data in all other bands were acquired by Swift-UVOT. **e, f,** Polarization degree and electric vector position angle (EVPA) of the optical polarization measured by the Kanata-TRISPEC in the *V*-band (dark blue) and by the KVA telescope without any filters (light blue). Note that EVPA has $\pm 180^\circ \times n$ (where $n = 1, 2\ldots$) ambiguity. The horizontal dashed lines in **f** refer to EVPAs of 50° and –130°. **g, h,** Near-infrared flux F_{NIR} and radio fluxes measured by ground-based telescopes. Kanata-TRISPEC measured the *J* and K_s NIR bands, OVRO measured the 15 GHz radio band and GASP-WEBT measured the *J*, *H*, *K* and several millimetre and radio bands. All UV, optical and NIR data are corrected for the Galactic absorption.

(where νF_ν is the energy flux measured in the millimetre band [$\sim 10^{11.5}$ Hz]), which is consistent with the limit provided by the shortest doubling timescales of the γ-ray flux variations.

The gradual rotation of the polarization angle is unlikely to originate in a straight, uniform axially symmetric, matter-dominated jet because any compression of the jet plasma by, for example, a perpendicular shock moving along the jet and viewed at a small but constant angle to the jet axis would change the degree of polarization, but would not result in a gradual change of EVPA. Instead, it could reflect a non-axisymmetric magnetic field distribution (as in, for example, ref. 14), a swing of the jet across our line of sight (which in turn does not require any source/pattern propagation), or a curved trajectory of the dissipation/emission pattern. The last possibility may be due to propagation of an emission knot following a helical path in a magnetically dominated jet as was recently investigated in the context of the optical polarization event seen in BL Lacertae[12], or may involve the 'global' bending of a jet. The magnetic field in the emission region is anisotropic (presumably concentrated in the plane of a shock or disturbance propagating along the jet), so the degree and angle of observed polarization then depends on the instantaneous angle θ of the direction of motion of the radiating material to the line of sight. The maximum rotation rate of the polarization

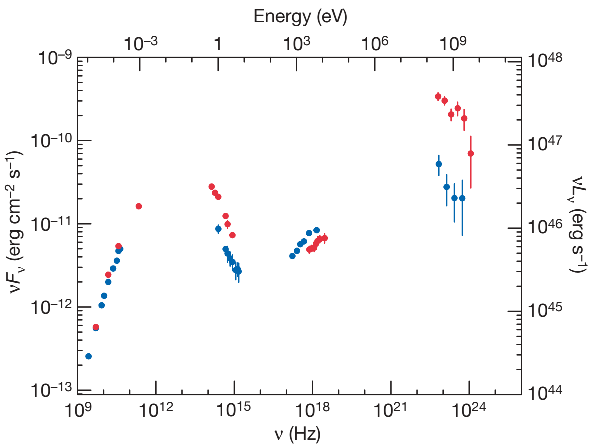

Figure 2 | Energy spectrum from radio to γ-ray band of 3C 279 at two different epochs. The red points were taken between 54880 and 54885 MJD, corresponding to the first five days of the sharp γ-ray flare accompanying the dramatic polarization change event (epoch 1). The blue points were taken between 54950 and 54960 MJD, around the peak of the isolated X-ray flare (epoch 2). The γ-ray spectra were measured by Fermi-LAT. In the X-ray band, the flux points are obtained by the RXTE-PCA in epoch 1 (red) and by Swift-XRT in epoch 2 (blue). The fluxes in the UV range were measured by Swift-UVOT. Observations in the optical-to-radio bands were performed by ground-based telescopes as given in Fig. 1 (with additional radio coverage provided by the Effelsberg radio telescope[25]). Each data point represents an average source flux and the error bar represents ±1 s.d. of the flux during each epoch. Each data point is already corrected for Galactic absorption. Note that the total energy associated with the X-ray flare is relatively modest, about 30 times less than the energy associated with the γ-ray flare accompanying the dramatic polarization change, and the γ-ray emission is still dominant, having five times the X-ray energy flux even during the X-ray flare event.

angle would correspond to $\theta = \theta_{\min}$ and the polarization degree would be highest for $\theta \approx 1/\Gamma_{\rm jet}$. The 'bent jet' scenario can explain the observed polarization event (the change of angle as well as the magnitude of polarization) provided the jet curvature is confined to the plane inclined to the line of sight at an angle $\theta_{\min} < 1/\Gamma_{\rm jet}$ and configured in such a way that the jet trajectory projected on the sky turns by almost 180°. Similar geometry—albeit on larger scales—has been observed in another blazar[15], PKS 1510-089. Nonetheless, in both scenarios, the coherent polarization event is produced by a density pattern co-moving along the jet, and so it is possible to estimate the distance travelled by the emitting material during the flare, $\Delta r_{\rm event}$; this in turn allows us to constrain the distance of the dissipation region (where flaring occurs) from the black hole, $r_{\rm event}$, because $r_{\rm event} \geq \Delta r_{\rm event}$. With this, $r_{\rm event} \geq \Delta r_{\rm event} \approx 10^{19}(\Delta t_{\rm event}/20\ {\rm days})(\Gamma_{\rm jet}/15)^2$ cm, which is about five orders of magnitude larger than the gravitational radius of the black hole in 3C 279.

The constraints on the distance of the dissipation region can be relaxed under 'flow-through' scenarios, in which the emission patterns may move much more slowly than the bulk speed of the jet or not propagate at all: one such example is the model involving swings ('wobbling') of the jet associated with jet instabilities such that its boundary moves relative to our line of sight. In this case, the timescale for the observed variation is the timescale for the jet motion. Consequently, the emission region can easily be much closer (by a factor $\Gamma_{\rm jet}^2$) to the black hole than in the 'helical' or 'bent jet' scenarios, because the natural radial scale for $\Delta t_{\rm event} \approx 20$ days is $r_{\rm event} \approx c\Delta t_{\rm event} \approx 500$–1,000 gravitational radii (see, for example, ref. 16). Under this scenario, the angle the jet makes with the line of sight must change by at least $\sim\Gamma_{\rm jet}^{-1}$ to explain the large swing of polarization. Here, the jet motion can be imposed at its base, be caused by deflection due to external medium, or be a consequence of dynamical instability.

This leaves us with three viable possibilities. Both the scenario involving a knot propagating along the helical magnetic field lines and the 'flow-through' scenario above imply that the rotation of the polarization angle should be preferentially following the same direction, because in those two models the twist presumably originates in the inner accretion disk. In our case, we observe the rotation of the polarization angle to be opposite in direction to that measured previously[9], leaving us with the 'bent jet' model combined with a small swing of the jet as the most compelling scenario.

The dominant source of 'seed' photons for inverse-Compton scattering depends on the distance of the dissipation event from the central black hole[17]. At the parsec distances predicted by the 'helical' or 'bent jet' scenarios that involve the radiating material co-moving with the jet, the seed radiation fields are dominated by infrared radiation emitted by a warm dust located in the circum-nuclear molecular torus and by synchrotron radiation produced within the jet. At the sub-parsec distances implied by the 'flow-through' scenarios, this photon field could be the broad emission line region[13] (clearly detected in this object[18], as expected in a quasar possessing a luminous accretion disk[19]), as well as the direct radiation of such a disk[20] or its corona[21]. In any case, the $\sim$20-GeV electrons and positrons producing the highest-energy γ rays and the polarized optical radiation lose their energy on timescales shorter than the light travel-time from the black hole, and so must be accelerated locally.

In summary, the close association of the energetically dominant γ-ray flare with the smooth, continuous change of the optical polarization angle suggests co-spatiality of the optical and γ-ray emission and provides evidence for the presence of highly ordered magnetic fields in the regions of γ-ray production. Provided the emission pattern is co-moving with the jet, we can measure the distance of the coherent event to be of the order of 10^5 gravitational radii away from the black hole. While the available data cannot exclude the theoretically less explored 'flow-through' scenarios—in which the dissipation events may take place at much smaller distances, down to $\sim10^3$ gravitational radii—that the observed direction of rotation of the optical polarization angle is opposite to the direction previously measured appears to support the jet bending at larger distances as the best explanation of the available data. Furthermore, the detection of the isolated X-ray flare challenges the simple, one-zone emission models, rendering them too simple. However, the Fermi satellite has been in operation for only just over a year, and the outlook for a more comprehensive picture of these enigmatic objects, primarily via multi-band campaigns including well-sampled optical polarimetry, is excellent.

Received 6 October 2009; accepted 14 January 2010.

1. Ulrich, M.-H., Maraschi, L. & Urry, C. M. Variability of active galactic nuclei. *Annu. Rev. Astron. Astrophys.* **35,** 445–502 (1997).
2. Hartman, R. C. *et al.* Detection of high-energy gamma radiation from quasar 3C 279 by the EGRET telescope on the Compton Gamma Ray Observatory. *Astrophys. J.* **385,** L1–L4 (1992).
3. Kniffen, D. A. *et al.* Time variability in the gamma-ray emission of 3C 279. *Astrophys. J.* **411,** 133–136 (1994).
4. Wehrle, A. E. *et al.* Multiwavelength observations of a dramatic high-energy flare in the blazar 3C 279. *Astrophys. J.* **497,** 178–187 (1998).
5. Albert, J. *et al.* Very-high-energy gamma-rays from a distant quasar: how transparent is the Universe? *Science* **320,** 1752–1754 (2008).
6. Nilsson, K. *et al.* The host galaxy of 3C 279. *Astron. Astrophys.* **505,** 601–604 (2009).
7. Woo, J.-H. & Urry, C. M. Active galactic nucleus black hole masses and bolometric luminosities. *Astrophys. J.* **579,** 530–544 (2002).
8. Jorstad, S. G. *et al.* Polarimetric observations of 15 active galactic nuclei at high frequencies: jet kinematics from bimonthly monitoring with the Very Long Baseline Array. *Astron. J.* **130,** 1418–1465 (2005).
9. Larionov, V. M. *et al.* Results of WEBT, VLBA and RXTE Monitoring of 3C 279 during 2006–2007. *Astron. Astrophys.* **492,** 389–400 (2008).
10. Laing, R. A. A model for the magnetic-field structure in extended radio sources. *Mon. Not. R. Astron. Soc.* **193,** 439–449 (1980).
11. Atwood, W. B. *et al.* The Large Area Telescope on the Fermi Gamma-Ray Space Telescope Mission. *Astrophys. J.* **697,** 1071–1102 (2009).
12. Marscher, A. P. *et al.* The inner jet of an active galactic nucleus as revealed by a radio-to-gamma-ray outburst. *Nature* **452,** 966–969 (2008).
13. Sikora, M., Begelman, M. C. & Rees, M. J. Comptonization of diffuse ambient radiation by a relativistic jet: the source of gamma-rays from blazars? *Astrophys. J.* **421,** 153–162 (1994).

14. Konigl, A. & Choudhuri, A. R. A model of the polarization position-angle swings in BL Lacertae objects. *Astrophys. J.* **289,** 188–192 (1985).
15. Homan, D. C. *et al.* PKS 1510–089: a head-on view of a relativistic jet. *Astrophys. J.* **580,** 742–748 (2002).
16. Lyutikov, M., Pariev, V. I. & Blandford, R. Polarization of prompt gamma-ray burst emission: evidence for electromagnetically dominated outflow. *Astrophys. J.* **597,** 998–1009 (2003).
17. Sikora, M., Stawarz, L., Moderski, R., Nalewajko, K. & Madejski, G. Constraining emission models of luminous blazar sources. *Astrophys. J.* **704,** 38–50 (2009).
18. Netzer, H. *et al.* The optical-ultraviolet-gamma-ray spectrum of 3C279. *Astrophys. J.* **430,** 191–195 (1994).
19. Pian, E. *et al.* Ultraviolet and multiwavelength variability of the blazar 3C 279: evidence for thermal emission. *Astrophys. J.* **521,** 112–120 (1999).
20. Dermer, C., Schlickheiser, R. & Mastichiadis, A. Gamma-rays from extragalactic radio sources. *Astron. Astrophys.* **256,** L27–L30 (1992).
21. Blandford, R. D. & Levinson, A. Pair cascades in extragalactic jets: 1: Gamma-rays. *Astrophys. J.* **441,** 79–95 (1995).
22. Abdo, A. A. *et al.* Early Fermi Gamma-ray Space Telescope observations of the quasar 3C 454.3. *Astrophys. J.* **699,** 817–823 (2009).
23. Villata, M. *et al.* The correlated optical and radio variability of BL Lacertae. WEBT data analysis 1994–2005. *Astron. Astrophys.* **501,** 455–460 (2009).
24. Watanabe, M. *et al.* TRISPEC: a simultaneous optical and near-infrared imager, spectrograph, and polarimeter. *Publ. Astron. Soc. Pacif.* **117,** 870–884 (2005).
25. Fuhrmann, L., Zensus, J. A., Krichbaum, T. P., Angelakis, E. & Readhead, A. C. S. Simultaneous radio to (sub-) mm-monitoring of variability and spectral shape evolution of potential GLAST blazars. *AIP Conf. Proc. (1st GLAST Symp.)* 921 249–251 (2007).

Acknowledgements The Fermi-LAT Collaboration acknowledges support from a number of agencies and institutes for both development and the operation of the LAT as well as scientific data analysis. These include NASA and DOE in the United States, CEA/Irfu and IN2P3/CNRS in France, ASI and INFN in Italy, MEXT, KEK and JAXA in Japan, and the K. A. Wallenberg Foundation, the Swedish Research Council and the National Space Board in Sweden. Additional support from INAF in Italy for science analysis during the operations phase is also gratefully acknowledged. The GASP-WEBT observatories participating in this work are Abastumani, Calar Alto, Campo Imperatore, Crimean, Kitt Peak (MDM), L'Ampolla, Lowell (Perkins-PRISM), Lulin, Roque de los Muchachos (KVA and Liverpool), San Pedro Mártir, St Petersburg for the optical–NIR bands, and Mauna Kea (SMA), Medicina, Metsahovi, Noto and UMRAO for the millimetre radio band, and are supported in part by the Georgian National Science Foundation, the Spanish "Ministerio de Ciencia e Innovación", the NSF and NASA and the Smithsonian Institution in the United States, the UK Science and Technology Facilities Council, the Academia Sinica in Taiwan, the Russian RFBR and the Academy of Finland. M.H. is supported by the JSPS for the Postdoctoral Fellowship for Research Abroad. J. Conrad is a Royal Swedish Academy of Sciences Research Fellow, funded by a grant from the K. A. Wallenberg Foundation. L.T. is partially supported by the International Doctorate on Astroparticle Physics (IDAPP) programme.

Author Contributions All authors contributed to the work presented in this paper. M. Uemura and R. Itoh led the Kanata observations and data analysis. M. Villata organized the optical-radio observations by GASP-WEBT as the president of the collaboration.

Author Information Reprints and permissions information is available at www.nature.com/reprints. The authors declare no competing financial interests. Correspondence and requests for materials should be addressed to M. Hayashida (hayasida@stanford.edu) and G. M. Madejski (madejski@slac.stanford.edu).

The Fermi-LAT Collaboration: A. A. Abdo[1,2], M. Ackermann[3], M. Ajello[3], M. Axelsson[4,5], L. Baldini[6], J. Ballet[7], G. Barbiellini[8,9], D. Bastieri[10,11], B. M. Baughman[12], K. Bechtol[3], R. Bellazzini[6], B. Berenji[3], R. D. Blandford[3], E. D. Bloom[3], D. C.-J. Bock[13,14], J. R. Bogart[3], E. Bonamente[15,16], A. W. Borgland[3], A. Bouvier[3], J. Bregeon[6], A. Brez[6], M. Brigida[17,18], P. Bruel[19], T. H. Burnett[20], S. Buson[10], G. A. Caliandro[21], R. A. Cameron[3], P. A. Caraveo[22], J. M. Casandjian[7], E. Cavazzuti[23], C. Cecchi[15,16], Ö. Çelik[24,25,26], A. Chekhtman[1,27], C. C. Cheung[1,2], J. Chiang[3], S. Ciprini[16], R. Claus[3], J. Cohen-Tanugi[28], W. Collmar[29], L. R. Cominsky[30], J. Conrad[5,31], S. Corbel[7,32], R. Corbet[24,26], L. Costamante[3], S. Cutini[23], C. D. Dermer[1], A. de Angelis[33,34], F. de Palma[17,18], S. W. Digel[3], E. do Couto e Silva[3], P. S. Drell[3], R. Dubois[3], D. Dumora[35,36], C. Farnier[28], C. Favuzzi[17,18], S. J. Fegan[19], E. C. Ferrara[24], W. B. Focke[3], P. Fortin[19], M. Frailis[33,34,37], L. Fuhrmann[38], Y. Fukazawa[39], S. Funk[3], P. Fusco[17,18], F. Gargano[18], D. Gasparrini[23], N. Gehrels[24,40,41], S. Germani[15,16], B. Giebels[19], N. Giglietto[17,18], P. Giommi[23], F. Giordano[17,18], M. Giroletti[42], T. Glanzman[3], G. Godfrey[3], I. A. Grenier[7], J. E. Grove[1], L. Guillemot[35,36,38], S. Guiriec[43], Y. Hanabata[39], A. K. Harding[24], M. Hayashida[3], E. Hays[24], D. Horan[19], R. E. Hughes[12], G. Iafrate[8,37], R. Itoh[39], M. S. Jackson[5,44], G. Jóhannesson[3], A. S. Johnson[3], W. N. Johnson[1], M. Kadler[25,45,46,47], T. Kamae[3], H. Katagiri[39], J. Kataoka[48], N. Kawai[49,50], M. Kerr[20], J. Knödlseder[51], M. L. Kocian[3], M. Kuss[6], J. Lande[3], S. Larsson[5,31], L. Latronico[6], M. Lemoine-Goumard[35,36], F. Longo[8,9], F. Loparco[17,18], B. Lott[35,36], M. N. Lovellette[1], P. Lubrano[15,16], J. Macquart[52], G. M. Madejski[3], A. Makeev[1,27], W. Max-Moerbeck[53], M. N. Mazziotta[18], W. McConville[24,41], J. E. McEnery[24,41], S. McGlynn[5,44], C. Meurer[5,31], P. F. Michelson[3], W. Mitthumsiri[3], T. Mizuno[39], A. A. Moiseev[25,41], C. Monte[17,18], M. E. Monzani[3], A. Morselli[54], I. V. Moskalenko[3], S. Murgia[3], I. Nestoras[38], P. L. Nolan[3], J. P. Norris[55], E. Nuss[28], T. Ohsugi[39], A. Okumura[56], N. Omodei[6], E. Orlando[29], J. F. Ormes[55], D. Paneque[3], J. H. Panetta[3], D. Parent[1,27,35,36], V. Pavlidou[53], T. J. Pearson[53], V. Pelassa[28], M. Pepe[15,16], M. Pesce-Rollins[6], F. Piron[28], T. A. Porter[57], S. Rainò[17,18], R. Rando[10,11], M. Razzano[6], A. Readhead[53], A. Reimer[3,58], O. Reimer[3,58], T. Reposeur[35,36], L. C. Reyes[59], J. L. Richards[53], L. S. Rochester[3], A. Y. Rodriguez[21], M. Roth[20], F. Ryde[5,44], H. F.-W. Sadrozinski[57], D. Sanchez[19], A. Sander[12], P. M. Saz Parkinson[57], J. D. Scargle[60], C. Sgrò[6], M. S. Shaw[3], C. Shrader[25], E. J. Siskind[61], D. A. Smith[35,36], P. D. Smith[12], G. Spandre[6], P. Spinelli[17,18], L. Stawarz[3,62], M. Stevenson[53], M. S. Strickman[1], D. J. Suson[63], H. Tajima[3], H. Takahashi[39], T. Takahashi[64], T. Tanaka[3], G. B. Taylor[65], J. B. Thayer[3], J. G. Thayer[3], D. J. Thompson[24], L. Tibaldo[7,10,11], D. F. Torres[21,66], G. Tosti[15,16], A. Tramacere[3,67], Y. Uchiyama[3], T. L. Usher[3], V. Vasileiou[25,26], N. Vilchez[51], V. Vitale[54,68], A. P. Waite[3], P. Wang[3], A. E. Wehrle[69], B. L. Winer[12], K. S. Wood[1], T. Ylinen[5,44,70], J. A. Zensus[38], M. Ziegler[57]

External members of the 3C 279 multi-band campaign: M. Uemura[71], Y. Ikejiri[39], K. S. Kawabata[71], M. Kino[72], K. Sakimoto[39], M. Sasada[39], S. Sato[72], M. Yamanaka[39], M. Villata[73], C. M. Raiteri[73], I. Agudo[74], H. D. Aller[75], M. F. Aller[75], E. Angelakis[38], A. A. Arkharov[76], U. Bach[38], E. Benítez[77], A. Berdyugin[78], D. A. Blinov[78,79], M. Boettcher[80], C. S. Buemi[81], W. P. Chen[82], M. Dolci[83], D. Dultzin[77], N. V. Efimova[76,79], M. A. Gurwell[84], C. Gusbar[80], J. L. Gómez[74], J. Heidt[85], D. Hiriart[86], T. Hovatta[87], S. G. Jorstad[88], T. S. Konstantinova[79], E. N. Kopatskaya[79], E. Koptelova[82], O. M. Kurtanidze[89], A. Lahteenmaki[87], V. M. Larionov[79], E. G. Larionova[79], P. Leto[81], H. C. Lin[82], E. Lindfors[78], A. P. Marscher[88], I. M. McHardy[90], D. A. Melnichuk[79], M. Mommert[85], K. Nilsson[78], A. Di Paola[91], R. Reinthal[78], G. M. Richter[92], M. Roca-Sogorb[74], P. Roustazadeh[80], L. A. Sigua[89], L. O. Takalo[78], M. Tornikoski[87], C. Trigilio[81], I. S. Troitsky[79], G. Umana[81], C. Villforth[78], K. Grainge[93], R. Moderski[94], K. Nalewajko[94], M. Sikora[94]

[1]Space Science Division, Naval Research Laboratory, Washington, District of Columbia 20375, USA. [2]National Research Council Research Associate, National Academy of Sciences, Washington, District of Columbia 20001, USA. [3]W. W. Hansen Experimental Physics Laboratory, Kavli Institute for Particle Astrophysics and Cosmology, Department of Physics and SLAC National Accelerator Laboratory, Stanford University, Stanford, California 94305, USA. [4]Department of Astronomy, Stockholm University, SE-106 91 Stockholm, Sweden. [5]The Oskar Klein Centre for Cosmoparticle Physics, AlbaNova, SE-106 91 Stockholm, Sweden. [6]Istituto Nazionale di Fisica Nucleare, Sezione di Pisa, I-56127 Pisa, Italy. [7]Laboratoire AIM, CEA-IRFU/CNRS/Université Paris Diderot, Service d'Astrophysique, CEA Saclay, 91191 Gif sur Yvette, France. [8]Istituto Nazionale di Fisica Nucleare, Sezione di Trieste, I-34127 Trieste, Italy. [9]Dipartimento di Fisica, Università di Trieste, I-34127 Trieste, Italy. [10]Istituto Nazionale di Fisica Nucleare, Sezione di Padova, I-35131 Padova, Italy. [11]Dipartimento di Fisica "Galileo Galilei", Università di Padova, I-35131 Padova, Italy. [12]Department of Physics, Center for Cosmology and Astro-Particle Physics, The Ohio State University, Columbus, Ohio 43210, USA. [13]Combined Array for Research in Millimeter-wave Astronomy (CARMA), Big Pine, California 93514, USA. [14]Radio Astronomy Laboratory, University of California, Berkeley, California 94720, USA. [15]Istituto Nazionale di Fisica Nucleare, Sezione di Perugia, I-06123 Perugia, Italy. [16]Dipartimento di Fisica, Università degli Studi di Perugia, I-06123 Perugia, Italy. [17]Dipartimento di Fisica "M. Merlin" dell'Università e del Politecnico di Bari, I-70126 Bari, Italy. [18]Istituto Nazionale di Fisica Nucleare, Sezione di Bari, 70126 Bari, Italy. [19]Laboratoire Leprince-Ringuet, École polytechnique, CNRS/IN2P3, F-91128 Palaiseau, France. [20]Department of Physics, University of Washington, Seattle, Washington 98195-1560, USA. [21]Institut de Ciencies de l'Espai (IEEC-CSIC), Campus UAB, 08193 Barcelona, Spain. [22]INAF-Istituto di Astrofisica Spaziale e Fisica Cosmica, I-20133 Milano, Italy. [23]Agenzia Spaziale Italiana (ASI) Science Data Center, I-00044 Frascati (Roma), Italy. [24]NASA Goddard Space Flight Center, Greenbelt, Maryland 20771, USA. [25]Center for Research and Exploration in Space Science and Technology (CRESST) and NASA Goddard Space Flight Center, Greenbelt, Maryland 20771, USA. [26]Department of Physics and Center for Space Sciences and Technology, University of Maryland Baltimore County, Baltimore, Maryland 21250, USA. [27]George Mason University, Fairfax, Virginia 22030, USA. [28]Laboratoire de Physique Théorique et Astroparticules, Université Montpellier 2, CNRS/IN2P3, 34095 Montpellier, France. [29]Max-Planck Institut für extraterrestrische Physik, 85748 Garching, Germany. [30]Department of Physics and Astronomy, Sonoma State University, Rohnert Park, California 94928-3609, USA. [31]Department of Physics, Stockholm University, AlbaNova, SE-106 91 Stockholm, Sweden. [32]Institut universitaire de France, 75005 Paris, France. [33]Dipartimento di Fisica, Università di Udine, I-33100 Udine, Italy. [34]Istituto Nazionale di Fisica Nucleare, Sezione di Trieste, Gruppo Collegato di Udine, I-33100 Udine, Italy. [35]CNRS/IN2P3, Centre d'Études Nucléaires Bordeaux Gradignan, UMR 5797, Gradignan, 33175, France. [36]Université de Bordeaux, Centre d'Études Nucléaires Bordeaux Gradignan, UMR 5797, Gradignan, 33175, France. [37]Osservatorio Astronomico di Trieste, Istituto Nazionale di Astrofisica, I-34143 Trieste, Italy. [38]Max-Planck-Institut für Radioastronomie, Auf dem Hügel 69, 53121 Bonn, Germany. [39]Department of Physical Sciences, Hiroshima University, Higashi-Hiroshima, Hiroshima 739-8526, Japan. [40]Department of Astronomy and Astrophysics, Pennsylvania State University, University Park, Pennsylvania 16802, USA. [41]Department of Physics and Department of Astronomy, University of Maryland, College Park, Maryland 20742, USA. [42]INAF Istituto di Radioastronomia, 40129 Bologna, Italy. [43]Center for Space Plasma and Aeronomic Research (CSPAR), University of Alabama in Huntsville, Huntsville, Alabama 35899, USA. [44]Department of Physics, Royal Institute of Technology (KTH), AlbaNova, SE-106 91 Stockholm, Sweden. [45]Dr Remeis-Sternwarte Bamberg, Sternwartstrasse 7, D-96049 Bamberg, Germany. [46]Erlangen Centre for Astroparticle Physics, D-91058 Erlangen,

Germany. [47]Universities Space Research Association (USRA), Columbia, Maryland 21044, USA. [48]Research Institute for Science and Engineering, Waseda University, 3-4-1, Okubo, Shinjuku, Tokyo, 169-8555 Japan. [49]Department of Physics, Tokyo Institute of Technology, Meguro City, Tokyo 152-8551, Japan. [50]Cosmic Radiation Laboratory, Institute of Physical and Chemical Research (RIKEN), Wako, Saitama 351-0198, Japan. [51]Centre d'Étude Spatiale des Rayonnements, CNRS/UPS, BP 44346, F-30128 Toulouse cedex 4, France. [52]ICRAR/Curtin Institute of Radio Astronomy, Bentley, Western Australia 6102, Australia. [53]Cahill Center for Astronomy and Astrophysics, California Institute of Technology, Pasadena, California 91125, USA. [54]Istituto Nazionale di Fisica Nucleare, Sezione di Roma "Tor Vergata", I-00133 Roma, Italy. [55]Department of Physics and Astronomy, University of Denver, Denver, Colorado 80208, USA. [56]Department of Physics, Graduate School of Science, University of Tokyo, 7-3-1 Hongo, Bunkyo-ku, Tokyo 113-0033, Japan. [57]Santa Cruz Institute for Particle Physics, Department of Physics and Department of Astronomy and Astrophysics, University of California at Santa Cruz, Santa Cruz, California 95064, USA. [58]Institut für Astro- und Teilchenphysik and Institut für Theoretische Physik, Leopold-Franzens-Universität Innsbruck, A-6020 Innsbruck, Austria. [59]Kavli Institute for Cosmological Physics, University of Chicago, Chicago, Illinois 60637, USA. [60]Space Sciences Division, NASA Ames Research Center, Moffett Field, California 94035-1000, USA. [61]NYCB Real-Time Computing Inc., Lattingtown, New York 11560-1025, USA. [62]Astronomical Observatory, Jagiellonian University, 30-244 Kraków, Poland. [63]Department of Chemistry and Physics, Purdue University Calumet, Hammond, Indiana 46323-2094, USA. [64]Institute of Space and Astronautical Science, JAXA, 3-1-1 Yoshinodai, Sagamihara, Kanagawa 229-8510, Japan. [65]University of New Mexico, MSC07 4220, Albuquerque, New Mexico 87131, USA. [66]Institució Catalana de Recerca i Estudis Avançcats (ICREA), 08010 Barcelona, Spain. [67]Consorzio Interuniversitario per la Fisica Spaziale (CIFS), I-10133 Torino, Italy. [68]Dipartimento di Fisica, Università di Roma "Tor Vergata", 00133 Roma, Italy. [69]Space Science Institute, Boulder, Colorado 80301, USA. [70]School of Pure and Applied Natural Sciences, University of Kalmar, SE-391 82 Kalmar, Sweden. [71]Hiroshima Astrophysical Science Center, Hiroshima University, Higashi-Hiroshima, Hiroshima 739-8526, Japan. [72]Department of Physics and Astrophysics, Nagoya University, Chikusa-ku Nagoya 464-8602, Japan. [73]INAF, Osservatorio Astronomico di Torino, I-10025 Pino Torinese (TO), Italy. [74]Instituto de Astrofisica de Andalucía, CSIC, 18080 Granada, Spain. [75]Department of Astronomy, University of Michigan, Ann Arbor, Michigan 48109-1042, USA. [76]Pulkovo Observatory, 196140 St Petersburg, Russia. [77]Instituto de Astronomía, Universidad Nacional Autónoma de México, CP 04510 México, D.F., México. [78]Tuorla Observatory, University of Turku, FI-21500 Piikkiö, Finland. [79]Astronomical Institute, St Petersburg State University, St Petersburg, Russia. [80]Department of Physics and Astronomy, Ohio University, Athens, Ohio 45701, USA. [81]Osservatorio Astrofisico di Catania, 95123 Catania, Italy. [82]Graduate Institute of Astronomy, National Central University, Jhongli 32054, Taiwan. [83]INAF-Osservatorio Astronomico di Collurania, 64100 Teramo, Italy. [84]Harvard-Smithsonian Center for Astrophysics, Cambridge, Massachusetts 02138, USA. [85]Landessternwarte, Universität Heidelberg, Königstuhl, D 69117 Heidelberg, Germany. [86]Instituto de Astronomía, Universidad Nacional Autónoma de México, CP 22860 Ensenada, B.C., México. [87]Aalto University Metsähovi Radio Observatory, FIN-02540 Kylmälä, Finland. [88]Institute for Astrophysical Research, Boston University, Boston, Massachusetts 02215, USA. [89]Abastumani Observatory, Mt. Kanobili, 0301 Abastumani, Georgia. [90]School of Physics and Astronomy, University of Southampton, Southampton SO17 BJ, UK. [91]Osservatorio Astronomico di Roma, 00040 Monte Porzio Catone, Italy. [92]Astrophyisikalisches Institut Potsdam, D-14482 Potsdam, Germany.[93]Cavendish Laboratory, Cambridge CB3 0HE, UK. [94]Nicolaus Copernicus Astronomical Center, 00-716 Warsaw, Poland.

The Astronomical Journal, 139:757–764, 2010 February
doi:10.1088/0004-6256/139/2/757

THE TAIWAN–AMERICAN OCCULTATION SURVEY PROJECT STELLAR VARIABILITY. I. DETECTION OF LOW-AMPLITUDE δ SCUTI STARS

D.-W. Kim[1,2,3], P. Protopapas[1,2], C. Alcock[1], Y.-I. Byun[3], J. Kyeong[4], B.-C. Lee[4], N. J. Wright[1], T. Axelrod[5], F. B. Bianco[1,6], W.-P. Chen[7], N. K. Coehlo[8], K. H. Cook[9], R. Dave[2], S.-K. King[10], T. Lee[10], M. J. Lehner[1,6,10], H.-C. Lin[7], S. L. Marshall[9,11], R. Porrata[12], J. A. Rice[8], M. E. Schwamb[13], J.-H. Wang[7,10], S.-Y. Wang[10], C.-Y. Wen[10], and Z.-W. Zhang[7,10]

[1] Harvard Smithsonian Center for Astrophysics, Cambridge, MA 02138, USA
[2] Initiative in Innovative Computing, School of Engineering and Applied Sciences, Harvard, Cambridge, MA 02138, USA
[3] Department of Astronomy, Yonsei University, Seoul 120-749, Republic of Korea
[4] Korea Astronomy & Space Science Institute, Daejeon 305-348, Republic of Korea
[5] Steward Observatory, 933 North Cherry Avenue, Room N204 Tucson, AZ 85721, USA
[6] Department of Physics and Astronomy, University of Pennsylvania, 209 South 33rd Street, Philadelphia, PA 19104, USA
[7] Institute of Astronomy, National Central University, No. 300, Jhongda Rd, Jhongli City, Taoyuan County 320, Taiwan
[8] Department of Statistics, University of California Berkeley, 367 Evans Hall, Berkeley, CA 94720, USA
[9] Institute for Geophysics and Planetary Physics, Lawrence Livermore National Laboratory, Livermore, CA 94550, USA
[10] Institute of Astronomy and Astrophysics, Academia Sinica, P.O. Box 23-141, Taipei 106, Taiwan
[11] Kavli Institute for Particle Astrophysics and Cosmology, 2575 Sand Hill Road, MS 29, Menlo Park, CA 94025, USA
[12] Department of Astronomy, University of California Berkeley, 601 Campbell Hall, Berkeley, CA 94720, USA
[13] Division of Geological and Planetary Sciences, California Institute of Technology, 1201 E. California Blvd., Pasadena, CA 91125, USA
Received 2009 September 29; accepted 2009 December 6; published 2010 January 14

ABSTRACT

We analyzed data accumulated during 2005 and 2006 by the Taiwan–American Occultation Survey (TAOS) in order to detect short-period variable stars (periods of $\lesssim$1 hr) such as δ Scuti. TAOS is designed for the detection of stellar occultation by small-size Kuiper Belt Objects and is operating four 50 cm telescopes at an effective cadence of 5 Hz. The four telescopes simultaneously monitor the same patch of the sky in order to reduce false positives. To detect short-period variables, we used the fast Fourier transform algorithm (FFT) in as much as the data points in TAOS light curves are evenly spaced. Using FFT, we found 41 short-period variables with amplitudes smaller than a few hundredths of a magnitude and periods of about an hour, which suggest that they are low-amplitude δ Scuti stars. The light curves of TAOS δ Scuti stars are accessible online at the Time Series Center Web site (http://timemachine.iic.harvard.edu).

Key words: stars: variables: delta Scuti – methods: data analysis – surveys

1. INTRODUCTION

δ Scuti stars (hereinafter, δ Sct stars) are pulsating variables inside the classical instability strip and on or close to the main sequence. They are typically placed lower on the instability strip than RR Lyrae stars or Cepheids and thus they are fainter than RR Lyrae stars or Cepheids. Their spectral types are between A and late F. Their periods are between ~0.02 days and ~0.25 days, which is relatively shorter than other types of variables (e.g., γ Dor; Henry et al. 2001). Based on these characteristics, δ Sct stars can be separated from other types of variable stars such as RR Lyrae, β Cepheid, γ Dor, etc. (Breger 2000a).

The majority of the δ Sct stars are low-amplitude δ Sct stars (LADS) with amplitudes from a millimagnitude to a few tens of a millimagnitude. LADS are mainly non-radial p-mode pulsators (Breger 2000a). Another subgroup of δ Sct stars is the high-amplitude δ Sct stars (HADS), whose amplitudes are bigger than ~0.3 mag. HADS are radial pulsators (Breger 2000a; Rodríguez et al. 1996). In addition to LADS and HADS, there is another interesting type of pulsation star called SX Phe variable stars, which exhibits a type of pulsation similar to the δ Sct stars. They are relatively old and evolved Population II stars, whereas most of the δ Sct stars are Population I stars. Stellar evolutionary theory is not yet successful at explaining these SX Phe variable stars (Rodríguez & López-González 2000). Most of the SX Phe show similar properties with HADS such as high amplitude and short period. More detailed review of δ Sct stars is presented in Breger (2000a, and references therein).

Because of their great number of radial and non-radial modes, it is known that δ Sct stars are suitable for asteroseismology research, which enables study of stellar interior structures (Brown & Gilliland 1994). For a better understanding of pulsating δ Sct stars and thus stellar structure, several authors studied δ Sct stars and detected their multiple frequencies of pulsation using either ground-based observations or space-based observations (Breger et al. 2002, 2005; Ripepi et al. 2003; Buzasi et al. 2005; Bruntt et al. 2007; Pribulla et al. 2008). Due to the better photometric precision, space-based observation data show better results on the analysis of multiple frequencies than ground-based observation data (Bruntt et al. 2007; Pribulla et al. 2008). However, some authors have pointed out that ground-based observations using multiple-site telescopes are still valuable because, with a baseline longer than space-based observations, they are useful for detecting long-period pulsation (for more details, see Breger et al. 2005; Bruntt et al. 2007, and references therein). Moreover, by parameterizing the amplitude ratio and the phase differences in different filters (e.g., $ubvy$), it is possible to derive the spherical harmonic degree, l (Garrido et al. 1990; Balona & Evers 1999; Moya et al. 2004), which is an important parameter for the asteroseismology studies. Therefore, ground-based telescopes that are more feasible for multiple-site and multiple-filter observations (e.g., Delta Scuti Network, Zima et al. 2002) are nonetheless useful for the identification of pulsation modes and thus for the study of interior structures.

Another interesting feature of δ Sct stars is that some of them show period and amplitude variations (Breger & Pamyatnykh 1998; Breger 2000b; Arentoft et al. 2001). The period variation $(1/P)\ dP/dt$, based on observations, is about 10^{-7} per year for both period increases and decreases with equal distribution. On the other hand, theoretical models give 10 times smaller period variation than observed; they also predict that period increases should be dominant over period decreases (Breger & Pamyatnykh 1998). Amplitude variations and timescales of the variations are different from star to star, ranging from a few millimagnitudes to several tens of millimagnitudes and from a few tens of days to a few hundreds of days (Arentoft et al. 2001). These period and amplitude variations are thought to be caused not by evolutionary effects but by some other mechanism (e.g., light-time effect because of the orbital motion in binaries or nonlinear mode interactions). However, the true origin of the variations is still unknown. For more details, see Breger & Pamyatnykh (1998) and references therein.

McNamara et al. (2007) investigated HADS in the Large Magellanic Cloud (LMC) and their period–luminosity (*P–L*) relation to test if they can be used as the standard distance candles. They found that the distance modulus for LMC derived using δ Sct stars is consistent with the distance moduli for LMC derived using RR Lyrae and Cepheids, which implies the *P–L* relation of δ Sct stars can help to determine distances of *long-distance* objects such as objects in the LMC.

In this paper, we present the detection of 41 δ Sct candidate stars from the Taiwan-American Occultation Survey (TAOS) data accumulated during 2005 and 2006 observation (hereinafter, TAOS δ Sct stars). Among the 41 detections, there is one previously known "suspected variable" star, NSV 3816, from the Suspected Variable Stars and Supplement (Samus et al. 2009, no period or type is provided in that catalog). The rest of the 40 TAOS δ Sct stars are newly detected by this study. Only 14 of the detected TAOS δ Sct stars have spectral types. Twelve of those have spectral types from A to F, which are typical for δ Sct stars. The remaining two have B8 and G5 spectral types, which are peculiar spectral types. Using spectroscopic instruments—BOES (Kim et al. 2007) and FAST (Fabricant et al. 1998)—we obtained spectra for those two stars. As a result we found that the B8 star is an A5 star and the G5 star is an F0 star. Even though the rest of the detected stars do not have spectral-type information, their low amplitudes, short periods, and morphologies of light curves strongly suggest that they are LADS.

In Section 2, we present a TAOS overview, data reduction processes, and the detection algorithm we used to detect δ Sct stars in TAOS two-year data. We provide a list of the detected TAOS δ Sct stars and their physical parameters (e.g., magnitude, period, amplitude, spectral type, etc.) in Section 3. In Section 4, we present summaries.

2. TAOS δ Sct STARS

2.1. TAOS Overview

TAOS aims to detect stellar occultations caused by small-sized Kuiper Belt Objects (KBOs) at a distance of Neptune's orbit or beyond (Alcock et al. 2003; Chen et al. 2007; Lehner et al. 2009). Because of the short duration (<1 s) and the rareness of occultation events, TAOS monitors several hundreds of stars in a wide field of view (3 deg^2) with a high sampling rate. To reduce false positives, TAOS uses four 50 cm telescopes which simultaneously monitor the same patch of the sky. Due to the high sampling rate, TAOS data are also useful for detecting short-period variable stars such as δ Sct stars. Moreover, TAOS telescopes keep monitoring the same field up to 1.5 hr and can thus obtain full-phase light curves of variable stars whose periods are shorter than 1.5 hr. To detect such short-period variable stars, we analyzed TAOS data accumulated during 2005 and 2006. The data set consists of 117 TAOS observation fields, which cover 351 deg^2 of the sky. It consists of $\sim$200 *runs*, where a run is a set of multiple (two or three[14]) telescope observations for a given field and a given date. Note that the TAOS telescopes occasionally visit the same observation field multiple times according to the telescopes' observation schedules, which enables detecting the same variable stars multiple times. In such a case, we are able to derive multiple frequencies of the stars as explained in Section 3.1.

2.2. Data Reduction

To detect periodic signals, we analyzed the light curves generated by the TAOS photometry pipeline (Zhang et al. 2009). The pipeline was developed by the collaboration to extract light curves of each star from zipper images. The zipper images are generated by the unique telescope operation mode called zipper mode which was developed in order to achieve high-speed photometry (Lehner et al. 2009).

After obtaining the light curves using the TAOS photometry pipeline, we applied further cuts to the light curves. Some of the individual measurements are flagged as invalid. This happens when the star moves out of the field of view because of temporary telescope vibrations or tracking error, thus yielding no photometrical measurements. We therefore applied a B-spline (de Boor 1978) and replaced the flagged measurements with values interpolated from the spline fit. After the interpolation process, in order to increase the signal-to-noise ratio (S/N), we binned each light curve using a fifty-point window (10 s). During the binning process, we used the average time of the 50 data points as the time of the binned data.

We then removed the systematic variations that are common across light curves of the same run. Such systematic variations, which we call trends, could be caused by air mass, temporary telescope vibrations, noise in CCD images, etc. To remove such trends, we applied the Photometric DeTrending algorithm (PDT, Kim et al. 2009) to each individual run. PDT first calculates the correlation between whole light curves as a measure of similarity between light curves. PDT then uses the hierarchical clustering algorithm (Jain et al. 1999) to group similar light curves together and determines one master trend per group by summing weighted light curves in the group. Using the determined master trends, PDT finally removes trends from each individual light curve by minimizing the residual between the master trends and the light curve. For more details about PDT, see Kim et al. (2009).

Figure 1 shows an example of a TAOS δ Sct star's light curve before and after the detrending process. The *x*-axis is time in minutes, and the *y*-axis is flux. As the figure shows, periodic signals are clearly recovered after detrending. We show the errors for each photometric measurement before detrending, propagated from the errors estimated by the TAOS photometry pipeline (Zhang et al. 2009).

[14] During 2005 and 2006 observational season, one of the four TAOS telescopes was not operational.

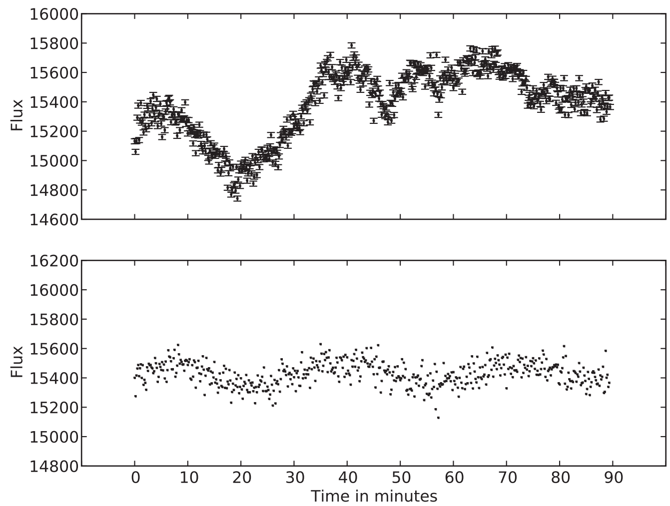

Figure 1. Example light curve of a TAOS δ Sct star. The x-axis is time in minutes and the y-axis is flux. The top panel is the light curve before detrending and the bottom panel is the light curve after detrending. The periodic signals contaminated by unstable weather (e.g., moving clouds) are successfully recovered after detrending. We show the errors for each photometric measurement of the raw light curve.

2.3. *Detection of Short-period Variable Stars*

After we finished the preprocessing, explained in the previous section, we applied the fast Fourier transform algorithm (FFT; Brigham 1974) to each light curve in order to detect periodic signals. Note that the individual measurements of TAOS light curves are evenly spaced with a 5 Hz sampling rate.[15] Thus FFT is appropriate for the detection of periodic signals. We focused on the detection of short-period variable stars whose periods are $\lesssim$1.5 hr because TAOS monitors a given field for a maximum of 1.5 hr.

We describe the basic steps of the detection process below.

1. We apply FFT to each detrended light curve and derive the power spectrum of the light curve. We then examine if there exists a frequency (or frequencies) whose power is bigger than five times the standard deviation of powers of the background frequencies. The standard deviation of powers is calculated after removing outliers using 3σ clipping.[16] We identify the star as a variable candidate if there is a frequency higher than five times the standard deviation.
2. For each candidate variable, we check if the periodic signal is detected on the other telescopes' light curves of the same run. If it is not detected by the other telescopes, we remove the star from the candidate list.
3. We visually inspect all raw zipper images for the candidates and remove false positives caused by moving asteroids, photometry defects, or other contamination due to various noise sources. For instance, the flux of stars in the neighborhood of fast-moving objects could be increased and decreased within an hour, which resembles periodic signals.
4. We cross-match all of the candidates with SIMBAD (Wenger et al. 2000) and remove the false positives that are confirmed to be other types of variable stars (e.g., eclipsing binary stars).
5. Finally, we remove the variable stars whose periods are longer than 1.5 hr.

3. DETECTION RESULTS

With the detection algorithm described in the previous section, we found 41 δ Sct candidate stars whose periods are shorter than 1.5 hr and whose amplitudes are within a few hundredth of a magnitude (hereinafter, TAOS δ Sct stars). Among those 41 TAOS δ Sct stars, one of them is a previously *suspected* variable star, NSV 3816, from the Suspected Variable stars and Supplement (Samus et al. 2009). However, the period and amplitude of NSV 3816 have never been published before. The remaining 40 TAOS δ Sct stars are newly detected by this study.

After the TAOS δ Sct stars were identified, we extracted the physical parameters of each star by cross-matching them with various astronomical catalogs. We show catalogs we used in Table 1. We found that 12 of the detected 41 TAOS δ Sct stars have spectral types from A0 to F5, which are typical spectral types for δ Sct stars. Unfortunately, the rest of them, except for two peculiar δ Sct stars—discussed in Section 3.3—do not have spectral information. Nevertheless, their short period and low amplitude strongly suggest that they are LADS rather than other types of variables, such as RR Lyrae or Cepheids, whose periods and amplitudes are relatively longer and larger than those of δ Sct stars.

As a byproduct of our analysis, we detected a previously known variable star with δ Sct pulsation, GM Leo, which is actually a λ Bootis star (Handler et al. 2000). Some λ Bootis stars show δ Sct pulsations (Paunzen 2004) and can have spectral types from late B to early F, which makes it difficult to distinguish them from δ Sct stars. In such cases, there are no clear differences between δ Sct stars and λ Bootis stars except the metal abundance (Balona 2004); λ Bootis stars show weak metal lines such as the Mg II λ4481 line (Paunzen 2004).

We also checked several preexisting catalogs of δ Sct stars to see if there are previously known δ Sct stars in the TAOS observation fields. Table 2 shows the preexisting catalogs we checked. As a result of this search, we found only one previously known δ Sct pulsation star to be in the TAOS observation fields. That turns out to be GM Leo, which, as mentioned above, we successfully detected. Although GCVS classified GM Leo as δ Sct star based on the work by Handler et al. (2000), Handler et al. (2000) in their paper claimed GM Leo is not a δ Sct star but a λ Bootis star. Thus we removed GM Leo from our detection list.

3.1. *List of the Detected 41 δ Sct Stars*

Table 3 shows the 41 TAOS δ Sct stars' physical information such as positions, magnitudes, frequencies, amplitudes, spectral types, etc.

We used the FFT algorithm to detect periodic signals; however, we used PERIOD04 to derive their physical parameters such as period and amplitude.[17] This is because PERIOD04 improves the frequency by fitting the light curve with a combination of sine curves. Moreover PERIOD04 also provides errors for the derived frequencies. Figure 2 shows a comparison result of power spectra derived from an FFT method and PERIOD04 for a single TAOS δ Sct star. The x-axis is frequency in counts/day and the y-axis is scaled power. The solid line is

[15] Binned light curves are evenly spaced as well.

[16] Those outliers are only removed for the calculation of the standard deviation. They are included in the search of periodic signals.

[17] Since PERIOD04 gives half of the full amplitudes, we doubled amplitudes derived by PERIOD04 as Rodríguez et al. (2000) and other authors do.

Table 1
Catalogs Used to Extract Additional Parameters

Catalog	Reference
GCVS	Perryman & ESA (1997)
All-Sky Compiled Catalogue of 2.5 million stars	Kharchenko (2001)
HD	Cannon & Pickering (1993)
Catalog of Stellar Spectral Classifications	Skiff (2009)
Tycho-2 Catalogue of the 2.5 Million Brightest Stars	Høg et al. (2000)
Guide Star Catalog (GSC)	Lasker et al. (2008)
USNO-B 1.0	Monet et al. (2003)
SAO Star Catalog J2000	SAO Staff (1995)
Catalog of Projected Rotational Velocities	Glebocki & Stawikowski (2000)
Rotational Velocity Determinations for 118 δ Sct Variables	Bush & Hintz (2008)

Table 2
Preexisting Catalogs of δ Sct Stars

Catalog	Source Surveys	Number of δ Sct Stars	Reference
R2000[a]	MACHO, OGLE, Hipparcos, etc	$\sim$600	(Rodríguez et al. 2000)
ROTSE[b]	ROTSE	6	(Jin et al. 2003)
ASAS[c]	ASAS	$\sim$500	(Pojmanski et al. 2006)
GCVS[d]	Various surveys	$\sim$500	(Samus et al. 2009)
TAOS	TAOS	41	This paper
Others			
	5 new γ Doradus and 5 new δ Sct survey	5	(Henry et al. 2001)
	Case study for HD 173977	1	(Chapellier et al. 2004)
	Case study for HD 8801	1	(Henry & Fekel 2005)
	The first HADS in an eclipsing binary star	1	(Christiansen et al. 2007)
	Variable stars in NGC 2099	9	(Kang et al. 2007)
	Transit survey of M37	2	(Hartman et al. 2008)
	ASAS variable stars in the Kepler field of view	4	(Pigulski et al. 2009)

Notes.
[a] The catalog compiled by Rodríguez et al. (2000).
[b] Robotic Optical Transient Search Experiment.
[c] All-Sky Automated Survey.
[d] General Catalog of the Variable Stars.

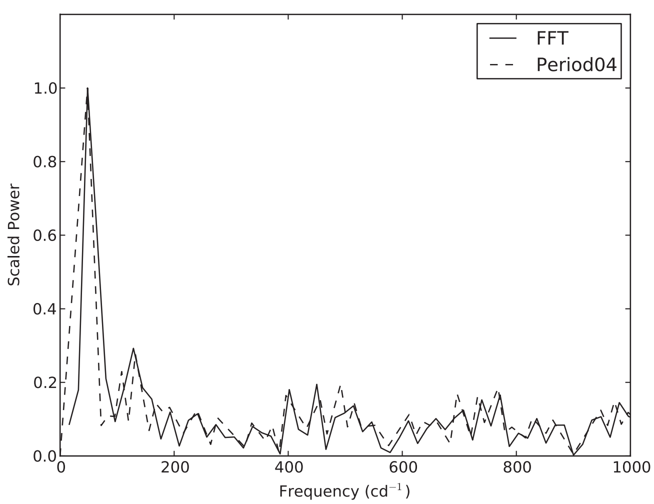

Figure 2. Comparison result of the power spectrum derived from an FFT method and from PERIOD04. The x-axis is frequency in counts/day and the y-axis is scaled power. The solid line is the power spectrum derived from an FFT method, and the dashed line is the power spectrum derived from PERIOD04. The two spectra appear almost identical.

a power spectrum derived from an FFT method, and the dashed line is a power spectrum derived from PERIOD04. As the figure shows, the two spectra are almost consistent.

As we mentioned in the previous section, TAOS operates multiple telescopes simultaneously monitoring the same patch of the sky. Thus we have a maximum of three simultaneous light curves for all TAOS δ Sct stars for a given zipper run. To derive more precise frequencies and amplitudes, for each identified δ Sct star we summed the light curves from each of the telescopes. Moreover, the TAOS telescopes occasionally visit same fields multiple times. In such cases, we merge all corresponding normalized light curves[18] of each identified δ Sct star into a single but longer light curve. Having longer light curves we were able to extract multiple frequencies using PERIOD04. Among the extracted frequencies, we selected the frequencies whose S/N is bigger than 5. The S/N of each frequency was calculated using PERIOD04 as well.[19] As a result, we found 16 TAOS δ Sct stars having multiple frequencies (see Table 3). Note that we did not attempt to extract multiple frequencies if the star is detected only once (i.e., detected in only a single zipper run). It is also worth mentioning that we lose detectability on relatively long-period pulsations because we normalized the light curves while merging them.

All detected δ Sct stars are relatively bright as shown in the table (the faintest star's m_V is around 12). This is because the limiting magnitude of TAOS zipper mode is relatively bright at $\sim$13.5 (Lehner et al. 2009) and also because high S/N is needed to detect low-amplitude variations of a few millimagnitudes. To

[18] We normalized each light curve by their mean values.
[19] Although other authors have suggested a threshold of S/N > 4 (Breger et al. 1993; Christiansen et al. 2007), we empirically found that a threshold of S/N > 4 produces false positives and thus we set the S/N threshold to 5.

Table 3
TAOS δ Sct Stars in TAOS Two-year Data

No.	ID[a]	R.A. (hh:mm:ss)	Decl. (dd:mm:ss)	m_V	m_B	Frequency (cd^{-1})	Δm_V[b] (mmag)	S/N[c]	Epoch (MJD)	Spectral Type	#/#[d]	Note
1	124.00003	00:52:40	+06:39:55	8.89	9.20	$24.421 \pm 3.975e^{-4}$	3.83 ± 0.20	6.5	53626.7469	A2	4/7	
2	038.00124	02:56:54	+34:23:20	11.60	12.00	$23.598 \pm 4.775e^{-1}$	7.95 ± 0.44	11.9	53678.6909		1/2	
3	053.00009	03:37:02	+18:21:51	8.48	8.80	$20.544 \pm 2.314e^{-4}$	5.99 ± 0.14	18.5	53671.7396	A2	3/8	
4	059.00115	03:42:41	+17:55:01	12.12	12.60	$25.836 \pm 7.587e^{-4}$	9.19 ± 0.68	13.6	54021.6614		3/8	
						$32.116 \pm 8.434e^{-4}$	7.97 ± 0.66	11.8	54021.6579			
						$12.034 \pm 1.291e^{-3}$	4.94 ± 0.58	7.5	54021.5979			
						$40.403 \pm 1.713e^{-3}$	3.53 ± 0.62	5.25	54021.6523			
5	059.00005	03:46:01	+18:34:00	9.14	9.46	$33.115 \pm 2.022e^{-4}$	8.00 ± 0.20	15.7	54006.7013	A5	7/8	B8[e]
						$18.068 \pm 4.793e^{-4}$	3.26 ± 0.20	6.4	54006.7020			
6	049.00056	04:03:21	+19:21:31	10.91	11.48	$24.205 \pm 3.694e^{-4}$	9.15 ± 0.34	13.7	54029.8147		6/16	
						$17.761 \pm 6.312e^{-4}$	4.98 ± 0.36	7.5	54029.7806			
						$29.544 \pm 8.243e^{-4}$	4.00 ± 0.34	6.0	54029.8094			
7	068.00053	04:30:06	+20:55:00	11.45	12.36	$32.504 \pm 2.402e^{-5}$	10.17 ± 0.28	15.5	53643.8513	F0	8/15	G5[f]
						$26.117 \pm 5.939e^{-5}$	4.10 ± 0.28	6.24	53643.8542			
8	060.00151	04:48:37	+21:10:33	11.44	11.64	$43.180 \pm 3.709e^{-4}$	5.13 ± 0.26	8.4	54012.7340	F5	6/32	
9	022.00001	04:56:14	+21:34:20	7.34	7.70	$21.582 \pm 1.709e^{-4}$	3.97 ± 0.12	12.9	54021.7647	F0	7/25	
						$21.146 \pm 3.268e^{-4}$	2.15 ± 0.12	6.94	54021.7495			
						$40.637 \pm 4.339e^{-4}$	1.57 ± 0.12	5.12	54021.7926			
10	020.00206	05:08:38	+22:49:37	11.85	12.16	$53.575 \pm 5.075e^{-1}$	7.62 ± 0.46	9.9	53705.6765		1/3	
11	020.00141	05:09:24	+23:16:05	11.40	12.29	$31.535 \pm 6.862e^{-1}$	6.87 ± 0.52	5.7	53705.6877		1/3	
12	021.00011	05:09:40	+21:50:05	8.99	9.21	$41.754 \pm 1.493e^{-4}$	8.05 ± 0.18	17.7	53975.7771		5/7	
						$37.264 \pm 4.476e^{-4}$	2.73 ± 0.18	5.9	53975.7883			
13	020.00135	05:10:14	+23:01:24	10.90	11.78	$39.254 \pm 6.865e^{-1}$	5.11 ± 0.40	6.3	53705.6974		1/3	
14	024.00234	05:15:19	+22:53:41	11.93	12.39	$25.804 \pm 2.471e^{-1}$	35.35 ± 1.04	12.8	53679.7864		1/2	
15	160.00106	06:01:30	+21:27:38	10.38	10.69	$21.063 \pm 3.878e^{-4}$	7.44 ± 0.22	13.9	53680.8125		3/8	
16	160.00004	06:04:05	+21:29:39	7.81	7.97	$25.827 \pm 5.607e^{-4}$	4.70 ± 0.16	15.5	53680.8193		3/8	
						$22.395 \pm 7.432e^{-4}$	3.55 ± 0.14	11.7	53680.8406			
						$38.868 \pm 1.077e^{-3}$	1.59 ± 0.12	5.2	53680.8298			
17	160.00199	06:04:26	+21:21:55	10.96	11.16	$43.741 \pm 9.070e^{-4}$	4.12 ± 0.26	11.0	53680.8119		3/8	
18	052.00132	07:39:07	+21:39:20	11.14	11.67	$23.802 \pm 3.343e^{-3}$	4.69 ± 0.30	7.2	53699.7766		2/3	
19	052.00069	07:39:09	+20:48:41	10.43	10.85	$21.288 \pm 7.664e^{-4}$	7.51 ± 0.28	11.6	53682.7645		3/3	
						$29.627 \pm 1.666e^{-3}$	3.41 ± 0.28	5.2	53682.7835			
20	052.00159	07:39:20	+21:11:22	11.25	11.59	$18.793 \pm 2.293e^{-3}$	9.59 ± 0.42	18.8	53699.7682		2/3	
						$27.366 \pm 3.345e^{-3}$	6.69 ± 0.42	13.4	53699.7680			
						$41.107 \pm 6.306e^{-3}$	3.19 ± 0.32	6.2	53699.7687			
21	054.00014	07:56:31	+21:52:29	9.50	9.74	$20.310 \pm 6.086e^{-5}$	2.89 ± 0.14	8.5	53702.8142	A5	9/19	NSV 3816
						$45.725 \pm 7.022e^{-5}$	2.16 ± 0.14	6.3	53702.8211			
						$23.012 \pm 7.570e^{-5}$	2.32 ± 0.14	6.8	53702.8130			
22	054.00075	07:58:27	+21:36:24	10.80	11.11	$22.591 \pm 3.776e^{-5}$	7.21 ± 0.026	12.9	53702.8148		5/19	
23	064.00006	08:43:26	+16:53:00	8.80	9.11	$19.763 \pm 3.791e^{-1}$	6.84 ± 0.34	8.3	53812.5164		1/2	
24	064.00050	08:43:45	+17:25:00	10.60	10.94	$20.148 \pm 4.392e^{-1}$	7.47 ± 0.44	8.6	53812.5238		1/2	
25	066.00003	08:44:07	+15:55:51	8.56	8.71	$54.890 \pm 9.400e^{-1}$	6.37 ± 0.38	10.6	53774.6133	A0	1/2	
26	062.00060	09:05:56	+17:47:27	10.90	11.50	$38.163 \pm 8.580e^{-4}$	11.24 ± 0.70	7.4	53753.6878	A5	3/9	
						$46.333 \pm 1.213e^{-3}$	7.94 ± 0.68	5.2	53753.7126			
27	062.00030	09:09:53	+17:41:08	10.18	10.40	$21.098 \pm 3.614e^{-5}$	7.64 ± 0.22	9.0	53753.6725		4/9	
28	107.00023	13:10:39	−06:25:01	10.25	10.51	$20.214 \pm 1.921e^{-4}$	10.58 ± 0.30	10.4	53767.8800	A0	4/10	
29	099.00087	15:58:40	−19:27:14	11.62	12.46	$19.673 \pm 3.479e^{-1}$	19.86 ± 0.92	12.4	53903.6396		1/1	
30	148.00060	16:51:54	+07:36:44	10.80	11.10	$24.652 \pm 4.632e^{-4}$	27.71 ± 0.64	14.3	53812.7968	A5	2/12	
31	012.00024	19:51:31	−22:23:03	9.84	10.20	$27.102 \pm 7.279e^{-1}$	8.22 ± 0.78	6.0	53959.6073	A6III	1/4	
32	153.00128	20:04:47	−20:32:05	11.63	12.34	$19.313 \pm 5.077e^{-1}$	43.72 ± 2.92	6.4	53919.7373		1/1	
33	121.00214	21:01:43	+16:39:37	11.20	11.57	$23.471 \pm 6.650e^{-4}$	9.20 ± 0.48	6.2	53559.7694		2/10	
34	121.00043	21:03:25	+15:21:26	9.13	17.53	$30.376 \pm 1.866e^{-3}$	3.61 ± 0.16	12.8	53750.7027		3/10	
35	028.00439	21:54:03	+25:11:07	12.85	13.54	19.445 ± 6.747^{-5}	32.02 ± 1.16	18.4	53575.7487		5/9	
						$21.088 \pm 1.405e^{-4}$	15.39 ± 1.02	8.8	53575.7599			
						$8.847 \pm 1.238e^{-3}$	9.79 ± 1.02	5.7	53575.7475			
36	028.01026	22:01:08	+24:44:33	13.01	13.42	$33.008 \pm 5.843e^{-5}$	36.45 ± 1.72	11.5	53575.7736		5/9	
37	003.00147	22:01:53	−12:28:52	12.24	12.23	$17.731 \pm 2.283e^{-4}$	32.24 ± 1.14	18.5	53947.6845		4/4	
						$41.446 \pm 1.392e^{-3}$	12.43 ± 1.28	7.4	53947.7181			
						$30.608 \pm 8.642e^{-4}$	9.26 ± 1.26	5.4	53947.7213			
38	138.00022	22:05:55	+28:02:32	9.54	10.05	$17.767 \pm 6.301e^{-5}$	5.11 ± 0.20	12.0	53781.7689	A3	6/13	
						$18.090 \pm 9.286e^{-5}$	3.50 ± 0.20	8.2	53781.7733			
39	138.00110	22:09:41	+28:12:40	10.80	11.30	$16.877 \pm 1.751e^{-4}$	7.87 ± 0.32	12.6	53584.7897		4/13	
40	030.00019	22:59:23	+37:14:33	9.26	9.65	$20.199 \pm 9.589e^{-4}$	5.21 ± 0.20	13.5	53657.6049	F2	4/8	
						$29.390 \pm 1.564e^{-3}$	2.60 ± 0.18	6.7	53657.6029			
						$19.757 \pm 1.579e^{-3}$	2.86 ± 0.20	7.4	53657.5702			
41	030.00195	23:02:06	+36:30:28	11.51	11.91	$22.278 \pm 5.635e^{-4}$	13.56 ± 0.42	21.4	53657.5695		5/8	
						$18.802 \pm 1.529e^{-3}$	5.14 ± 0.40	8.1	53657.6120			

Notes.
[a] Combination of TAOS field ID and TAOS star ID.
[b] We doubled amplitudes derived by PERIOD04.
[c] S/N of frequencies derived using PERIOD04.
[d] The number of identifications/the number of zipper runs. Note that we did not count zipper runs observed by only one telescope.
[e] The B8 star found to be an A5 star as explained in the text.
[f] The G5 star found to be an F0 star as explained in the text.

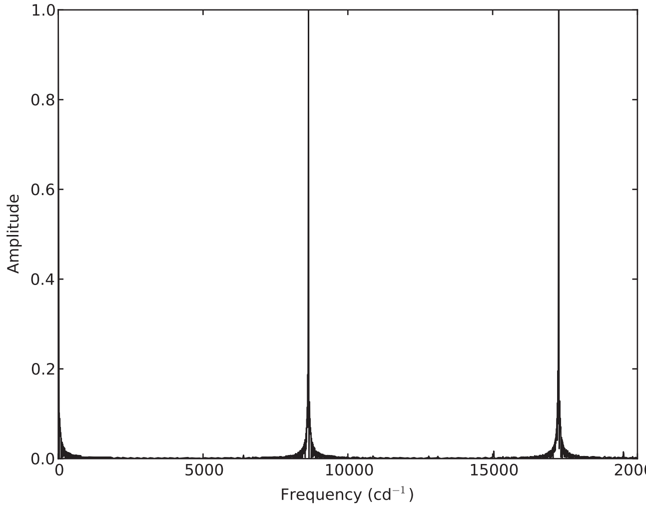

Figure 3. Example of a spectral window of a single zipper run. Peaks with regular intervals (two times of the Nyquist frequency) appear because points are equally spaced in a single zipper run.

find m_V, m_B, and spectral types, we used Centre de Données astronomiques de Strasbourg (CDS) Web service (Genova et al. 2000).

In Table 3, we also provide the number of the total observations (i.e., the number of the total zipper runs) and the number of identifications by the FFT analysis for each TAOS δ Sct star. Since the TAOS telescopes observe same fields multiple times, we have multiple light curves for stars in the fields. Note that we applied the FFT algorithm to each light curve to detect periodic signals. Nevertheless, as the table shows, not every light curve of the TAOS δ Sct stars was confirmed to have periodic signals. This is mainly because of the poor quality of some of the light curves caused by trends and noise (i.e., unstable weather, telescope vibration, etc.). Although we removed most of the trends using PDT, it is nearly impossible to recover the intrinsic periodic signal of a few millimagnitudes in the presence of large systematic errors.

3.2. *Spectral Windows and Power Spectra of TAOS δ Sct Stars*

In Figure 3, we show an example of a spectral window of a single zipper run. Since the observational times are almost equally spaced, peaks with regular intervals (two times the Nyquist frequency) are present in the spectral window (Deeming 1975). The Nyquist frequency is 4320 Hz since the gap between each consecutive binned data is 10 s.

Figures 4–6 show the spectral windows along with the power spectra of three TAOS δ Sct stars. Stars included in these figures are 020.00141 (Figure 4), 121.00043 (Figure 5), and 054.00014 (Figure 6), respectively. The top panels in each figure show the spectral windows, and the bottom panels (and the middle panel in Figure 6) show the power spectra of the stars. Dashed lines indicate the detected frequencies. Note that we improved the detected frequencies by fitting a combination of sine waves using PERIOD04. Thus the improved frequencies could be slightly shifted from the original peaks in the power spectra (e.g., see the bottom left panel in Figure 4) after the fitting.

As Table 3 shows, the star with ID 020.00141 was identified only once and is relatively fainter ($m_V = 11.40$) than other TAOS δ Sct stars. Its amplitude is one of the smallest amplitudes and its detected frequency S/N is the lowest among TAOS δ Sct stars. Thus the power spectrum of this star represents one of

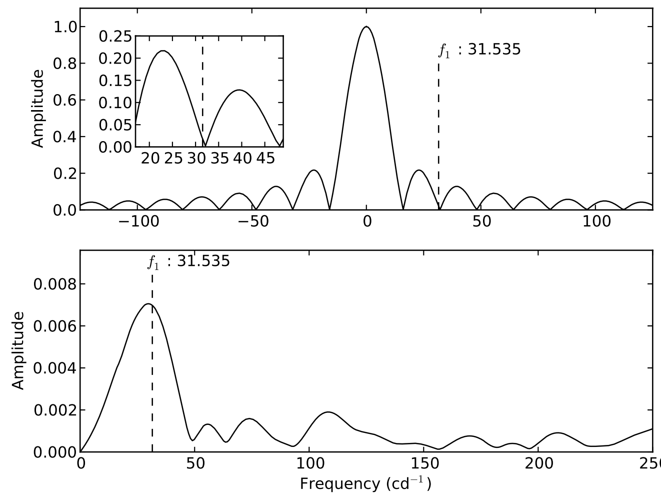

Figure 4. Spectral window and the power spectrum of the star ID 020.00141. The top panel shows the spectral window, and the bottom panel shows the power spectrum of the star. The dashed line shows the detected frequency. In the top panel, we magnified the spectral window to clearly show the detected frequency.

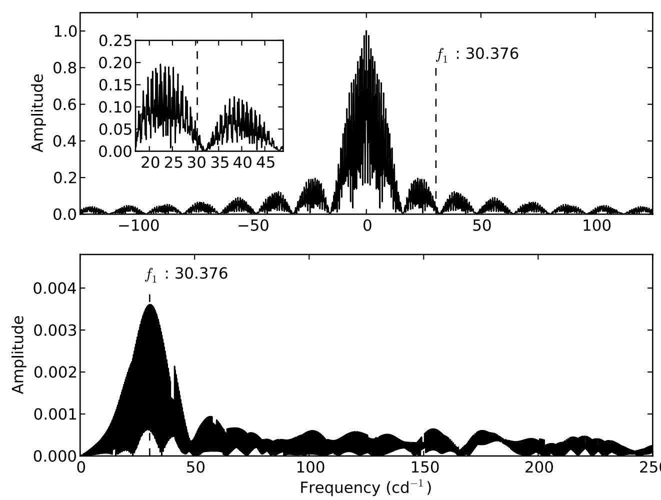

Figure 5. Spectral window and the power spectrum of the star ID 121.00043. The top panel shows the spectral window, and the bottom panel shows the power spectrum of the star. The dashed line shows the detected frequency. In the top panel, we magnified the spectral window to clearly show the detected frequency.

the "worst-case scenarios." We detected one single frequency for this star. The star with ID 121.00043 was identified three times and is relatively bright ($m_V = 9.13$). The spectral window and the power spectrum of the star could represent a "moderate-level scenario." We detected one frequency for this star. Finally, the star with ID 054.00014 was identified nine times and is relatively bright ($m_V = 9.50$). Thus its spectral window and power spectrum represent one of the "best-case scenarios." Using PERIOD04, we detected three frequencies for this star. As can be seen from the figures, there are no significant peaks in the spectral windows at the detected frequencies.

3.3. *Spectroscopy of Two Peculiar Spectral Type δ Sct Stars*

As we mentioned in the previous section, we found two peculiar spectral-type δ Sct stars which have B8 and G5 spectral types. These are the bluest and reddest spectral types of δ Sct stars ever detected. The spectral type of the B8 star was extracted from the Henry Draper Catalogue and Extension (HD; Cannon & Pickering 1993). Unfortunately, we could not find any spectroscopic literature for the G5 star so we suspect that the

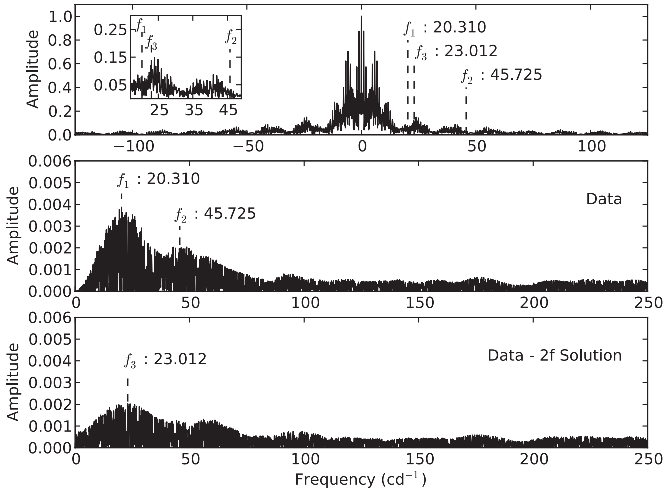

Figure 6. Spectral window and the power spectrum of the star ID 054.00014. We detected three frequencies (dashed lines) using PERIOD04. The top panel shows the spectral window. The middle panel shows the first two frequencies. The bottom panel is the power spectrum after whitening the two frequencies. In the top panel, we magnified the spectral window to clearly show the detected frequencies.

spectral type is most likely derived from its color information. The spectral type of the G5 star was extracted from SIMBAD. To confirm their spectral types, we observed the two stars with spectroscopic instruments.

For the B8 star, we used the BOES[20] of the 1.8 m telescope at the Bohyunsan Optical Astronomy Observatory (BOAO), South Korea (Kim et al. 2007). We used IRAF (Tody 1986, 1993) for the reduction of the obtained spectroscopic data. Figure 7 shows the normalized spectrum of the B8 candidate star. We indicate several important spectral lines in the figure. As the figure shows, the Ca II K line is very strong which is typical for A-type stars (Gray & Garrison 1987). B-type stars do not show such a strong Ca II K line. The spectrum also shows weak metallic lines (e.g., Ca I and Mg II lines) which are usually presented in A-type stars. Based on the strength of the Ca II K line, hydrogen lines, and metallic lines, the star is likely an A5-type star although the classification of sub-class is rather uncertain due to the low S/N of the spectrum.

In addition, to observe the G5 star, we used the FAST instrument mounted at the Fred Lawrence Whipple Observatory (FLWO) 1.5 m telescope, Mount Hopkins in Arizona (Fabricant et al. 1998). After comparing the observed data with standard spectral libraries (Pickles 1998), we found that the spectral type of the star is not a G5 but an F0. Therefore, the star is likely a typical δ Sct star.

4. SUMMARY

We analyzed the TAOS two-year data accumulated during 2005 and 2006 observations in order to find short-period variables. Using the TAOS photometry pipeline, we created photometric light curves. We removed systematic trends commonly appeared in the light curves using PDT. To detect periodic signals in the detrended light curves, we applied the FFT to each light curve. FFT is a simple but *powerful* algorithm for detection of periodic signals when data points are evenly spaced. We then chose light curves which possess a frequency (or frequencies) whose power is five times larger than the standard deviation of powers of all background frequencies in the power spectrum derived using FFT. We visually checked the light curves and raw images of all candidates to remove false positives caused by moving asteroids, photometry defects, etc. We also removed candidates which were detected by only one of the three telescopes. All remaining 41 variable candidates have periods about an hour and amplitudes less than a few hundredth of a magnitude, which strongly suggests that they are LADS.

We cross-matched the detected δ Sct candidate stars with many astronomical catalogs to extract additional information (e.g., magnitude, spectral type, variability type, etc.). As a result, we found that 14 stars have spectral types from A to F, which

[20] BoaO Echelle Spectrograph.

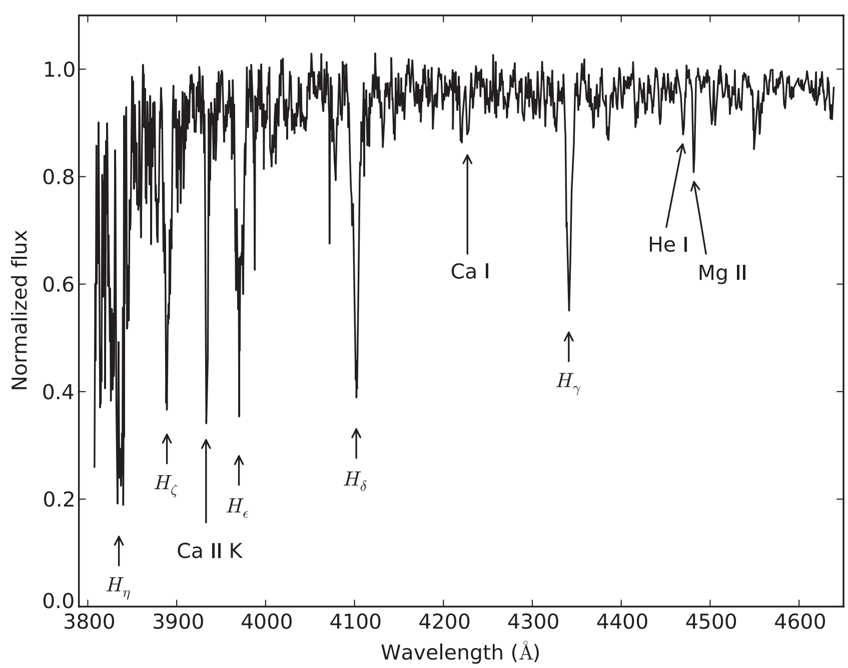

Figure 7. Normalized spectrum of the B8 candidate star. There are strong Ca II K line and weak metallic lines, which is typical for A-type stars. The star is likely an A5-type star rather than a B8-type star.

are typical spectral types for δ Sct stars. The rest of the detected δ Sct stars do not have spectral information.

The light curves of TAOS δ Sct stars are accessible at the Time Series Center (TSC, http://timemachine.iic.harvard.edu), Initiative in Innovative Computing (IIC) at Harvard. PERIOD04 project files of each star is also provided. The project files contain complete light-curve data, power spectrum, frequency, and amplitude information.

Y.-I. Byun acknowledges the support of the National Research Foundation of Korea through Grant 2009-0075376. The work at National Central University was supported by the grant NSC 96-2112-M-008-024-MY3. Work at Academia Sinica was supported in part by the thematic research program AS-88-TP-A02. Work at the Harvard College Observatory was supported in part by the National Science Foundation under grant AST-0501681 and by NASA under grant NNG04G113G. S.L.M.'s work was performed under the auspices of the U.S. Department of Energy by Lawrence Livermore National Laboratory in part under Contract W-7405-Eng-48 and by Stanford Linear Accelerator Center under Contract DE-AC02-76SF00515. K. H. Cook's work was performed under the auspices of the U.S. Department of Energy by Lawrence Livermore National Laboratory in part under Contract W-7405-Eng-48 and in part under Contract DE-AC52-07NA27344. We also thank J. D. Hartman at Harvard-Smithsonian Center for Astrophysics for useful discussion.

The detrending and the analysis of data sets in this paper were run on the Odyssey cluster supported by the FAS Research Computing Group at the Harvard. This research has made use of the SIMBAD database, operated at CDS, Strasbourg, France. IRAF is distributed by the National Optical Astronomy Observatories, which are operated by the Association of Universities for Research in Astronomy, Inc., under cooperative agreement with the National Science Foundation.

REFERENCES

Alcock, C., et al. 2003, Earth Moon Planets, 92, 459

Arentoft, T., et al. 2001, A&A, 374, 1056

Balona, L. A. 2004, in IAU Symp. 224, The A-Star Puzzle, Pulsations of A stars, ed. J. Zverko, J. Ziznovsky, S. J. Adelman, & W. W. Weiss (Dordrecht: Kluwer), 325

Balona, L. A., & Evers, E. A. 1999, MNRAS, 302, 349

Breger, M. 2000a, in ASP Conf. Ser. 210, Delta Scuti and Related Stars, δ Scuti Stars (Review), ed. M. Breger & M. Montgomery (San Francisco, CA: ASP), 3

Breger, M. 2000b, MNRAS, 313, 129

Breger, M., & Pamyatnykh, A. A. 1998, A&A, 332, 958

Breger, M., et al. 1993, A&A, 271, 482

Breger, M., et al. 2002, MNRAS, 336, 249

Breger, M., et al. 2005, A&A, 435, 955

Brigham, E. O. 1974, The fast Fourier Transform (Englewood Cliffs, NJ: Prentice-Hall)

Brown, T. M., & Gilliland, R. L. 1994, ARA&A, 32, 37

Bruntt, H., et al. 2007, A&A, 461, 619

Bush, T. C., & Hintz, E. G. 2008, AJ, 136, 1061

Buzasi, D. L., et al. 2005, ApJ, 619, 1072

Cannon, A. J., & Pickering, E. C. 1993, VizieR Online Data Catalog, 3135, 0

Chapellier, E., et al. 2004, A&A, 426, 247

Chen, W. P., et al. 2007, in IAU Symp. 236, Search for Small Trans-Neptunian Objects by the TAOS Project, ed. G. B. Valsecchi, D. Vokrouhlický, & A. Milani (Dordrecht: Kluwer), 65

Christiansen, J. L., et al. 2007, MNRAS, 382, 239

de Boor, C. 1978, A Practical Guide to Splines (New York: Springer), 87

Deeming, T. J. 1975, Ap&SS, 36, 137

Fabricant, D., Cheimets, P., Caldwell, N., & Geary, J. 1998, PASP, 110, 79

Garrido, R., Garcia-Lobo, E., & Rodriguez, E. 1990, A&A, 234, 262

Genova, F., et al. 2000, A&AS, 143, 1

Glebocki, R., & Stawikowski, A. 2000, Acta Astron., 50, 509

Gray, R. O., & Garrison, R. F. 1987, ApJS, 65, 581

Handler, G., Gray, R. O., & Shobbrook, R. R. 2000, IBVS, 4876, 1

Hartman, J. D., et al. 2008, ApJ, 675, 1254

Henry, G. W., & Fekel, F. C. 2005, AJ, 129, 2026

Henry, G. W., et al. 2001, AJ, 122, 3383

Høg, E., et al. 2000, A&A, 355, L27

Jain, A. K., Murty, M. N., & Flynn, P. J. 1999, ACM Comput. Surv., 31, 264

Jin, H., et al. 2003, A&A, 404, 621

Kang, Y. B., et al. 2007, PASP, 119, 239

Kharchenko, N. V. 2001, Kinematika Fiz. Nebesnykh Tel, 17, 409

Kim, D.-W., et al. 2009, MNRAS, 397, 558

Kim, K.-M., et al. 2007, PASP, 119, 1052

Lasker, B. M., et al. 2008, AJ, 136, 735

Lehner, M. J., et al. 2009, PASP, 121, 138

McNamara, D. H., Clementini, G., & Marconi, M. 2007, AJ, 133, 2752

Monet, D. G., et al. 2003, AJ, 125, 984

Moya, A., Garrido, R., & Dupret, M. A. 2004, A&A, 414, 1081

Paunzen, E. 2004, in IAU Symp. 224, The A-Star Puzzle, The λ Bootis stars, ed. J. Zverko, J. Ziznovsky, S. J. Adelman, & W. W. Weiss (Dordrecht: Kluwer), 443

Perryman, M. A. C., & ESA (ed.) 1997, The *HIPPARCOS* and *TYCHO* Catalogues. Astrometric and Photometric Star Catalogues Derived from the ESA HIPPARCOS Space Astrometry Mission (ESA Special Publication, Vol. 1200; Noordwijk: ESA)

Pickles, A. J. 1998, PASP, 110, 863

Pigulski, A., et al. 2009, Acta Astron., 59, 33

Pojmanski, G., et al. 2006, VizieR Online Data Catalog, 2264, 0

Pribulla, T., et al. 2008, MNRAS, 391, 343

Ripepi, V., et al. 2003, A&A, 408, 1047

Rodríguez, E., & López-González, M. J. 2000, A&A, 359, 597

Rodríguez, E., López-González, M. J., & López de Coca, P. 2000, A&AS, 144, 469

Rodríguez, E., et al. 1996, A&A, 307, 539

Samus, N. N., et al. 2009, VizieR Online Data Catalog, 1, 2025

SAO Staff 1995, VizieR Online Data Catalog, 1131, 0

Skiff, B. A. 2009, VizieR Online Data Catalog, 1, 2023

Tody, D. 1986, Proc. SPIE, 627, 733

Tody, D. 1993, in ASP Conf. Ser. 52, Astronomical Data Analysis Software and Systems II, IRAF in the Nineties, ed. R. J. Hanisch, R. J. V. Brissenden, & J. Barnes (San Francisco, CA: ASP), 173

Wenger, M., et al. 2000, A&AS, 143, 9

Zhang, Z. W., et al. 2009, PASP, 121, 1429

Zima, W., et al. 2002, in ASP Conf. Ser. 259, Radial and Nonradial Pulsationsn as Probes of Stellar Physics, The Delta Scuti Network: Steps Towards Successful Asteroseismology of Delta Scuti Stars, ed. C. Aerts, T. R. Bedding, & J. Christensen-Dalsgaard (San Francisco, CA: ASP), 598

PUBLICATIONS OF THE ASTRONOMICAL SOCIETY OF THE PACIFIC, **122**:959–975, 2010 August

The TAOS Project: Statistical Analysis of Multi-Telescope Time Series Data

M. J. LEHNER,[1,2,3] N. K. COEHLO,[4] Z.-W. ZHANG,[1,5] F. B. BIANCO,[2,3,6,7] J.-H. WANG,[1,5] J. A. RICE,[4] P. PROTOPAPAS,[3,8]
C. ALCOCK,[3] T. AXELROD,[9] Y.-I. BYUN,[10] W. P. CHEN,[5] K. H. COOK,[11] I. DE PATER,[12] D.-W. KIM,[3,8,10]
S.-K. KING,[1] T. LEE,[1] S. L. MARSHALL,[11,13] M. E. SCHWAMB,[14] S.-Y. WANG,[1] AND C.-Y. WEN[1]

Received 2010 February 18; accepted 2010 June 2; published 2010 June 30

ABSTRACT. The Taiwanese-American Occultation Survey (TAOS) monitors fields of up to ~1000 stars at 5 Hz simultaneously with four small telescopes to detect occultation events from small (~1 km) Kuiper Belt Objects (KBOs). The survey presents a number of challenges, in particular the fact that the occultation events we are searching for are extremely rare and are typically manifested as slight flux drops for only one or two consecutive time series measurements. We have developed a statistical analysis technique to search the multi-telescope data set for simultaneous flux drops which provides a robust false-positive rejection and calculation of event significance. In this article, we describe in detail this statistical technique and its application to the TAOS data set.

1. INTRODUCTION

The Taiwanese-American Occultation Survey operates four small telescopes (Bianco et al. 2010; Wang et al. 2009; Zhang et al. 2008; Lehner et al. 2009) at Lulin Observatory in central Taiwan to search for occultations by small (~1 km diameter) KBOs (Schlichting et al. 2009; Wang et al. 2010; Bianco et al. 2009; Bickerton et al. 2009, 2008; Nihei et al. 2007; Chang et al. 2007; Roques et al. 2006; Cooray 2003; Cooray & Farmer 2003; Roques et al. 2003). Occultation surveys are the only method available to detect these objects, as objects smaller than about 20 km in diameter have magnitudes $R > 30$, which is beyond the limit of direct observation. Occultation events are extremely rare (estimated rates range from 10^{-4} to 10^{-2} events $\mathrm{star}^{-1}\,\mathrm{yr}^{-1}$), they are very short in duration ($\lesssim$200 ms), and at the 5 Hz observing cadence used by TAOS, they result in measured flux drops of typically $\lesssim 30\%$ in one or two consecutive points. This presents a number of challenges, in particular the identification of false-positive events of statistical origin and candidate events which are in fact of terrestrial origin (e.g., birds, airplanes, and extreme scintillation events). We reject these false-positive events by requiring simultaneous detection in multiple telescopes.

A second challenge is finding a robust method to determine the statistical significance of any candidate events. The noise distribution of each light curve is not known a priori, due to non-Poisson and non-Gaussian processes on the tails of the flux distributions. The typical stars in our fields have magnitudes $R \sim 13$ and a signal-to-noise ratio (S/N) of ~10. Moreover, TAOS monitors fields for durations of up to 1.5 hr, and changes in atmospheric transparency and air mass introduce further uncertainties into the flux measurements.

To overcome these difficulties, we have developed nonparametric techniques using *rank statistics*. Rank statistics facilitate a simultaneous analysis of multi-telescope photometric measurements to enable a robust determination of event significance and false-positive rejection, which are independent of the underlying noise distributions of the light curves being analyzed. Occultation events and the application of rank statistics to detect such events in the TAOS data are described in the following sections. In § 2 we review the characteristics of occultation events and describe how such events would appear in the data. In § 3 we discuss the rank product statistical test used to calculate event significance and the false-positive rate. In § 4 we describe the light-curve filtering techniques and diagnostic tests used to ensure that the rank product statistical test is valid,

[1] Institute of Astronomy and Astrophysics, Academia Sinica. P.O. Box 23-141, Taipei 106, Taiwan; mlehner@asiaa.sinica.edu.tw.
[2] Department of Physics and Astronomy, University of Pennsylvania, Philadelphia, PA 19104.
[3] Harvard-Smithsonian Center for Astrophysics, Cambridge, MA 02138.
[4] Department of Statistics, University of California Berkeley, Berkeley, CA 94720.
[5] Institute of Astronomy, National Central University, No. 300, Jhongda Rd, Jhongli City, Taoyuan County 320, Taiwan.
[6] Department of Physics, University of California, Santa Barbara CA 93106-9530
[7] Las Cumbres Observatory Global Telescope Network, Inc., Santa Barbara, CA 93117.
[8] Initiative in Innovative Computing, Harvard University, Cambridge, MA 02138.
[9] Steward Observatory, Tucson, AZ 85721.
[10] Department of Astronomy, Yonsei University, 134 Shinchon, Seoul 120-749, Korea.
[11] Institute of Geophysics and Planetary Physics, Lawrence Livermore National Laboratory, Livermore, CA 94550.
[12] Department of Astronomy, University of California, Berkeley, CA 94720.
[13] Kavli Institute for Particle Astrophysics and Cosmology, Menlo Park, CA 94025.
[14] Division of Geological and Planetary Sciences, California Institute of Technology, Pasadena, CA 91125.

and in § 4.4 we describe a new and more robust set of diagnostics tests.

The following definitions apply throughout the remainder of this article. We define a *data run* as a consecutive series of multi-telescope observations of a given star field made at a cadence of 5 Hz. Typical data runs last 1.5 hr, comprising 27,000 time series images on each telescope. We define a *light-curve set* as a set of multi-telescope light curves of a single star during a given data run. There are typically 300–500 stars in an image, and hence 300–500 light-curve sets in a data run. We adopt the standard statistical notation wherein we denote a random variable with an upper case letter, and use the corresponding lower case letter for an actual value for that variable (e.g., Z is a random variable which could take on a value of z). We use the function $p()$ to describe a probability density distribution, and $\mathbb{P}()$ to describe an actual probability. Finally, we note that the four telescopes are labeled TAOS A, TAOS B, TAOS C, and TAOS D. TAOS C came online in 2008 August, and to date no data from this telescope have been analyzed. All example light curves shown in this article come from telescopes A, B, and D.

2. OCCULTATIONS BY KUIPER BELT OBJECTS

An occultation event occurs when an object passes between the telescope and a distant star (Bickerton et al. 2009; Nihei et al. 2007; Roques et al. 2003). The Earth and the occulting object are in relative motion, inducing a variation in the measured stellar flux over time. The target population for TAOS is small ($\sim$1 km diameter) KBOs, whose sizes are on the order of the *Fresnel scale*, which is given by

$$F = \sqrt{\frac{\lambda\Delta}{2}},$$

where λ is the wavelength of observation and Δ is the observer–KBO distance. For TAOS, the median wavelength of observation is $\lambda \approx 600$ nm, and the typical distance to KBOs is 43 AU, resulting in $F = 1.4$ km. Occultation events by KBOs with diameters $D \lesssim 10$ km thus show significant diffraction effects. This is illustrated in the left panel of Figure 1, which shows a simulated occultation "shadow" from a 3 km diameter KBO projected onto the surface of the Earth.

The timescale of an occultation event is set by the relative velocity between the KBO and observer, the size of the occultation shadow, and the impact parameter (minimum distance between the KBO and the line of sight to the target star). Assuming a circular orbit, the relative velocity between the Earth and KBO in the plane of the sky is given by

$$v_{\rm rel} = v_{\rm E}\left[\cos\phi - \left(\frac{1\rm AU}{\Delta}\right)^{\frac{1}{2}}\left(1 - \frac{1\rm AU^2}{\Delta^2}\sin^2\phi\right)^{\frac{1}{2}}\right], \quad (1)$$

where ϕ is the angle of observation between the occulted star and opposition, and $v_{\rm E} = 29.8\ {\rm km\,s^{-1}}$ is the velocity of the Earth around the Sun. The event width (the length of the chord across the occultation shadow where it crosses the telescope) is given by

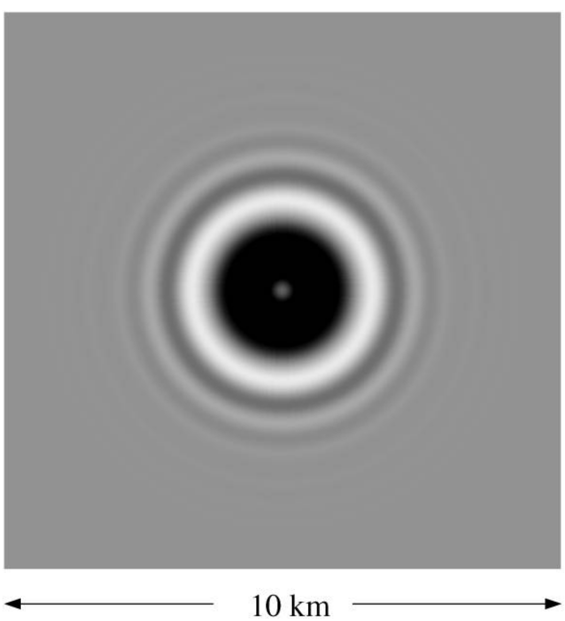

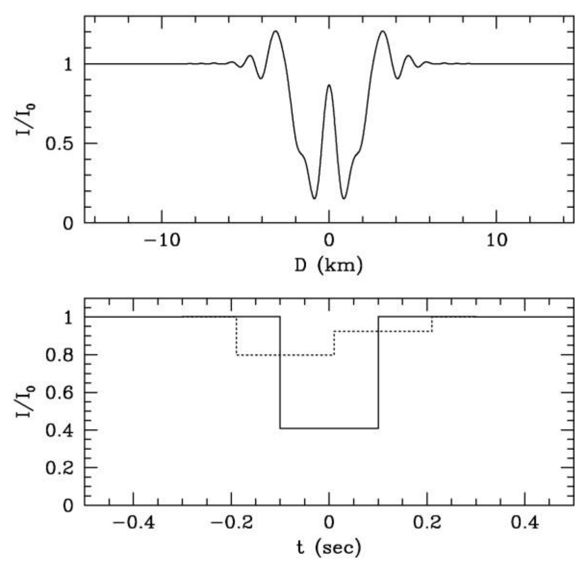

FIG. 1.—*Left panel:* diffraction shadow projected onto the surface of the Earth from a 3 km diameter KBO at 43 AU. *Right panel, top:* perfectly sampled light curve assuming zero impact parameter. *Right panel, bottom:* same light curve as sampled by the TAOS system at 5 Hz. *Solid curve* has measurements centered on event, *dotted line* shows light curve where sampling is out of phase with event.

$$W = \sqrt{H^2 - b^2},$$

where b is the impact parameter, and H is the event cross section, which we define as the diameter of the first Airy ring of the diffraction shadow, and which can be approximated by (Nihei et al. 2007)

$$H \approx [(2\sqrt{3}F)^{\frac{3}{2}} + D^{\frac{3}{2}}]^{\frac{2}{3}} + \theta_* \Delta, \quad (2)$$

where θ_* is the angular size of the occulted star.

For the very small objects ($D \lesssim 1$ km) targeted by this survey and stars with small angular diameters (the vast majority of stars covered by this survey), the minimum event cross section is set by the Fresnel scale:

$$H_{\text{min}} \approx 2\sqrt{3}F. \quad (3)$$

At 43 AU, $H_{\text{min}} \approx 5$ km. At opposition ($\phi = 0$), $v_{\text{rel}} \approx 25\ \text{km}\,\text{s}^{-1}$, and with $b = 0$ the resulting event duration is 200 ms, with the duration getting smaller as b is increased.

This is illustrated in the right panels of Figure 1. The top panel shows a slice through the simulated diffraction shadow, assuming the KBO crosses the line of sight to the star ($b = 0$). Note that the event width, given by the distance between the two top peaks, is about 5 km. (In this case, the event width is dominated by the Fresnel scale, so the approximation given in eq. [3] applies.) The bottom panel shows this event as it would be measured by the TAOS system at 5 Hz. The solid line shows the light curve which would be measured if the sampling was in phase with the event, that is, the measurement at $t = 0$ is centered on the epoch when the KBO is centered on the line of sight to the target star. The dotted line shows the same event with the sampling out of phase with the event.

Typical occultation events for small KBOs at opposition will thus manifest themselves in the TAOS data as a reduction in flux on one or two consecutive photometric measurements of a star with an otherwise flat light curve. However, when observing away from opposition, the relative velocity decreases, as indicated by equation (1). Furthermore, TAOS is also sensitive to objects more distant than the Kuiper Belt. The discovery of Sedna (Brown et al. 2004) indicates the possibility of a large, heretofore unknown population of objects at distances of 100 to 1000 AU (see Wang et al. 2009 and references therein). Such events will also be of a longer duration due to the increased angular size of the Fresnel scale, as indicated by equation (2). Figure 2 shows a simulated light curve with an occultation by a 5 km object at 500 AU, observed at 70° from opposition. The width of the event is about 22 km, and with a relative velocity of about 9 $\text{km}\,\text{s}^{-1}$, the event duration is about 2.5 s, corresponding to a total of 13 measurements at our cadence of 5 Hz. (Once again, the approximation for the event width given in eq. [3] applies.)

The goals of the TAOS statistical analysis described in this article are to find as many such events as possible, minimize the false-positive rate, and provide a method to robustly estimate the statistical significance of any candidate event. The statistical technique should be sensitive to both the one- and two-point events shown in Figure 1 and the longer duration events such as that shown in Figure 2. In the following sections the application of rank statistics to meet these goals will be described. The discussion will begin with a focus on single-point events, and the extension of the statistical technique to multipoint observations will be presented in § 3.4.

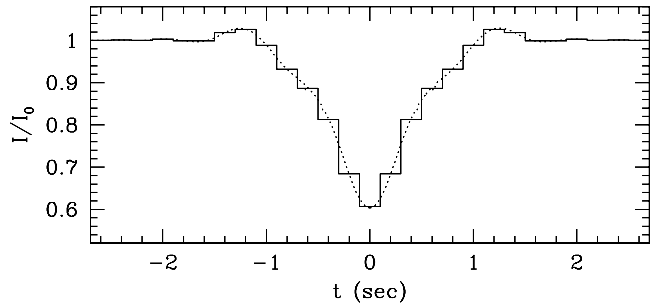

FIG. 2.—Simulated light curve with an occultation by a 5 km object at 500 AU, measured at 70° from opposition. Diffraction features are smoothed out due to finite angular size of the occulted star. *Dotted line* is the infinitesimally sampled light curve, and the *solid line* indicates the light curve as would be measured with 5 Hz sampling. See Nihei et al. (2007) for a discussion of occultation events from objects at such distances.

3. RANK STATISTICS

The idea of rank statistics is quite simple, and is best introduced with a single series. Take a time series of flux measurements $f_1, \ldots, f_{N_p}$ from one telescope, where N_p is the number of points in the time series. Replace each flux measurement f_j with its rank r_j. That is, the lowest f_j will be assigned rank 1 and the highest assigned rank N_p. If we use a total of T telescopes, we replace the time series for each telescope with its rank within the light curve from that telescope, giving a set of T rank time series r_{ij}. Thus for each time point t_j, we have a *rank tuple*

$$(r_{1j}, \ldots, r_{Tj}).$$

If, for each telescope i, the rank r_{ij} follows a uniform distribution on $\{1, \ldots, N_p\}$ at each time point t_j, and if the light curves f_{ij} are independent between the different telescopes, then each rank tuple combination is equally likely at each time point, and we can calculate exact probability distribution of these rank tuples. The calculation of the probability distribution of the raw data is impossible to perform on the original time series measurements, since the underlying distributions of the flux measurements f_{ij} in each light curve are unknown. That is, by working with the ranks, we replace something unknown, the distribution of the data, with something known, the distribution of the ranks.

A time series is *stationary* if the distribution of any finite subset of the series is invariant under time shift. A stationary time series f_j is *ergodic in mean* if, for any function G with an expected value $\mathbb{E}(G(f)) < \infty$, we have the following convergence with probability of 1 (law of large numbers):

$$\lim_{n\to\infty} \frac{1}{n}\sum_{i=1}^{n} G(f_i) \to \mathbb{E}(G(f)).$$

It can be shown that if a time series f_j of length N is ergodic in mean, then the distribution of ranks r_j/N will converge to the uniform distribution for any sequence $1 \leq j \leq N$, and it is well known that ergodicity in mean can be assured under very weak assumptions on temporal dependence within a light curve. This proof is beyond the scope of this article, but it is published in Coehlo (2010).

Therefore, if the data f_j are stationary and ergodic in mean, this implies that at each time point t_j, r_j will be uniform on $\{1, \ldots, N_p\}$. In addition, if the light curves from different telescopes are independent, then the rank tuples $(r_{1j}, \ldots, r_{Tj})$ will be uniform on

$$\{1, 2, \ldots, N_p\}^T,$$

and we can calculate exact probability distributions of the rank tuples. However, most of the light-curve sets exhibit slowly varying trends that are highly correlated between the different telescopes, so our light curves are neither uncorrelated nor stationary. We have developed a filtering algorithm to remove these trends, and in most cases the resulting individual light curves can be plausibly modeled as stationary and ergodic in mean. In most cases the correlations between the light curves from different telescopes are also removed by the application of the filter. This filtering algorithm will be described in § 4.

Figure 3 introduces the *rank-rank diagram*, which is a scatter-plot of the ranks on two telescopes. Similar plots will be used throughout the remainder of the article to illustrate various statistical tests. Note that each rank must occur once and only once in each time series. Thus there must be exactly one point in each row and in each column. The ranks within a single light curve are thus not independently distributed. However, if the conditions on ergodicity in mean and no dependence between telescopes are met, then the rank pairs will be uniformly distributed throughout the diagram.

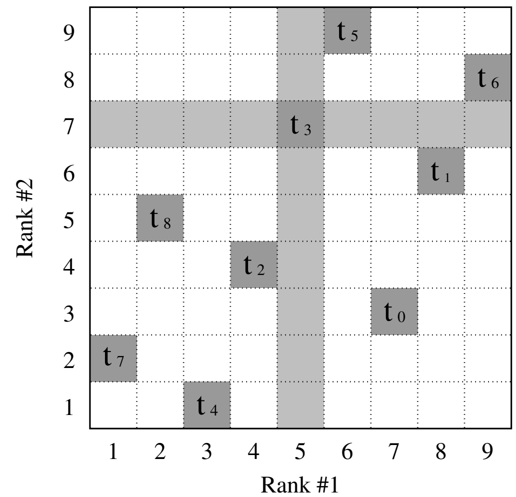

FIG. 3.—Schematic of a rank-rank diagram, with $N_p = 9$. Axes are ranks of photometric intensity for individual data points on two different telescopes. A single two-telescope photometric measurement will correspond to a rank doublet on this plot. These are marked with the *dark squares* and labeled with the time at which they where measured. For example, note the highlighted rank pair at (5,7), measured at time t_3. Note that each rank value occurs once and only once in the time series for each telescope.

3.1. The Rank Product Test Statistic

As can be seen in Figure 1, events consistent with occultations by KBOs will appear as one or two consecutive flux drops in all four telescopes. Our test is thus designed to find those rank tuples where all of the ranks are small, corresponding to a region toward the lower left corner of the rank-rank diagram shown in Figure 3 (expanded to T dimensions, where T is the number of telescopes). The assumptions on the rank statistics and conditions placed on the raw data allow us to calculate the significance level α of various test statistics corresponding to this region.

The statistical analysis is designed to use each rank tuple $(r_{1j}, \ldots, r_{Tj})$ to perform a hypothesis test that there is an event at time t_j. Each measurement r_{ij} can be used as a test statistic for the null hypothesis of no occultation event versus the alternative that there is an occultation, yielding a p-value given by

$$\mathbb{P}(R \leq r_{ij}) = \frac{r_{ij}}{N_p}.$$

The goal is to use the tuple of T p-values at time t_j to calculate a single test of significance. Fisher proposed that the product of the p-values be used as a test statistic for this general problem (Fisher 1958; Mosteller & Fisher 1948). Given the product of ranks at time t_j over all telescopes T

$$y_j = \prod_{i=1}^{T} r_{ij},$$

we define our rank product statistic as

$$z_j = -\ln\left(\frac{y_j}{N_p^T}\right). \tag{4}$$

Event detection based on the rank product statistic was described in Lehner et al. (2006) and Zhang et al. (2008). In the description presented in Lehner et al. (2006), we made the assumption that the distribution of p-values r_{ij}/N_p was uniform on the *continuous* interval $[0, 1]$. In this case, it can be shown that the rank product distribution has a distribution of the form

$$p(z_j) = \frac{1}{\Gamma(T)} z_j^{T-1} e^{-z_j}, \quad (5)$$

which is simply the Γ distribution. However, the distribution of ranks is in fact uniform on the *discrete* set $\{1/N_p, 2/N_p, \ldots, 1\}$, and we found that the assumption of a continuous distribution leads to substantial errors for large values of z. The true distribution of the rank product can be calculated using the function $K(n; T, N_p)$, which we define as the number of ways to get a product of n by multiplying T integers (number of telescopes) between 1 and N_p (number of points in the light curves). This function can be calculated numerically, and we have developed a simple algorithm to calculate $K(n; T, N_p)$ when $n \le N_p$ (see Appendix). Some values of this function for $T = 4$ telescopes are shown in Table 1. Note that this function is independent of N_p if $n \le N_p$.

Rather than using the function K to calculate the probability density of the rank product statistic z, it is simpler to calculate the distribution as a function of the rank product y as

$$p(y) = \frac{1}{N_p^T} K(y; T, N_p).$$

We thus calculate the significance, or p-value, of any candidate event as

$$\mathbb{P}(Y \le y) = \frac{1}{N_p^T} \sum_{i=1}^{y} K(i; T, N_p). \quad (6)$$

However, for clarity we continue to display results in terms of the rank product statistic z because candidate events are more easily distinguished on the tail of the distribution (see Fig. 4). Given the relation between z and y, it clearly follows that

$$\mathbb{P}(Z \ge z(y)) = P(Y \le y).$$

Note that the results published in Zhang et al. (2008) and Bianco et al. (2010) use the correct probability distribution based on the discrete rank distribution.

The efficacy of the rank product method is shown in Figure 4 (right panel). A three-telescope (top) and a four-telescope (bottom) data run were simulated. On the three-telescope run, an event was added with a rank triplet $\{10, 10, 10\}$, and on the four-telescope run, an event was added with ranks $\{10, 10, 10, 10\}$. The four-telescope event has a p-value of 3.7×10^{-12} under the null hypothesis, while the three-telescope event has a p-value of 1.5×10^{-9}. This simple example illustrates the value of using multiple telescopes, in that the absence of the fourth telescope decreases the significance of the event by more than 2000, while keeping the false-positive rate fixed.

The rank product test statistic is based on subsets of the rank tuples where events would plausibly be expected to be found. However, in general, the subset of rank tuples that provides the most sensitive detection is composed of those tuples which are most likely in the event of an occultation. We could imagine identifying this subset by running an enormous simulation of occultations which produced a probability for each of the T^{N_p} tuples. The rejection region for the test would then be composed of the quadruplets with largest probabilities, the number

TABLE 1

RANK QUADRUPLETS USED TO CALCULATE $K(z; T, N_p)$ FOR $T = 4$ AND $z \le N_p$

$K(1) = 1$	$K(2) = 4$	$K(3) = 4$	$K(4) = 10$	$K(5) = 4$	$K(6) = 16$
1111	1112	1113	1114	1115	1116
	1121	1131	1141	1151	1161
	1211	1311	1411	1511	1611
	2111	3111	4111	5111	6111
			1122		1123
			1212		1132
			2112		1213
			1221		1312
			2121		2113
			2211		3112
					1231
					1321
					2131
					3121
					2311
					3211

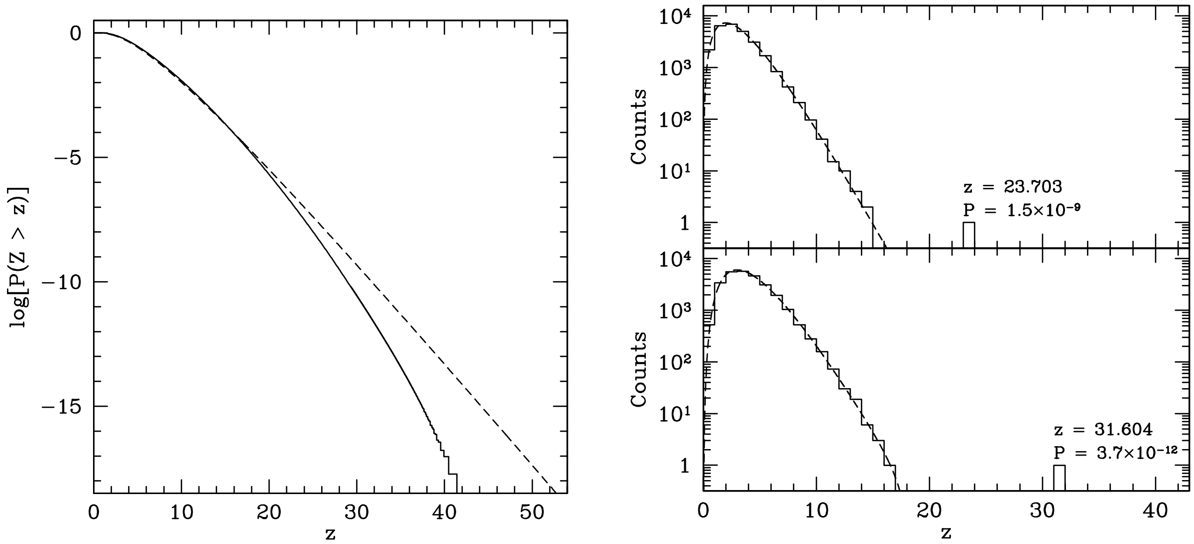

FIG. 4.—*Left panel:* event significance as a function of z (*solid line*), assuming $N_p = 27,000$ and $T = 4$. Also shown for comparison is the event significance calculated using the Γ distribution approximation (*dashed line*). *Right panels:* the results of two simulations illustrating the power of the rank product method for event selection. On the *top panel,* the histogram shows the parameter z for $T = 3$ and $N_p = 27,000$, and the *dashed line* shows the true distribution given the null hypothesis. The rank triplet on the tail has ranks $\{10, 10, 10\}$. The *bottom plot* is the same, but with $T = 4$, and the outlier arises from a rank quadruplet of $\{10, 10, 10, 10\}$.

being determined by the desired false-positive rate. Note that the rejection region might not be symmetric in the telescopes (invariant to the telescope labels), which might be desirable if light curves from some telescopes had much better signal to noise ratios than from others. We have not carried out such a simulation, but a modest simulation indicates that the rejection region determined by the rank product statistic is sufficient for the purpose of event detection.

3.2. False-Positive Rate

The methodology we employ is to search for an event at every time point in every light-curve set that the survey has collected. Hence, the total number of hypotheses tested is

$$N_{\text{hyp}} = \sum_l N_p(l),$$

where the sum is over all light-curve sets l in the data set.

If we set a significance threshold of α to declare an event at time point t_j in light-curve set l, and we use the same significance threshold at all times in all light curves, then the expected number of declared events due to chance would be

$$\alpha \times N_{\text{hyp}} = \alpha \times \sum_l N_p(l).$$

Therefore, to control false positives we must make α very small. For the results published in Zhang et al. (2008), the data set (after diagnostic cuts, see § 4.3 for details) comprised a total of 2.3×10^9 tuples, and the threshold used was $\alpha = 10^{-10}$, which gives a predicted 0.23 false-positive events. To keep the false-positive rate low for the larger data set (9.0×10^9 tuples) used in Bianco et al. (2010), we used $\alpha = 3 \times 10^{-11}$, corresponding to an expected number of 0.27 false positives.

In all likelihood there will be at most one occultation in a light-curve set, and if an occultation occurred over consecutive time points it would only be counted once. Hence, one could consider performing a hypothesis test over the entire light-curve set rather than at each time point by looking at the minimum of the rank product over all time points in the light-curve set:

$$\beta = \min_j \prod_i r_{ij}.$$

If we test based on β at level α', then the expected number of false positives is

$$\sum_l \alpha' = \alpha' \times \text{number of light-curve sets}.$$

The distribution of β can be evaluated numerically, but it is much easier to work with the rank product at every time point. Given a constraint on the false-positive rate, and given the lengths of the series of interest, and the part of the distribution we are interested in (the tail), it has been found (Coehlo 2010) that there is little difference if we work with β or with the rank product at all time points; the same events will be detected.

3.3. Power of Rank Product Test

The primary advantage of the rank product test is that one can calculate the exact *level* of the test, that is, the probability of measuring a particular rank product under the null hypothesis (no event is present). However, the replacement of the original data by the ranks leads to a loss of *power* of the test, that is, the probability of detection under the alternative hypothesis (an event *is* present). This is due to the loss of information when mapping the photometric measurements onto the rank space.

It is impossible to know how much power is lost by using the rank product test since the underlying distributions of the photometric measurements are not known. However, we can calculate the loss of power when the data are Gaussian by comparing the rank product with the power of the likelihood ratio test (after co-adding the light curves in a light-curve set), which is optimal under the Gaussian assumption. We have performed such a simulation, using $T = 3$ telescopes and light curves of length $N_p = 27,000$. For the simulation, we generated a total of 10^5 light-curve sets. Each light curve is generated with a mean value μ and a noise level σ. To each light-curve set we added a single-point occultation event of depth

$$\delta = a \times \mu,$$

where a is a free parameter. We then found how many events were recovered by each test, using a threshold level of $\alpha = 10^{-10}$. It can be shown (Coehlo 2010) that the power of each statistical test is a function of

$$c = \frac{\delta}{\sigma} = a \times \mathrm{S/N},$$

and is otherwise independent of μ and σ. We thus repeated the test for several values of c, and the results are shown in Figure 5. The top panel of Figure 5 shows the power of the Gaussian and rank product tests as a function of the event depth c, and the bottom panel shows the ratio of the powers of the rank product and Gaussian tests. The power of both tests is very low for occultation event depths $c < 3$. For values of $c \approx 3$, the power of the rank product test is about 70% of the power of the Gaussian test, and for larger values the ratio rapidly approaches one. Also note that for $c > 5$, nearly every event is detected by both tests. Since many occultations produce values of c outside the $3 < c < 5$, and the power reduction is modest inside $3 < c < 5$, we conclude that we do not lose much power in the Gaussian case.

3.4. Detection of Multipoint Occultation Events

If we had an occultation from a large object in the Kuiper Belt, it would cause a substantial flux drop for several consecutive time points, resulting in several values of the rank product that pass the significance threshold. On the other hand, if the object were at 200 AU, it might cause a modest flux drop

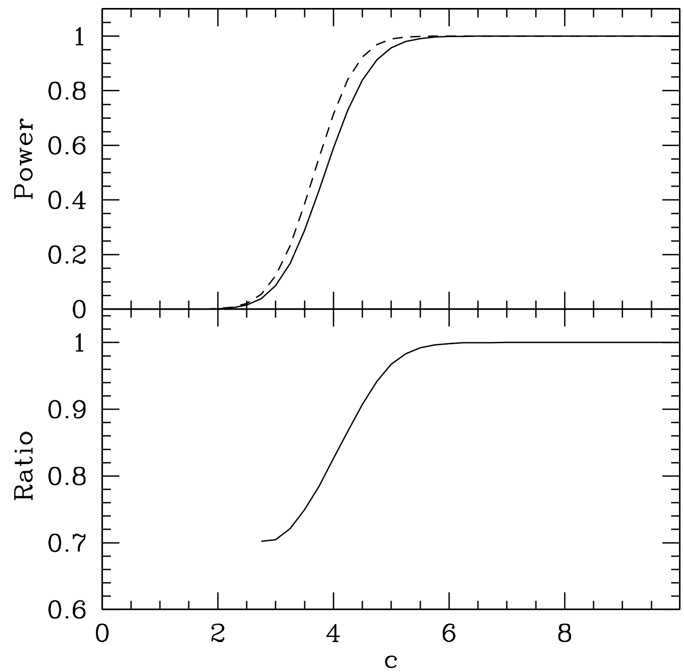

FIG. 5.—*Top panel:* power of the rank product test (*solid line*) and Gaussian test (*dashed line*) as a function of occultation depth c. *Bottom panel:* ratio of the power of the rank product test and the power of the Gaussian test as a function of occultation depth c.

for several time points, none of them big enough to pass the threshold. In the latter case, it is useful to consider functions of the data that look at neighboring time points for detection.

Let our original time series be $f_1, \ldots, f_N$, and suppose we form a new series by

$$a_j = b(f_{j-k}, \ldots, f_j, \ldots, f_{j+k}).$$

For example, b could be a moving average:

$$b(f_{j-k}, \ldots, f_j, \ldots, f_{j+k}) = \frac{1}{2k+1}(f_{j-k} + \ldots + f_{j+k}).$$

The series a_j might show a larger response at the center of the modest signal than f_j, leading to better detection efficiency. Another possibility for b is to take the inner product with some signal. For example, a series of event templates could be used as the function b to search for occultation events from objects of specific sizes and distances, which is what was done by Schlichting et al. (2009), Wang et al. (2010), and Bickerton et al. (2008).

Such manipulation of the data will introduce significant autocorrelation into the light curves. However, if the series f_j is stationary and ergodic in mean, and if k is small relative to the length of the light curves, then it follows that a_j will also be stationary and ergodic in mean, so the rank product distribution will still be satisfied. This is because the autocorrelation structure is expected to be the same throughout the light curve. See Coehlo (2010) for a detailed discussion.

4. LIGHT CURVE FILTERING

As discussed in § 3, the tests based on rank statistics are valid only if the light curves from each telescope are stationary, ergodic in mean, and independent of those from other telescopes. However, in the actual data, significant correlations and nonstationarity are evident, as can be seen in the top left panel of Figure 6. Trends like those evident in the light curves in Figure 6 can arise due to changing air mass and atmospheric transparency throughout the duration of a run. The bottom left panel of Figure 6 shows the rank-rank diagram corresponding to this light-curve set (telescopes A and B are shown). Under the assumption of independence, the points should be distributed uniformly across the diagram; clearly this is not the case.

To solve this problem, we apply a *mean filter* to the light curves in order to remove the slowly varying trends. Each photometric measurement f_j in a light curve is replaced with

$$g_j = f_j - \bar{f}_j,$$

where $\bar{f}_j$ is defined as a 3σ-clipped (Bertin & Arnouts 1996; Da Costa 1992) mean taken over a window of size W_μ which is centered on the point f_j.

After application of the mean filter, we found many light curves that exhibit fluctuations in variance over time. In periods of higher variance, more extreme high or low rank values are more likely, and our assumption on the uniform distribution of ranks throughout a light curve is invalid. We thus correct for changes in the variance by applying a *variance filter*, where we replace every point g_j with

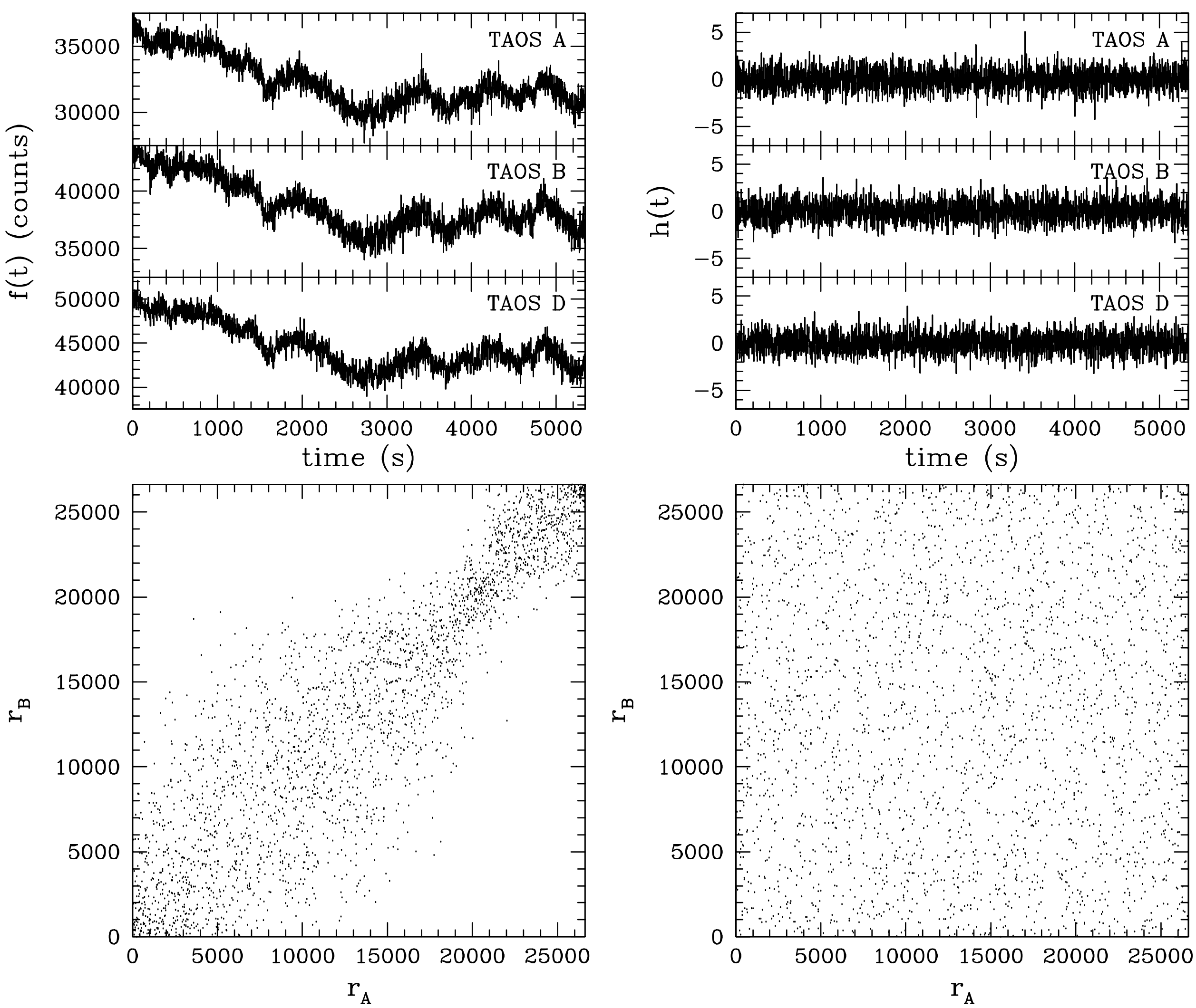

FIG. 6.—*Top left:* an unfiltered three-telescope light-curve set for a single star. Note the correlated variations in the light curves. *Bottom left:* rank-rank diagram for telescopes A and B. *Top right:* same light-curve set after filtering. *Bottom right:* rank-rank diagram after filtering. All four plots are reproduced from Zhang et al. (2008).

$$h_j = \frac{g_j}{\sigma_j},$$

where the standard deviation σ_j is calculated over a window of size W_σ centered on the point g_j, and 3σ clipping is applied here as well.

We want to choose the window sizes to be small enough to accurately correct for high frequency trends, but we also want them large enough to enable accurate determination of $\bar{f}$ and σ. After testing various window sizes, we found that $W_\mu = 33$ and $W_\sigma = 151$ work best (the variance fluctuates much more slowly than the mean, hence the larger window size).

We note that much work has been done in the past on removing such trends from light curves, most of which involves removing correlated trends in light curves from different stars in the same series of images (for example, see Kovács et al. 2005; Tamuz et al. 2005; Bianco et al. 2009). The simpler approach we have adopted works well enough for our purposes, but we are considering adopting similar techniques for future analysis.

The top right panel of Figure 6 shows the same light-curve set shown in the left panel, after filtering. The trends in the mean and variance have clearly been removed. The rank-rank diagram of the filtered light-curve set is shown in the bottom right panel of Figure 6. No dependence is evident in this diagram.

Figure 7 shows autocorrelation functions (ACFs) after application of the mean and variance filters. Three of the panels show ACFs of light curves in the TAOS data after filtering (such as those shown in the top right panel of Fig. 6), and one of them shows the ACF of a synthetic light curve of white noise, after the same filters have been applied. The autocorrelation is insignificant in all cases after a time lag of 6.6 s, which corresponds to the window size W_μ of the mean filter. The ACF of the simulated light curve demonstrates that the observed features in the ACFs are consequences of the mean filter. The small feature in Figure 7a evident at time lag of 30 s is likely due to the variance filter which has a window size of $W_\sigma = 151$ points. The short timescale (relative to the length of the light curve) of the significant autocorrelation features is consistent with our modeling of the filtered light curves as stationary and ergodic in mean, as dependence over longer timescales would invalidate our assumptions that all possible ranks are equally likely at each time point (Coehlo 2010).

While the filter appears to work well on the example light-curve set shown in Figure 6, we still need to quantify how well it actually works. This is important because some data runs may exhibit variations that are not adequately corrected for by the filters we apply. In particular, data runs with extremely rapid fluctuations in the mean (due to fast-moving cirrus clouds or other phenomena) will not be removed if the event width is small when compared with W_μ. This is illustrated in Figure 8, which shows a light-curve set taken during a night with periods of fast-moving cirrus clouds. Significant correlations are evident in the filtered light curves. The corresponding rank-rank diagram of telescopes TAOS A and TAOS B is shown in Figure 9. Significant overdense regions are evident in the lower left and upper right corners of this diagram. In order for the application of the rank statistics to be valid, such data need to be flagged and cut from the data set before the application of the rank product test.

We have thus developed two diagnostic tests to be applied to each light-curve set to assess the quality of the data after the application of the filters. We have found that phenomena inducing correlations in the light-curve sets tend to affect the entire

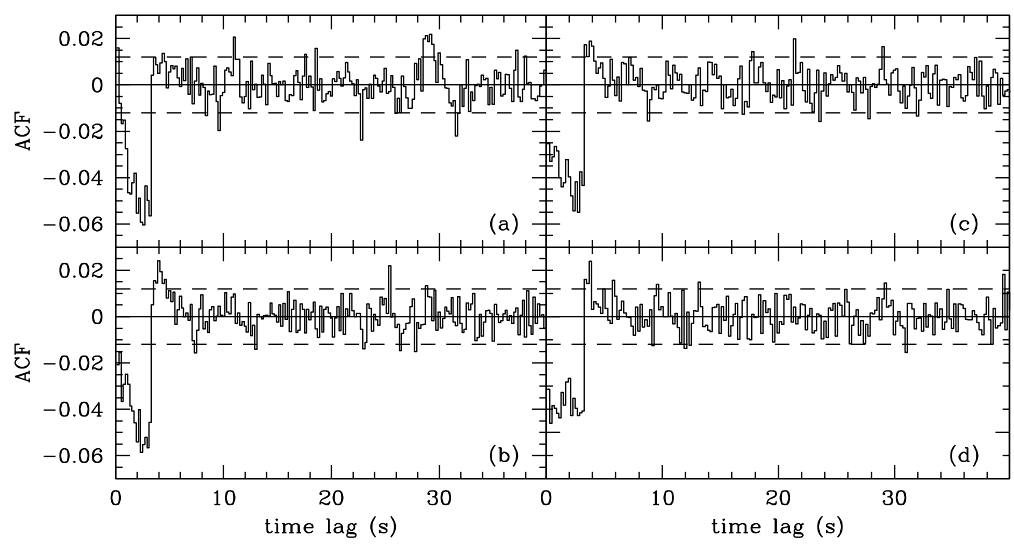

FIG. 7.—Autocorrelation plot from four light curves. Panels (*a*), (*b*), and (*c*): autocorrelation plots from three filtered TAOS light curves. Panel (*d*): autocorrelation plot from a synthetic white-noise light curve, after application of the mean and variance filters. *Dashed lines* are the 95% confidence level limits for what would be expected for randomly distributed light curves.

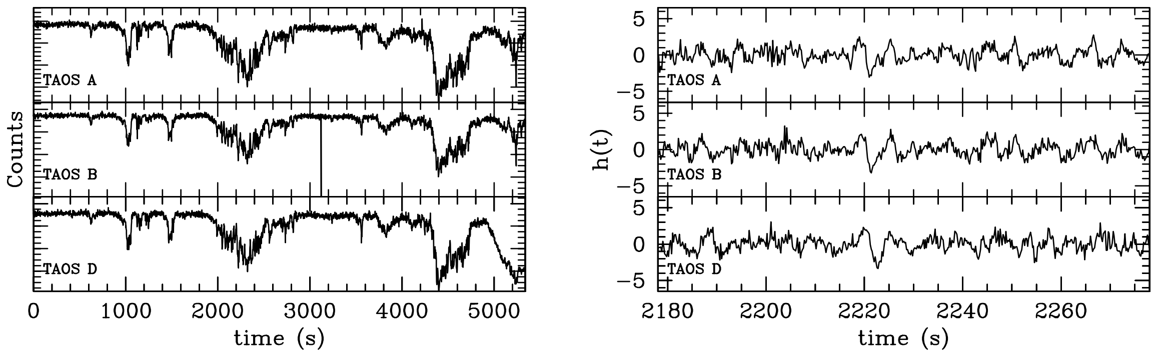

FIG. 8.—*Left panel:* An unfiltered light-curve set on a night with periods of cirrus cloud cover (during the periods of significant flux drops). *Right panel:* the same light-curve set after filtering, zoomed in to a period of cloud cover. Significant correlations are evident. Note that the correlation is stronger between telescopes TAOS A and TAOS B, which are close together (6 m separation). TAOS D, which is about 100 m away, has similar features but they are offset in time.

data run. Therefore, these diagnostic tests (described in the following subsections) are applied to entire data runs rather than individual light-curve sets. Data runs failing these tests are not considered for further analysis. The tests, described in the following subsections, were used in Zhang et al. (2008), Wang et al. (2009) and Bianco et al. (2010). An improved version of these tests has been developed for use in future analysis runs, and these new tests will be described in § 4.4.

4.1. Pearson's χ^2 Statistic

A simple test to determine if the light curves in a light-curve set are dependent is to divide the multi-telescope rank space into a grid and count the number of rank tuples in each grid element.

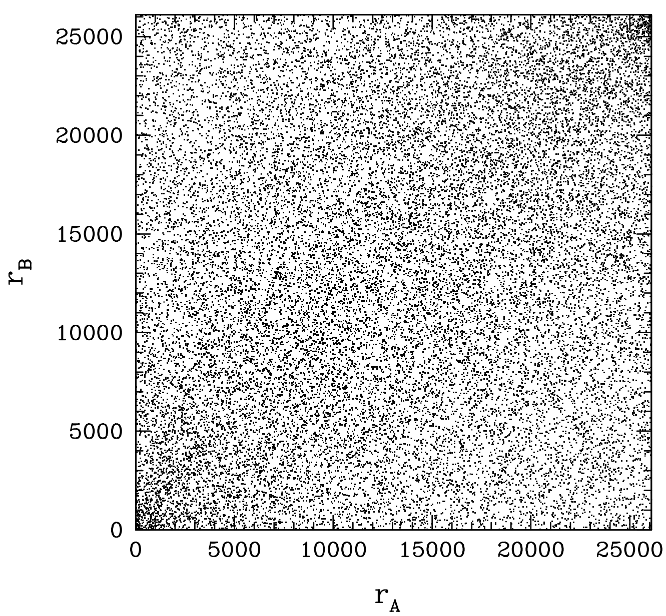

FIG. 9.—Rank-rank diagram (telescopes TAOS A and TAOS B) of the light-curve set shown in Fig. 8. The rank pairs are not uniformly distributed, as there are denser than average regions in the lower left and upper right corners.

This is illustrated in the left panel of Figure 10, in the case of two telescopes where the rank-rank diagram is divided into a $N_{\rm g} \times N_{\rm g}$ grid, where $N_{\rm g} = 3$. With $N_p = 9$ and 9 grid elements, the expected number of rank pairs in each grid element is 1.

One can then perform a Pearson's χ^2 test on the number of rank pairs in each grid element by calculating

$$\chi^2 = \sum_{i=1}^{N_{\rm g}^T} \frac{(O_i - \mathbb{E}_i)^2}{\mathbb{E}_i},$$

where O_i is the observed number of rank tuples in grid element i, and

$$\mathbb{E}_i = \frac{N_p}{N_{\rm g}^T}$$

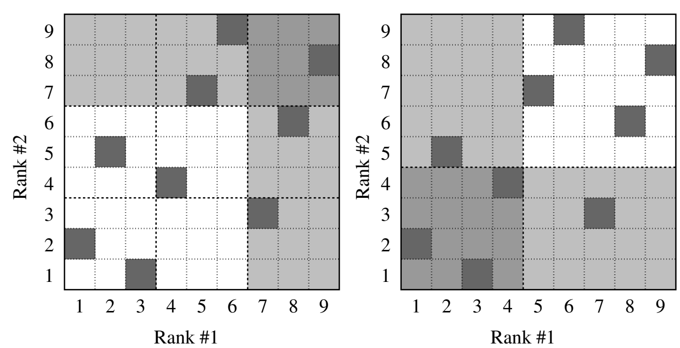

FIG. 10.—*Left panel:* rank-rank diagram illustrating the Pearson's χ^2 test. The rank-rank diagram is divided into a $N_{\rm g} \times N_{\rm g}$ grid ($N_{\rm g} = 3$ in this case), and the number of rank pairs in each box is tabulated and compared with the expected uniform distribution. Counts in the gray elements are not free parameters. *Right panel:* rank-rank diagram illustrating the hypergeometric test. The test counts the number of objects in the lower left corner (*dark shaded region*) of the rank-rank diagram, in this case with a box size of $R = 4$. Note that there are four rank doublets with $r_{1j} \leq 4$ and four rank doublets with $r_{2j} \leq 4$ (*light shaded regions*) since each rank must occur exactly once in a light-curve set for each telescope. In this case there are three rank doublets where $r_{ij} \leq 4$ for both telescopes.

is the expected number of rank tuples in grid element i. (Note that $\mathbb{E}_i$ may vary slightly among grid elements if N_p is not an exact multiple of N_{g}.)

For a given data run, we expect the distribution of the Pearson's χ^2 statistic to follow the χ^2 distribution, given by

$$p(u_c, \nu) = \frac{1}{2^{\nu/2}\Gamma(\nu/2)} u_c^{(\nu/2)-1} e^{-u_c/2}, \tag{7}$$

where $u_c = \chi^2$ and ν is the number degrees of freedom. The derivation of ν can be illustrated by Figure 10. It is important to note that every rank must appear once and only once in the time series for each telescope, and this constrains the value of ν. The degrees of freedom is the number of cells in the grid minus the number of independent constraints. First, the cell counts must sum to N_p, giving one constraint. Secondly, the counts in each grid row and each grid column must sum to three, giving two constraints on the three rows and on the three columns which are independent of each other and of the first constraint. Thus the total degrees of freedom are $9 - 2 - 2 - 1 = 4$. To illustrate, note that in the left grid column, the ranks 1, 2, and 3 must appear in telescope 1. Therefore, for telescope 2, since there are two doublets in the bottom left grid element and one doublet in the middle left grid element, there must be zero doublets in the top left element. The gray grid elements in the rank-rank diagram are thus not free parameters. For an arbitrary number of telescopes T, the number of degrees of freedom can be shown to be equal to

$$\nu = N_{\mathrm{g}}^T - T(N_{\mathrm{g}} - 1) - 1.$$

4.2. The Hypergeometric Test

While the Pearson's χ^2 test validates that the rank tuples are spread uniformly over $\{1 \ldots N_p\}^T$, it is also useful to demonstrate that there is no bias toward rank quadruplets with all ranks relatively low, since these are the target events in the survey. Given a rank limit R, we define the variable u_{h} as the number of rank quadruplets with $r_{ij} \leq R$ for all telescopes i. This is illustrated in the case of two telescopes in the right panel of Figure 10, where we choose $R = 4$. In this figure, $u_{\mathrm{h}} = 3$ is the number of rank doublets in the shaded lower left corner of the rank-rank diagram. Note that with $R = 4$ there are exactly four rank doublets with both $r_{1j} \leq R$ and $r_{2j} \leq R$. The probability distribution of the number of rank doublets with *both* ranks $r_{ij} \leq R$ is given by the hypergeometric distribution

$$\mathbb{P}(U = u_{\mathrm{h}}) = \frac{\binom{R}{u_{\mathrm{h}}}\binom{N_p - R}{R - u_{\mathrm{h}}}}{\binom{N_p}{R}}, \tag{8}$$

where $u_{\mathrm{h}} \leq R$ (if $u_{\mathrm{h}} > R$ then $\mathbb{P} = 0$).

To expand this calculation to more than two telescopes, we use the *law of total probability* to calculate

$$\mathbb{P}(U_{i+1} = u_{\mathrm{h}}) = \sum_{l=u_{\mathrm{h}}}^{R} [\mathbb{P}(U_{i+1} = u_{\mathrm{h}} | U_i = l) \times \mathbb{P}(U_i = l)], \tag{9}$$

where u_{h} is the number of measurements with $r \leq R$ on all telescopes 1 to $i + 1$. The conditional probability is defined as

$$\mathbb{P}(U_{i+1} = u_{\mathrm{h}} | U_i = l) = \frac{\binom{R}{u_{\mathrm{h}}}\binom{N_p - R}{l - u_{\mathrm{h}}}}{\binom{N_p}{l}}, \tag{10}$$

given that each rank must occur exactly once for each telescope,

$$\mathbb{P}(U_1 = l) = \delta_{lR},$$

and one can thus expand equation (9) to include an arbitrary number of telescopes.

4.3. Application of Diagnostic Statistics

To date, the TAOS project has only analyzed data sets with light curves from three telescopes (Bianco et al. 2010; Wang et al. 2009; Zhang et al. 2008). Therefore we only describe the application of the diagnostic tests to three-telescope data. The development of these tests was a work in progress when the results presented in Bianco et al. (2010); Wang et al. (2009); Zhang et al. (2008) were calculated, and an improved method is described in § 4.4. However, we now present the original methods used to apply the diagnostic tests to the data to illustrate what was done to derive our previously published results. We note that for any analysis of TAOS data we will perform in the future, we will use the improved methods described in § 4.4.

For each data run, we apply both the Pearson's χ^2 statistic u_c and the hypergeometric test statistic u_{h} to each light-curve set. For the Pearson's χ^2 test, we use a grid size of $N_{\mathrm{g}} = 5$, which corresponds to a total of $\nu = 112$ degrees of freedom. For the hypergeometric test, we set $R = N_p/5$, rounding to the nearest integer. (A typical 90 minute data run will have $N_p = 27,000$, but many runs are truncated due to bad weather.) Due to the fact that any correlations in the data may not show up in light curves with low S/N values, we perform the diagnostic tests only on those light-curve sets with S/N ≥ 10. Details of the algorithm used to calculate S/N values of our light curves are given in Zhang et al. (2009). To summarize, we first calculate a 5σ-clipped rolling mean similar to that calculated in the mean filter, and then average the value of the rolling mean to get the signal. We then subtract the rolling mean from the raw light curve, and calculate a 5σ-clipped standard deviation of the new light curve, which we use as an estimate of the noise.

Even in the case of completely independent light curves, random chance will give rise to a number individual light-curve sets with aberrant values of the test statistic. We therefore look at the ensemble of test statistics for each data run, and require a match to the theoretical distributions. A set of examples is shown in Figure 11. The top panels show histograms of u_c and $u_{\rm h}$ for all of the light-curve sets in a data run with no evident dependence among the light curves, and the bottom panels show the same data for the pathological data run that contains the light-curve sets shown in Figures 8 and 9. Clearly, the data shown in the top panels match the theoretical distribution quite well, while the data in the bottom panels do not.

To determine which data runs are to be rejected, we test the goodness of fit of the distribution of test statistics over the light-curve sets in a data run to their theoretical distributions. To set a threshold, for each data run we calculate the quantity $D_{\rm max}$, which is defined as the absolute value of the maximum difference between the cumulative distribution of measured test statistics and the theoretical cumulative probability distribution. This is analogous to the Kolmogorov-Smirnov test (see Press et al. 1994, and references therein). For each data run, we calculate $D_{\rm max}$ for both the Pearson's χ^2 test and the hypergeometric test. A scatter plot of these values is shown in Figure 12.

Data runs that fail either of the two tests are removed from the occultation event search. For data runs exhibiting widespread dependence between the light curves from different telescopes, we expect the measured distributions to differ significantly from the theoretical distributions, giving rise to large values of $D_{\rm max}$. Visual inspection of several data runs indicated that setting a cut on $D_{\rm max} > 0.2$ allowed us to reject nearly all of the runs where the light curves exhibit clear, widespread dependence.

4.4. Improved Application of Diagnostic Tests

While the diagnostic tests described in the previous section are sufficient to remove nearly all of the data runs with significant dependence between light curves from different telescopes, they suffer from some limitations which motivated us to improve the techniques. First, the threshold $D_{\rm max}$ was chosen somewhat arbitrarily after visual inspection of many data sets, since there is no way to determine empirically what the optimum threshold actually is. Second, in order for the measured statistical distributions to match the theoretical χ^2 and hypergeometric distributions, the original time series data in the light curves are required to be independent and identically distributed (i.i.d.), which is a stricter requirement than stationary and ergodic in mean. If some autocorrelation structure were present in the light curves, the light curves could still be stationary and independent from each other, however, the test statistics would not be expected to match the theoretical distributions. Finally, and most importantly, we would like to apply the same tests to light curves when searching for multipoint events. As discussed in § 3.4, for such event searches we would take a moving average of the light-curve data, or perhaps take the inner product of the light curve with some event template. Such filtering will induce autocorrelations into the light curves, and increase the S/N values as well. If we increase the S/N enough, some insignificant correlations between the light curves might in fact become significant in the filtered data. So it would be useful to apply the diagnostic tests to the data runs after the application of these

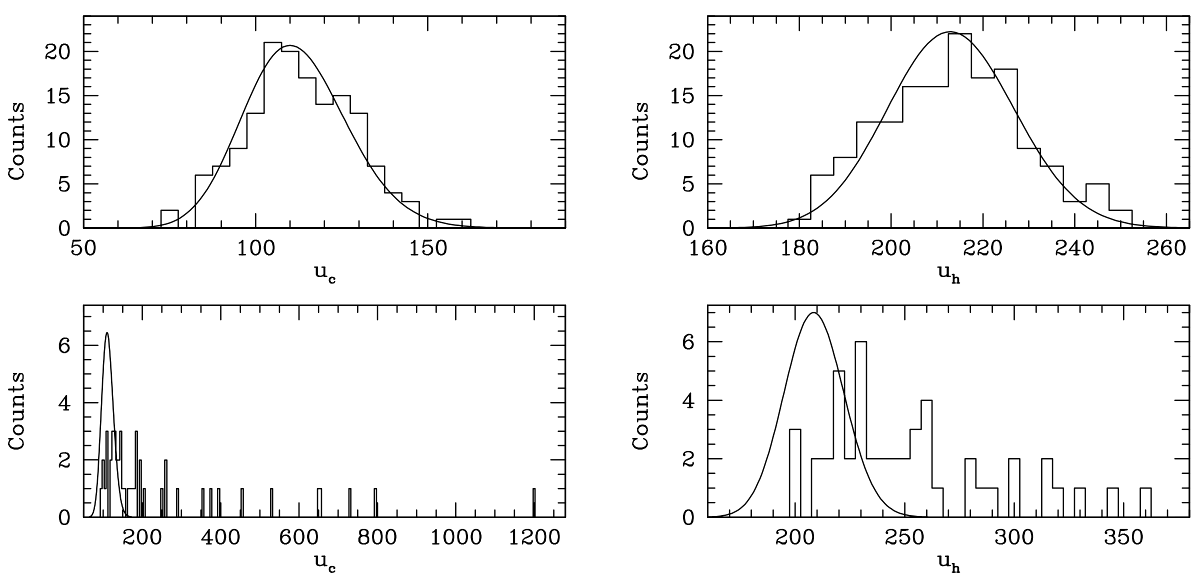

FIG. 11.—Results of diagnostic tests. *Histograms* indicate actual data, and *solid lines* indicate theoretical distributions. *Top panels:* Pearson's χ^2 test (*left*) and hypergeometric test (*right*) for a data run with no evident dependence between telescopes. *Bottom panels:* same as top panels, but for a data run with significant dependence between light curves. The light-curve set shown in Figs. 8 and 9 comes from this data run.

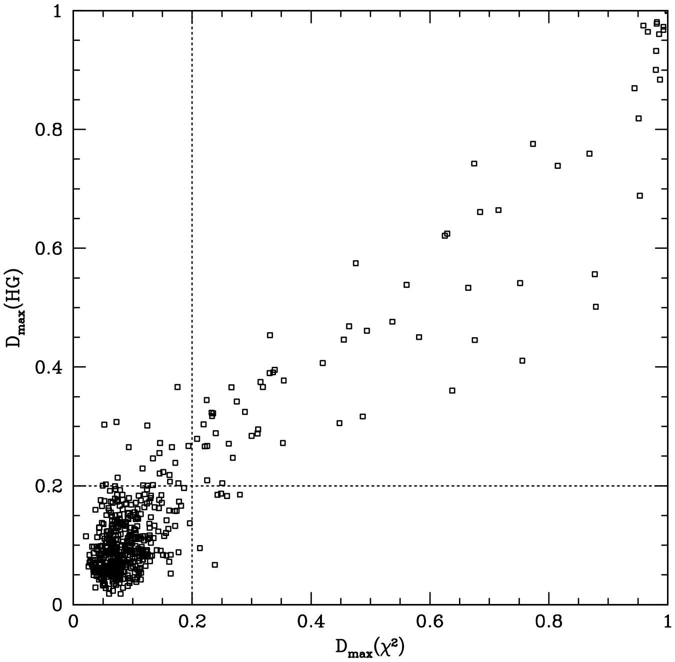

FIG. 12.—Scatter plot showing $D_{\max}$ values for the Pearson's χ^2 test (x-axis) and hypergeometric test (y-axis). Each point corresponds to a single data run. For each test statistic, we reject data runs with $D_{\max} > 0.2$ (*dotted lines*).

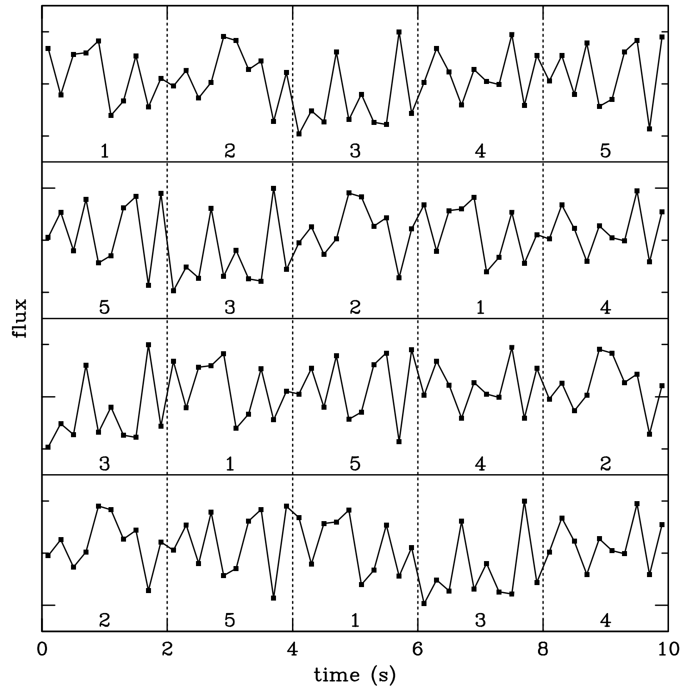

FIG. 13.—Illustration of the BBS test. *Top panel:* original light curve, divided into five blocks of data (*dotted lines*). *Bottom panels:* four light curves with the blocks permuted randomly. Blocks are labeled 1 through 5 for reference.

filters. However, the introduction of significant autocorrelations into the light-curve data will more or less guarantee that all of the data runs will fail the diagnostic tests since the light curves will not be i.i.d.

We have thus developed a new technique based on the Blockwise Bootstrap (Künsch 1989) method (hereinafter BBS), which uses both the Pearson's χ^2 statistic u_c and the hypergeometric statistic $u_{\rm h}$, described earlier, but requires no assumptions about the theoretical distributions for either statistic. The BBS test is implemented as follows. First, for a given light-curve set, we calculate both u_c and $u_{\rm h}$. Then we divide each light curve in the light-curve set into 100 subsets, or *blocks*, of data. We then permute the blocks randomly, with each light curve in the light-curve set undergoing a different random permutation, and recalculate the diagnostic test statistics. We repeat this step a total of 99 times, and we are thus left with 100 statistical measurements for each of the diagnostic tests.

This is illustrated schematically in Figure 13. The top panel shows the original, unpermuted light curve, divided into five blocks. The blocks are labeled 1 through 5 for clarity. The bottom four panels show the same light curve with the five blocks randomly permuted. Note that the data within each block remain unchanged.

For each diagnostic test, we have now calculated 100 different values, one for the original light-curve set and 99 for the randomly permuted light-curve sets. If we permute the blocks we still preserve the stationary structure as long as the block size is large in comparison to the time scale of any autocorrelation. So if the light curves are independent, our 100 values are like 100 independent draws from the same distribution. Thus, if we rank each of the series of 100 test statistics from 1 to 100 (where a rank of one corresponds to the largest value of u_c or $u_{\rm h}$, which would be the worst match to the expected distribution), the ranks should be uniform and we can calculate associated p-values as

$$\mathbb{P}(V < v_c) = \frac{v_c}{100} \tag{11}$$

and

$$\mathbb{P}(V < v_{\rm h}) = \frac{v_{\rm h}}{100}, \tag{12}$$

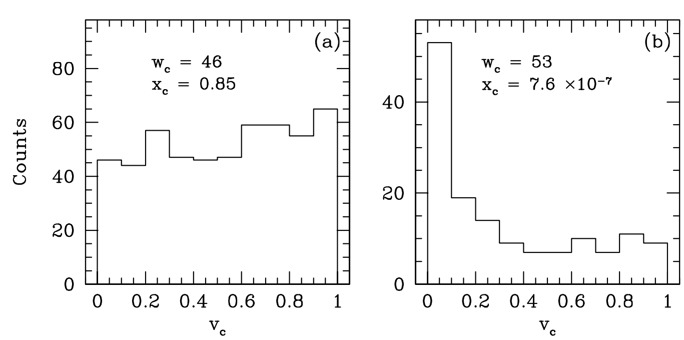

FIG. 14.—(a): distribution of p-values v_c from the Pearson's χ^2 test from a good data run. (b): same plot for a rejected data run.

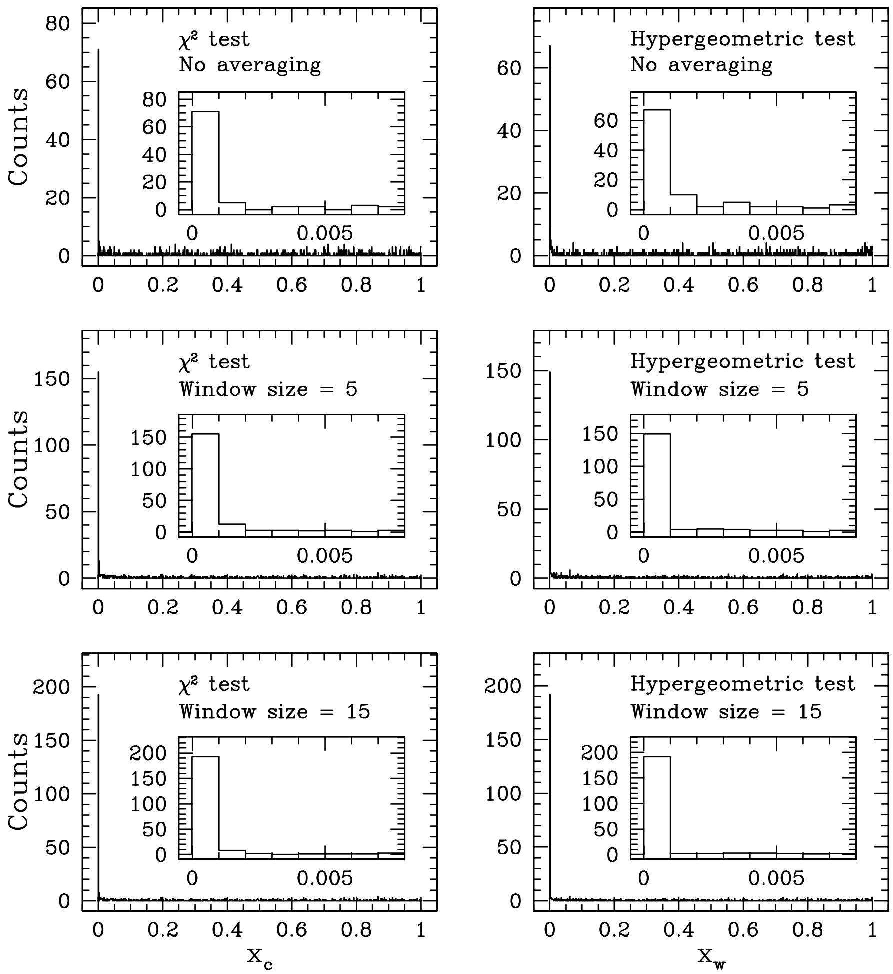

FIG. 15.—(*a*): Distribution of p-values from all data runs in the data set described in Bianco et al. (2010) for both the χ^2 and hypergeometric tests, with the original data and data after the application of moving average filters with window sizes of 5 and 15. *Inset plots* are zoomed in to the lowest p-values. The excess counts in the lowest bins are the runs exhibiting significant correlations between the telescopes.

where v_c and v_h correspond to the ranks of the test statistics u_c and u_h from the unpermuted (original) light-curve sets.

The BBS test is then performed on every light-curve set in a data run with $\mathrm{S/N} > 10$. In the case of a data run that does not exhibit any strong dependence between the telescopes, the p-values v_c and v_h should be uniformly distributed on $\{0.01, \ldots, 1\}$. However, in the case where there is significant dependence between the telescopes, we would expect the distributions of v to be clustered at small values, since any correlation between the telescopes would disappear when the blocks are randomly permuted. This is illustrated in Figure 14, which shows a histogram of the values v_c from each light-curve set in two different data runs. The histogram in Figure 14a shows the results from a data run with little dependence between the telescopes, while Figure 14b shows a data run with strong dependence.

In order to quantify the amount of dependence between the telescopes in a data run, we define two new test statistics, w_c and w_h, which are defined as the number of light-curve sets in a data run with $v_c < v_\mathrm{t}$ and $v_\mathrm{h} < v_\mathrm{t}$ respectively, where we choose $v_\mathrm{t} = 0.1$[15] (This corresponds to the lowest bin in the histograms shown in Fig. 14). In the case of independence between telescopes, the distributions of w_c and w_h follow the binomial distribution of the form

$$p(w_c) = \binom{L}{w_c} v_\mathrm{t}^{w_c}(1 - v_\mathrm{t})^{L-w_c},$$

$$p(w_\mathrm{h}) = \binom{L}{w_\mathrm{h}} v_\mathrm{t}^{w_\mathrm{h}}(1 - v_\mathrm{t})^{L-w_\mathrm{h}},$$

where L is the number of light-curve sets with $\mathrm{S/N} > 10$ in the data run that are used to calculate the test statistics u_c and u_h.

[15] Tests have shown that as long as v_t is relatively small, the exact value chosen for v_t has no significant effect on the final results.

Using these distributions, we can calculate two test statistics for the entire data run, which we define as

$$x_c(w_c) = \mathbb{P}(W > w_c), \qquad x_\mathrm{h}(w_\mathrm{h}) = \mathbb{P}(W > w_\mathrm{h}).$$

For the data run in Figure 14a, we thus calculate $x_c = 0.85$, while for the data run in Figure 14b, we have $x_c = 7.6 \times 10^{-7}$.

We can now reject a data run for significant dependence by setting thresholds on x_c and x_h. In the absence of any significant dependence, the values of x_c and x_h should be distributed uniformly on the interval $[0, 1]$. Plots of the distributions of x_c and x_h statistics are shown in Figure 15. In order to illustrate the application of the BBS test to multipoint occultation searches, we also show the distributions after taking moving averages on the light curves with bin sizes of 5 and 15. The histograms shown have a bin size of 0.001, and with a total of 524 data runs we expect a value of about 0.5 for each bin. However, while the distributions appear to be uniform over most of the ranges in x values, note the large number of counts in the lowest bins. These are the light-curve sets that show dependence between telescopes. Note that some of the histograms show a slight excess in the second bin as well. By rejecting all data runs that appear in the first two bins ($x_c \leq 0.002$ and $x_\mathrm{h} \leq 0.002$), we are clearly rejecting nearly all of the data runs exhibiting widespread dependence between the telescopes. Note that we only expect a total of one data run in the first two bins from random chance.

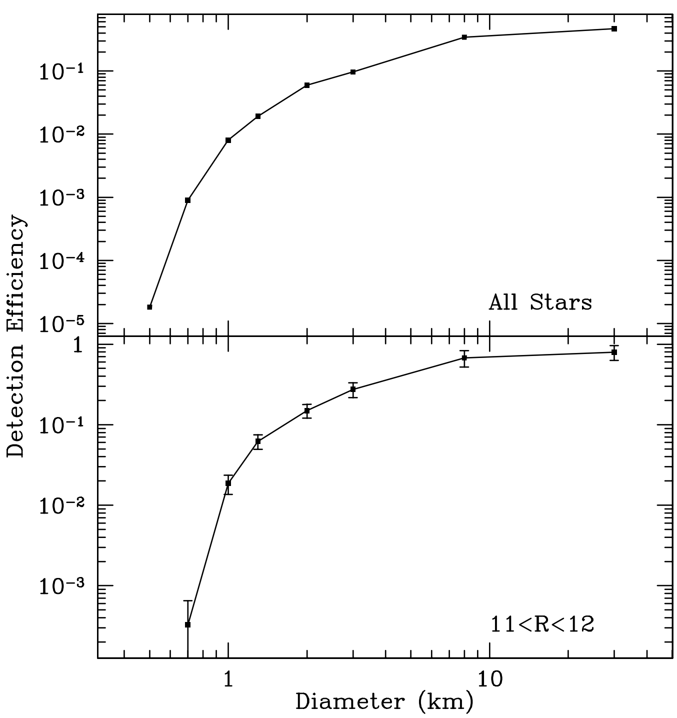

FIG. 16.—*Top panel:* detection efficiency vs. diameter for results published in Bianco et al. (2010) for all stars in the data set. *Bottom panel:* same as top panel, but only for stars with magnitudes $11 < R < 12$.

Note that our thresholds on x_c and x_h of 0.002 are based on the fact that the distributions of these values are uniform above these thresholds as expected, and there are spikes where we expect to find the worst data runs. These are reasonable choices of thresholds, given the clear changes in the distributions of x values from each of the tests. However, we note that there is no underlying theory which would allow one to set an optimal threshold. Our choice of threshold is thus context and data driven and not motivated by optimality conditions. The thresholds on these values will thus be determined on a case by case basis for future analyses.

Finally, note that in Figure 15, the larger the bin size on the moving average, the more data runs that are rejected. This is because of low level correlations that are insignificant in the unbinned data, but become significant in the binned data due to the increased S/N of the binned light curves.

The BBS test is clearly a superior method to the simple comparison of the test statistics to their theoretical distributions. It is very clear where the thresholds on x_c and x_h should be, the test will not reject data runs where the light curves are stationary but not i.i.d., and the tests are capable of robustly rejecting data runs when performing searches for multipoint occultation events.

5. CONCLUSION

We have developed a technique to search for extremely rare coincident events in voluminous multivariate (multi-telescope) time series data. Using rank statistics, this technique enables robust determination of event significance and false-positive rate, *independent of the underlying noise distributions in the time series data.* Furthermore, we have developed a method to test for widespread dependence between light curves in a data run, which allows us to reject runs with inherent characteristics that could possibly give rise to a larger false-positive rates. We note that while the method described in this article is sufficient for the calculation of the rate of false-positive events that arise due to random statistical chance, it is not capable of estimating the background event rate due to systematic errors in the TAOS photometry (Zhang et al. 2009). For example, tracking errors or moving objects in the images could give rise to false detections in the data set. A description of how such background events are handled is described in Bianco et al. (2010).

This method has been used to search for rare occultation events by KBOs in over 500 data runs comprising a total of nearly 370,000 light-curve sets (Bianco et al. 2010). To calculate the upper limit on the size distribution, we performed a simulation in which simulated events were added to the light-curve data. A search algorithm based on the statistical algorithm described in this article was then used to measure our detection efficiency. The results are shown in Figure 16. The top panel shows our detection efficiency as a function of object diameter averaged over all of the light-curve sets in the data set. In this plot, all of the detection efficiency at the small end comes from the brightest stars with the highest S/N. At the larger end, the efficiency reaches a maximum of about 47%. This is due to the inclusion of many faint stars in the data set with such low S/N values that any event is virtually undetectable. (Note that the inclusion of these stars in the data set has no bearing on the final upper limit). In order to better illustrate the effectiveness of the search algorithm, we plot the detection efficiency as a function of diameter only for those stars with magnitudes $11 < R < 12$ in the bottom panel of Figure 16. (We thus exclude the very bright stars with the highest S/N, as well as the faint stars with which no events are detectable). The detection efficiency is very high for objects with diameters $D \gtrsim 3$ km, and drops rapidly when $D < 1$ km.

Finally, we note that the rank product test is useful only for the rejection of the null hypothesis that no occultation event is present, and to estimate the false-positive rate. In order to definitively show that outer solar system objects have been detected, a number of events would need to be detected in order to correlate the surface density with ecliptic latitude. Any physical parameters of an occulting object (such as size and distance) can be estimated for high S/N events from the shape of the light curves (Nihei et al. 2007). However, this would be difficult to do with the TAOS data, primarily due to the relatively slow cadence of the TAOS observations. (Some limited size and distance information could be determined for occultations by objects well beyond 100 AU [Wang et al. 2009]). Surveys with a higher readout rate would in fact be able to make reasonable estimates of these physical parameters for high S/N events (Schlichting et al. 2009; Bickerton et al. 2009, 2008; Roques et al. 2006, 2003; Chang et al. 2007), and a next generation multi-telescope occultation survey (TAOS II, currently in the early development stage), which will operate with a readout cadence of 20 Hz, will also be able to do so after using the rank product method to identify candidate events.

This work was supported in part by the thematic research program AS-88-TP-A02 at Academia Sinica. N. K. C.'s work was supported in part by the National Science Foundation under grant DMS-0636667. Work at the Harvard College Observatory was supported in part by the National Science Foundation under grant AST-0501681 and by NASA under grant NNG04G113G. The work at National Central University was supported by the grant NSC 96-2112-M-008-024-MY3. J. A. R.'s work was supported in part by the National Science Foundation under grant AST-00507254. S. L. M.'s work was performed under the auspices of the US Department of Energy by Lawrence Livermore National Laboratory in part under Contract W-7405-Eng-48 and by Stanford Linear Accelerator Center under Contract DE-AC02-76SF00515. Y. I. B. acknowledges the support of National Research Foundation of Korea through Grant 2009-0075376. K. H. C.'s work was performed under the auspices of the US Department of Energy by Lawrence Livermore National Laboratory in part under Contract W-7405-Eng-48 and in part under Contract DE-AC52-07NA27344.

APPENDIX

EVALUATION OF THE *K* FUNCTION

Here we present an algorithm to evaluate $K(x; k, n)$, the number of ways to get a product of x by multiplying k integers between 1 and n, which is applicable when $x \leq n$.

Note that $K(1; k, n) = 1$. For $x > 1$, consider the prime decomposition of x where the ps are unique primes and d is their degree so that:

$$x = p_1^{d_1} \times p_2^{d_2} \times \ldots \times p_m^{d_m},$$

where m is the total number of prime factors of x.

We claim that

$$K(x; k, n) = \prod_{i=1}^{m} \binom{d_i + k - 1}{k - 1}.$$

A1. Proof

Suppose $A_1 \times A_2 \times \ldots \times A_k = x$ and take prime decompositions of each number

$$\begin{aligned}
A_1 &= p_1^{d_{1,1}} \times p_2^{d_{1,2}} \times \ldots \times p_m^{d_{1,m}} \\
A_2 &= p_1^{d_{2,1}} \times p_2^{d_{2,2}} \times \ldots \times p_m^{d_{2,m}} \\
\vdots \quad &\quad \vdots \\
A_k &= p_1^{d_{k,1}} \times p_2^{d_{k,2}} \times \ldots \times p_m^{d_{k,m}}.
\end{aligned}$$

Note that

$$\sum_{i=1}^{k} d_{i,j} = d_j \quad \forall\ j.$$

Hence,

$$K(x; k, n) = \prod_{i=1}^{m} S(d_i; k),$$

where $S(d; k)$ is the number of ways to get a sum of d by adding k integers where $0 \leq k \leq d$. The calculation of the function S is best illustrated with an example. Consider the case of $d = 10$ and $k = 4$. If we illustrate the sum $d = 10$ with 10 dots in the top row of Figure 17, the function S is simply the number of ways to divide the dots into 4 groups (using the bars shown).

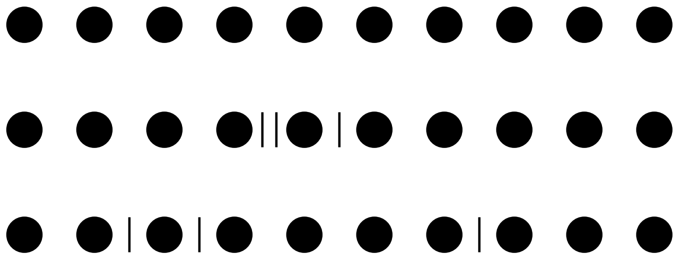

FIG. 17.—Schematic illustrating the calculation of the function $S(d;k)$. In this case, $d = 10$, as indicated by the top row of 10 dots. The bars in the bottom two rows indicate possible ways to split the 10 dots into four addends. The second row indicates the tuple (4,0,1,5), and the third row indicates the tuple of (2,1,4,3).

For example, the second row of Figure 17 corresponds to a tuple of (4,0,1,5), while the third row corresponds to a tuple of (2,1,4,3). So the number of possible 4-tuples is the number of ways to choose 3 bar locations in a total $10 + 3 = 13$ possibilities. This gives

$$S(d;k) = \binom{d+k-1}{k-1}.$$

For example, to calculate $K(6;4,n)$ where $n \geq 6$, we note that $6 = 2 \times 3$ is the product of two primes to the first power, and in the four-telescope case it is equal to

$$K(6;4,n) = \binom{1+4-1}{4-1}^2 = \binom{4}{3}^2 = 4^2 = 16,$$

in agreement with Table 1. Note that this formulation is only valid if $x \leq n$. For example, $K(6;4,5) = 12$, since any of the rank tuples with a rank value of 6 would be impossible in a light-curve set containing only 5 points.

As a second example, for the case of $360 = 2^3 \times 3^2 \times 5$, we have three primes with degrees 3, 2, and 1. We thus have (for $n \geq 360$)

$$K(360;4,n) = \binom{3+4-1}{4-1}\binom{2+4-1}{4-1}\binom{1+4-1}{4-1}$$
$$= \binom{6}{3}\binom{5}{3}\binom{4}{3} = 20 \times 10 \times 4 = 800.$$

REFERENCES

Bertin, E., & Arnouts, S. 1996, A&AS, 117, 393
Bianco, F. B., et al. 2009, AJ, 138, 568
———. 2010, AJ, 139, 1499
Bickerton, S. J., Kavelaars, J. J., & Welch, D. L. 2008, AJ, 135, 1039
Bickerton, S. J., Welch, D. L., & Kavelaars, J. J. 2009, AJ, 137, 4270
Brown, M. E., Trujillo, C., & Rabinowitz, D. 2004, ApJ, 617, 645
Chang, H.-K., et al. 2007, MNRAS, 378, 1287
Coehlo, N. K. 2010, Ph.D thesis, Univ. California, Berkeley
Cooray, A. 2003, ApJ, 589, L97
Cooray, A., & Farmer, A. J. 2003, ApJ, 587, L125
Da Costa, G. S. 1992, in ASP Conf. Ser. 23, Astronomical CCD Observing and Reduction Techniques, ed. S. B., Howell, 90
Fisher, R. A. 1958, Statistical Methods for Research Workers (New York: Hafner)
Kovács, G., Bakos, G., & Noyes, R. W. 2005, MNRAS, 356, 557
Künsch, H. R. 1989, Ann. Stat., 17, 1217
Lehner, M. J., et al. 2006, Astron. Nachr., 327, 814
———. 2009, PASP, 121, 138
Mosteller, F. J., & Fisher, R. J. 1948, The American Statistician, 2, 30
Nihei, T. C., et al. 2007, AJ, 134, 1596
Press, W. H., et al. 1994, Numerical Recipes in C (New York: Cambridge Univ. Press)
Roques, F., et al. 2003, ApJ, 594, L63
———. 2006, AJ, 132, 819
Schlichting, H. E., et al. 2009, Nature, 462, 895
Tamuz, O., Mazeh, T., & Zucker, S. 2005, MNRAS, 356, 1466
———. 2009, AJ, 138, 1893
———. 2010, AJ, 139, 2003
Zhang, Z.-W., et al. 2009, PASP, 121, 1429
Zhang, Z.-W., et al. 2008, ApJ, 685, L157

The Astronomical Journal, 139:2026–2033, 2010 May
doi:10.1088/0004-6256/139/5/2026

THE TAIWANESE–AMERICAN OCCULTATION SURVEY PROJECT STELLAR VARIABILITY. II. DETECTION OF 15 VARIABLE STARS

S. Mondal[1,2], C. C. Lin[1], W. P. Chen[1], Z.-W. Zhang[1], C. Alcock[3], T. Axelrod[4], F. B. Bianco[3,5,6,7], Y.-I. Byun[8], N. K. Coehlo[9], K. H. Cook[10], R. Dave[11], D.-W. Kim[8], S.-K. King[12], T. Lee[12], M. J. Lehner[3,5,12], H.-C. Lin[1], S. L. Marshall[10,13], P. Protopapas[3,11], J. A. Rice[9], M. E. Schwamb[14], J.-H. Wang[1,12], S.-Y. Wang[12], and C.-Y. Wen[12]

[1] Institute of Astronomy, National Central University, 300 Jhongda Road, Jhongli 32054, Taiwan; soumen@aries.res.in
[2] Aryabhatta Research Institute of Observational Sciences, Manora Peak, Nainital-263129, India
[3] Harvard-Smithsonian Center for Astrophysics, 60 Garden Street, Cambridge, MA 02138, USA
[4] Steward Observatory, 933 North Cherry Avenue, Room N204, Tucson, AZ 85721, USA
[5] Department of Physics and Astronomy, University of Pennsylvania, 209 South 33rd Street, Philadelphia, PA 19104, USA
[6] Department of Physics, University of California Santa Barbara, Mail Code 9530, Santa Barbara, CA 93106-9530, USA
[7] Las Cumbres Observatory Global Telescope Network Inc., 6740 Cortona Dr., Suite 102, Santa Barbara, CA 93117, USA
[8] Department of Astronomy, Yonsei University, 134 Shinchon, Seoul 120-749, Republic of Korea
[9] Department of Statistics, University of California Berkeley, 367 Evans Hall, Berkeley, CA 94720, USA
[10] Institute for Geophysics and Planetary Physics, Lawrence Livermore National Laboratory, Livermore, CA 94550, USA
[11] Initiative in Innovative Computing at Harvard, 120 Oxford Street, Cambridge, MA 02138, USA
[12] Institute of Astronomy and Astrophysics, Academia Sinica, P.O. Box 23-141, Taipei 106, Taiwan
[13] Kavli Institute for Particle Astrophysics and Cosmology, 2575 Sand Hill Road, MS 29, Menlo Park, CA 94025, USA
[14] Division of Geological and Planetary Sciences, California Institute of Technology, 1201 East California Boulevard, Pasadena, CA 91125, USA
Received 2009 September 22; accepted 2010 March 8; published 2010 April 8

ABSTRACT

The Taiwanese–American Occultation Survey (TAOS) project has collected more than a billion photometric measurements since 2005 January. These sky survey data—covering timescales from a fraction of a second to a few hundred days—are a useful source to study stellar variability. A total of 167 star fields, mostly along the ecliptic plane, have been selected for photometric monitoring with the TAOS telescopes. This paper presents our initial analysis of a search for periodic variable stars from the time-series TAOS data on one particular TAOS field, No. 151 (R.A. = $17^{\mathrm{h}}30^{\mathrm{m}}6^{\mathrm{s}}.7$, decl. = $27°17'30''$, J2000), which had been observed over 47 epochs in 2005. A total of 81 candidate variables are identified in the 3 deg^2 field, with magnitudes in the range $8 < R < 16$. On the basis of the periodicity and shape of the light curves, 29 variables, 15 of which were previously unknown, are classified as RR Lyrae, Cepheid, δ Scuti, SX Phonencis, semi-regular, and eclipsing binaries.

Key words: methods: data analysis – stars: imaging – stars: variables: Cepheids – stars: variables: delta Scuti – stars: variables: general – stars: variables: RR Lyrae – surveys

1. INTRODUCTION

The Taiwanese–American Occultation Survey (TAOS) project aims to search for stellar occultation by small (∼1 km diameter) Kuiper Belt Objects (KBOs). The KBO population consists of remnant planetesimals in our solar system, which typically have low to intermediate (below 30°) inclination orbits and heliocentric distances between 30 and 50 AU (Edgeworth 1949; Kuiper 1951; Morbidelli & Levison 2003). The size distribution of large KBOs shows a broken power law with the break occurring ∼30–100 km which indicates a relative deficiency of small KBOs. Such a broken power law is believed to be the consequence of competing processes of agglomeration to form progressively larger bodies versus collisional destruction. The size distribution thus provides critical information of the dynamical history of the solar system. The stellar occultation technique, namely the dimming of a background star by a passing KBO, is the only technique capable of detecting cometary-sized bodies, which are too faint for direct imaging even with the largest telescopes (King et al. 2001; Alcock et al. 2003; Zhang et al. 2008). So far, TAOS has collected several billion stellar photometric measurements, and no occultation events have been detected, indicating a significant depletion of small KBOs (Zhang et al. 2008; Bianco et al. 2010).

Several projects have discovered numerous variable stars as byproducts, for instance the MACHO (Alcock et al. 1995, 1998), EROS (Beaulieu et al. 1995; Derue et al. 2002), OGLE (Cieslinski et al. 2003; Wray & Paczynski 2004), and ROTSE-I (Akerlof et al. 2000; Kinemuchi et al. 2006; Hoffman et al. 2009). Such data have enriched our knowledge of stellar variability in the Galactic fields and the Magellanic Clouds, which not only improves the number statistics, but also has helped to shed light on the detailed mechanisms of stellar variability. Knowledge of the variability has been so far still relatively poor for even the bright stars. Recent large-area sky survey projects, however, have started to turn up large numbers of variable stars. These projects include the All Sky Automated Survey (ASAS; Pojamanski et al. 2005), the observations by the Hungarian Automated Telescope (HAT[15]; Bakos 2001), the Northern Sky Variability Survey (NSVS; Wozniak et al. 2004), and ROTSE-I. Variable stars, notably Cepheids, RR Lyrae-type, δ Scuti-type, SX Phonenicis-type, semi-regular variables, and eclipsing binaries are shown to be ubiquitous in Galactic fields and in clusters. The next-generation projects like the cyclic all-sky survey by the Panoramic Sky Survey And Rapid Response System (Pan-STARRS) no doubt will provide a much more complete variable star census and characterization to enhance vastly our understanding of the cosmos in the time domain.

While the main goal of the TAOS project is to conduct a KBO census by detecting stellar occultations, the plethora of time-series stellar photometry renders the opportunity to identify and characterize variable stars spanning a wide range of timescales,

[15] http://www.cfa.harvard.edu/∼bakos/HAT

from less than a second to a few years. The first paper of the series of the TAOS stellar variability studies deals with the detection of low-amplitude δ Scuti stars (Kim et al. 2009). The current paper, the second in the series, presents the effort to identify variable stars in a targeted star field.

2. OBSERVATIONS AND DATA REDUCTION

The TAOS telescope system consists of an array of four 50 cm, fast optics (f/1.9), wide-field robotic telescopes, sited at Lulin Observatory (longitude 120°52′25″E; latitude 23°28′07″N, elevation 2862 m) in central Taiwan. Each telescope is equipped with a 2048 × 2048 SI-800 CCD camera, with a pixel scale of 2.″9, yielding about a 3 deg^2 field of view on the sky. The TAOS system uses a custom-made filter which, together with the sensitivity of the CCD, has a response function close to that of a standard broad R-band filter.

All TAOS telescopes observe the same star field simultaneously so as to eliminate the false detection of occultation events by KBOs. Each observing session begins with regular imaging ("*stare mode*") of the star field, followed by a special CCD readout operation ("*zipper mode*"). In the zipper mode, the camera continues to read out a block of pixels at a time while the shutter remains open. A stellar occultation by a km-sized KBO is expected to last for only a fraction of a second, and it is this pause-and-shift charge transfer operation that allows 5 Hz photometric sampling to detect such an event. The zipper-mode data are most suitable for studying truly fast varying phenomena such as stellar flaring, but they were not used in the results reported in this paper so will not be discussed further. Technical details of the TAOS operation can be found in Lehner et al. (2009).

The primary purpose of the stare-mode observations is to provide guidance of the pointing of the star field, particularly for photometric processing of the zipper-mode images, but the stare-mode data also can be used for stellar variability studies. A set of stare-mode observations consists of nine telescope pointings, each with three frames of images, dithered around the center of the target field. The frames covering the central position were used in the analysis reported here.

There are a total of 167 TAOS star fields, mostly along the ecliptic plane. These fields have been selected to have few exceedingly bright ($R < 7$) stars, and to have a sufficient number of stars to maximize occultation probability, yet not too crowded to hamper accurate stellar photometry. The number of stars brighter than about $R \sim 16$ ranges from a few hundreds to several thousands in each of our target fields.

This paper presents the variable stars found in a particular field, No. 151, which has the central coordinates R.A. = 17$^{\rm h}$30$^{\rm m}$6.$^{\rm s}$67, decl. = 27°17′30″(J2000). After excluding data taken under inferior sky conditions, the data presented here include 93 good photometric measurements taken at 47 epochs from 2005 April 11 to 2005 August 2. Each photometric measurement came from a stare-mode image with a 4 s exposure.

Photometry was performed using the *SExtractor* package (Bertin & Arnouts 1996) with a 3σ source-detection limit. For each detected source, the output provides the x–y position, instrumental magnitude, magnitude error, FWHM, etc. Astrometry was done using the *imwcs* task of *WCSTools*[16] (Mink 1999) with the USNO-B1.0 catalog (Monet et al. 2003). Then the CCD x–y positional output from *SExtractor* was converted to sky coordinates (R.A. and decl.) for individual images using the *xy2sky* task of *WCSTools*.

The stellar position was matched with the USNO-B1.0 and Two Micron All Sky Survey (2MASS; Cutri et al. 2003) catalogs. The USNO-B1.0 catalog was derived from images of digitization of sky-survey photographic plates, and gives the position, proper motions, photographic magnitude in each of the five passbands (B1, B2, R1, R2, I), and star/galaxy estimators for some 1,042,618,261 objects. The 2MASS Point Source Catalog essentially covers the whole sky in three near-infrared bands J, H, and K_s, down to a limiting magnitude of $J \sim 15.8$ mag with a signal-to-noise ratio of 10. Optical magnitudes, USNO unique identification numbers (USNO ID), and 2MASS magnitudes of the detected sources in our images were obtained by matching the position to the USNO-B1.0 and 2MASS catalogs. A matching radius of 10″ was used, which gives unambiguous identifications in all but a few cases. The catalog for each image provides the unique USNO_id, TAOS instrumental magnitude, optical magnitude (B2, R2), 2MASS_id, and infrared (J, H, K_s) magnitudes.

We then created the light curve for each star, containing the modified Julian date (MJD), calibrated TAOS magnitude, and error in magnitude. Photometric calibration of the TAOS instrumental magnitude will be discussed in the following section. Only data with good photometric quality, judged on the basis of the number of detected sources, were used in the analysis. Best images are those with more than 3000 detected sources. In the results reported here, we only considered images having more than 2500 detected sources. For variability analysis, only sources with more than 80 photometric measurements were considered. Finally, we obtained the light curves of 2915 sources, mostly with 93 photometric measurements.

2.1. Photometric Calibration

TAOS images are obtained with a filter close (but not identical) to the standard R optical band. We used the R2 magnitude in the USNO-B1.0 catalog to calibrate our TAOS instrumental magnitude with a linear fit, under the assumption that most stars are not variable. Despite the large photometric scattering intrinsic to the USNO-B1.0 catalog (derived from photographic plates), the calibration gives a consistent rescaling of the TAOS instrumental magnitude for each star so as to remove run-to-run variable sky transparency, atmospheric extinction due to different airmasses, and telescope system variations. One such calibration curve for a particular image is shown in Figure 1.

2.2. Periodicity Analysis

We used the Lomb–Scargle (LS) periodogram (Lomb 1976; Scargle 1982) to determine the most likely period of a variable star. The LS method computes the Fourier power over an ensemble of frequencies, and finds significant periodicities even for unevenly sampled data. We used the LS algorithm taken from the publicly available Starlink[17] software database. The periods were further verified with the software *Period04*[18] (Lenz & Breger 2005) for stars displaying obvious periodic variation. *Period04* also provides the semi-amplitude of the variability in a light curve. For any star showing a possibly spurious period, we carefully checked the phased light curve for that particular period.

[16] Package available at http://tdc-www.harvard.edu/software/wcstools/.

[17] http://starlink.jach.hawaii.edu/starlink

[18] http://www.univie.ac.at/tops/Period04

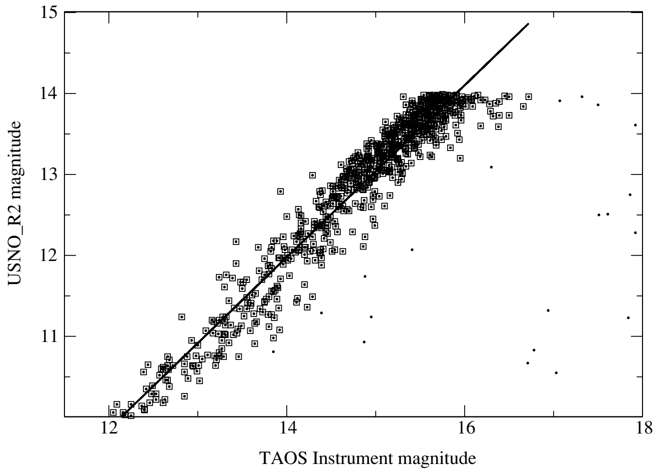

Figure 1. TAOS instrument magnitude vs. the R2 magnitude in the USNO-B1.0 catalog. The dots show all the TAOS measurements, whereas the squares mark those stars with a corresponding R2 magnitude between 10 and 14 used in the linear fitting, shown as the solid line. Outliers, i.e., TAOS detections with mismatched USNO magnitudes, are caused by the photometric scattering of the USNO-B1.0 photometry or bad pixels in the TAOS images.

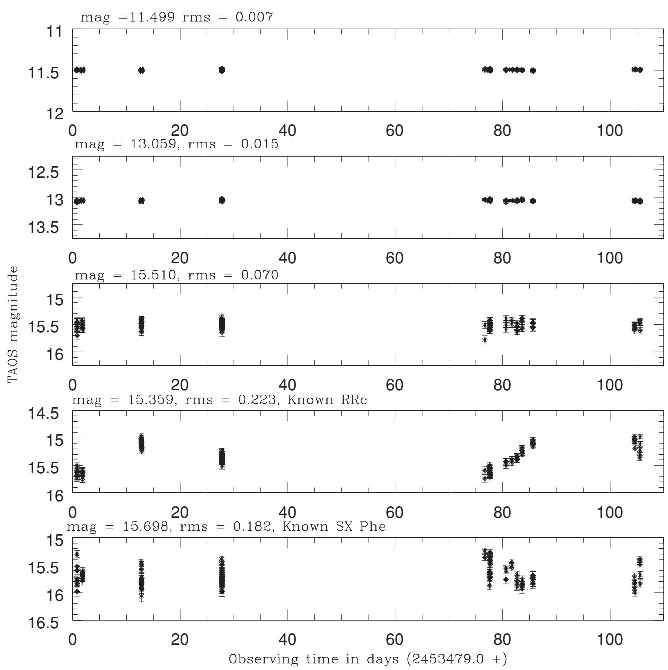

Figure 2. Example light curves of a few apparently nonvariable stars (top three panels) and known variable stars.

3. RESULTS

3.1. Candidate Variables

Because a large number of stars have been observed, the random errors of the differential magnitudes are well determined. These amount to ∼0.02 mag at TAOS magnitude $\lesssim$14 but increase to ∼0.1 mag at ∼16 mag. To illustrate this, Figure 2 shows the light curves of a few nonvariable stars (per our analysis) as well as known variable stars. Figure 3 shows the variations of the light curves of 2900 stars in the selected field. Each point represents the rms of 80–93 measurements of a particular star over 105 days. One sees that most stars behave "normally," i.e., the signal-to-noise ratio decreases for fainter stars, as expected. The increase of rms at the bright end (<8 mag) is due to saturation. An outlier, that is, a star with a large rms value for its magnitude, is then considered a likely variable.

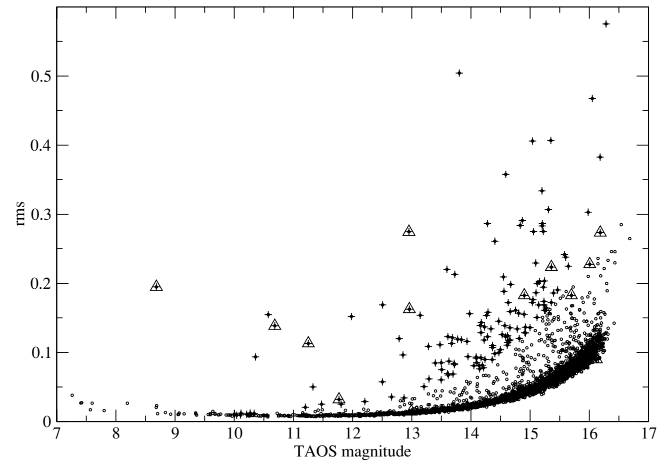

Figure 3. rms of the magnitudes of some 2900 stars in the 2.9 deg^2 field of the TAOS Field 151 (R.A. = $17^h30^m6^s.67$, decl. = $27°17'30''$). Each dot represents the rms of the light curve of each of the 2900 stars in the field. The triangles mark known variables. The plus symbols tag the sources having more than 3σ variability in the light curves, hence are variable candidates.

A total of 143 variable star candidates were identified on the basis of 3σ above the average rms in a magnitude bin. Visual inspection of the light curves indicated that 62 stars show large rms values because of flux drops of only a few data points, e.g., as the result of bad pixels or cosmic rays. These were excluded from the variable list. At the end we had the final count of 81 candidate variables.

3.2. Previously Known Variables

We have searched the International Variable Star Index (VSX)[19] of the American Association of Variable Star Observers (AAVSO) for known variables in our field. The VSX database is populated with the General Catalogue of Variable Stars (GCVS; Kholopov et al. 1998), the New Catalog of Suspected Variable Stars (Kukarkin et al. 1982), and the published data from sky surveys, e.g., NSVS (Wozniak et al. 2004), the ASAS (Pojamanski et al. 2005), and the Optical Gravitational Lensing Experiment-phase 2 (OGLE-II; Wozniak et al. 2002).

A total of 19 variables from the VSX database are found in our field, and we recovered 14 of them, listed in Table 1. Missing objects in our list of known variables include one star that is brighter than our saturation limit so was not included in our analysis. Two stars, namely ASAS J172907+2749.4 (Pojamanski 2002) and ROTSE1 J172907.35+274928.6 (Akerlof et al. 2000), with a $3''.6$ coordinate difference, are classified as RRABs with similar periods. They should be the same star, and we recovered the object as USNO-B1 ID 1178.0358793 with a similar period. Another two entries in the VSX, namely ROTSE1 J173203.69+272225.1 from ROTSE-I data (Akerlof et al. 2000) and ASAS J17320+2722.4 from HAT data (Pojamanski 2002), also with a $3''.6$ difference in the published coordinates, have only one counterpart in our data as USNO-B1 ID 1173.0334705. They are detected as one star by the TAOS telescope system, which has a large $3''$ pixel scale. We suspect the $3''.6$ coordinate difference to be a systematic offset in the ASAS catalog, and these two entries actually refer to the same star. This star is classified as a long-period variable (LPV) by

[19] http://www.aavso.org/vsx/

Table 1
Known Variable Stars

USNO ID	Star Name	Vmag	Tmag	Frames	σ_T	Type	P_{known}	P_{LS}	Period04	Semiamp
1178.0360412	NT Her	10.0–10.6	8.33–8.96	90	0.192	LB	NA	74.5240	74.8600	0.309
1169.0319910	V1097 Her	10.7–11.3	10.51–11.00	88	0.133	EW	0.3608	0.1804	0.1805	0.179
1173.0334705	ASAS J173204+2722.4	11.51(0.336)	11.10–11.40	93	0.113	MISC	...	∼104	∼104	0.19
	ROTSE1 J173203.69+272225.1					LPV				
1177.0363083	V1060 Her	12.1–12.8	11.72–11.90	92	0.032	EA	1.5768	0.7012	1.5873	0.220
1169.0316280	V0486 Her	12.8–13.6	12.70–13.25	89	0.161	RRAB	0.8059	0.8061	0.8059	0.190
	ROTSE1 J172638.42+265616.5	13.551(0.497)R1				RRAB	0.8056			
	ASAS J172638+2656.3	12.769(1.202)				CW-FU	4.203			
1178.0358793	ASAS J172907+2749.4	12.406(0.785)	12.43–13.31	93	0.274	RRAB	0.46883	0.469	0.48871	0.310
	ROTSE1 J172907.35+274928.6	12.85–13.50(R1)				RRAB	0.46885			
1171.0322166	1RXS J172719.4+270858	12.9(0.12)	12.96–13.03	93	0.0143	UV	...	0.7486	0.7489	0.011
1174.0340307	V0420 Her	14.5–15.6	14.37–15.18	86	0.179	RRAB	0.6003	0.7464	0.5997	0.220
1179.0338666	[WM2007] 772	15.29(0.17)	14.99–15.27	93	0.053	VAR	...	0.1061	0.1107	0.026
1167.0305285	V0413 Her	15.6–16.3	14.97–15.74	90	0.223	RRC	0.5137	0.5131	0.5126	0.271
1180.0314388	V0879 Her	15.2–15.8	15.24–16.06	82	0.175	SXPhe	0.0569	0.0569	0.0538	0.193
1179.0338257	[WM2007] 771	16.28(0.18)	15.94–16.36	67	0.091	VAR	...	0.9682	1.0172	0.04
1169.0316908	V0404 Her	16.0–16.8	15.51–16.57	72	0.2276	RR	0.55509	0.20918	0.6616	0.195
1169.0316979	V0405 Her	15.8–17.0	15.76–16.79	47	0.2733	RRAB	0.5879	0.5880	1.4287	0.296

ROTSE-I without period determination. We estimated the period to be about 104 days.

Of the three stars, V0486 Her, ROTSE1 J172638.42+265616.5 and ASAS J172638+2656.3, the first two have the same coordinates, period (0.8059/0.8056 days), and classification (RRAB), but as separate entries in the VSX database. The third star, again 3$''$.6 away, should also be the same star, though ASAS gave a similar brightness but classified it as a CW-FU with a different period (4.203 days). We recovered one variable as USNO ID 1169.0316280 in the position, with a period of 0.8061 days. We hence caution others on the possible multiple entries of the same variable star in the VSX database.

The VSX database provides information on the variable type, period, and magnitude range. Table 1 lists the period and semi-amplitude of known variables derived from our new data, together with VSX information. The first two columns are the star name and the USNO identification number (ID). The third and fourth columns provide the visual magnitude range in the VSX database and our TAOS magnitude range. Columns 5–7 give, respectively, the number of observed frames, rms in TAOS magnitude and the variable classification from the VSX database (such as the pulsating types of LB and LPV, RRAB, and RRC, and the eclipsing binary types of EW end EA, and the δ Scuti type of SX Phe). Column 8 provides the period taken from the VSX catalog, while the ninth and tenth columns give the periods we derived using the LS method and *Period04*, described in Section 2.2. Column 11 provides the semi-amplitude determined by *Period04*. The star NT Her is a known LB variable, but without a published period. Our data suggest a long period, ∼74 days with a large uncertainty. For the rest of known variables, the periods we determined are consistent, except in harmonics in some cases, with those listed in the VSX. The light curves of the 14 previously known variable stars are shown in Figure 4.

3.3. Newly Found Variables

Of the 67 previously uncataloged variable candidates, 15 stars show clearly perceived phased light curve patterns with periods well determined by the LS algorithm. Periods derived from the two LS methods generally matched well. The remaining 52 candidates either did not show any significant periods, perhaps because of insufficient phase coverage of our data, or the phased light curves did not show patterns readily recognizable. Table 2 summarizes the properties of the 15 newly found variables. The first four columns are the TAOS star identifier, R.A. and decl. coordinates taken from the USNO-B1.0 catalog (both in degrees), and the ID in the USNO catalog. Columns 5 and 6 give the calibrated TAOS magnitude and its error. The seventh and eighth columns are the magnitude rms of the light curve and the number of observations used in the analysis. Column 9 is the derived period and Column 10 gives the variable classification on the basis of the shape of light curves, periods, and semi-amplitudes.

The phased light curves of the 15 classified variables are shown in Figure 5. Among these, four are RR Lyrae (RR) variables, three are semi-regular (SR) variables, five are broadly classified as eclipsing binaries (EW), and one each has been classified as a δ Scuti (Dsct), Cepheid (Cep), or SX Phonencis (SX Phe) variable.

Cepheids (Cep) are massive stars with a spectral class of F at maximum light while G to K at minimum; they generally have periods in the range of 1–70 days with an amplitude variation of 0.1–2.0 mag in V. RR Lyrae-type (RR) stars are radially pulsating giants with a spectral class A–F; they have periods of 0.2–2.0 days with an amplitude variation of 0.3–2.0 mag in V. The δ Scuti-type variable stars are A3-F0 main-sequence or sub-giant stars located in the lower part of the classical instability strip in the Hertzsprung–Russell diagram, with short pulsating periods ranging from 0.02 to 0.3 days and amplitudes less than 0.1 mag in V. The SX Phonencis (SX Phe) stars are pulsating sub-dwarfs with a spectral type A2–F5. Their light variations resemble those of δ Scuti variables, but with shorter periods, 0.04–0.08 days, and larger magnitude variations, up to 0.7 mag in V. Semi-regular (SR) variables are generally giants or supergiants of intermediate or late (K-M) spectral types. SRs show noticeable periodicity in their light curves, with periods in the range from 20 to 1000 days and amplitudes varying in the range from 0.1 to 2.0 mag in V. Eclipsing binaries are binary systems with the orbital plane lying near the line of sight of the observer.

Table 3 presents the USNO B, R2, and 2MASS J, H, K_s magnitudes of the previously known variable stars and the variables found by our analysis, i.e., those listed in Tables 1 and 2. In addition to light curves, the color information of the stars

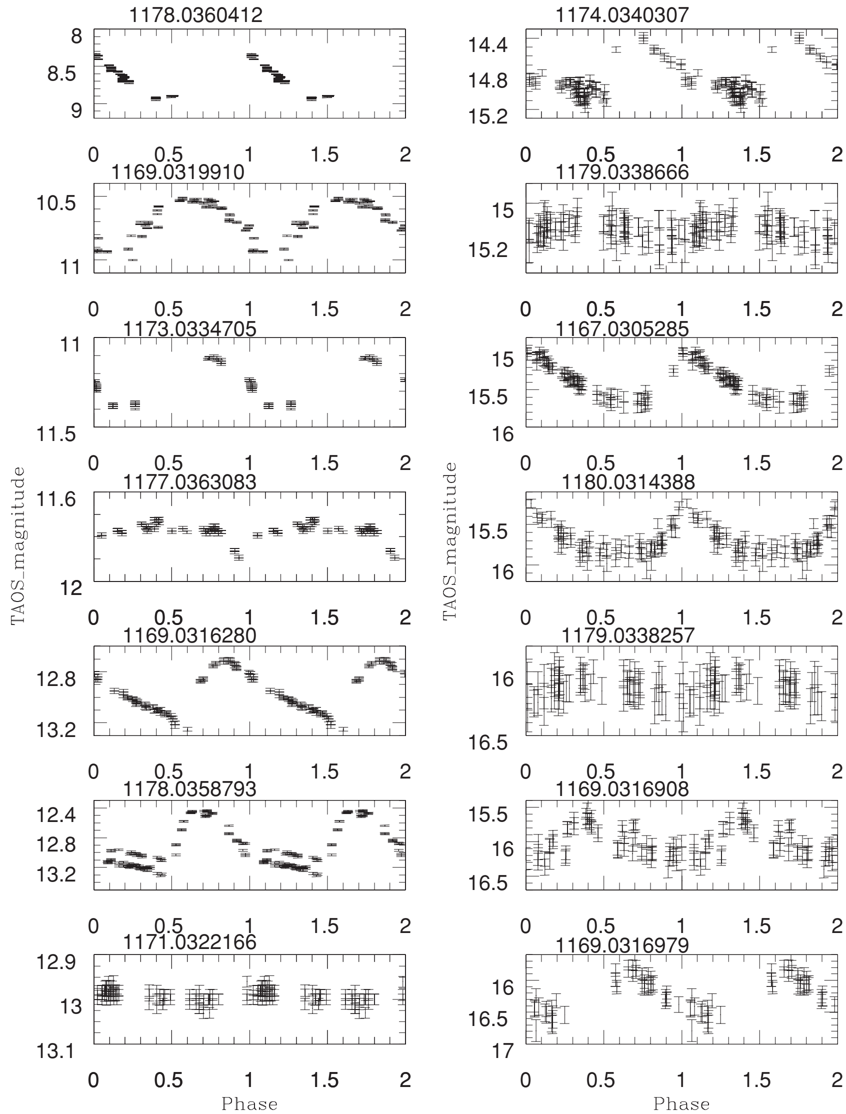

Figure 4. Phased light curves of known variables in Table 1.

Table 2
Previously Unknown Variables

ID	R.A. (J2000) (deg)	Decl. (J2000) (deg)	USNO ID	TAOS_mag (mag)	mag_err (mag)	rms (mag)	Frame No	Period (days)	Classification
TAOS 151-01	262.0523250	+27.2035170	1172.0333288	11.330	0.005	0.0501	93	22.065	SR1
TAOS 151-02	261.7864306	+27.0041889	1170.0320366	11.806	0.007	0.0251	93	59.891	SR2
TAOS 151-03	262.5683400	+27.8393820	1178.0359464	12.503	0.009	0.0574	93	34.936	SR3
TAOS 151-04	261.6632700	+27.3628750	1173.0332057	12.659	0.010	0.0356	92	2.409	Cep
TAOS 151-05	263.3984850	+27.6555000	1176.0347892	12.869	0.011	0.0342	93	0.439	RR1
TAOS 151-06	262.7197200	+27.6675860	1176.0346875	13.498	0.016	0.0850	92	0.147	SXPhe
TAOS 151-07	262.3019550	+27.6931360	1176.0346036	13.722	0.019	0.0823	93	0.280	EW1
TAOS 151-08	261.9320400	+27.6780570	1176.0345244	14.088	0.023	0.0934	93	0.622	RR2
TAOS 151-09	263.3462100	+26.7278840	1167.0306057	14.497	0.031	0.1040	93	0.401	RR3
TAOS 151-10	262.6746600	+26.4792490	1164.0287321	14.619	0.033	0.1243	93	0.264	Dsct
TAOS 151-11	263.1983550	+27.1243050	1171.0324737	14.672	0.035	0.1985	93	0.174	EW2
TAOS 151-12	262.9039200	+26.4763810	1164.0287687	15.121	0.048	0.1998	87	0.264	EW3
TAOS 151-13	262.8258600	+26.4790000	1164.0287567	15.158	0.049	0.2028	93	0.264	EW4
TAOS 151-14	263.4367250	+26.5488583	1165.0285251	15.235	0.052	0.1686	84	0.430	EW5
TAOS 151-15	263.2523100	+27.1410000	1171.0324817	15.680	0.171	0.156	93	0.621	RR4

could be used to cross-check the classification of variable stars. TAOS data do not provide color information, so we used the 2MASS data (Cutri et al. 2003) for this purpose. The 2MASS observations were taken simultaneously in the J, H, and K_s bands, thus the colors $(J - H)$ and $(H - K_s)$ are sampled at the same phase of a variable's light cycle. The near-infrared colors of RRab stars are in the range $(J - H) = -0.1$ to 0.5 mag and $(H - K_s) = -0.1$ to 0.25 mag (Kinemuchi et al. 2006).

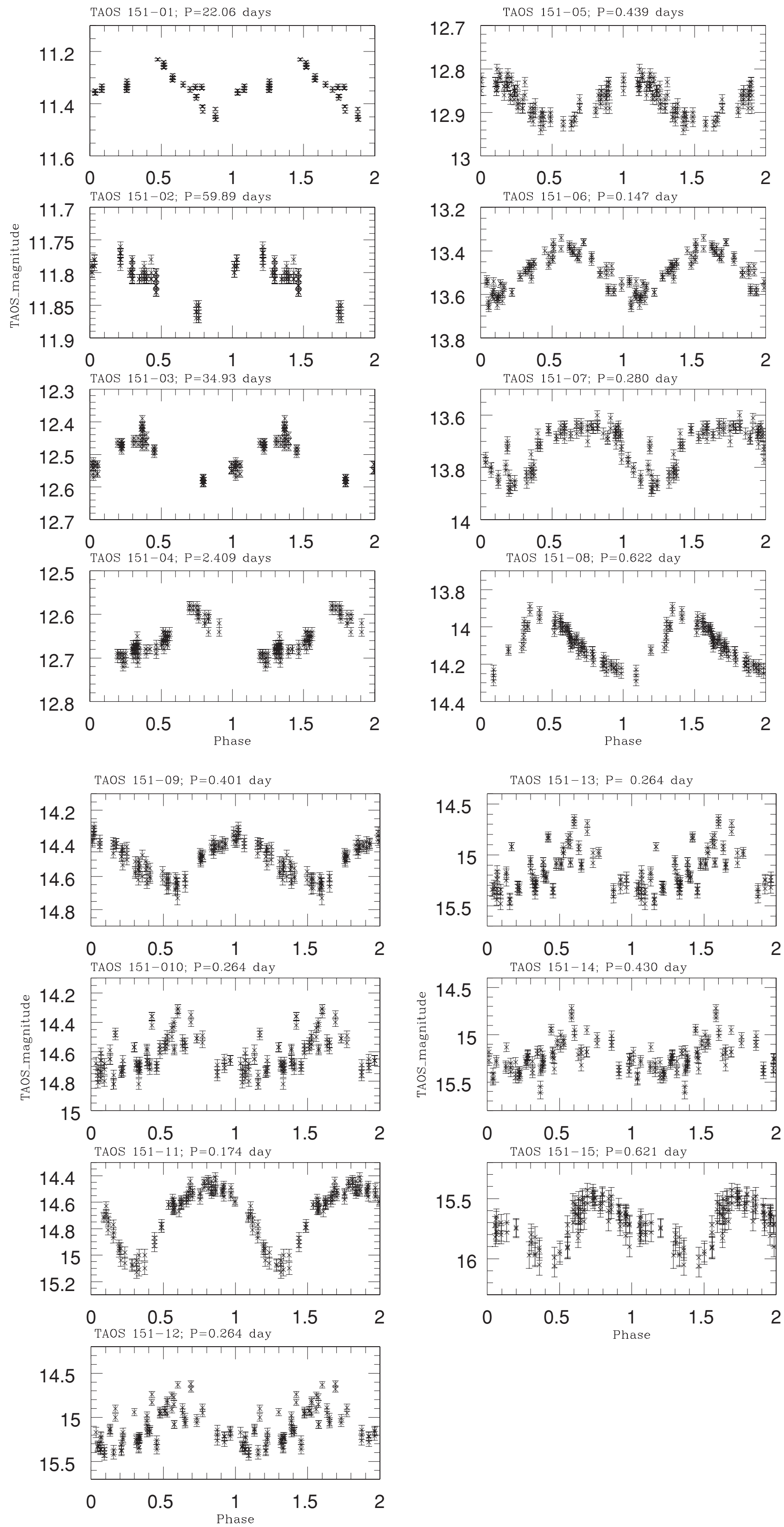

Figure 5. Phased light curves of newly identified variables with the TAOS data.

Figure 6 displays the 2MASS colors of the variable stars listed in Table 3, along with the loci of dwarfs, giants, and supergiants (Bessell & Brett 1998) for reference. With a few exceptions, the location of each variable is reasonably positioned in the color–color diagram according to its class.

4. SUMMARY AND FUTURE WORK

We have identified a total of 81 candidate variable stars in a particular field, No. 151 (R.A. = $17^{h}30^{m}6\overset{s}{.}67$, decl. = $27^{\circ}17'30''$, J2000) in the TAOS survey. Among these, 29 vari-

Table 3
Catalog for Variable Stars

USNO ID	ΔDiff ($''$)	USNOB2 (mag)	USNOR2 (mag)	J (mag)	H (mag)	K_s (mag)
Known variables						
1178.0360412	0.252	10.18	8.61	4.640	3.650	3.171
1169.0319910	0.540	11.38	10.64	9.889	9.591	9.510
1173.0334705	0.072	12.53	11.24	9.150	8.497	8.342
1177.0363083	0.432	12.54	11.49	10.431	9.933	9.779
1169.0316280	0.576	13.72	13.20	11.970	11.760	11.715
1178.0358793	0.504	14.08	12.61	12.398	12.124	12.115
1171.0322166	0.252	14.77	12.60	9.796	9.213	8.970
1174.0340307	0.972	15.32	15.16	13.799	13.561	13.549
1179.0338666	0.324	15.80	14.85	14.165	13.906	13.861
1167.0305285	0.900	...	15.00	14.681	14.420	14.159
1180.0314388	0.396	15.91	15.72	14.969	14.774	14.801
1179.0338257	0.720	16.95	15.90	15.094	14.713	14.683
1169.0316908	0.288	16.32	15.74	15.359	15.126	15.155
1169.0316979	0.396	16.44	16.10	15.299	15.133	15.039
Unknown variables						
1172.0333288	0.864	12.64	11.02	8.264	7.392	7.129
1170.0320366	0.828	14.47	11.24	10.491	9.901	9.852
1178.0359464	0.540	14.61	12.64	9.097	8.221	7.947
1173.0332057	0.180	13.63	12.83	11.360	10.852	10.715
1176.0347892	0.756	13.18	12.11	11.830	11.486	11.416
1176.0346875	0.648	14.12	13.25	12.211	11.731	11.632
1176.0346036	0.468	14.69	13.91	12.796	12.479	12.406
1176.0345244	0.612	15.19	14.12	13.134	12.902	12.835
1167.0306057	1.440	15.01	14.59	14.071	13.906	13.840
1164.0287321	0.252	15.96	14.92	13.404	12.843	12.747
1171.0324737	0.252	15.43	14.86	13.428	13.063	13.039
1164.0287687	0.468	17.31	15.46	13.453	12.824	12.594
1164.0287567	0.180	16.56	15.64	14.701	14.319	14.343
1165.0285251	7.056	20.09	18.65	16.687	16,198	15.663
1171.0324817	0.684	16.31	15.88	14.738	14.372	14.403

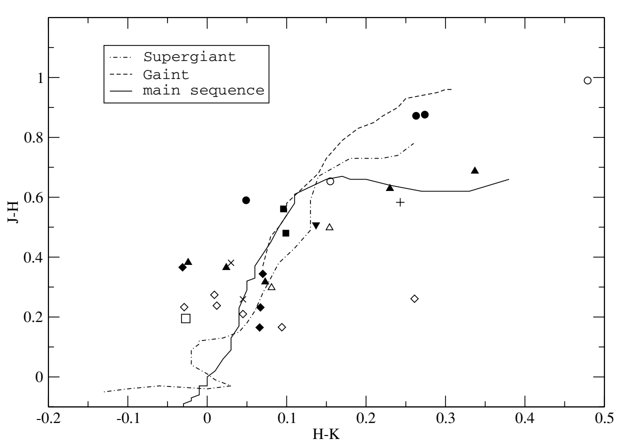

Figure 6. 2MASS $(J - H)$ vs. $(H - K_s)$ colors of variables stars. The loci of dwarfs, giants, and supergiants are taken from Bessell & Brett (1998). The open and filled symbols represent previously known and newly found variables. Different symbols are for various variable classes: circles for SR, LPV, LB, diamonds for RRAB, RRC, upward triangles for EW, EA, squares for SX Phe, DSct, downward triangles for Cep, pluses for UV, and crosses for VAR.

ables can be classified (including 15 that were previously uncataloged) as Cepheids, RR Lyrae stars, semi-regular variables, eclipsing binaries, or δ Scuti-type variables. Their light curves, derived periods, semi-amplitudes, and hence the variable classification are presented here and the data are available on the TAOS Web site, http://taos.asiaa.sinica.edu.tw/var2.php. With the same methodology we expect to produce variable star lists in other TAOS fields, now with observations covering more than four years (2005–2009). In addition to stare-mode photometry, the zipper-mode observations provide data sampled at 5 Hz, so may be particularly useful for fast stellar variability (Kim et al. 2009). The TAOS database hence has the unique potential to study several thousand stars at timescales from less than a second to a few years.

The work at National Central University was supported by the grant NSC 96-2112-M-008-024-MY3. Y.I.B. acknowledges the support of the National Research Foundation of Korea through grant 2009-0075376. Work at Academia Sinica was supported in part by the thematic research program AS-88-TP-A02. Work at the Harvard College Observatory was supported in part by the National Science Foundation under grant AST-0501681 and by NASA under grant NNG04G113G. S.L.M.'s work was performed under the auspices of the U.S. Department of Energy by Lawrence Livermore National Laboratory in part under Contract W-7405-Eng-48 and by Stanford Linear Accelerator Center under Contract DE-AC02-76SF00515. K.H.C.'s work was performed under the auspices of the U.S. Department of Energy by Lawrence Livermore National Laboratory in part under Contract W-7405-Eng-48 and in part under Contract DE-AC52-07NA27344.

REFERENCES

Akerlof, C., et al. 2000, AJ, 119, 1901
Alcock, C., et al. 1995, AJ, 109, 1653
Alcock, C., et al. 1998, AJ, 115, 1921
Alcock, C., et al. 2003, Earth Moon Planets, 92, 459

Bakos, G. 2001, Publ. Astron. Dep. Eötvös Univ., 11, 107
Beaulieu, J. P., et al. 1995, A&A, 303, 137
Bertin, E., & Arnouts, S. 1996, A&AS, 117, 393
Bessell, M. S., & Brett, J. M. 1998, PASP, 100, 1134
Bianco, F. B., et al. 2010, AJ, 139, 1499
Cieslinski, D., et al. 2003, PASP, 115, 193
Cutri, R. M., et al. 2003, 2MASS All Sky Catalog of Point Sources (Pasadena, CA: IPAC)
Derue, F., et al. 2002, A&A, 389, 149
Edgeworth, K. E. 1949, MNRAS, 109, 600
Hoffman, D. I., Harrison, T. E., & McNamara, B. J. 2009, AJ, 138, 466
Kholopov, P. N., et al. 1998, Combined General Catalogue of Variable Stars, GCVS, SIMBAD (Moscow: Sternberg Astron. Inst.)
Kim, D.-W., et al. 2009, AJ, 139, 757
Kinemuchi, K., Smith, H. A., Wo̓zniak, P. R., & Mckay, T. A. 2006, AJ, 132, 1202
King, S. K. 2001, in ASP Conf. Ser. 246, Small-Telescope Astronomy on Global Scales, ed. W. P. Chen, C. Lemme, & B. Paczynski (San Francisco, CA: ASP), 253
Kuiper, G. P. 1951, in Astrophysics, ed. J. A. Hynek (New York: McGraw-Hill), 357
Kukarkin, B. V., et al. 1982, New Catalogue of Suspected Variable Stars (Moscow: Nauka)
Lehner, M. J., et al. 2009, PASP, 121, 138
Lenz, P., & Breger, M. 2005, Commun. Asteroseismol., 146, 53
Lomb, N. R. 1976, Ap&SS, 39, 447
Mink, D. J. 1999, in ASP Conf. Ser. 172, Astronomical Data Analysis Software and Systems VIII, ed. D. M. Mehringer, R. L. Plante, & D. A. Roberts (San Francisco, CA: ASP), 498
Monet, D. G., et al. 2003, AJ, 125, 984
Morbidelli, A., & Levison, H. F. 2003, Nature, 422, 30
Pojamanski, G. 2002, Acta Astron., 52, 397
Pojamanski, G., Pilecki, B., & Szczygiel, D. 2005, Acta Astron., 55, 275
Scargle, J. D. 1982, ApJ, 263, 835
Wozniak, P. R., et al. 2002, Acta Astron., 52, 129
Wozniak, P. R., et al. 2004, AJ, 127, 2436
Wray, J. J., & Paczynski, B. 2004, MNRAS, 349, 1059
Zhang, Z. W., et al. 2008, ApJ, 685, L157

Dust Coma Morphology of Comet 81P/Wild 2 and 103P/Hartley 2 in 2010

Lin, Z.-Y. [(1)] , Lara, L.M. [(1)] and Ip, W.-H. [(2)]

(1) Instituto de Astrofisica de Andalucia – CSIC, Granada, Spain (zlin@iaa.es)

(2) Institute of Astronomy, National Central University, Taiwan

Comet 81P/Wild 2

1. Introduction

Comet 81P/Wild 2 (hereafter Wild 2) is a Jupiter family comet (JCF) discovered by Paul Wild in early January 1978. Due to a close encounter with Jupiter in 1974 at a distance of 0.006 AU from the planet, the orbital parameters changed such that the perihelion distance decreased by 3.5 AU from 4.9 AU to 1.4 AU allowing the cometary surface to receive a higher radiation from the Sun. The orbital period of comet Wild 2 changed from 57 years to 6.4 years (Sekanina 2003). This relatively young photometric age of 13cy, a parameter related to cometary activity, was estimated by using the secular light curves obtained in 1990, 1997 and 2003 apparitions (Ferrin 2007). Because of this young age, comet Wild 2 has probably encountered fewer intense heating episodes than other JFCs and new and pristine material would be expected to be detected in coming apparitions. Comet Wild 2 was the target of NASA's Stardust mission with close encounter on 2 January 2004. The Stardust project was primarily a dust sample return mission and its primary goal was to collect the sub-millimeter particles for laboratory analysis (Brownlee et al. 2004). During its flyby, Stardust also obtained many high resolution images. These images revealed large numbers of jets projected nearly around the entire perimeter of the nucleus. The highly collimated jets indicated that the source regions on cometary surface or subsurface were small and this phenomenon was also seen in comet 19P/Borrelly (Yelle et al. 2004; Soderblom et al. 2004). Unfortunately, the observing condition of ground-based telescopes during the 2003 perihelion and flyby time was extremely poor because the comet was in conjunction with the Sun. Under such bad condition, only very few data were obtained at very high arimass (Farnham et al. 2005). Besides, most of the quality data were taken in May and in June 2004.

In 2010, the distance was only 0.67AU to the Earth, it represented, therefore, a good chance to have relatively good spatial resolution to study the morphology of cometary coma.

2. Observation

The observational program using the One-meter Telescope at Lulin Observatory in Taiwan was planned from January 14th to August 1st 2010. During this observational period, the comet passed through its perihelion (1.598 AU) on 22 February and made its closest approach to Earth (0.673AU) on 5 April 2010. The observations of coma morphology were done using Asahi R broadband filter and the narrowband filters of Rosetta filter set. The camera (PI 1300B) has a pixel scale 0.516 " and a field of view of 11.2' X 11.6'. Details of our observations of comet Wild 2 are given in Table 1.

Table 1: Log of 81P/Wild 2 observations performed at the Lulin observatory

Date (UT)	r_H (AU)	Δ (AU)	Solar P.A. (degree)	P.A.	Pixel scale (km)
Jan. 14	1.64	1.10	112.7	35.5	410.8
Jan. 15	1.64	1.09	112.6	35.4	407.1
Jan. 16	1.64	1.08	112.5	35.4	404.0
Jan. 17	1.64	1.07	112.5	35.4	399.7
Jan. 18	1.64	1.03	112.4	35.3	384.7
Feb. 26	1.60	0.78	106.8	28.7	291.3
Apr. 7	1.66	0.67	84.8	10.3	250.3
Apr. 24	1.71	0.70	0.5	4.8	264.2
May 4	1.74	0.75	319.2	8.7	281.0
May 20	1.81	0.86	302.2	16.1	322.0
May 31	1.86	0.96	297.8	20.1	358.9
Aug 1	2.19	1.80	286.6	27.3	672.7

Note: Δ and r_H are the geocentric and heliocentric distances in AU; Solar P.A. is the position angle of the projected solar direction, measured from North towards East. P.A. is the phase angel.

3. Coma Morphology

Apart from the dust tail (labeled T in Figure 1) we identified up to seven different dust structures in our images, summarized in Table 2. From 14 to 18 January 2010, three features are detected in the solar direction (labeled A, B, C in Figure 1. The structure A extends first towards the Sun before being bended in the tail direction by the radiation pressure force. Structures B and C do not display the same curvature, although this is very likely a projection effect. Notice that structure B is very close to structure A in the images and as the jet broadens when particles move away from the nucleus the bended part of structure B cannot be distinguished from structure A. In the image taken on 26 February, only structures A and B are detected. Since we have a very good signal over noise ratio in these images, the disappearance of structure C is not a bias in our observations but rather indicates a change in activity, probably the switch-off of one active region. Notice that Earth-comet observing geometry in January and February remained relatively constant. From early April to late May 2010, at least four new jets appear in addition to structures A and B (there are labeled D, E, F, G in Figure 1). Three new jets can be indentified in April and one new additional jet was found at P.A. 8 degree in May, respectively. The last image in May suffers from the low signal/noise ratio and structures can barely be noticed, although they might be still present. In August, only one jet can be found in inner coma and this jet might have been present all the time from May to August because their morphology and the orbital configuration did not change during these months.

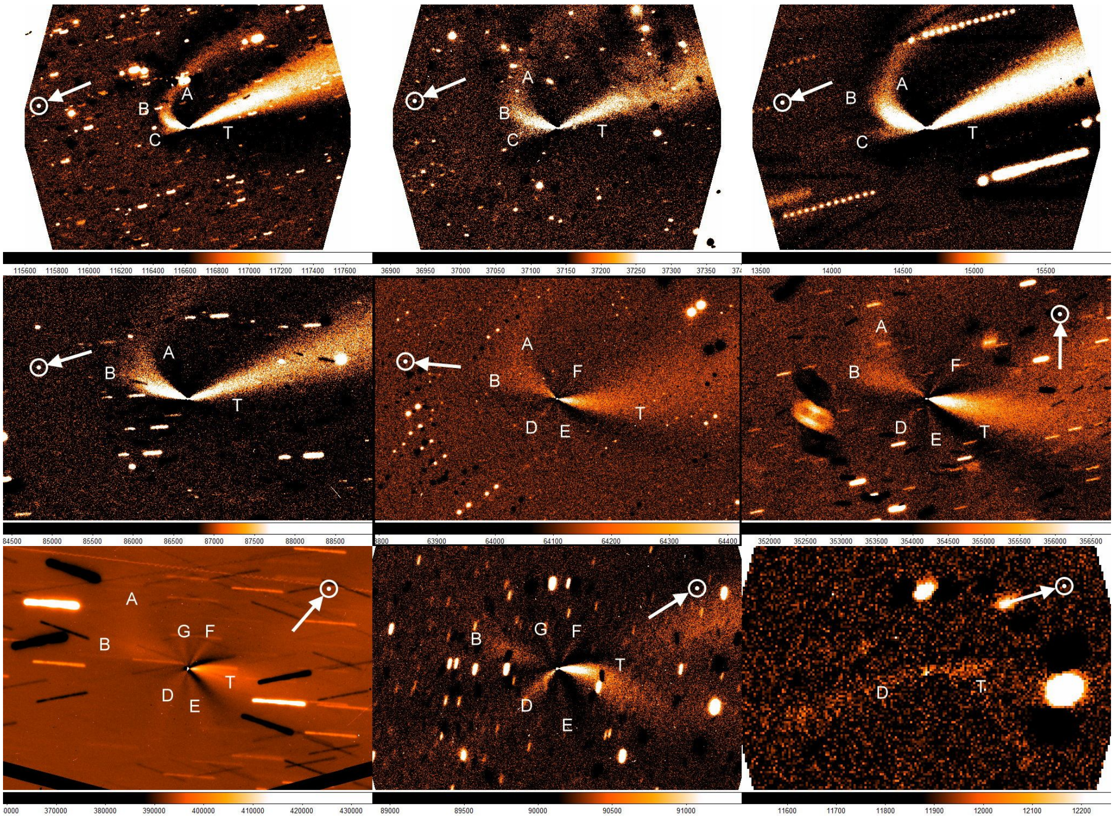

Fig. 1. Images processed by Larson-Sekanina algorithm and taken on Jan. 14, Jan. 15 and Jan. 18, (Top, from left to right,) Feb. 26, Apr. 7, and Apr. 24(middle, from left to right) May 4, May 20, Aug. 1 (Bottom, from left to right). In all images, North is up, East is to the left. The field of view is 5.85' X 3.87'. The arrow points solar projected direction. Structures are identified with capital letters, T marks the position of the dust tail. All images were obtained with a broadband R filter.

Table 2 Position of jet feature of dust coma

Date (UT)	r_H (AU)	Δ (AU)	Solar P.A. (degree)	A (degree)	B (degree)	C (degree)	D (degree)	E (degree)	F (degree)	G (degree)
Jan. 14	1.64	1.10	112.7	55	80	105	-	-	-	-
Jan. 15	1.64	1.09	112.6	55	80	105	-	-	-	-
Jan. 16	1.64	1.08	112.5	55	80	105	-	-	-	-
Jan. 17	1.64	1.07	112.5	55	80	105	-	-	-	-
Jan. 18	1.64	1.03	112.4	55	80	105	-	-	-	-
Feb. 26	1.60	0.78	106.8	55	80	-	-	-	-	-
Apr. 7	1.66	0.67	84.8	40	67	-	140	200	320	-
Apr. 24	1.71	0.70	0.5	40	67	-	140	200	328	-
May 4	1.74	0.75	319.2	43	69	-	130	200	320	8
May 20	1.81	0.86	302.2		65	-	130	200	328	8
May 31	1.86	0.96	297.8	-	-	-	130	-	-	-
Aug 1	2.19	1.80	286.6	-	-	-	120	-	-	-

Comet 103P/Hartley 2

1. Introduction

Comet 103P/Hartley 2, hereafter Hartley 2, with an orbital period of 6.46 years was discovered photographically by Malcolm Hartley in March 1986. Because this comet is the second of three periodic comets discovered by M. Hartley, it goes by the name “Hartley 2”. Comet Hartley 2 was an interesting object in the end of 2010, not only because it becomes a naked-eye comet, but also because NASA’s Deep Impact vehicle is scheduled for a close flyby to study it on November 4 2010. This comet was the fifth comet nucleus visited by spacecraft (the other four are: 1P/Halley, 19P/Borrelly, 81P/Wild 2 and 9P/Tempel 1). Before the spacecraft flyby, comet Hartley 2 passed only 0.12 AU from Earth on October 20 and then reached perihelion of 1.06 AU from the Sun on October 28.

NASA’s EPOXI mission was known as Deep Impact when it flew past Comet 9P/Tempel in 2005. The spacecraft then consisted of two parts: a massive impactor, 370 kg, that collided with the comet and a flyby spacecraft that recorded the results. The impact created a bright flash of light as it vaporized a small chunk of the nucleus and this provided scientists with their first look at the material beneath the heavily processed surface of the comet (A’Hearn et al. 2005). After impact mission in 2005, the flyby craft lives on as EPOXI. On November 4 2010 at 14:00 UT, the spacecraft made its closest approach to Comet Hartley 2 at a distance of about 700 kilometers. Those flyby images have been released by the EPOXI team and can be found in the website as following http://epoxi.umd.edu/ ..

2. Observation

The observational program using the One-meter Telescope at Lulin Observatory in Taiwan was planned from April 24th to December 2nd 2010. Our first image of comet Hartley 2 (Figure 3) was taken on April 24 2010 as comet at 2.4 AU far from the Sun and Earth. With 10 minute exposure time, the comet had no tail, but a round coma 5” wide. Its strong central condensation has a FWHM of 2.5″, compared to 1.5″ of stars in standard star field. The observations of dust coma were done using Asahi R broadband filter. Due to the moon influence, we did not have the broadband filter data as comet close approach its perihelion. A list of all the observations conducted at the Lulin one-meter telescope is given in Table3.

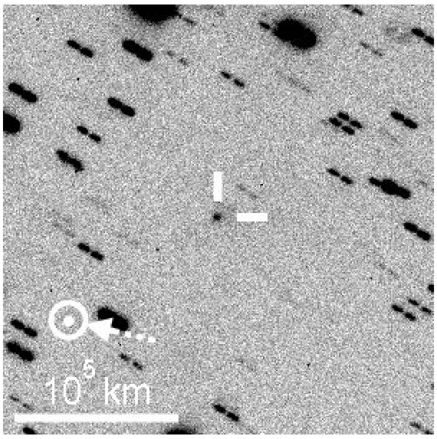

Fig. 3 The image of Hartley 2 was taken on April 24 2010. The comet had no tail, but a round coma 5" wide. Sun symbol and dash-arrow indicate the projected direction towards the Sun.

Table 3: Log of Observations performed at the Lulin observatory

Date (UT)	r_H (AU)	Δ (AU)	Solar P.A. (degree)	P.A.	Pixel scale (km)	Filter
April 24	2.424	2.363	76.2	24.2	884.4	R
May 11	2.283	2.026	72,1	26.3	758.3	R
May 15	2.249	1.948	71.0	26.7	729.0	R
May 16	2.240	1.928	70.8	26.8	721.6	R
May 20	2.206	1,851	69.7	27.1	692.9	R
July 14	1.721	0.924	46.9	29.0	345.9	R
August 1	1.562	0.694	32.9	29.3	259.6	R
August 19	1.409	0.503	15.5	31.1	188.3	R
August 20	1.402	0.494	14.5	31.2	185.0	R
August 21	1.392	0.483	13.3	31.4	180.9	R
August 29	1.329	0.412	05.6	33.3	154.2	R
September 29	1.130	0.192	02.1	44.2	71.7	R
September 30	1.125	0.186	03.8	44.6	69.6	R
October 2	1.116	0.175	08.3	45.3	65.4	R
October 3	1.112	0.170	11.1	45.6	63.7	R
October 10	1.087	0.140	35.9	48.0	52.3	R
October 11	1.084	0.136	40.3	48.4	51.0	R
October 25	1.059	0.126	89.8	55.9	47.0	R
October 29	1.059	0.135	96.9	57.7	50.6	R
November 2	1.061	0.150	102.0	58.7	55.8	R
November 5	1.064	0.157	104.2	58.8	58.8	R
November 21	1.112	0.239	118.8	53.2	60.2	R
December 2	1.116	0.295	128.9	46.4	74.6	R

Note: Δ and r_H are the geocentric and heliocentric distances in AU; Solar P.A. is the position angle of the projected solar direction, measured from North towards East. P.A. is the phase angel. R is the broad band filter.

3. Coma Morphology

Here, we show two methods (Larson-Sekanina algorithm and mean-media profile subtraction) of image processing in Figure 4. In April and May, the signal to noise ratio of images obtained by Lulin observatory are quite lower and therefore we didn't get any structure in inner coma even the dust tail is too faint to detect. In

July and August, we only detected the dust tail which is roughly toward to the anti-solar direction. In the end of September, we found a dust jet at Sunward direction and this jet feature can be detected from the end of September until the beginning of December when is our last observation at Lulin observatory. The dust jet feature sometimes looks like a prominent jet but sometimes it shows the multiple jets features. Mostly, we didn't find the dust jet changed from prominent jet to multiple jets in one night observation. But we do fortunately observe this phenomenon during two whole nights. There are two dust jets found on October 10 and October 11, the main one that streams toward the Sun does not change a lot but another one that perpendicular to Sun-tail direction is to switch on at the end time of these two days. This particular jet switched on/off could be a seasonal effect or caused by the projected effect during our observation run.

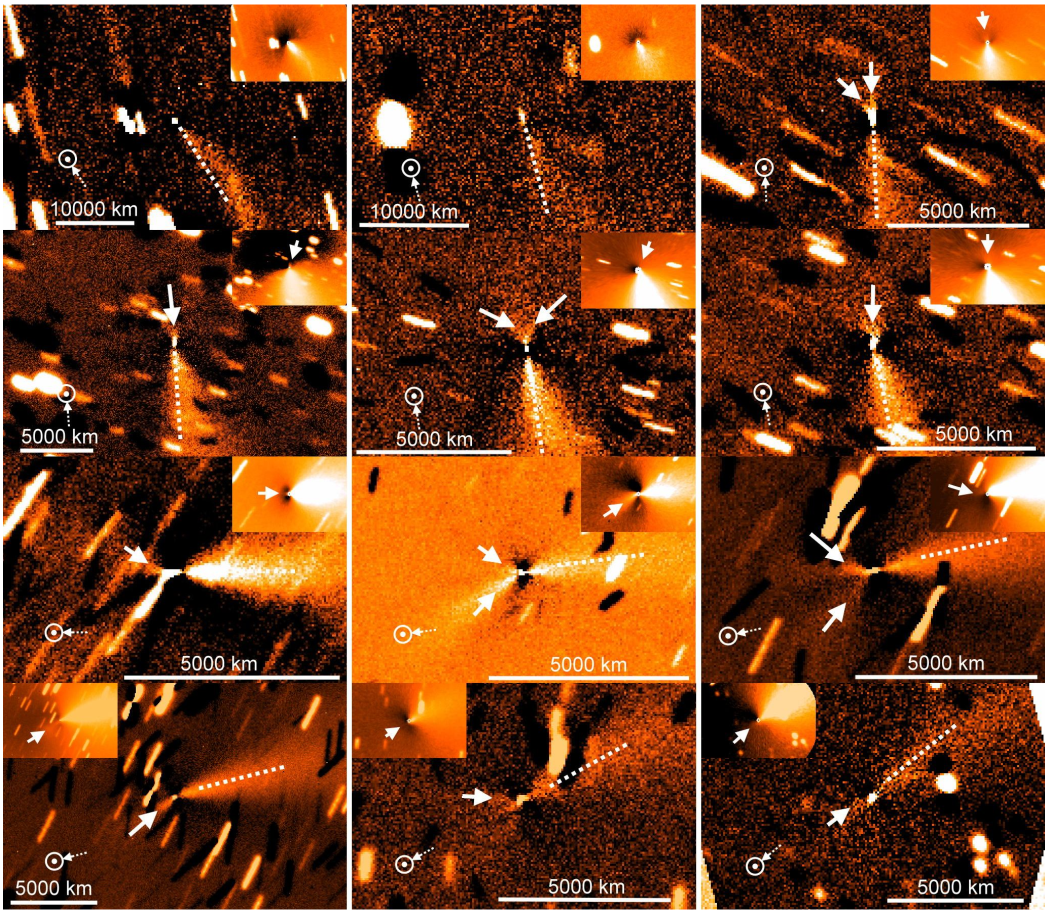

Fig. 4. Images were all processed by Larson-Sekanina algorithm (larger) and mean-media profile subtraction (smaller). All images were taken on Aug. 1, Aug. 20 and Sep. 29 (Top, from left to right); Sep. 30, Oct. 2, and Oct. 3 (upper-middle, from left to right); Oct. 25, Oct. 29, Nov. 2 (middle, from left to right); Nov. 5, Nov. 21. and Dec.2 (bottom, from left to right). In all images, North is up, East is to the left. The dash-arrow points the solar projected direction and the dash-line shows the anti-solar direction. Structures are identified with solid-arrow.

Reference :
1. A'Hearn, M.F., et al., 2005. Deep Impact: Excavating Comet Tempel 1 Science, 310, 258
2. Boehnhardt, H. and Birkle, K., Time variable coma structures in comet P/Swift-Tuttle, A&A, 107, 101
3. Brownlee, D.E. et al., 2004. Surface of Young Jupiter Family Comet 81 P/Wild 2: View from the Stardust Spacecraft, Science, 304, 1764
4. Farnham, T.L. et al., 2005. Physical and compositional studies of Comet 81P/Wild 2 at multiple apparitions, Icarus, 173, 533
5. Ferrin, I., 2007. Secular light curve of Comet 28P/Neujmin 1 and of spacecraft target Comets 1P/Halley, 9P/Tempel 1, 19P/Borrelly, 21P/Giacobinni Zinner, 26P/Grigg Skjellerup, 67P/Churyumov Gerasimenko, and 81P/Wild 2, Icarus, 191, 22
6. Larson, S. M. and Sekanina, Z. Coma morphology and dust-emission pattern of periodic Comet Halley. I - High-resolution images taken at Mount Wilson in 1910, AJ, 89, 571
7. Lin, Z.-Y., et al., 2007. Photometry and Imaging of Comet C/2004 Q2 (Machholz) at Lulin and La Silla, A&A, 469, 771
8. Lin, Z.-Y., et al., 2009. The Outburst of Comet 17P/Holmes, AJ, 138, 625
9. Sekanina, Z., 2003. A model for comet 81P/Wild 2, Journal of Geophysical Research, 108, SRD 2-1
10. Soderblom, L.A., et al., 2004. Imaging Borrelly, Icarus, 167, 4
11. Yelle, R. V., et al., 2004. Formation of jets in Comet 19P/Borrelly by subsurface geysers, Icarus, 167, 30

2010 年鹿林一米望遠鏡伽瑪射線爆光學餘暉後續觀測

黃麗錦(中研院天文所)，浦田裕次，蔡佩剛，莊佳蓉（中央大學天文所）

2010 年觀測結果總結

2010 年總共觀測了 8 個伽瑪射線爆光學餘暉。其中 GRB100302A 為高紅移 (z=4.8)伽瑪射線爆，許多天文台的觀測並沒有在 R 波段偵測到光學餘暉。們使用 R 和 I 波段觀測，發現鹿林 R 波段幾乎沒有餘暉，但 I 波段有偵測到餘暉，立即將我們的觀測結果通報伽瑪射線爆即時訊息系統(GCN)。由於我們的觀測，八米雙子星望遠鏡立即對餘暉拍攝光譜，證實為紅移 4.8 的伽瑪射線爆，可說是鹿林一米望遠鏡發現的高紅移伽瑪射線爆。GRB100424A,我們在爆發後 2 小時使用 z 波段觀測，不過並沒有偵測到餘暉影像。

而 GRB100814A 和 GRB100816A 皆偵測到餘暉影像。其中以 GRB100814A 最為明亮，其光變曲線極為特殊。鹿林分別於伽瑪射線爆爆發後 0.6 天、2.6 天以及 3.6 天在 g,r,i,z 四個波段皆偵測到伽瑪射線爆餘暉。我們的光變資料，與韓國合作者首爾大學的觀測資料結合一起，發現此伽瑪射線爆在爆發後 0.6 天光變曲線竟然變亮，一直到 2 天後才變暗（圖一）。

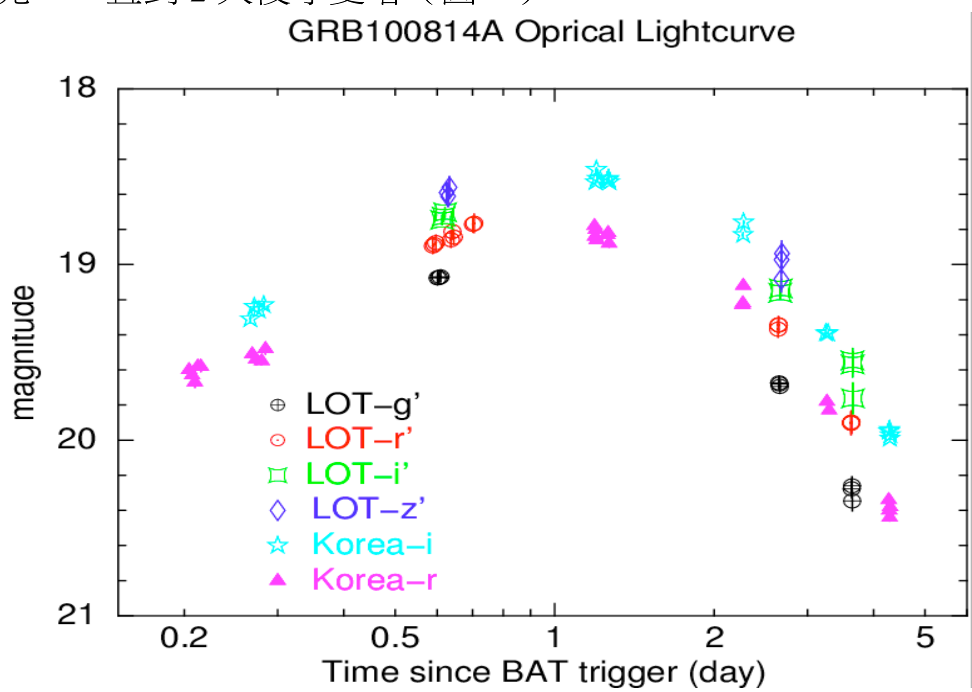

圖一： GRB 100814A 光變曲線。圖中的光學資料點是由台灣鹿林一米望遠鏡以及韓國的望遠鏡所觀測。

Swift/UVOT 團隊邀請我們參與 GRB100814A 的論文合作，若將 UVOT 的結果與鹿林 g,r,i,z 波段資料以及 X 射線資料結合一起，即可做出從 X 射線到 z 波段的光譜能量分布（SED)，並做模型模擬。這樣可以得知可見光波段和 X 射線的來源是否一致，進而解析可見光部份的來源。要做多波段光譜能量分析，並把不同天文台的資料以相同基準點修正，伽瑪射線爆星場的標準星觀測極為重要，因此我們利用鹿林天文台於 9 月 14 日的測光夜對伽瑪射線爆星場做標準星校正，並將結果提供給其他天文台修正伽瑪射線爆光學餘暉星等以相同基準修正。

(2)計畫發表論文：

2-1 GRB 071112C

GRB071112C 論文大致完成，準備投稿。此論文除了使用鹿林的觀測資料外，還使用 ROTSE、TAOS、北京天文台的 0.8 米望遠鏡資料以及日本岡山天文台 50cm 光學望遠鏡資料。主要討論早期的 R 波段的早期平緩光度演化來源以及探討光學與 X 射線光變演化的不一致。我們的觀測結果與其他的理論模型以及其他伽瑪射線爆觀測比較後，認為 R 波段在爆發後 100 秒所產生的平緩光變，應是伽瑪射線爆餘暉剛形成時所呈現的平緩凸狀光變曲線(圖二)。

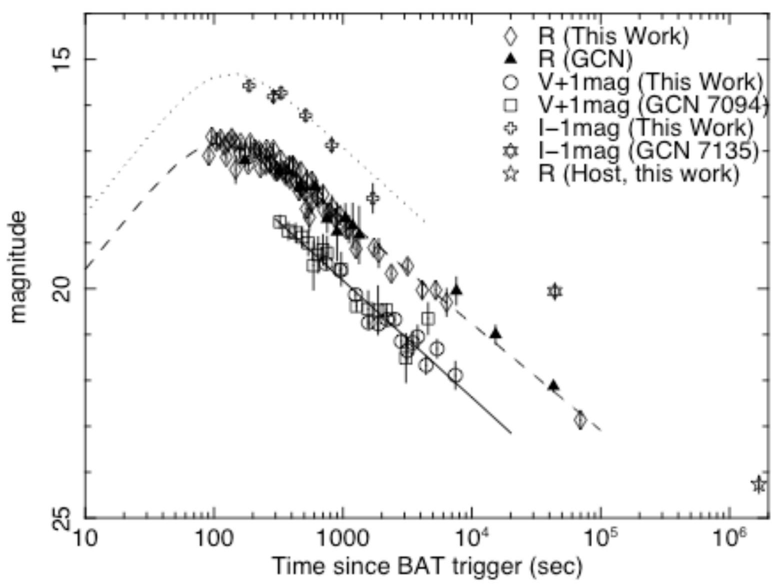

圖二： GRB 071112C V,R, I 波段光變曲線。

將擁有許多資料點的 R 波段與 X 射線光變曲線比較，發現這兩波段其冪次演化斜率不同，且與餘暉模型所預測的 X 射線和光學演化的冪次斜率不符。也就是說，這兩波段的能量發射的機制可能不一樣。由於 GRB0711112C X 射線光變曲線在爆發

後 500 秒左右有X射線瞬閃，類似情形也在其他的伽瑪射線爆的X射線光變中被發現。天文學者認為，這些X射線瞬閃與伽瑪射線爆的能量釋放活躍度有相關。若是如此，則 GRB071112C 的X射線光度有可能包含著伽瑪射線爆的高能訊息，而不是單純的餘暉演化。因此，我們從R波段的光度曲線演化認為可見光已經是進入餘暉時期，而遵守餘暉模型的預測結果。接下來，我們從R波段的觀測性質，根據餘暉模型擬合預測的X射線餘暉亮度（圖三）。結果發現餘暉模型預測的X射線餘暉亮度在爆發後幾千秒後遠遠小於觀測的X射線亮度。也就是說，我們所觀測到的X射線光變曲線，一開始由伽瑪射線爆持續釋放的高能能量所主導，並於爆發後約幾千秒後亮度減弱到比餘暉還暗，進而後期演化由餘暉所主導。這解釋為何餘暉模型無法同時完美解釋可見光與X射線的整體演化。

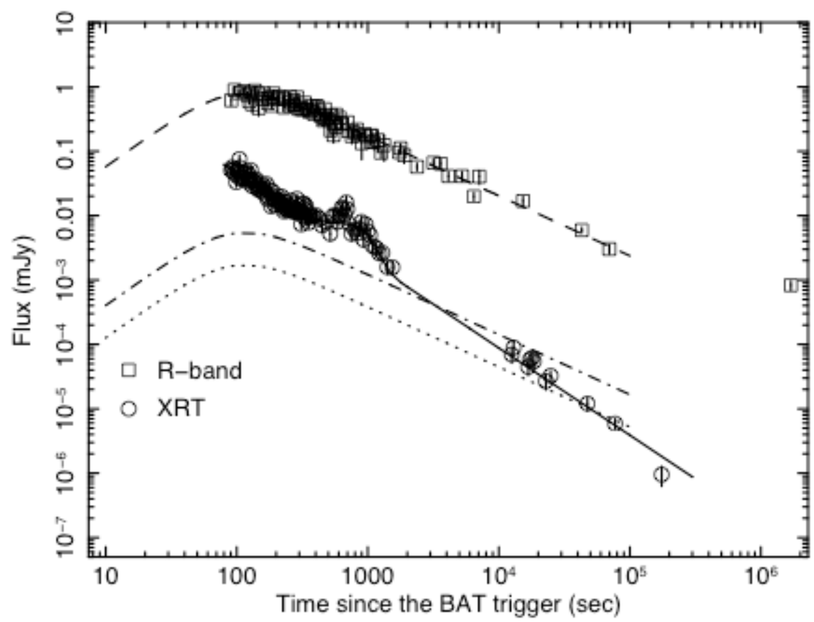

圖三： GRB 071112C R波段與X射線得光變曲線。其中點線為預測的X射線餘暉亮度。

2-2 GRB 090424

GRB090424，這個伽瑪射線爆非常有趣，可見光的光變曲線演化竟與X射線不相同且可見光本身的資料也相當有趣。此伽瑪射線爆非常亮，在爆發後97秒時，餘暉光度達12.5等，持續以冪次曲線變暗，然後冪次斜率從陡峭轉成平緩變暗，然後在爆發後1.6天候在一次快速變暗。乍看之下，GRB090424與其它伽瑪射線爆餘暉一樣以冪次分布變暗。然而從完整的興隆0.8米、1米、鹿林一米、韓國一米及印度一米望遠鏡的觀測顯示（圖四，五），其早期有比普通光變演化陡峭的冪次斜率，而完整的X射線光變曲線可以以多個高斯曲線擬合，表示此伽瑪射線爆在早期演化複雜，可能與伽瑪射線爆的活躍程度有關，或者是周圍星際物質密度高，造成這樣的光變曲線。為了瞭解這些複雜演化的來源及探討X射線以及可見

光波段的關係，多波段光譜能量分析是必須的。目前我已將可見光部分光變曲線分析解析完成以及將不同波段的星等資料修整，並用多個冪次加高斯分佈擬合可見光變曲線，列出參數，並和X射線光變曲線比較。接下來要進行X射線光譜的分析再加上可見光資料，來解析X射線和可見光餘暉的關係。

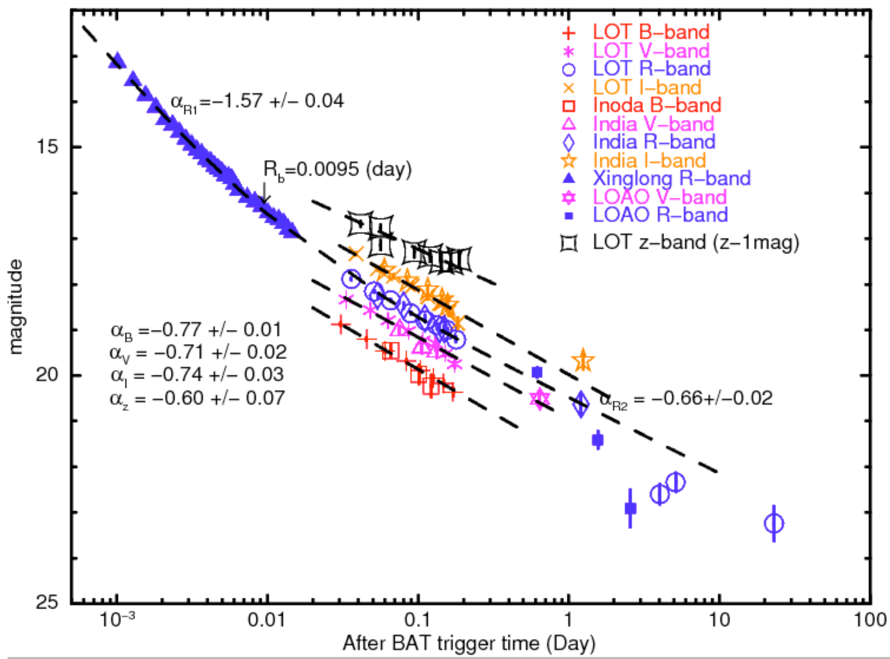

圖四：GRB 090424 的多波段光變曲線以及演化斜率。

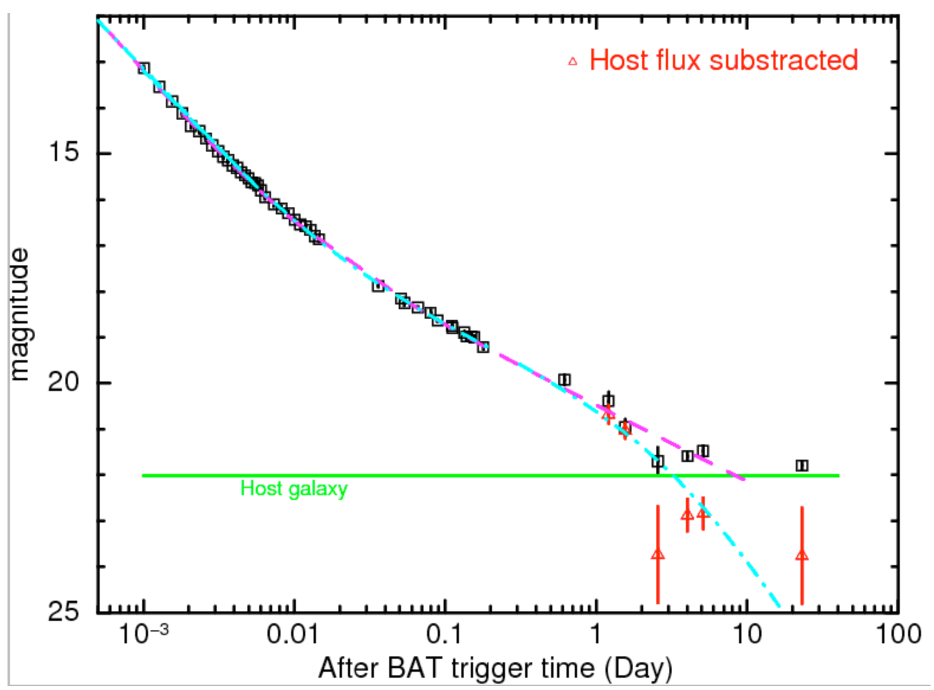

圖四：GRB 090424 的R波段光變曲線。

Simultaneous Observations of Classical Be Stars

Chien-De Lee, Wen-Ping Chen, Chien-Hui Kao and Li-Wen Hung

National Central University, Graduate Institute of Astronomy

In 2010, we carried out the optical and near-infrared simultaneous photometric and spectroscopic observations using the LOT, SLT, Okayama Astrophysical Observatory in Japan, and Xinglong Observatory in China. We had five runs (19 nights) at Lulin, with more than 70% clear time with data. We collected spectra of some 70 classical Be stars with different time scales, from hours, days to months. Limited by the sky conditions at Okayama, only two nights were available for simultaneous optical spectroscopic and near-infrared photometric observation. Otherwise we carried out near-simultaneous observations.

Our targets are all bright (Vmag < 11); more than one thousand images were obtained in total. The data are being processed by the pipeline we developed. Preliminary results have been presented as an oral and a poster papers at the IAU Symposium 272, held in Paris in 2010. Both will be published in the proceedings. Our work was awarded one of the "Best Posters" at the 2010 Annual Meeting of Physical Society of the ROC.

Emission lines and near-infrared excess

Fig. 1 shows the near-infrared excess and Balmer activity of CBe stars. Stars with both H*β* and H*α* in absorption --- signifying less gas activity --- show little near-infrared excess. Those with H*α* in emission, but H*β* and higher Balmer lines in absorption, have moderate near-infrared excess. CBe stars with H*α* and H*β* both in emission are highly active, and exhibit large near-infrared excess. Some CBe stars have excess emission extending to far-infrared or longer, so must be accounted for by dust emission. Fig. 2 displays some sample spectra with different near-infrared excess. An extreme case is MWC 623, which has very large NIR excess and with Hα, Hβ, and Hγ all in emission.

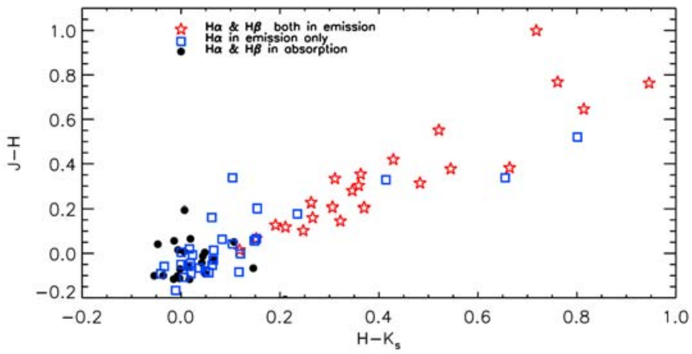

Figure 1. The emission lines and near-infrared excess of CBe stars.

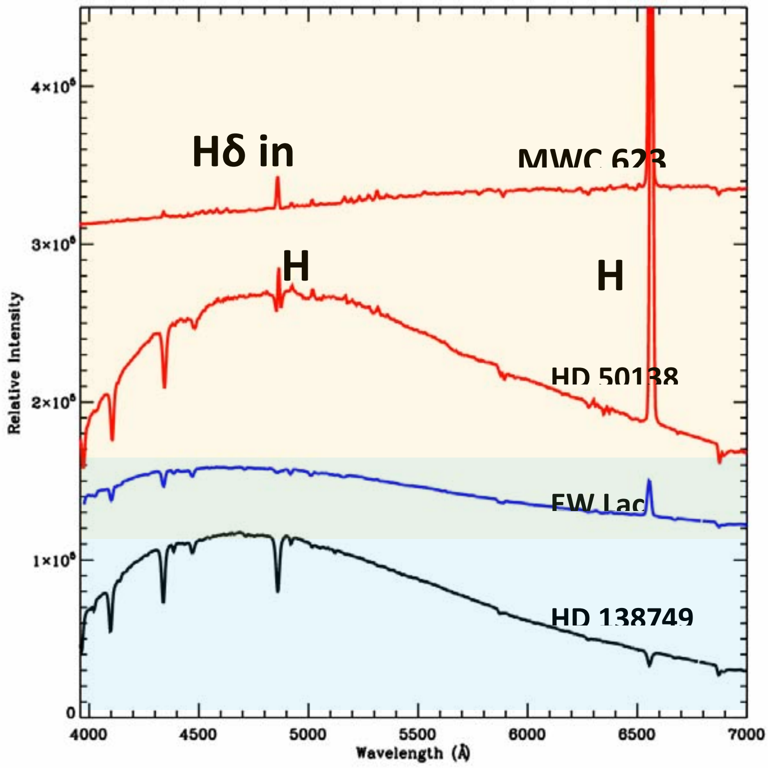

Figure 2. CBe spectra with different near-infrared excess.

Observations of two lensed quasars with LOT in 2010

E. Koptelova[1], W.P. Chen[2], D.C. Chang[3]

[1]Department of Physics, National Taiwan University, Wenshan Chiu, 116 Taipei, Taiwan

[2]Graduate Institute of Astronomy, Jhongli City, Taoyuan County 320, Taiwan

Background

Variability in UV/optical/IR wavelengths is an intrinsic property of all quasars. In case of the lensed quasars when we observe two (or sometimes more) images of the same source (the quasar), all quasar images will repeat the variations of the source quasar but not simultaneously. The quasar variability in the multiple images will be seen at different times due to the difference in lengths of the paths which take light rays to form the images of the quasar. This difference in time (known as lensing time delay between variations in two images A and B of quasar, t_{AB}) is related to the Hubble constant H_0 as t_{AB}~$1/H_0$ (Refsdal 1964, MNRAS 128, 307). This relation gives a direct method of the Hubble constant determination which is independent of a distance ladder. The time delay between variations in the quasar images can be measured using cross-correlation analysis of the light curves of the images. The lensed systems with accurately measured time delays can give the Hubble constant value which is less uncertain than that estimated based on Cepheids and cosmic microwave background radiation. Thus, the key idea of the observations of the lensed quasars is to obtain well-sampled and accurate light curves of the quasar images that can give an accurately measured time delay (with accuracy of several per cent) and that, in turn, can give us an accurate estimate of the Hubble constant.

Aim of the observations

During the 2010A (from February to May) and 2010B semester (starting from November) we have been observing two gravitationally lensed quasars RXJ0921+4529 and SDSS1206+2623 with the 1m Lulin telescope in the R band. The total number of data points obtained for RXJ0921+4529 and SDSS1206+2623 is 12. The goal of our observations was to obtain accurate and homogeneous light curves which can be used to measure the lensing time delays in systems RXJ0921+4529 and SDSS1206+2623. Note, that delays in RXJ0921+4529 and SDSS1206+2623 have not been measure until now.

These quasars are wide separation double lensed systems. The large image separation makes them good targets for observations with small ground-based telescopes. There are presently 18 gravitationally lensed systems with measured time delays of varying accuracy. We have also measured time delays in several lensed quasars (Ullán, Goicoechea, Zheleznyak, Koptelova et al., 2006; Goicoechea, Shalyapin, Koptelova et al. 2008; Shalyapin V.N., Goicoechea L.J., Koptelova E. et al., 2008; Koptelova et al.,

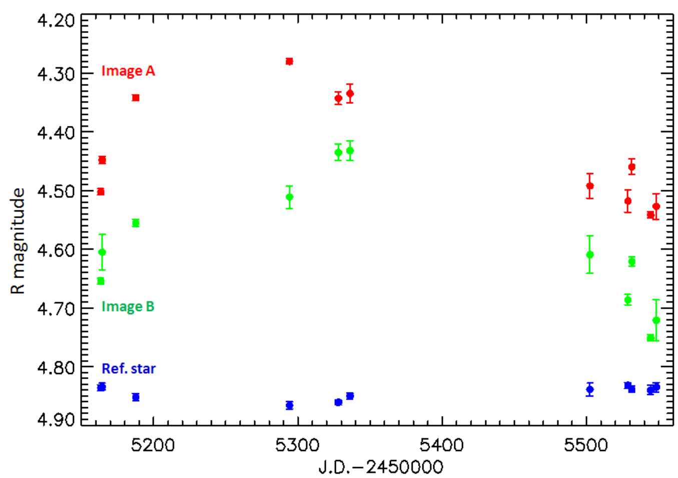

Figure1. R-band light curves of image A (red) and image B (green) of quasar RXJ0921+4529 based on observations obtained with the 1m LOT telescope from November 27, 2009 to December 17, 2010. The light curve of the reference star is shown in blue.

2010). Among the quasars with measured time delays, the number of lensed systems which can give an estimate of H0 with accuracy compared with other methods is still limited (e.g. Jackson 2007, LLR 10, J4). It makes new time delays measurements in the newly discovered lensed systems an important task.

Targets

RXJ0921. The lensed system RX0921 consists of two images of the quasar with the image separation of about 6 arcsec (see Fig. 1). Both images of the quasar have been found to be variable (e.g. Paraficz et al. 2006, A&A 455, 1P). Therefore RX0921 is a good candidate for accurate determination of time delay. We have been observing RX0921 in the 2010A and 2010B semesters. The light curves of the quasar images obtained during the observations are shown in Fig. 1. We found that the images of RXJ0921 are variable both on a relatively short (about 50 days) and long (several months) timescales. The global behaviour of the light curves of the quasar images is similar, gradual brightening followed by gradual fading. It means that we probably observe the variations as a result of quasar variability. These variations should be similar for both quasar images but separated in time. We experimented with the light curves of the images and found that the time delay between brightness variations seen in the images can be in the range of 80-110 days. This is in good agreement with theoretical expectations. Thus, from our observations of RXJ0921 in the 2010A and 2010B semesters we determined the range of possible time delays between the quasar images. The next step is to constrain it more and to find the exact value of the delay. After shifting by this time delay value the light curves of the A and B images should convincingly match each other. In order to measure the time delay, we continue observations of RX0921 in the 2011A semester. We expect that the new observations of the system can better constrain the time delay between images of RX0921.

SDSS1206. The lensed system SDSS1206 is also a double lensed quasar with the separation between images of about 3 arcsec. We have been observing SDSS1206 in the 2010A and 2010B semesters. The observations showed that both quasar components changed their brightnesses up to 0.2 magnitudes during observations in the first and second semesters (see Fig. 2). We detect a significant brightening of the A and B quasar images in the 2010B semester (based on the recent observations of the system in December). This brightening will probably be changed by the fading of the images in next months. This event provides good chances to measure the lensing time delay. Already now, based on our observations of SDSS1206 during the 2010A and 2010B semesters, we obtain a preliminary estimate of the time delay between the SDSS1206 images of about 20 days (see Fig. 2). At the same time theoretically predicted time delay for this system is about 80 days. Therefore, we need carefully check our estimate of the delay. If it is really 20 days, than the model of the lensing galaxy for this system should be revised in order to reproduce the observed time delay. To confirm our preliminary estimates of the delay in SDSS1206, we continue observations of the system in the 2011A semester.

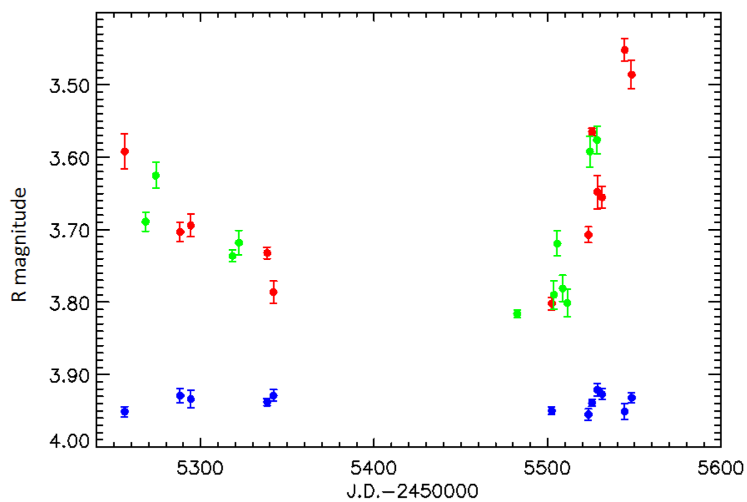

Figure 2. R-band light curves of image A (red) and image B (green) of quasar SDSS1206+2623 based on observations obtained with the 1m LOT telescope from February 28, 2010 to December 17, 2010. Image B is shifted by the delay of 20 days. The light curve of the reference star is shown in blue.

Progress Report

Rotationally Resolved Spectroscopic and Photometric Observations of Asteroids

Tai, Chih-Yang[1], Cheng, Yu-Chi[1], Ip, Wing-Huen[1,2]
1. Institute of Astronomy, National Central University
2. Institute of Space Science, National Central University

The original proposal requested 10 full nights of LOT with Hiyoyu. In the end, 10 half-nights are allocated. ~5 half-nights were under bad weather condition, For the remaining ~5 half-nights 11 asteroids were observed, as shown in Table 1.

Number	Name	Type	Period(h)
5	Astraea	S	16.8
7	Iris	S	7.139
23	Thalia	S	12.3122
37	Fides	S	7.3335
44	Nysa	E	6.422
49	Pales	C	10.42
52	Europa	C	5.633
65	Cybele	C	4.401
89	Julia	S	11.387
144	Vibilia	C	13.819
554	Peraga	C	13.63

Table 1 Asteroids observed

This report shows preliminary spectroscopic results. Fig. 1 is a spectrum of S-type asteroid (7)Iris, which was combined from three consecutive exposures, each of exposure time = 1 min. The spectrum was normalized to 1 at 5500 Å. The raw data of (7)Iris cover an interval of 0.6~0.7 rotation phase. A comparison of the sample spectrum matches rather well with the achived spectrum from the SMASS dataset. However, most of the spectra are invalid data after reduction. This problem was due to misuse of the flux/G2V standard star during observation and weather instability.

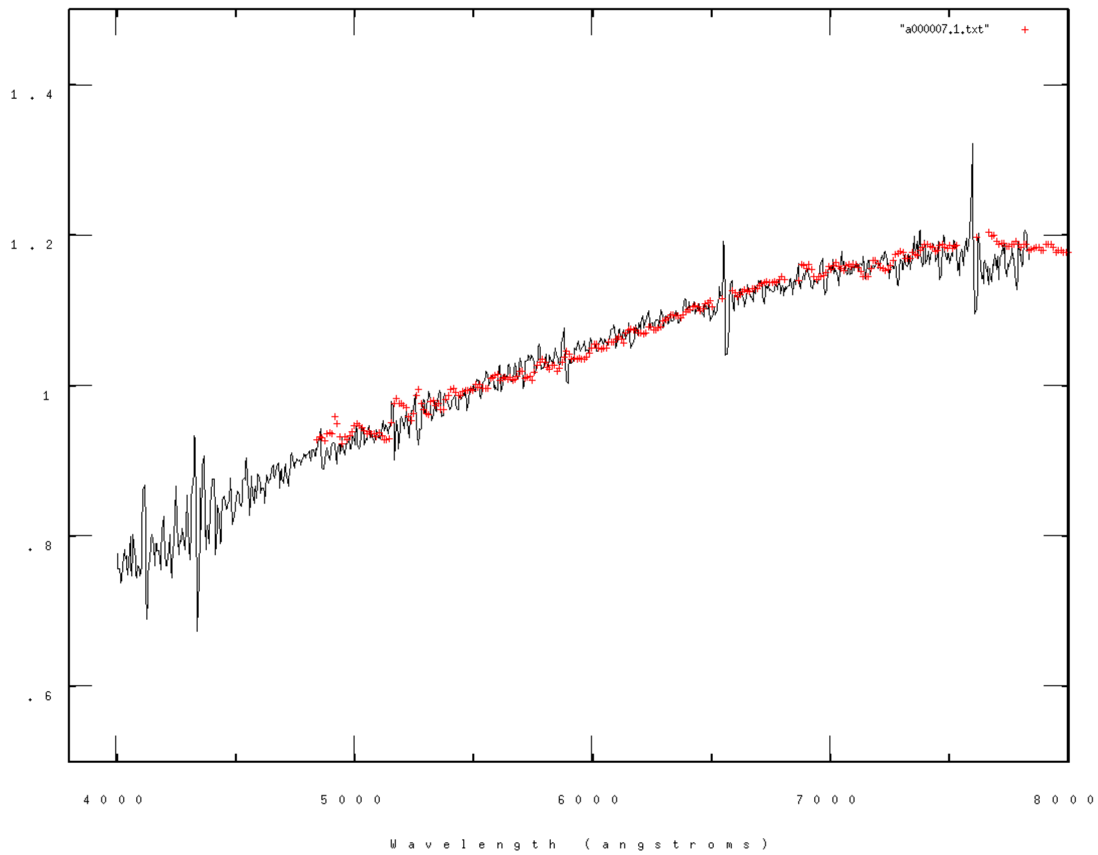

Figure 1 The spectra of (7) Iris for comparison. The black line is processed data of Hiyoyu observed at 2010-12-23 19:17:55 (UT); the red cross points were downloaded SMASS data. Both were normalized to same scale.

PS1 Follow-up : The Trigger Mechanism of Cometary Activity

Ying-Tung Chen, Hsing-Wen Lin, Wing-Huen Ip and Kinoshita Daisuke
Institute of Astronomy, NCU

The active Solar system objects such as comets are so miraculous that people started to study them for thousand years. The development of classical dynamics in .the Middle Ages was inspired by Halley’s comet observations. These kinds of objects have very inseparable connection with Earth and human life. The comet which connected to meteor showers and probably falls into the Earth was believed that it is one of sources of water on Earth. However, we only have very limited knowledge about these kinds of objects. Where did they come from? What is their composition? What is the trigger source of cometary activity? Although there are speculative answers for the above questions, they are poorly proofed by statistical results. Here we focus on the origin of the activities and their compositions.

The Comets, Main Belt Comets, Centaurs, TNOs etc, the cometary activities, were researched independently in several decades. There are three explanations for the cometary activity: (1)Solar Heating, (2)Tidal destruction, (3)Collision. These three scenarios have different feature of distribution according to the survey of large sky. By Panoramic Survey Telescope & Rapid Response System (Pan-Starrs, PS1) data, we try to monitor candidates of solar system objects, and distinguishing the active mechanisms.

In 2010B semester, we observed 4 centaurs (2060, 8405, 31824, 54598) which are the candidates of active Centaurs. Depend on object visibility, the images with Sloan filter (g, r, i, z) were obtained from 2010/08/01 to 2011/01/26. However, the image quality of them is too poor to distinguish the cometary activity, even for known active Centaur 2060 Chiron (Fig 2). For this kind of case, we are trying to develop new algorithm for analyzing the PSF profile by subtraction with PSF model of nearby background star. The new algorithm will also apply to PS1 postage stamp images of Centaurs. We believe that the combination of 2010B, 2011A and PS1 postage stamp images will reveal first step in resolution of cometary activity.

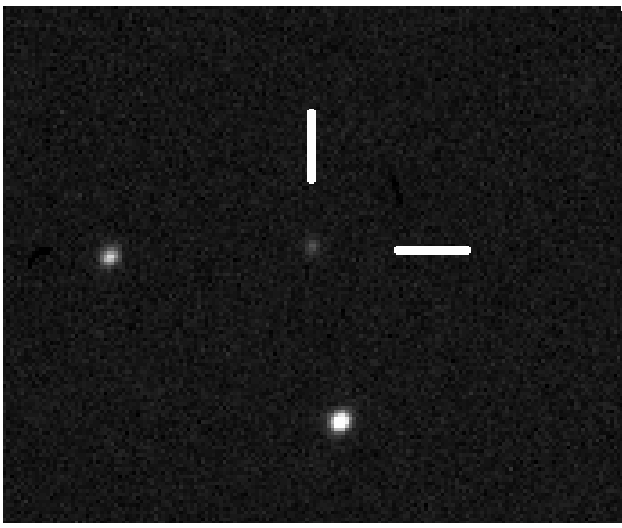

Fig The image of 8405 Centaur

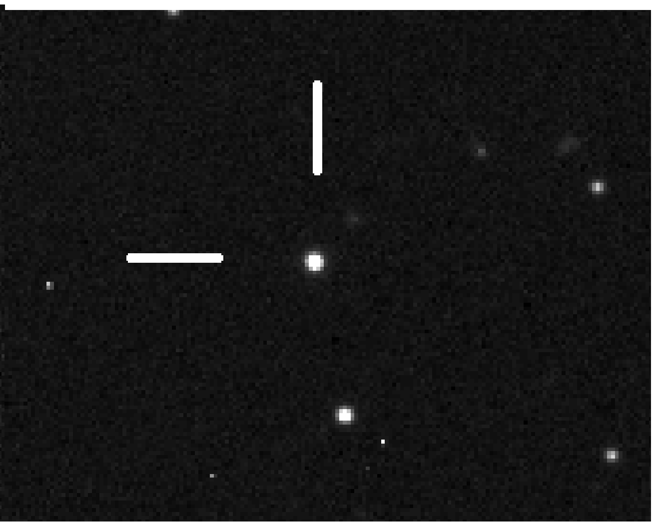

Fig 1 The image of 2060 Centaur

Scientific Results by the SLT in Global Monitoring of AGNs and Blazars

Reported by W. P. Chen (NCU/Astronomy)

2011 February 16

We continued to participate in the GASP (GLAST-AGILE Support Program), on the basis of the Whole Earth Blazar Telescope (WEBT) consortium. Using the SLT, a few targets, AGNs or Blazars, in the fields of GLAST/Fermi or AGILE would be observed every clear night, typically a couple frames in the R band. The images would be analyzed and photometry be summarized to the leading scientist of a particular program. GASP papers are always published in high ranking international journals, with multiwavelength data (radio, mm, IR, visible, X rays to gamma rays) to study the variability and hence emission mechanisms of the central engines of supermassive black holes. The author list for the paper of such a global monitoring program is inevitably long, up to hundreds, including normally 2-4 from NCU faculty, postdoc, or staff members.

In 2010, we were part of these publications:

1. Another look at the BL Lacertae flux and spectral variability: Observations by GASP-WEBT, *XMM-Newton*, and *Swift* in 2008–2009, Raiteri, C. M., Villata, M., Bruschini, L., et al. (The GASP collaboration with XMM-Newton and Swift teams, including Chen, W. P., Shiao, H. Y., and Koptelova, E. from NCU), 2010, *Astron. & Astrophy.*, 524, 43

2. *Fermi* Large Area Telescope and Multiwavelength Observations of the Flaring Activity of PKS 1510-089 between 2008 September and 2009 June, Abdo, A. A., Ackermann, M., Agudo, I. et al.

(*Fermi* Team and GASP collaboration including Chen, W. P., and Koptelova, Ekaterina from NCU), 2010, *Astrophy. J.*, 721, 1425

3. THE 2009 DECEMBER GAMMA-RAY FLARE OF 3C 454.3: THE MULTIFREQUENCY CAMPAIGN, Pacciani, I., Vittorini, V., Tavani, M., et al. (including Lin, C. S. from NCU), 2010, Astrophy. J. Lett., 716, L170

4. The Spectral Energy Distribution of *Fermi* Bright Blazars, Giommi, P. et al. (GASP Collaboration including Chen, W. P., and Koptelova, Ekaterina from NCU), 2010, *Astrophy. J.*, 716, 30

5. Multiwavelength Observations of 3C 454.3. III. Eighteen Months of Agile Monitoring of the "Crazy Diamond", Vercellone, S., D'Ammando, F., Vittorini, V., et al. (GASP collaboration including Chen, W. P. Hsiao, H. Y., Koptelova, E. from NCU), 2010, *Astrophy. J.*, 712, 405

6. A Change in the Optical Polarization Associated with a Gamma-Ray Flare in the Blazar 3C 279, Abdo, A. A., Ackermann, M. A., Ajello, M., et al. (The Fermi-LAT Collaboration, and the GASP collaboration including Chen, W. P., Koptelova, E., and Lin, H. C. from NCU), 2010, *Nature*, 463, 919

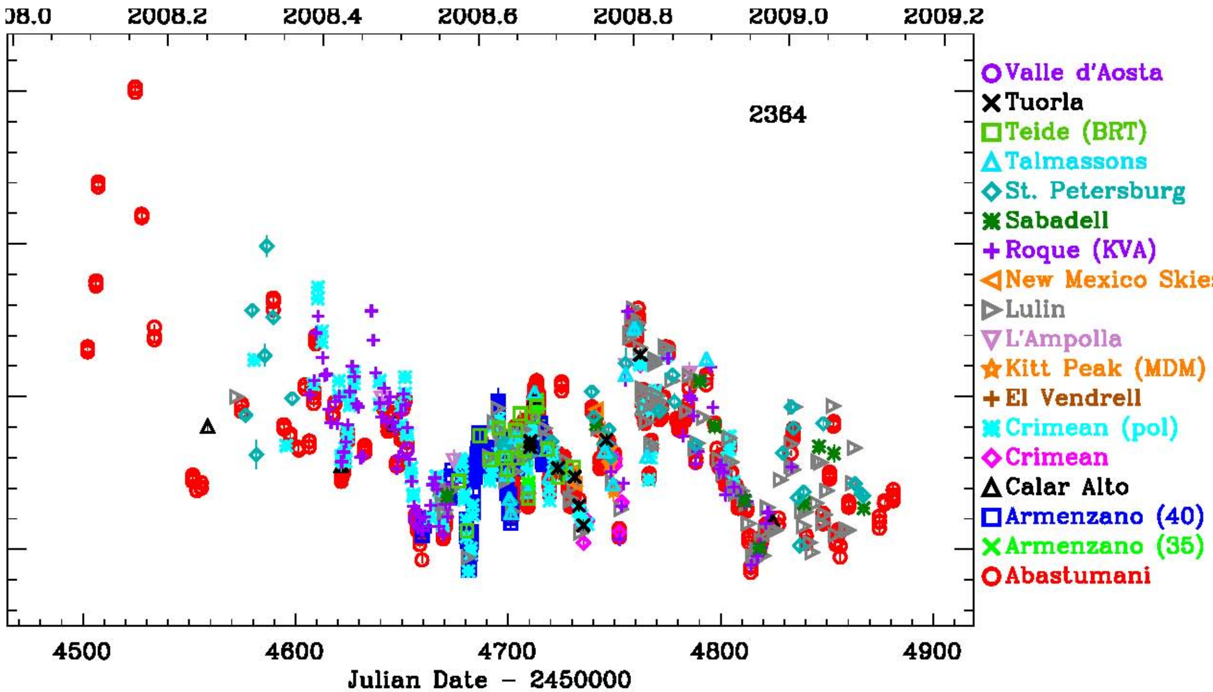

An example light curve of BL Lac showing the photometric variation measured by the WEBT telescopes, including the SLT contribution (figure taken from 2010 A&A., 524, 43)

尋找木星特洛伊小行星群中的雙星系統

林省文

在我們的研究中，我們試圖瞭解木星特洛伊小行星群的來源，並推測太陽系的演化。木星特洛伊小行星群聚集於木星的兩個拉格朗日點(Lagrangian point)，研著木星的軌道繞行太陽。這類小行星的起源仍然未知，不過目前科學家們相信有兩種可能的來源：

1. 太陽系形成初期，物質就聚集在木星的兩個拉格朗日點，進而形成小行星群。
2. 這些小行星在其他地區形成，可能在太陽系外圍的古柏帶 (Kuiper Belt)。後來因爲某些因數造成的不穩定使這些小行星進入內太陽系被木星捕捉於兩個拉格朗日點。

我們在這裡提出兩個可以觀測得到的物理量來瞭解以上哪個理論可能是正確的：

1. 雙星率：小行星雙星靠著彼此微弱的重力連結，如果雙星在其他地方形成，經過擾動進入內太陽系被木星捕捉這種劇烈的變動很可能就會崩解。如果我們發現特洛伊小行星群有極高的雙星率，那麼對於來源 2 這個理論很不利。
2. 小行星密度： 研小行星雙星互相繞行的週期與軌道，我們可以得到這個系統的質量，加上一些假設我們可以估算出小行星的密度。這有助於瞭解這些特洛伊小行星的來源，如果它們由古柏帶來，或許會有類似的密度。

目前爲止我們利用中央大學的鹿林天文台一米望遠鏡與中國科學院雲南天文台的二點四米望遠鏡調查了一百多顆特洛伊小行星發現其中三顆有很大的光變現象，爲可能的雙星系統（圖一）。正利用鹿林天文台一米望遠鏡與亞歷桑納州的 Tenagra 七十六公分往遠鏡進行後續觀測後所得的光度曲線如圖二。我們試圖使用 Lomb-Scargle periodogram 尋找這三顆小行星的自轉或是互繞週期，然而這一季的觀測取得的數據太過於分散，使用 Lomb-Scargle periodogram 沒有找到可信的週期。目前我們嘗試使用 PDM 來尋找可能的週期。初估小行星(4946)的週期大概在 8~9 小時左右。
此外我們還發現在兩個拉格朗日點的小行星群可能有不同的光度變化分布（圖三）。這代表這兩群小行星有不同的形狀分布，其中ㄧ群可能比較破碎。至於是否代表這兩群小行星有不同的來源，目前我們不得而知。

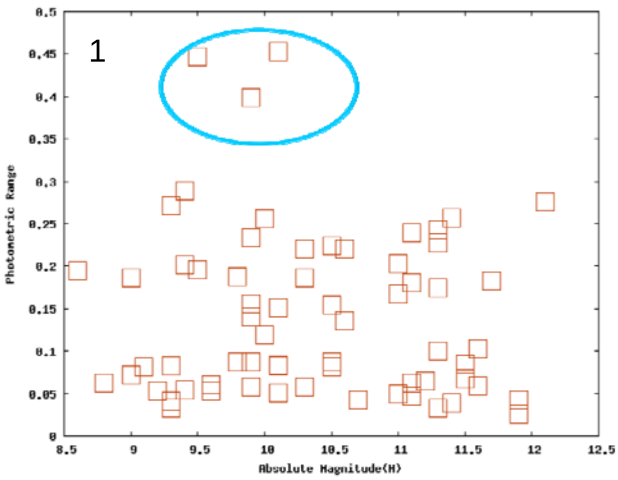

圖一：小行星光度變化強度, 藍色圈圈中的三個小行星有特別大的光度變化, 是 可能的雙星系統。

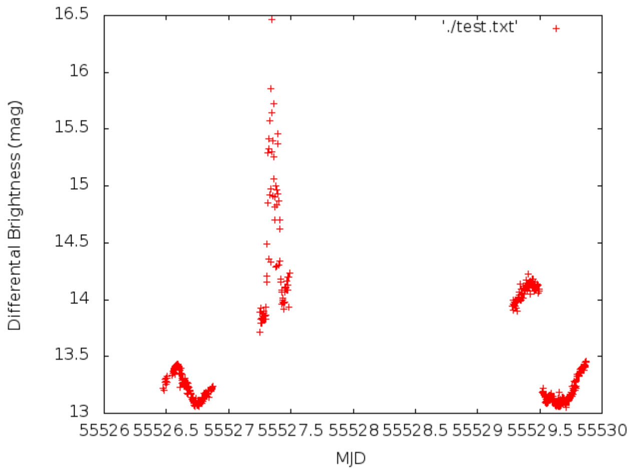

圖二：小行星(4946)的光度曲線。

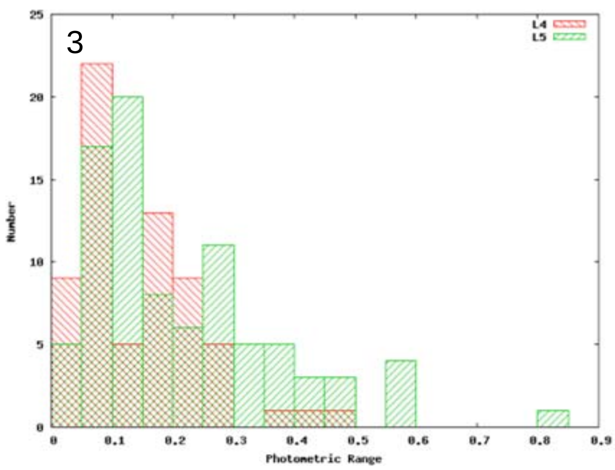

圖三：小行星光度變化強度分布圖, 可以看出在兩個不同的拉格朗日點的小行星群, 分別用紅色和綠色來表示, 有不同的分布趨勢。

TAOS Project: Searching for Variable Stars in the Selected TAOS Fields and Optical Follow-up Observations

K.S. Pan[1], C.C. Ngeow[1], W.P. Chen[1], D.C. Chang[2], Z.W. Zhang[3]

[1] Graduate Institute of Astronomy, NCU
[2] Department of Physics, NCU
[3] Academia Sinica Institute of Astronomy and Astrophysics (ASIAA)

The goal of our project is to obtain follow up time series observations for the unknown variable stars found in the TAOS project, and study these variables in details based on the data from TAOS and our project. The TAOS photometry allowed us to find roughly about 50 candidates (out of total of 2654 stars) in TAOS-060 field using the well developed variable stars finding algorithm. These 50 candidates were continuously observed in BVRI filters using the LOT and SLT telescopes available at the Lulin Observatory of Taiwan. The BVRI photometry will permit some important parameters, for example extinction, colors and brightness, to be derived for these candidates. We used IRAF to reduce the imaging data, and applied SExtractor for cataloging and photometry measurement. We present the preliminary results in this presentation.

Introduction

– Finding Variable Stars in Selected TAOS Field

- In addition to the KBO study, the long duration (~4 years) and dense sampling of TAOS (Taiwan-American Occultation Survey) data can be used to find new variable stars.
- In this project, we search for variable stars in TAOS 060 Field, located at RA: $04^h48^m00^s$ DEC:$+20^d46^m20^s$ (with limiting mag. Of ~15mag at S/N=10), using the stare mode data.
- Stars in TAOS 060 Fields have measurements up to ~500 points, spanning for ~150 days.
- Variables were searched using the sigma-deviation (n-sigma deviated from the means, illustrated in **Figure 1**) method and Stetson's J-index (Stetson 1996, PASP 108:851).
- Out of the ~2600 stars, we found ~50 variable candidates using both methods, including three previously known variables in the field.

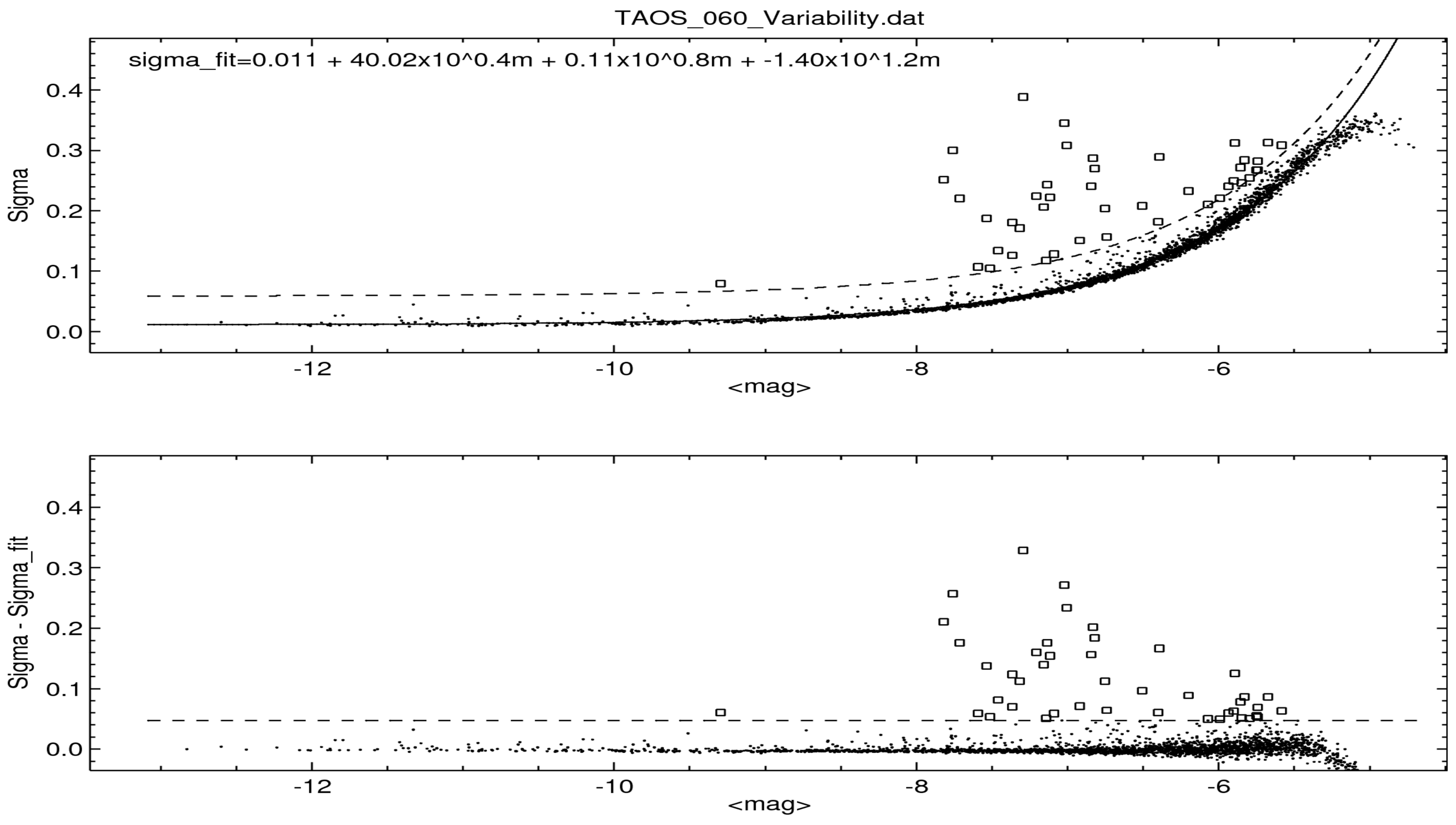

Figure 1: Variable candidates searched from using the sigma-deviation method. An empirical equation (solid curve in upper panel) was fitted to the mean magnitudes (expressed in term of the TAOS instrumental magnitudes) and the standard deviations of the means. A cut at certain threshold of the fitted curves (dashed line in the bottom panel) was used to select the variable candidates (open squares) from the "constant" stars (dots).

num	Coords (J2000)	Period (days)	Amplitude
1	04:44:54.1 +20:03:02	0.377998	0.6
2	04:49:06.6 +21:08:13	0.286447	1
3	04:47:18.4 +20:34:46	0.548221	0.6
4	04:50:18.7 +21:14:53	0.638394	0.8
5	04:48:48.8 +20:55:09	0.717851	2
6	04:45:32.3 +21:15:01	0.633039	1

Table 1 : Some examples we can recognize them surely are variable stars.

Figure 2: We select six variable stars examples to show their light-curve form TAOS 060 field

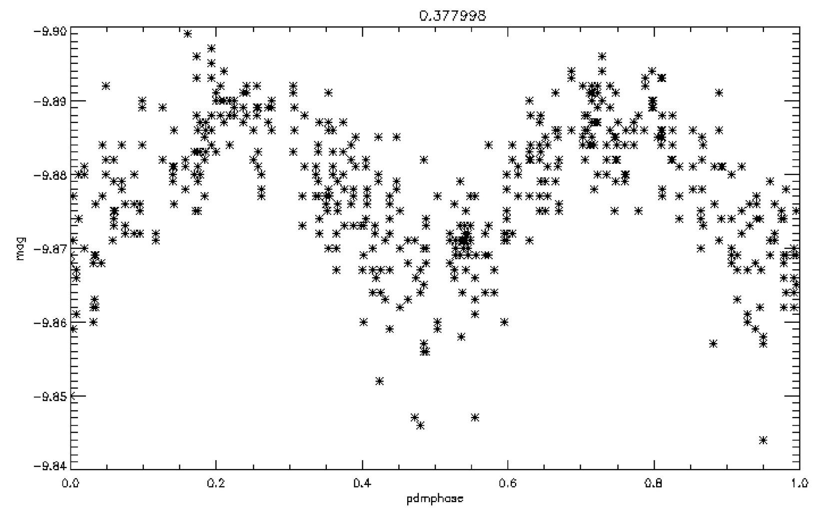

Figure 2-1

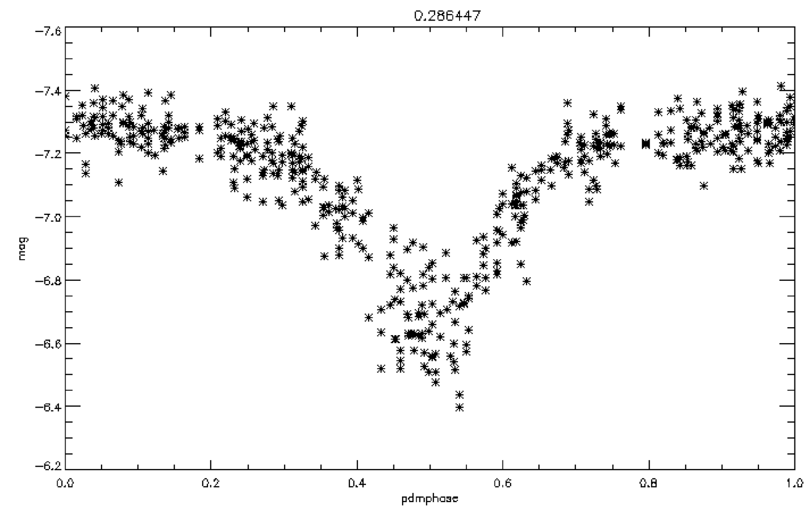

Figure 2-2

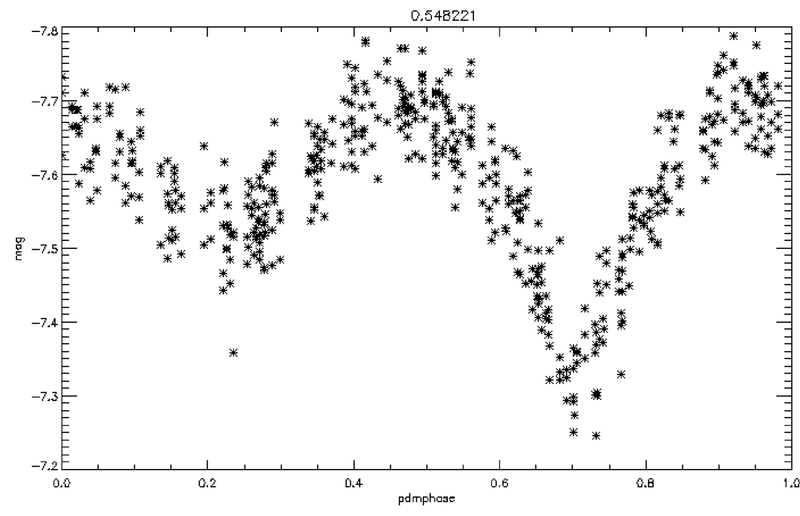

Figure 2-3

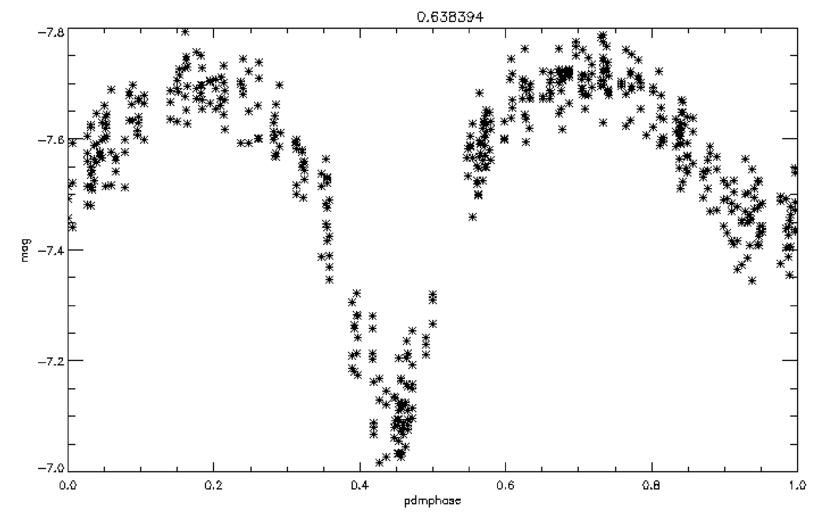

Figure 2-4

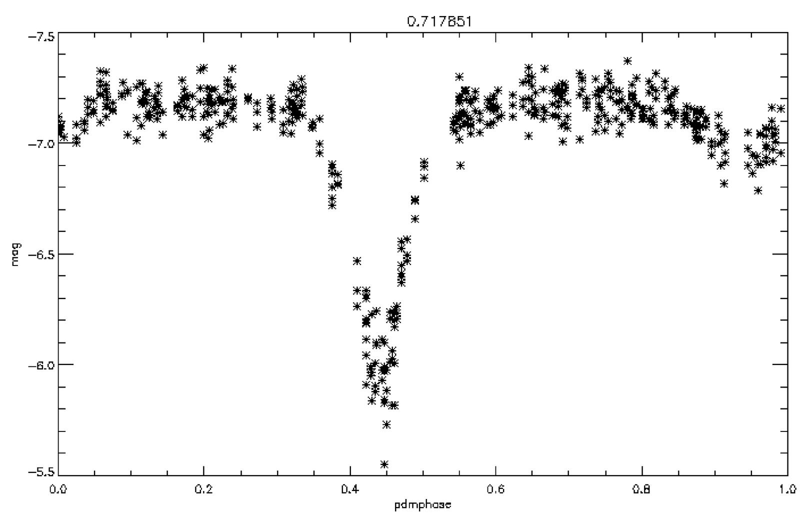

Figure 2-5

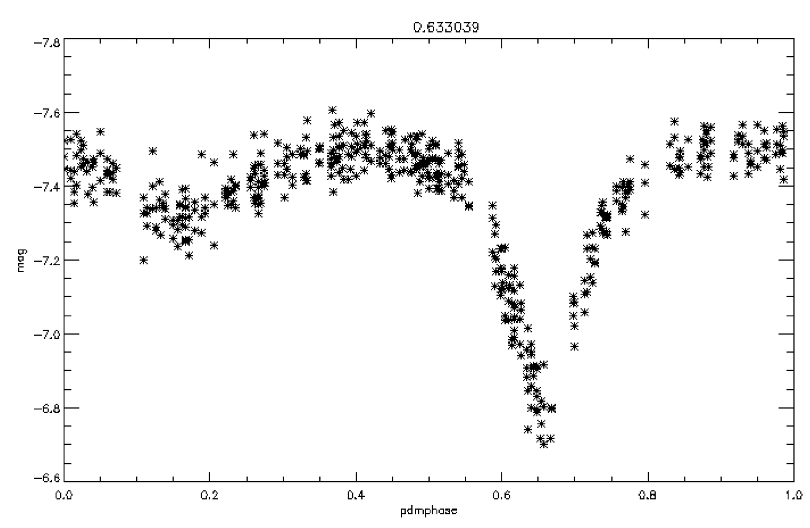

Figure 2-6

Observation & Analysis

– Optical Follow-Up of the Candidates

- TAOS observations were conducted using a customized broad-band filter. Hence an optical follow-up program were initiated to observe and construct the light curves of the TAOS 060 candidate variables in the *BVRI* bands, using the Lulin's One-Meter telescope (LOT) and the SLT telescope (0.4m aperture), from the Lulin Observatory, as well as the 0.81m telescope from the Tenagra II Observatory.
- The multi-band optical follow-up observation will help in improving the classification of these candidates, estimate their *BVRI* mean magnitudes, colors as well as extinction. This will enable a wide range of research in astrophysics for these variables.
- By selecting images form one night as reference images, other 25 nights of images were used to calculate the magnitude difference. **Figure 3** shows the diagram with reference magnitude R-band to differenced mag. The median differenced mag. is 12.3035. For each band, the mag. of the targets were subtracted by this differenced mag. Then plots the light-curve phased diagram (Figure 4.) .

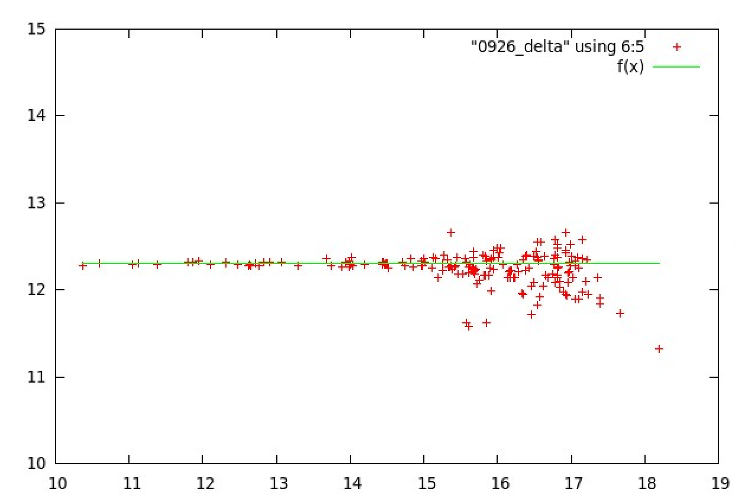

Figure 3 : This plot can help us to calculate the difference is 12.3035.

Figure 4 : The light-curve result for multi-band optical BVRI. The target is the **Figure** which Coords(J2000) is 04:47:18.4 +20:34:46 and Period (days) in our analysis is 0.633637..

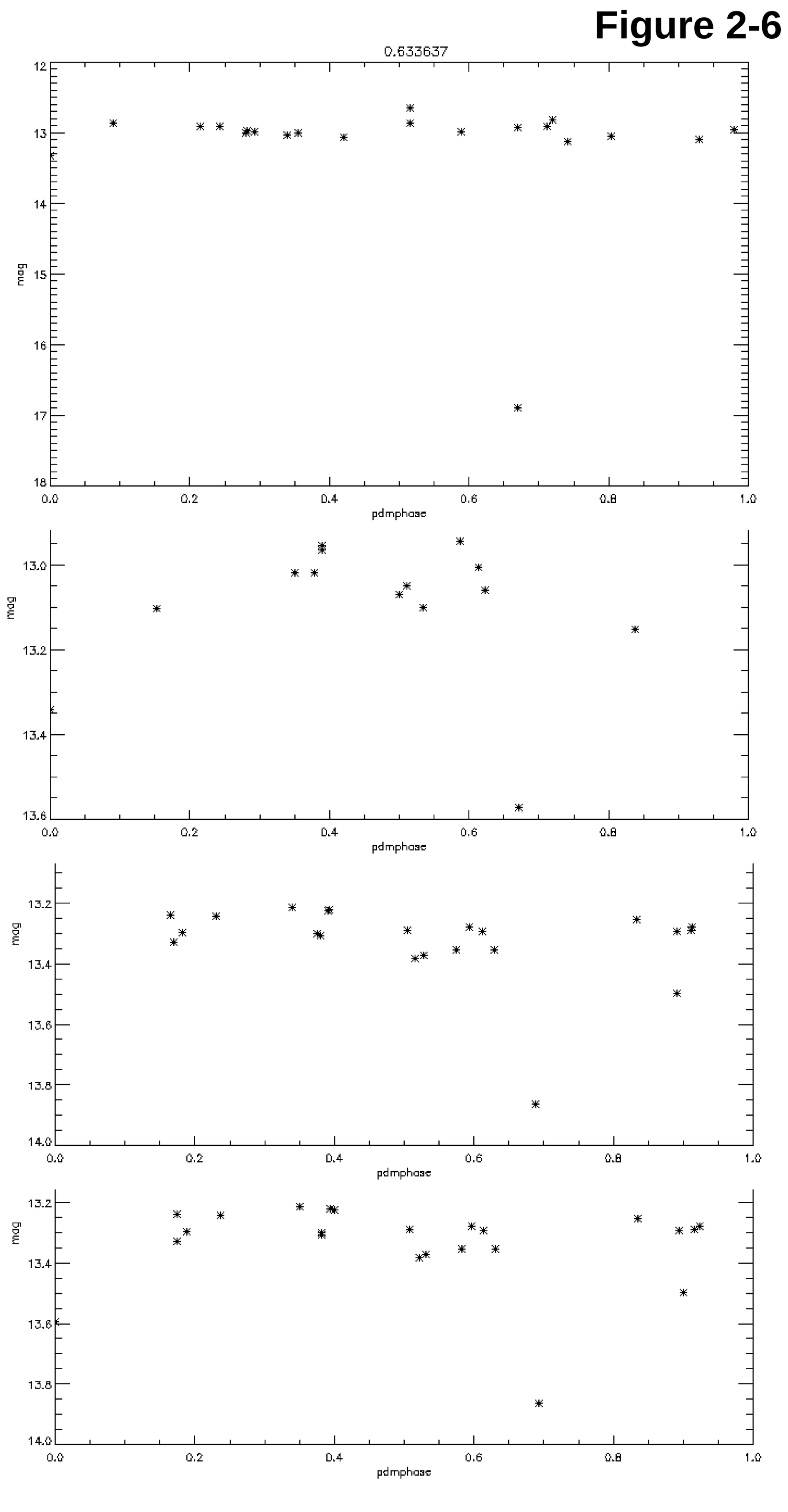

Acknowledgement: CCN thank the funding from National Science Council (of Taiwan) under the contract NSC 98-2112-M-008-013-MY3.

Ground-Based Optical Follow-Up Observation of Cepheid Candidates in *Kepler's* Field

C.-C. Ngeow[1], R. Szabo[2], L. Szabados[2], A. Derekas[2,4], P. Moskalik[5], J. Nuspl[2], H. Lehmann[6], G. Furesz[7], J. Molenda-Zakowicz[8], S. T. Bryson[9], A. A. Henden[10], D. W. Kurtz[11], D. Stello[12], J. M. Nemec[13], J. M. Benko[2], L. Berdnikov[14,15], H. Bruntt[16], N. R. Evans[17], N. A. Gorynya[18], E. N. Pastukhova[18], R. J. Simcoe[14], J. E. Grindlay[19], E. J. Los[19], A. Doane[19], S. G. Laycock[19], D. J. Mink[17], G. Champine[19], A. Sliski[19], G. Handler[3], L. L. Kiss[2], Z. Kollath[2], J. Kovacs[20], J. Christensen Dalsgaard[21], H. Kjeldsen[21], W. J. Borucki[9]

[1]Graduate Institute of Astronomy, National Central University; [2]Konkoly Observatory of the Hungarian Academy of Sciences; [4]Department of Astronomy, Eotvos University; [5]Copernicus Astronomical Center; [6]Thuringer Landessternwarte Tautenburg, Karl-Schwarzschild-Observatorium; [7]Harvard-Smithsonian Center for Astrophysics; [8]Astronomical Institute, University of Wroclaw; [9]NASA Ames Research Center; [10]American Association of Variable Star Observers; [11]Jeremiah Horrocks Institute of Astrophysics, University of Central Lancashire; [12]Sydney Institute for Astronomy, School of Physics, The University of Sydney; [13]Department of Physics & Astronomy, Camosun College; [14]Sternberg Astronomical Institute, Moscow University; [15]Isaac Newton Institute of Chile, Moscow Branch; [16]LESIA, UMR 8109, Observatoire de Paris; [17]Smithsonian Astrophysical Observatory; [18]Institute of Astronomy, Russian Academy of Sciences;[19]Harvard College Observatory; [20]Gothard Astrophysical Observatory; [21]Department of Physics and Astronomy, Aarhus University

The Kepler Space Telescope

- NASA's mission aimed to find Earth size and larger planets around other stars.
- Almost un-interrupted observation of a 105 deg^2 field near Galactic Plane, with ~223,000 stars in the field.

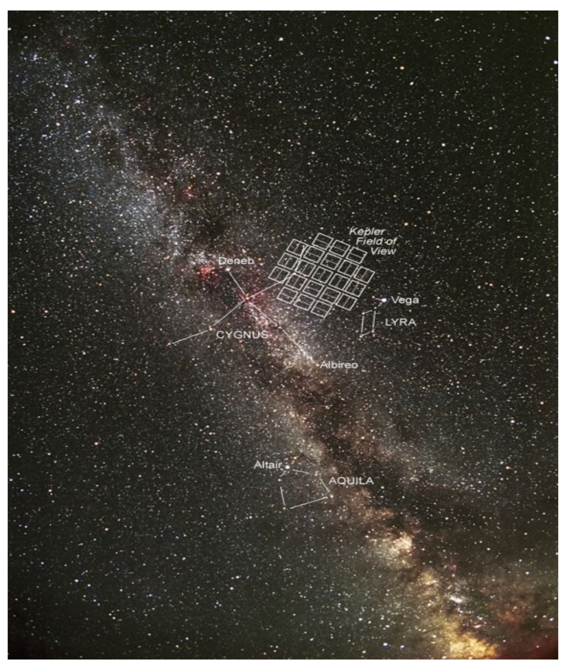

Kepler Asteroseismic Science Consortium

- In addition to finding extra-solar planets, *Kepler's* observation can also be used for asteroseismology and stellar variability studies.

  → Goal for **KASC** (http://astro.phys.au.dk/KASC/)
- Total there are 13 Working Group within KASC, WG #7 is dedicated to Cepheid study.

The Cepheid Variables

- Intrinsic pulsating variables that are crossing the instability strip in the Hertzsprung-Russell diagram, named after prototype delta Cepheid.
- Yellow supergiants with mass between ~3 to ~11 M_{sun} and surface temperature from ~4500K to ~6500K. Pulsating period range from ~1 to ~100 days, and obey the period-luminosity relation.
- Important astrophysical tools for (a) distance scale studies; and (b) stellar pulsation/evolution studies.

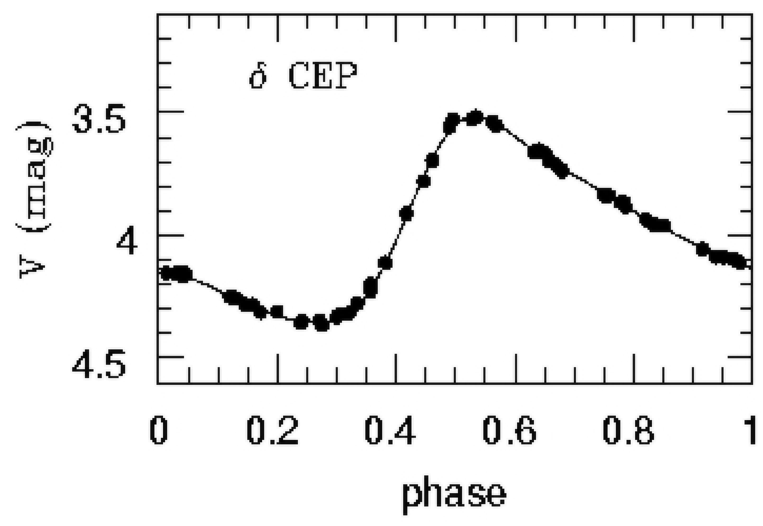

Cepheid Within The Kepler's Field

- Two previously known Cepheids in the field:

  V1154 Cyg & V2279 Cyg
- Additional Cepheid candidates selected from published catalogs of variable stars (including ASAS, ROTSE and HAT), and the *Kepler's* Input Catalog for stars located inside or near the instability strip. Total of ~40 initial targets were selected.
- However, after release of first *Kepler's* light curves, only few Cepheid candidates remained. We focused on V1154 Cyg and V2279 Cyg in this presentation.

Ground-Based Optical Follow-Up Observations

- *Kepler's* magnitude system, *Kp*, is based on broad band (430 – 900 nm) transmission of the telescope and detector. Hence, ground-based multicolor (and spectroscopic) follow-up observation is needed to complement the *Kepler's* light curve.
- Time-series observation (more than 3 months) were conducted with the following telescopes:

  I. Lulin One-meter Telescope (LOT) @ Lulin Observatory, Taiwan: 1.00-m Cassegrain telescope with PI1300B CCD.

  II. SLT @ Lulin Observatory, Taiwan: 0.40-m Ritchey-Chretien telescope with Apogee U9000 CCD.

  III. Tenagra telescope (TNG) @ Tenagra II Observatory, Arizona (USA): 0.81-m robotic telescope with STIe CCD.

  IV. Sonoita Research Observatory (SRO) @ Arizona (USA): 0.35-m robotic telescope with SBIG STL-1001E CCD.
- Imaging data process involved the following steps:

  I. Standard IRAF reduction (bias and dark subtracted, flat-fielding).

  II. Cataloging and aperture photometry using SExtractor.

  III. Calibration to standard magnitudes using Landolt standard stars.

Result From The Observation

- The resulted *BVRI* light curves for these two Cepheids are presented below. For clarity, error-bars were plotted for data points with errors > 0.02mag.

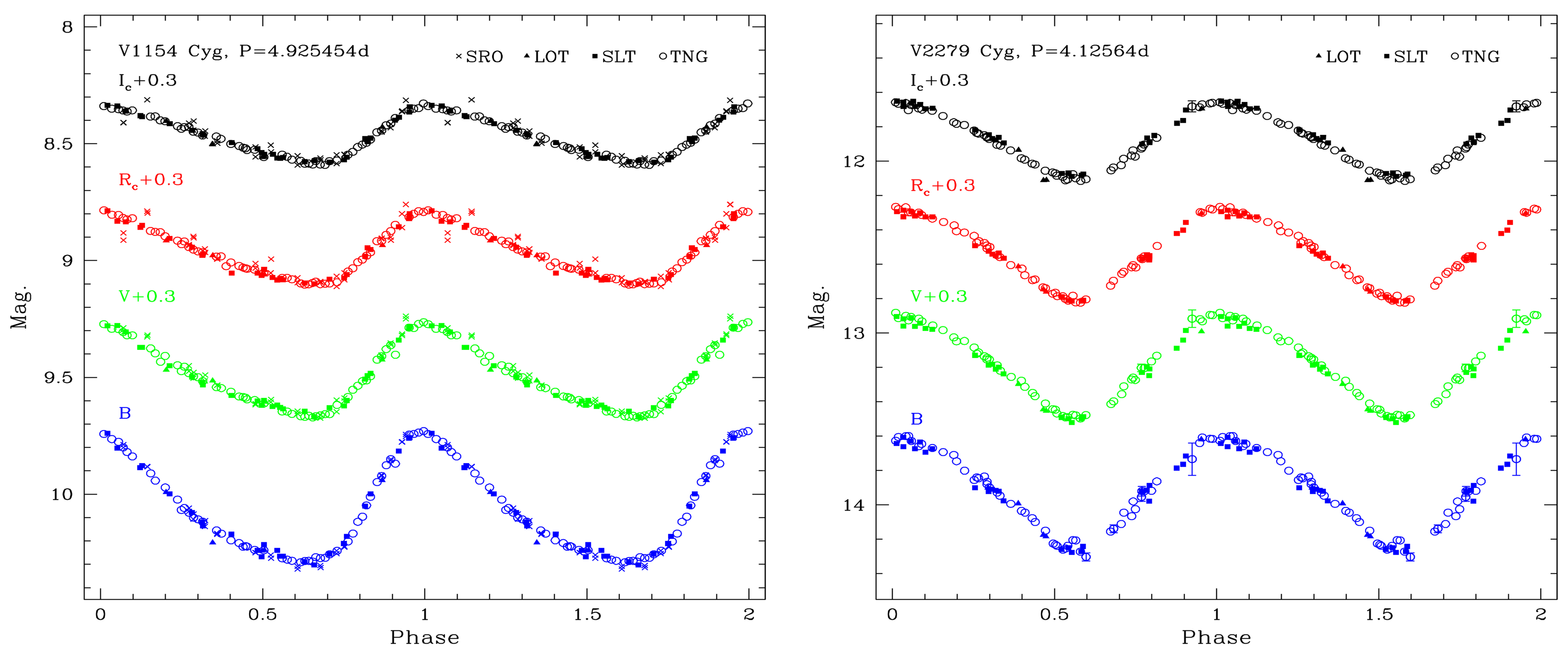

- *BVRI* light curves properties (amplitudes and Fourier decomposition) suggested V2279 Cyg is *not* a Cepheid.
- Flares shown up in *Kepler's* light curves.
- Additional spectroscopic observations confirmed non-Cepheid nature of this star, and most likely being a rotation star.

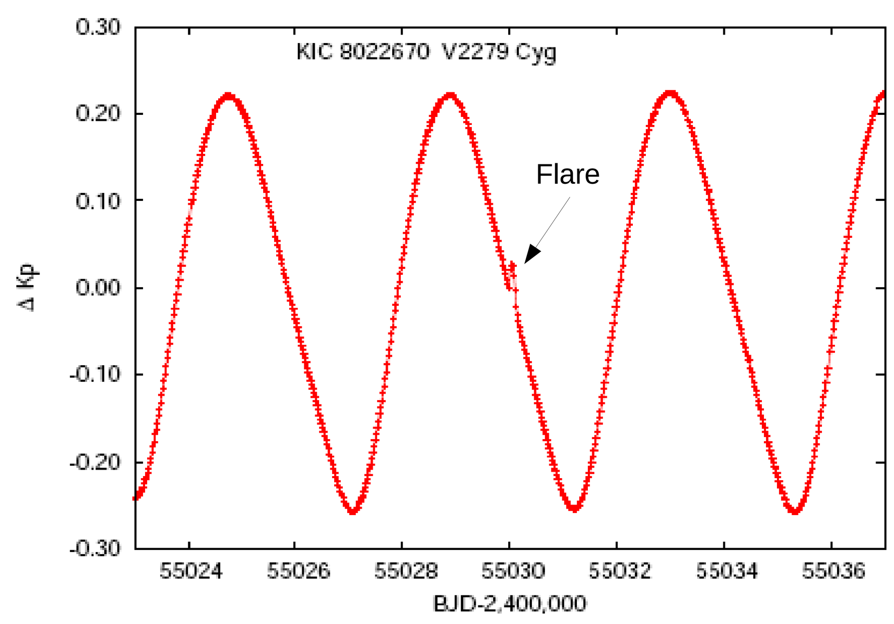

- *BVRI* light curves properties and radial velocity measurement from spectroscopic observation suggested V1154 Cyg is a *bona-fide* fundamental mode Cepheid.
- Very stable light curve behavior from *Kepler's* ultra-precision photometry.

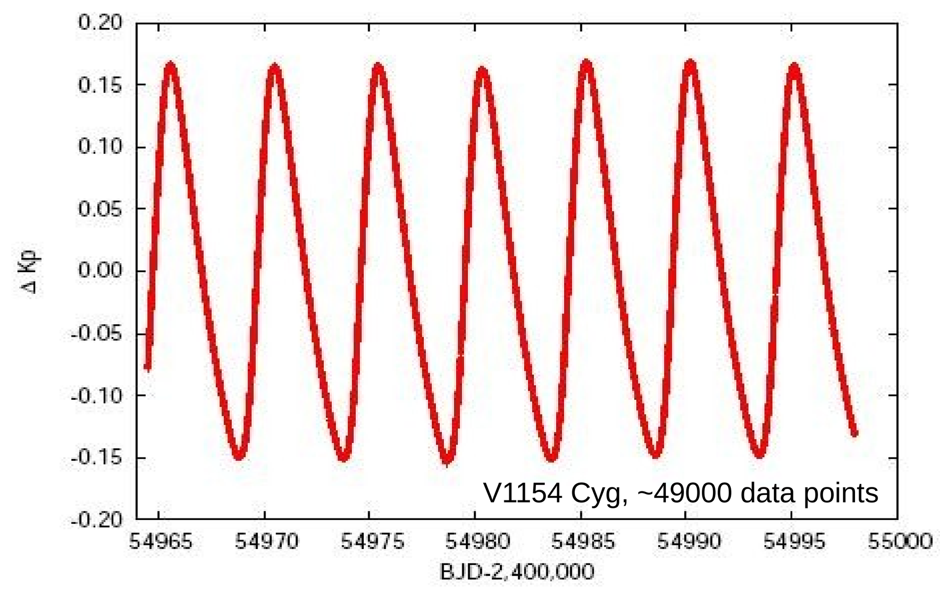

- *BVRI* and *Kepler's* light curves also ruled out other candidates being Cepheid. V1154 Cyg remained the only Cepheid in *Kepler's* field.

CCN thanks the funding from National Science Council (of Taiwan) under the contract NSC 98-2112-M-008-013-MY3. Funding for Kepler mission is provided by NASA's Science Mission Directorate.

Contact email: cngeow@astro.ncu.edu.tw

TAOS Project: Searching for Variable Stars in the Selected TAOS Fields and Optical Follow-up Observations

C.-C. Ngeow[1], D.-C. Chang[1], K.-S. Pan[1], T.-A. Chung[1], E. Koptelova[1]
& the TAOS Collaboration
([1] National Central University, Taiwan)

The Taiwan-American Occultation Survey (TAOS) Project

- Aim: to find small Kuiper Belt Objects (KBO, size from 500m to 30km) and measure their size distribution using the occultation technique.
- The TAOS project employed four 20-inch wide-field (F/1.9, 3 degree-squared FOV) telescopes, equipped with a 2K x 2K CCD, to simultaneously monitor the same patch of the sky.
- Two readout mode: (a) zipper mode for fast and continuous readout; (b) stare mode for regular imaging before zipper mode
- All four TAOS telescopes, which can be operated automatically, were located at the Lulin Observatory in central Taiwan (see **Figure 1**). The TAOS project has been continuously taking data since 2005.
- See http://taos.asiaa.sinica.edu.tw/index.php for more details.

Figure 1: A view of the Lulin Observatory. Two of the TAOS telescopes can be seen at the front of the picture. The third telescope is located at the upper-left corner (the fourth telescope is not shown). The building at the back hosted the 40cm SLT telescope, one of the main telescopes currently operated at the Lulin Observatory. (Image credit: The Lulin Observatory, operated by the National Central University)

Finding Variable Stars in Selected TAOS Field

- In addition to the KBO study, the long duration (~4 years) and dense sampling of TAOS data can be used to find new variable stars.
- In this project, we search for variable stars in TAOS 060 Field, located at RA: $04^h48^m00^s$ DEC:$+20^d46^m20^s$ (with limiting mag. Of ~15mag at S/N=10), using the stare mode data.
- Stars in TAOS 060 Fields have measurements up to ~500 points, spanning for ~150 days.
- Variables were searched using the sigma-deviation (n-sigma deviated from the means, illustrated in **Figure 2**) method and Stetson's J-index (Stetson 1996, PASP 108:851).
- Out of the ~2600 stars, we found ~50 variable candidates using both methods, including three previously known variables in the field.

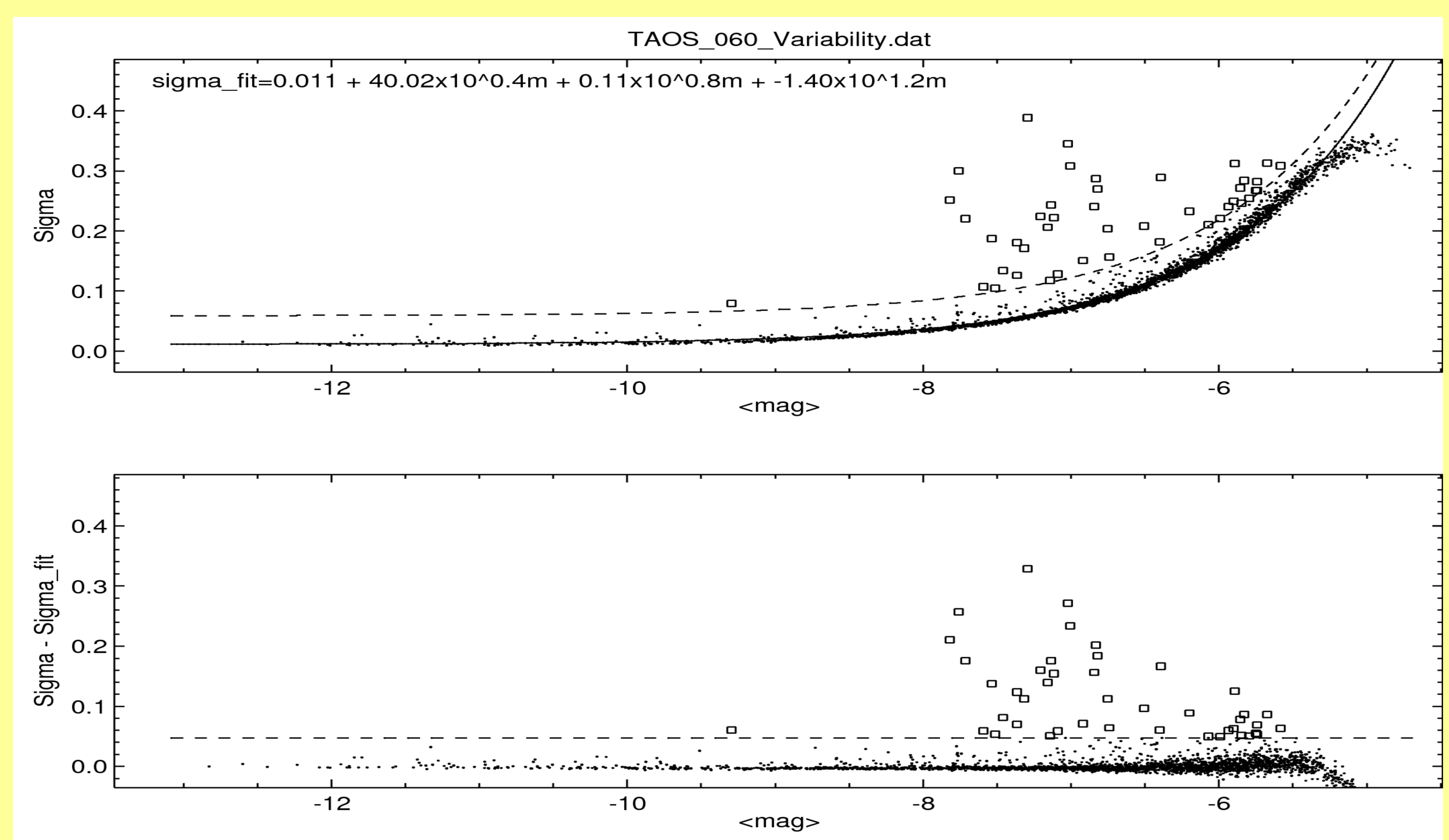

Figure 2: Variable candidates searched from using the sigma-deviation method. An empirical equation (solid curve in upper panel) was fitted to the mean magnitudes (expressed in term of the TAOS instrumental magnitudes) and the standard deviations of the means. A cut at certain threshold of the fitted curves (dashed line in the bottom panel) was used to select the variable candidates (open squares) from the "constant" stars (dots).

Optical Follow-Up of the Candidates

- TAOS observations were conducted using a customized broad-band filter. Hence an optical follow-up program were initiated to observe and construct the light curves of the TAOS 060 candidate variables in the *BVRI* bands, using the Lulin's One-Meter telescope (LOT) and the SLT telescope (0.4m aperture), from the Lulin Observatory, as well as the 0.81m telescope from the Tenagra II Observatory.
- The multi-band optical follow-up observation will help in improving the classification of these candidates, estimate their *BVRI* mean magnitudes, colors as well as extinction. This will enable a wide range of research in astrophysics for these variables.
- **Table 1** summarized the available nights, the telescopes used and the image qualities in each bands for our observation.
- **Figure 3** shows the preliminary results from our optical follow-up observations for one of the candidates. This star is an Algol-type (EA) eclipsing binary.

Table 1: Summary of the follow-up observation for TAOS 060 Field. The FWHM (in arcsecond) is the median FWHM of the available images in a given band, for a particular night.

Night	Telescope	FWHM (B)	FWHM (V)	FWHM (R)	FWHM (I)
2009 Dec 26	LOT	2.30	2.31	2.29	1.98
2010 Jan 24	Tenagra	----	----	2.96	----
2010 Feb 01	Tenagra	2.58	2.62	2.47	2.35
2010 Feb 10	SLT	3.62	2.97	3.29	3.64
2010 Feb 11	SLT	3.64	2.90	2.77	2.98
2010 Feb 12	Tenagra	3.16	3.09	2..90	2.73
2010 Feb 13	Tenagra	2.74	2.70	2.51	2.26
2010 Feb 14	Tenagra	3.20	2.94	2.96	2.66
2010 Feb 15	Tenagra	2.95	2.81	2.65	2.56
2010 Feb 16	Tenagra	2.91	2.65	2.59	2.47
2010 Feb 17	Tenagra	2.84	2.74	2.57	2.53
2010 Feb 18	Tenagra	2.39	2.12	1.97	1.97
2010 Feb 19	Tenagra	2.44	2.29	2.16	2.13
2010 Feb 20	Tenagra	2.39	2.21	2.17	2.07
2010 Mar 01	LOT	1.70	1.58	1.40	1.39

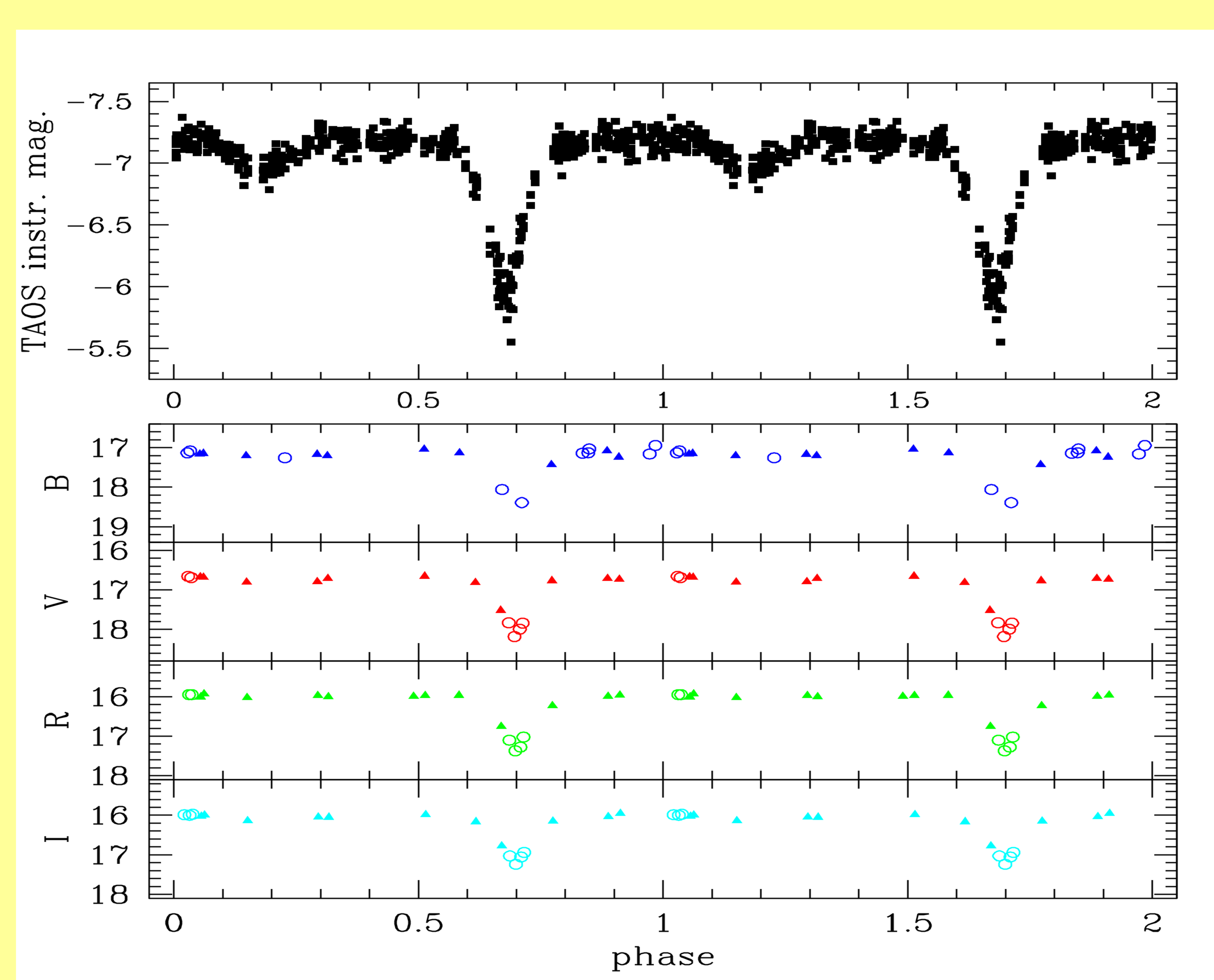

Figure 3: Light curves for one of the TAOS 060 candidates from TAOS (upper panel) and our optical follow-up observation (bottom panel; open circle=SLT; filled triangle=Tenagra). The period of this variable is 0.71791 days, obtained from using the phase dispersion minimization technique (Stellingwerf, 1978, ApJ 224:953). The *BVRI* photometry has been calibrated relatively, and not yet calibrated to the standard Johnson/Cousin system. Error-bars are omitted for clarity.

Acknowledgement: CCN thank the funding from National Science Council (of Taiwan) under the contract NSC 98-2112-M-008-013-MY3.

工作報告

Thermal Design of Dewar for CCD Camera

KINOSHITA Daisuke

02 April 2010

Abstract

This short report describes the calculation of the inflow of the heat into the dewar of our CCD camera which is being developed. The CCD is planned to be cooled down to -100°C. Before the manufacturing of the dewar, it is critically important to estimate the inflow heat flux into the dewar, and compare it with the cooling power of the cryocooler. To estimate the total heat inflow, the radiation from the dewar window, the radiation from the dewar wall, the conduction through the polycarbonate posts, and the conduction through the copper lines are considered. The result of the calculation shows that the heat inflow is $\sim$ 3W. It is small enough compared to the cooling power of the cryocooler.

1 Introduction

The astronomical instrument development team at the Institute of Astronomy of National Central University aims to develop a CCD camera for 2-m telescope which is being built at Lulin Observatory. The CCD chip must be cooled down the low temperature to reduce the noise. Typical operation temperature of CCD chip for research purpose camera is about -100°C. At this temperature, the dark current electron generation rate is negligible. We have to make sure that the cryocooler has enough cooling power to maintain the CCD temperature as low as the target operation temperature. In order to estimate the cooling capability, one needs to calculate the inflow heat flux into the dewar of the camera, and compare it to the cooling power of the cryocooler.

2 Dewar Structure

Here, I assume a cylindrical shaped dewar with the diameter of 150-mm and the height of 100-mm. The size of a circular window of the dewar is set to be $\phi = 90$-mm. A schematic drawing of the dewar structure is shown in Fig. 1.

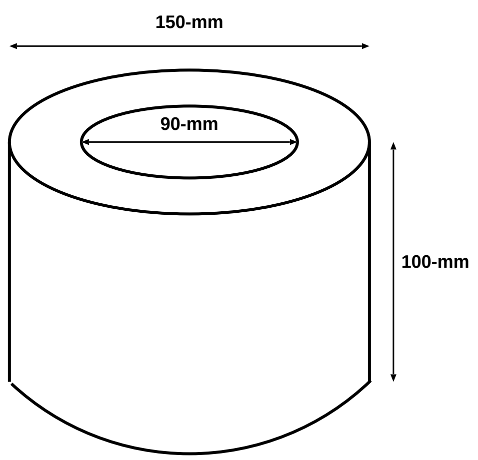

Figure 1: The schematic drawing of the structure of the dewar. It is a cylindrical shaped dewar with 150-mm diameter and 100-mm height. At the center of the top of the dewar, there is a fused silica window of $\phi = 90$-mm.

3 Calculations of Inflow Heat Flux

I calculated the total inflow heat flux into the dewar. Four heat sources were considered. Those are the radiation from the dewar window, the radiation from the dewar wall, the conduction through the polycarbonate posts, and the conduction through the copper lines. The calculations are based on the work by Okamura et al. (1996) and Miyazaki et al. (2002).

3.1 Radiation from Dewar Window

The incoming heat flux by the thermal transfer due to the radiation from the dewar window is expressed as

$$\dot{Q}_{win} = \sigma \left(T_{ambient}^4 - T_{CCD}^4 \right) A_{win} \frac{\epsilon_{win}\epsilon_{CCD}}{\epsilon_{win} + \epsilon_{CCD} - \epsilon_{win}\epsilon_{CCD}}. \tag{1}$$

Here, $\dot{Q}_{win}$ is the inflow heat flux by the radiation from the window, σ is the Stephan-Boltzmann constant ($\sigma = 5.67 \times 10^{-8}$ Wm^{-2}K^{-4}), A_{win} is the area of the dewar window, $T_{ambient}$ is the ambient temperature near the dewar window, T_{CCD} is the CCD operation temperature, ϵ_{win} is the emissivity of the fused silica window, ϵ_{CCD} is the emissivity of the CCD. The area of the dewar window is $A_{win} = \pi \left(\frac{D_{win}}{2} \right)^2 = 6.36 \times 10^{-3}\,\mathrm{m}^2$. The ambient temperature near the window and CCD temperature are chosen to be $T_{amb} = 283\,\mathrm{K}$ and $T_{CCD} = 173\,\mathrm{K}$, respectively. The emissivities of the window and CCD are assumed as $\epsilon_{win} = 1.0$ and $\epsilon_{CCD} = 0.5$, respectively. Then, the heat inflow by the radiation from the dewar window is estimated as

$$\dot{Q}_{win} = 1.0\,\mathrm{W}. \tag{2}$$

3.2 Radiation from Dewar Wall

The incoming heat flux by the thermal transfer due to the radiation from the dewar wall is expressed as

$$\dot{Q}_{wall} = \sigma \left(T_{ambient}^4 - T_{CCD}^4 \right) A_{wall} \frac{\epsilon_{Al}\epsilon_{CCD}}{\epsilon_{Al} + \epsilon_{CCD} - \epsilon_{Al}\epsilon_{CCD}}. \tag{3}$$

Here, $\dot{Q}_{wall}$ is the inflow heat flux by the radiation from the wall, A_{wall} is the area of the dewar wall, ϵ_{Al} is the emissivity of the dewar wall which is made of the aluminum. The area of the dewar wall is $A_{wall} = \pi \left(\frac{D_{win}}{2} \right)^2 = 5.84 \times 10^{-2}\,\mathrm{m}^2$. The emissivity of the aluminum are assumed as $\epsilon_{Al} = 0.06$. Then, the heat inflow by the radiation from the dewar wall is estimated as

$$\dot{Q}_{wall} = 1.0\,\mathrm{W} \tag{4}$$

3.3 Conduction through Polycarbonate Posts

The incoming heat flux by the thermal transfer due to the conduction through the polycarbonate post is expressed as

$$\begin{aligned} \dot{Q}_{post} &= \frac{A_{post}}{L_{post}} \int_{T_{amb}}^{T_{CCD}} \kappa_{post}(T) dT \\ &\sim \frac{A_{post}}{L_{post}} \bar{\kappa}_{post} \left(T_{amb} - T_{CCD} \right). \end{aligned} \tag{5}$$

Here, $\dot{Q}_{post}$ is the inflow heat flux by the conduction through a polycarbonate post, A_{post} is the cross-section of the polycarbonate post, L_{post} is the length of the polycarbonate post, κ_{post} is the thermal conductivity of the polycarbonate post, $\bar{\kappa}_{post}$ is the mean thermal conductivity of the polycarbonate post. The cross-section and length of the polycarbonate post are assumed to be $A_{post} = 20 \times 20$ mm^2 and $L_{post} = 40$ mm, respectively. The mean thermal conductivity of the polycarbonate is assumed as $\bar{\kappa}_{post} = 0.2$ W m^{-1} K^{-1}. The number of polycarbonate posts is 4. Then, the heat inflow by the conduction through the polycarbonate posts is extimated as

$$\dot{Q}_{posts} = \dot{Q}_{post} \times 4 = 0.9\,\mathrm{W}. \tag{6}$$

3.4 Conduction through Copper Lines

The incoming heat flux by the thermal transfer due to the conduction through the copper line is expressed as

$$\begin{aligned} \dot{Q}_{line} &= \frac{A_{line}}{L_{line}} \int_{T_{amb}}^{T_{CCD}} \kappa_{Cu}(T)dT \\ &\sim \frac{A_{line}}{L_{line}} \bar{\kappa}_{Cu} \left(T_{amb} - T_{CCD}\right). \end{aligned} \tag{7}$$

Here, $\dot{Q}_{line}$ is the inflow heat flux by the conduction through a copper line, A_{line} is the cross-section of a copper line, L_{line} is the length of a copper line, $\bar{\kappa}_{Cu}$ is the mean thermal conductivity of the copper. The cross-section and length of the copper line are assumed to be $A_{line} = 75 \times 18$ μm^2 and $L_{line} = 150$ mm, respectively. The mean thermal conductivity of the copper is assumed as $\bar{\kappa}_{post} = 420$ W m^{-1} K^{-1}. The number of copper lines is 50. Then, the heat inflow by the conduction through the copper lines is extimated as

$$\dot{Q}_{lines} = \dot{Q}_{line} \times 50 = 0.02\,\mathrm{W}. \tag{8}$$

3.5 Total Inflow Heat Flux

The total inflow heat flux Q_{total} is expressed by

$$\begin{aligned} \dot{Q}_{total} &= \dot{Q}_{win} + \dot{Q}_{wall} + \dot{Q}_{posts} + \dot{Q}_{lines} \\ &\sim 2.9\,W. \end{aligned} \tag{9}$$

A cryocooler which is planned to be used for the CCD camera is Polycold PT-30. The cooling power of PT-30 is about 22 W at 173 K. It is powerful enough to cool the CCD chip. To prevent the over-cooling and keep the stable CCD operation temperature, a resistance heater is required to be installed in the dewar.

4 Summary

The inflow heat flux into the dewar of the CCD camera was estimated. The radiation from the dewar window, the radiation from the dewar wall, the conduction through the polycarbonate posts, and the conduction through the copper lines were calculated. The estimated total heat inflow is 2.9 W. It is confirmed that the cooling power of the cryocooler is large enough compared to the inflow heat.

References

[1] Miyazaki et al., 2002, PASJ, 54, 833-853.

[2] Okamura et al., 1996, “Suprime-Cam Final Design Review”.

Thickness of Dewar Window of the CCD Camera

KINOSHITA Daisuke

01 April 2010

Abstract

This short report describes the calculation of the dewar window thickness for our CCD camera which is being developed. The size of the window is assumed to be 90-mm in diameter, and the material of the window is chosen to be the fused silica. The results of the calculations show that 5-mm thickness window is strong enough for the dewar of our CCD camera.

1 Introduction

The astronomical instrument development team at the Institute of Astronomy of National Central University aims to develop a CCD camera for 2-m telescope which is being built at Lulin Observatory. In order to have photons received by a CCD chip, there must be a window on the dewar. The material for the window has to have high transparency in visible wavelength region for higher observing efficiency. The thickness of the window should be carefully determined to be thick enough to be strong enough. The breaking of the window may end up with the destruction of a CCD chip. At the same time, the window thickness should be as thin as possible to minimize the chromatic aberration. The window thickness is also important that the thin window may result in the deformation which causes the degradation of the image quality.

2 Calculations of Dewar Window Thickness

Here, we choose the fused silica as the window material. The fused silica has excellent transparent properties at visible wavelength which is suitable for optical astronomical observations. Properties of fused silica is summarized in Table 1. The CCD chip which will be used for our camera is the fully depleted CCD manufactured by Hamamatsu Photonics. It is a 2K $\times$ 4K CCD with the pixel size of 15 μm. Hence, the size of the CCD chip is 30.7-mm $\times$ 61.4-mm. In order to have a full use of this size of CCD chip, the filter size is set to be 50-mm $\times$ 80-mm, and the shutter has an aperture of $\phi = 90$-mm. We assume $\phi = 90$-mm for the unsupported region of the fused silica window for the dewar.

Breaking strength	$F_a = 4.892 \times 10^7$ Pa
Young's modulus	$E = 6.966 \times 10^{10}$ Pa
Poisson ratio	$\nu = 0.17$

Table 1: The properties of fused silica. The data are from Okamura et al. (1996) and Miyazaki et al. (2002).

Now, here is a set of equations for the thickness of the dewar window.

$$\sigma_{max} = \frac{3P(3+\nu)}{32}\left(\frac{D}{t}\right)^2 < \frac{F_a}{S} \tag{1}$$

$$l = \frac{3P(1-\nu)(5+\nu)}{256E}\frac{D^4}{t^3} \tag{2}$$

$$R = \frac{l^2 + \left(\frac{D}{2}\right)^2}{2l} \tag{3}$$

Here, D is the diameter of the circular window, t is the thickness of the window, σ_{max} is the stress to the window surface at the window center, P is the pressure difference between the inside and outside of the dewar, ν is the Possion ratio, F_a is the breaking strength, S is the safety factor, l is the displacement of the window surface at the window center, E is the Young's modulus, and R is the curvature radius of the deformed window. According to Okamura et al. (1996) and Miyazaki et al. (2002), it is recommended to have safety factor of 4 or larger. Under the condition of the safety factor of 3 or smaller a small impact may break the window. The window thickness, window displacement at the center, and curvature radius of the deformed window are calculated for $S = 3, 4, 5, 6, 7, 8, 9$, and summarized in Table 2. The thickness of the window for the safety factor of 4 is calculated as 4.5-mm. We conclude to use a 5-mm thickness fused silica for the dewar window. The fused silica window must be anti-reflection coated before the installation.

S	t [mm]	l [μm]	R [m]
3	3.9	83	12.2
4	4.5	53	18.8
5	5.0	38	26.2
6	5.5	29	34.5
7	5.9	23	43.4
8	6.3	19	53.1
9	6.7	15	63.3

Table 2: Calculated window thickness, window displacement at the center, and curvature radius of the deformed window for given $S = 3, 4, 5, 6, 7, 8, 9$.

3 Summary

The thickness of the dewar window for given safety factor $S = 3, 4, 5, 6, 7, 8, 9$ assuming the $\phi = 90$-mm fused silica as the window material were calculated. To prevent the break of the window, the thickness of 5-mm is recommended.

References

[1] Miyazaki et al., 2002, PASJ, 54, 833-853.

[2] Okamura et al., 1996, "Suprime-Cam Final Design Review".

Development of Visible 4-color Simultaneous Imager

— Status Reports on Instrument, Laboratory, and Project Management —

KINOSHITA Daisuke[1] and CHEN Tse-Chuan[1]

[1] Institute of Astronomy, National Central University,
300 Jhongda Rd., Jhongli, Taoyuan, 32001, Taiwan

29 April 2011
for "Lulin Observatory Annual Report 2010"

Abstract

In order to carry out immediate follow-up observations for large scale astronomical surveys, a visible 4-color simultaneous imager is being developed. Three dichroic mirrors are used to split the beam from the telescope, and images at four different pass bands are recorded simultaneously by four CCD cameras. The main scope of this instrument is to conduct efficient and reliable color measurements of moving and transient celestial objects, such as asteroids and supernovae, even under relatively poor condition nights. Visible 4-color simultaneous imager also improves the observing efficiency. We report the scientific objectives, design, development strategy, current status of the instrument, status of the instrumentation laboratory, and the management of the project.

Key Words: Methods: observational – Instrumentation – Techniques: photometric

1 Introduction

Panoramic Survey Telescope and Rapid Response System (hereafter, Pan-STARRS) is an innovative and unique cyclical wide-field astronomical survey project (Kaiser 2004). A prototype telescope, PS1, is installed and operated at the summit of Haleakala on Maui island of Hawaii (Fig. 1). It is a telescope with the aperture of 1.8-m. Thanks to three sets of correcting lenses, a wide field-of-view of three degrees in diameter is achieved. A dedicated imaging instrument, named Giga Pixel Camera (hereafter, GPC) is attached to the telescope (Fig. 2). GPC is an wide-field imager with 1.4 giga pixels which covers the entire region of the focal plane of PS1 telescope. CCDs used for this instrument are orthogonal transfer CCDs. Orthogonal transfer CCDs are capable of moving electrical charges to neighbouring pixels in vertical and/or horizontal directions during the exposure, and hence offer the on-chip guiding to improve the image quality. PS1 system is one of the most powerful observing facilities in the world to perform astronomical wide-field imaging. The official surveys of PS1 has started in May 2011, and this telescope is now being used to carry out a sky survey for 75% of the sky which is observable from Hawaii. It is the first trial to image such a wide area of the sky repeatedly in a sysmatic way. PS1 provides unique data sets for time-domain astronomy, and it opens new opportunities for knowing variable universe. Intensive studies on moving objects in solar system, such as asteroids and trans-Neptunian objects, and transient objects, such as supernovae, and gamma-ray bursts, are expected.

In order to maximize scientific outputs of PS1 sky surveys, quick follow-up observations are essential to investigate physical properties, chemical compositions, and origin of newly discovered objects and mechanisms of observed phenomena. Note that PS1 keeps observing wide area of the sky, and cannot focus on small number of celestial objects to monitor. Telescopes exclusively used for follow-up observations are highly needed. For our case, a new 2-m telescope is being constructed at Lulin observatory in Taiwan. The primary mirror has an effective aperture of 2.0-m. The diameter of 2.0-m is chosen to make us possible to observe majority of PS1 discovered objects in imaging mode. The mirrors are made of low thermal expansion glass of Astro-Sitall, and the protective layer of SiO is coated on the surface after the aluminizing

Figure 1: A photo of PS1 dome at the summit of Haleakala taken by one of authors (KD) in November 2007.

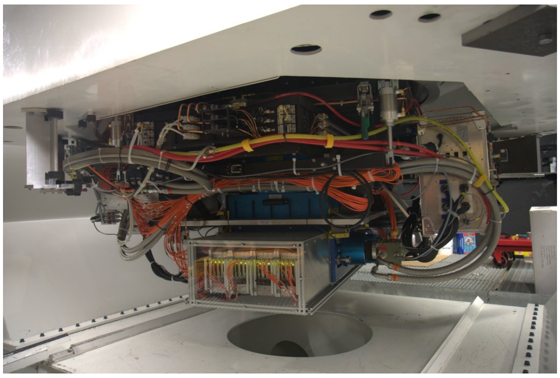

Figure 2: Giga Pixel Camera installed at PS1 telescope. This photo was taken by one of authors (KD) in November 2007.

of the mirrors. The optical system is a Ritchey-Chrétien, and the focal length of the system is 16.0-m for Cassegrain focus. This results in F/8, and it allows us to share some instruments with existing 1-m telescope at the same site. The mount of the telescope is alt-az mount. The expected image quality is 0.35 arcsec, and it is reasonably good considering a typical seeing condition of $\sim$ 1.5 arcsec at Lulin observatory. The pointing accuracy of 2 arcsec in RMS and tracking accuracy of 0.3 arcsec per 10 min are expected. The telescope is designed to have a maximum slew speed of 4 deg per second to enable efficient observations and quick response of sudden change of the observing plan. The telescope sometimes needs to do quick pointings right after the triggers of transient alert.

We have decided to build a visible 4-color simultaneous imager for the 2-m telescope to carry out sophisticated follow-up observations for PS1 sky surveys. This report describes scientific objectives, design, development strategy, current status of the instrument, and project management in following sections.

2 Visible 4-Color Simultaneous Imager

A visible 4-color simultaneous imager was selected to be the first generation instrument for the 2-m telescope. There are two reasons for this decision. First, the most important task of the 2-m telescope is to perform follow-up observations for celestial objects discovered by PS1 sky surveys. Then, majority of targets are (1) moving objects, such as asteroids, comets, and trans-Neptunian objects, and (2) transient objects, such as supernovae and gamma-ray bursts. Moving objects in solar system are irregularly shaped and are spinning in general. This fact suggests that these bodies change their cross-section and exhibit brightness variation. Color change may also be attributed to the rotation and heterogeneity of the surface. Needless to say, transient objects change the brightness and/or colors by their nature. It means that we need to complete the brightness measurements at two or more pass bands for accurate color determination before those objects change their brightness. Second, Lulin observatory is not the world's best observing site, like Mauna Kea in Hawaii and high altitude desert in northern Chile. The sky condition at Lulin is often unstable and is variable within a night. We see occasional cloud passing, and only have limited number of photometric nights. The utilization of poor condition nights has be well-considered, otherwise significant fraction of observing time may be wasted. To summarize, target objects intrinsically change their brightness and the transparency of the sky changes within a night under the typical condition. We need to measure colors of a target accurately in this situation.

Reliable and efficient color measurements of celestial objects are achieved by simultaneous imaging using a set of dichroic mirrors. The beam from the telescope is split into two or more, and images at different wavelength regions are recorded exactly at the same time. In this way, derived colors are less affected by intrinsic variability of targets and change of atmospheric conditions. It also makes the calibration and data analysis easier under the assumption that the transmittance of the cirrus is neutral over the wavelength coverage of the instrument, and the use of the simultaneous imager increases the number of observable nights. Furthermore, the simultaneous imaging improves the observing efficiency of the telescope. In conventional method of multi-color photometry by exchanging filters, the total amount of observing time needed T_c is given by

$$T_c = (t_{exp} + t_{ro}) \times N_{band}, \quad (1)$$

where t_{exp} is the integration time necessary for each band, t_{ro} is the readout time, and N_{band} is the number of filters used. On the other hand, the total amount of observing time needed for simultaneous imaging T_s is shown by

$$T_s = \frac{t_{exp}}{E_{throughput}} + t_{ro}, \quad (2)$$

where $E_{throughput}$ is the throughput of the additional optics in the instrument. Substituting values of t_{exp} = 60 sec, t_{ro} = 8 sec, N_{band} = 4, then we obtain $T_c/T_s \sim 3.3$, and the simultaneous imaging is suggested to be about three times more efficient than the conventional observations. These advantages are critically important for the operation and scientific productivity of Lulin observatory.

2.1 Scientific Objectives

In astronomy, color measurements are often used to obtain the first look of the physical conditions and chemical composition of celestial objects. An example of scientific objectives of this instrument is the color measurements of asteroids. Some asteroids are known to be rocky composition and classfied as S-type asteroids. Some other asteroids are known to be carbonaceous composition and classified as C-type asteroids. Color measurements are a technique to do the taxonomic classification. It gives us a clue to understand the chemical composition, origin, and evolution of the body. It is essential to know the taxonomic type of the object, when an asteroid with peculiar orbital properties is discovered. In addition, dozens of pairs of asteroids with extremely similar orbits have been identified recently. Color determination of pair asteroids is useful to support (or deny) the common origin (Kinoshita et al. 2007).

2.2 Design of the Instrument

In a conventional method of color measurements, we image the target using a filter, then later re-image the same object using another filter. In this way, there is a time lag between two measurements at different wavelength. Our targets, transient and moving objects, change their brightness with time, and the conventional color measurements may produce false colors.

A different and new approach is proposed here. That is, accurate measurements can be achieved by observing the target at two or more different wavelength regions simultaneously. This is realized by beam splitting using dichroic mirrors. The

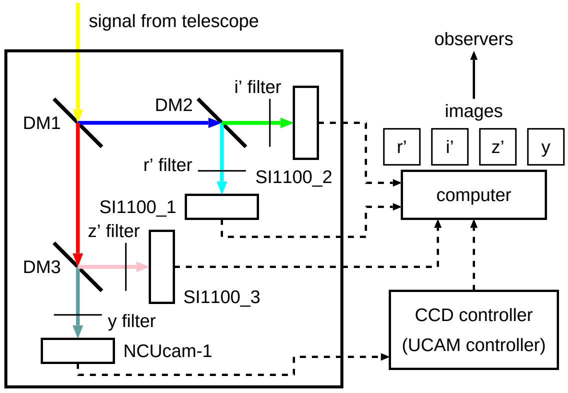

Figure 3: The conceptual design of the visible four-color simultaneous imager. Three dichroic mirrors, shown as DM1, DM2, and DM3, split the signal from the telescope into four, and four detectors acquire images at different wavelength regions at the same time.

dichroic mirror is an optical device that reflects the light shorter than the characteristic wavelength and transmits the light longer than the characteristic wavelength. By using three dichroic mirrors and four bandpass filters and detectors, one is able to measure the target flux at four different wavelength regions at the same time.

The conceptual design of the visible 4-color simultaneous imager is shown in Fig. 3. Three dichroic mirrors on the optical path split the light from the telescope into four components. These four beams pass through the bandpass filters (PS1 r', i', z', and y filters), and the signals are received by four detectors at the same time. In order to combine data both from PS1 in Hawaii and the 2-m telescope in Taiwan, the filter system of our visible 4-color simultaneous imager is designed to be compatible with those of PS1 filter system. The transmittance properties of PS1 r', i', z', and y filters are shown in Fig. 4. Four unit CCD cameras are used as detectors. Each camera is equipped with 4096 × 2048 pixels CCD chip. The pixel size is 15 μm, and resultant pixel scale with the 2-m telescope is 0.19 arcsec per pixel. 2 × 2 binning is planned for usual operation. These unit cameras provide a field-of-view of 13.2 arcmin × 6.6 arcmin. In order to reduce the noise, the CCD chips are cooled down to -100°C.

2.3 Development Strategy

When we have defined the development strategy, we have focused on following two aspects. First, it is important to deliver the instrument in timely fashion. If the project has a delay and the instrument is delivered after the PS1 mission, then

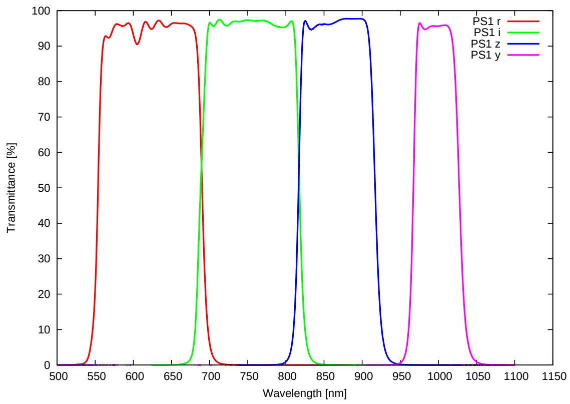

Figure 4: The measured transmittance properties of PS1 r', i', z', and y-band filters for our instrument. The filter system of visible four-color simultaneous imager will be compatible with those of PS1 filter system. These filters were manufactured by Asahi Spectra, Inc.

there will be less scientific impact and we have less scientific outputs from this instrument. Also, early scientific results are very appealing to the scientific community and funding agency. Significant delay of the project may affect to the future funding. Second, it is equally important to do in-house developments of some key components and accumulate experiences. If one uses commercially available products only for the research activities, then the uniqueless of the data is not easily emphasized. In this case, the competition with other facilities is higher. Meanwhile, in-house development may add unique functions to the instrument and/or achieve advantages in sensitivity / data quality, and one may be able to obtain a set of data that nobody else has. Unique and high quality data sets produce publications more easily.

CCD cameras are key components of our instrument, and we have reached to following conclusion for the development strategy. We have decided to purchase three commercially available CCD cameras to secure the delivery of the instrument by the telescope first-light, while fourth camera is developed by ourselves to let us learn from the development processes. This strategy fulfills both two aspects mentioned above. Even in the situation of the delay of fourth camera, the instrument is able to start the early-science observations as 3-color simultaneous imager, and it will not be a fatal problem for the project. Three CCD cameras for r', i', and z' bands, we have purchased SI1100 series cameras of Spectral Instruments, Inc. in USA. A reason that we have chosen this product is that the manufacturer allows us to select a CCD chip to install in the camera. The CCD chips we select are CCD 44-82-1-D23 of E2V, Inc.

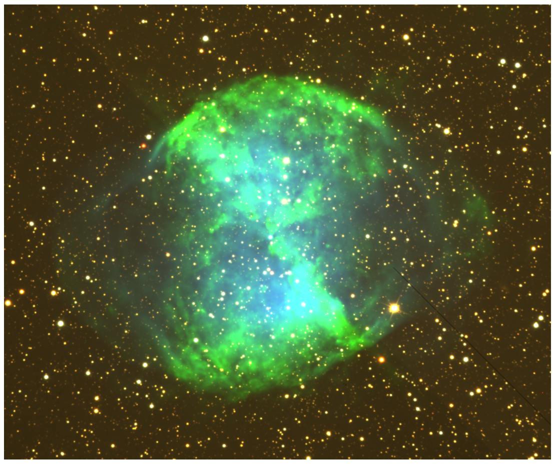

Figure 5: The first light image of the CCD camera SI1100-156. M27 was imaged using 1-m telescope at Lulin observatory at 17:10-17:54 on 20 July 2010. SDSS g', r', and i' filters were used for this observation. The integration time was 10 min for each band. The image shown here has the field-of-view of 10.0 arcmin $\times$ 8.3 arcmin.

It is a scientific grade (grade 1) CCD chip with 4K $\times$ 2K format. The pixel size of this CCD is 15 μm. The fringe suppression process is given to the chip, so that significant degradation of photometric accuracy due to the fringing on the image in z'-band is prevented. There are two amplifiers and A/D convertors for this CCD chip, and the readout time is shortened by using both two readout ports. Fourth camera, namely NCUcam-1, is developed by ourselves. NCUcam-1 will be used for imaging at y-band ($\lambda \sim 1\,\mu m$). We have decided to utilize a recently developed fully depleted CCD chip (Kamata et al. 2008). Majority of CCD chips used for astronomical observation at this moment are thinned back-illuminated CCDs. Because of thin depletion layer compared to the absorption depth of silicon, the sensitivity of thineed back-illuminated CCDs are very low at longer wavelength. Typical quantum efficiency of thinned back-illuminated CCDs at $\lambda \sim 1\,\mu m$ is about 10% or less. The low sensitivity of CCD at this wavelength region is critical problem for small aperture telescopes. To overcome the difficulty, we have decided to use a fully depleted CCD for NCUcam-1. The quantum efficiency of fully depleted CCD with 200 μm thickness reaches 40% at $\lambda \sim 1\,\mu m$, and it dramatically improves the sensitivity of y-band imaging.

2.4 Current Status

We first established a laboratory for the instrumentation at the Institute of Astronomy, National

Central University. We have arranged dark room with an optical table, clean room with class 1000, and mechanical assembly and testing area. We have been developing the instrument in this laboratory space since 2008. Three SI1100 series CCD cameras with E2V CCD 44-82-1-D23, namely SI1100-155, 156, and 157, were delivered in summer 2010. The first light of SI1100-156 was achieved in July 2011 (Fig. 5). We had number of observing runs with 1-m telescope at Lulin observatory to characterize these unit cameras. A set of photometric standard stars were observed to evaluate transformation cofficients and limiting magnitudes. The data sets are now under analysis. Through the experiences of test observations at Lulin, we learned a lot on the installation and operation of the instrument. For CCD camera which is cooled by cryocooler, a good consideration for the arrangement of the cryocooler tubes is needed. An attention to the cable lengths is always required. We are highly encouraged to make a detailed plan prior to the installation and operation at the place like high altitude observatory. More importantly, the safety is the highest priority. Here, the safety include both for human and instruments. NCUcam-1, the camera for y-band imaging, has been designed (Fig. 6) and mechanically assembled and some tests of vacuum condition and temperature control were carried out (Fig. 7). The analog electronics circuit works fine and the CCD temperature has been known to be well-controlled. The vacuum level of 10^{-5} torr is kept for about 3 days after turning off a vacuum pump. In December 2010, an engineering grade chip of the fully depleted CCD manufactured by Hamamatsu Photonics, Inc. was installed in the dewar. The CCD was drived by Lick/AET UCAM CCD controller (Jia et al. 2010), and the image was successfully acquired (Fig. 8). The readout noise of the CCD was estimated as ~ 5 e$^-$ under the sampling rate of 400 kHz. A set of r', i', z', and y filters were delivered in March 2011. Test observations using these filters and one of unit cameras were conducted at Lulin observatory in April 2011, and data were successfully obtained. The optics part of the instrument including a set of correcting lenses is planned to be delivered in May 2011. An assembling of the whole instrument and tests are scheduled in June/July 2011, and we hopefully start test observations at the end of 2011.

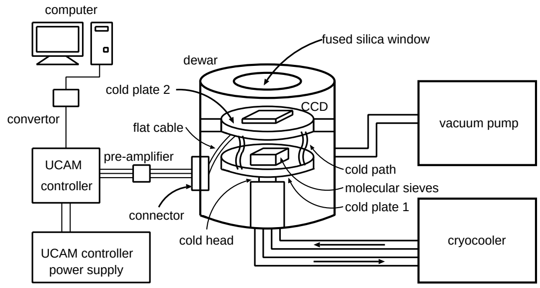

Figure 6: The schematic drawing of NCUcam-1. The CCD chip is installed in the dewar, and a vacuum pump and a cryocooler are connected to the dewar. The temperature control electronics and heaters are used to make the CCD temperature stable. UCAM CCD controller is used to acquire images.

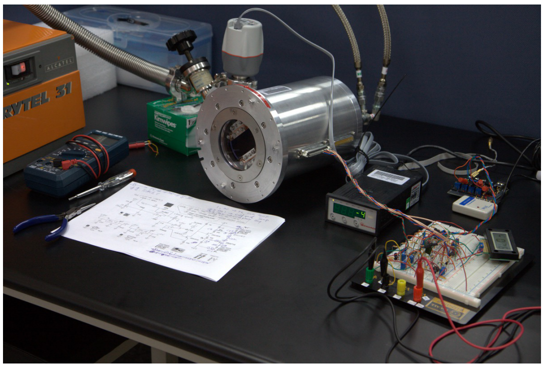

Figure 7: Assembled NCUcam-1 under testing in the laboratory. NCUcam-1 consists of the camera head, vacuum pump, cryocooler, temperature control electronics, and CCD readout electronics.

3 Project Management

To manage a project, one of the most important issues is to secure enough human resources, to assign tasks to each member, and to make a good arrangement of work load for each member. The instrumentation team now has three technicians, one graduate student, and one faculty. One administrative assistant is partly supporting us on budgetary issues. One thing that we stress is that the cooperation among researchers, technicians, and administrative staffs is crucial for a scientific project. The assignment of tasks are listed in Table 1. We intend to make duties of each member clear and let one person to plan, prepare, and complete the task as long as the amount of the work for a task is not too big. This makes us more responsible to the work that we are doing and will do in near future. A similar fashion applies also to domestic and international trips. For example, we clearly define the roles of each member when we arrange a trip. It lets us seriously prepare for a trip. We do not always demand the completion of a task, but we rather allow us to initiate a discussion if one finds the amount a work is too large or the difficulty of a task is too high.

Regular checks of the progress are essential for

Name	Tasks	Involvement
Chen, Tse-Chuan	optics, mechanics, detector characterization	since summer 2009
Huang, Ru-Huei	observation, data analysis	since summer 2009
Kinoshita, Daisuke	management, observation, data analysis	since 2007
Shen, I-Cheng	software development	from summer 2009 to summer 2010
Shen, Pei-Hsien	software development	since autumn 2010
Wu, Ching-Huang	electronics, mechanics	since spring 2008
Yang, Hui-Hsin	administration	since 2009

Table 1: Name, assignment of tasks, and involvement to the project of each project members.

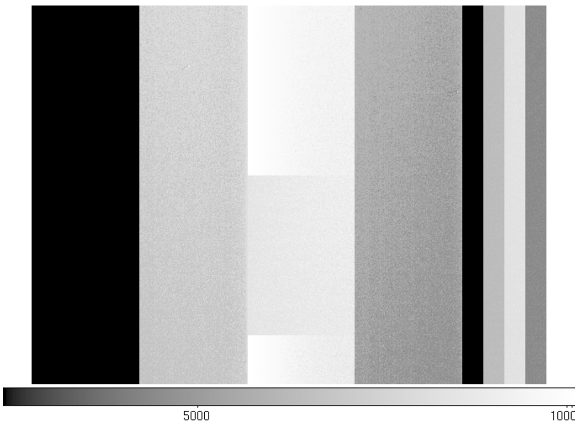

Figure 8: The bias frame obtained by NCUcam-1 with an engineering grade chip of the fully depleted CCD manufactured by Hamamatsu Photonics. The CCD was drived by UCAM controller. The CCD has four readout ports, and the mean levels of the bias for each region are slightly different. The most left side of the CCD was not working properly. Four narrow stripes on the right hand side are overscan regions.

good control of the schedule. We have weekly regular meetings. During the meeting, we report what has been done for a week, what will be done coming week, and point out problems and difficulties, if any. Pointing problems out is actually more important than reports of work smoothly done. We emphasize that it is no problem to have little progress for a difficult task, but it is rather essential to identify a difficulty or problem to be solved. Then, we are able to re-arrange the tasks and work loads. In this point of view, all the members has to join the meeting and report on what is being done, even if one thinks there is no progress to report. The most problematic situation is that one has not mentioned the difficulty for months, and he/she finally gives up without stating clearly what is the problem. Furthermore, it is highly expected to prepare a written report for the weekly meeting. One has to prepare a brief report for a meeting, and it actually benefits himself/herself because writing a report makes us clearer the progress, difficulties, problems we had, things we need to do coming weeks. Some may think that the work is perfectly planned and done by himself/herself and written reports at every meeting are not necessary. It may be a case for a very smart guy and a relatively simple and easy task. But, in order to prevent a mistake and failure, it is a good idea to assume that we are not that smart and tasks are not always simple and easy. Weekly meeting is also a place to make a decision. For important issues, a member is assigned for a study. Then, a report on the summary of the study is given at the meeting. We give a conclusion and make a decision after the discussion.

We also pay attention to the management of the laboratory space. We are advised to return tools to the original location after the usage. To avoid an accident, UPS is installed in the laboratory, and there is time to shutdown instruments when we have a sudden shortage of the power supply. Currently, we have cleaning of the laboratory every three months, and we check for missing tools every six months. It is needless to mention the importance of the cleaning. The check of missing tools is equally important for the project. If a tool necessary for upcoming work is missing or broken, then there might be a delay caused by the un-availability of a tool. In order to prevent such a situation, existence and functionality of tools are checked regularly. If a missing or unfunctional tool is identified, then we purchase a new one. Of course, consumable goods are supplemented if needed. We believe that it is also a key issue for future regular maintenance and stable operation of 2-m telescope and visible 4-color simultaneous imager.

We encourage us to do the calculation and evaluation during the design phase to estimate the functionality and error caused. Without a concrete understanding on what we are about to develop and the advantages and limitations, then a big problem may happen later on. For example, one cannot say “I don’t know how much cooling power is needed for a cryocooler, but I guess this product should be OK for our purpose..." or "I'm not sure how thick this part of the structure should be, but I hope the current design is OK...". We definitely need to do some calculations to check and evaluate correctly the design we give.

4 Summary

In order to realize quick follow-up observations for large scale astronomical surveys, such as Pan-STARRS, a visible 4-color simlutaneous imager is being developed. Efficient and reliable color measurements of moving objects in solar system and transient objects with this instrument even under relatively poor condition nights are expected. A instrumentation laboratory has been set up at the Institute of Astronomy at National Central University. Three cameras for r', i', and z' bands are now being characterized both at the laboratory using an integrating sphere and at Lulin with existing 1-m telescope. Fourth camera for y-band, NCUcam-1, is now being developed. We install a science grade CCD chip into the dewar at the end of April, and tests of CCD drive will be carried out in May 2011. The assembly of the whole instrument is scheduled in June/July 2011.

Acknowledgement

This work is supported by research grants by National Science Council of Taiwan "Follow-up Program for Pan-STARRS: Instrumentation Project for 2-m Telescope" (ID: 97-2911-M-008-010-MY2), "Comprehensive Understanding of Solar System Small Bodies" (ID: 96-2911-M-008-015-MY3), and "Break-up of asteroids and space-weathering on their surface" (ID: 99-2112-M-008-013). We are grateful to these supports. We also thank Prof. Wei Ming-Zhi at UCO / Lick observatory for his support on the CCD readout electronics, Prof. Ikeda Yuji at Kyoto-Sangyo University for his support on the optical design of visible 4-color simultaneous imager, and Dr. Wang Shiang-Yu at Institute of Astronomy and Astrophysics, Academia Sinica, for his support on the fully depleted CCD operation. Prof. Sako Takashi at STE Laboratory of Nagoya University provided valuable information and comments on the CCD readout electronics. Prof. Sato Shuji at Physics Department of Nagoya University kindly offers us an opportunity of training observations at Anpachi observatory near Nagoya city. Prof. Yanagisawa Kenshi and Dr. Kuroda Daisuke at Okayama Astrophysical Observatory of National Astronomical Observatory of Japan kindly provided useful information on the 3-color simultaneous imager that they have developed.

References

[1] Jia, L., Wei, M., Zou, S., Luo, Y., "The UCAM CCD system of LAMOST", 2010, Proceedings of the SPIE, Volume 7733, pp. 77335E-77335E-11.

[2] Kaiser, N., "Pan-STARRS: a wide-field optical survey telescope array", 2004, Proceedings of the SPIE, vol. 5489, pp. 11-22.

[3] Kamata, Y., Miyazaki, S., Nakaya, H., Tsuru, T. G., Tsunemi, H., Miyata, E., Muramatsu, M., Suzuki, H., Miyaguchi, K., "Evaluation of the fully-depleted back-illuminated CCD for Subaru Suprime-Cam", 2008, Proceedings of the SPIE, vol. 7021, pp. 70211S-70211S-9.

[4] Kinoshita, D., Ohtsuka, K., Sekiguchi, T., Watanabe, J., Ito, T., Arakida, H., Kasuga, T., Miyasaka, S., Nakamura, R., Lin, H.-C., "Surface heterogeneity of 2005 UD from photometric observations", 2007, A&A, 466, 1153-1158.

四色成像儀軟體設計之工作報告

Software Design for 4-Color Simultaneous Imager

沈霈嫻(Pei-Hsien Shen) and Instrument Team

一、簡介

我們正在開發四色成像儀的控制軟體同時需裝附到鹿林天文台的 2 米望遠鏡上。該軟體包含：

（1） Spectral Instrument‘s 1100 (SI 1100) Series camera controller
（2） NCUcam-1 controller
（3） Environment monitor
（4） Concurrent control layer
（5） User interface

我們有兩種不同類型的相機，三台 SI 1100 相機及一台 AET UCAM 相機，需要開發每台相機的控制軟體。除了相機控制軟體，我們也需要環境控制軟體來監控環境的溫度及濕度，同步控制階層來同時控制四台相機，和使用者介面，使觀測人員容易操作儀器。我們描述了軟體的設計和功能的各個組件。我們也報告了目前實作的狀況和未來工作的內容。

二、軟體設計架構圖介紹

下圖圖一為我們的軟體設計架構圖,總共分為六大階層:

第(1)階層:

為硬體部分，主要為兩大類不同的相機，包含 SI 相機及 AET UCAM 相機，自不同廠商購買而來的，而 FITS FILE 也是由此層產生。

第(2)階層:

為各硬體的驅動程式部分，這階層部分已經有廠商及相關開發者提供，但 SI 部分是使用不同型號之驅動，是否相容尚在測試中。

第(3)階層:

由相機廠商所提供的函式庫，提供 AP 呼叫以控制硬體。

第(4)階層:

為各相機實作需控制部分，不同相機有不同的設定，例如: SI 有三台相機，操作步驟都相同，實作起來也都相同。NCUcam-1 則是另一種相機，實作用來操作 AET UCAM controller，我們必須透過 TCP/IP 通訊協定來控制 NCUcam；[Write Filts]區塊專為我們生成 Fits 圖像格式,將有四個圖像和我們特定的標頭檔。

第(5)階層:

是同步控制階段，主要為將 UI 傳送的指令傳遞給各個不同控制程式部分，也接收從不同控制程式傳回來的指令。

第(6)階層:

為 UI(User Interface)，設計給使用者輸入指令的介面。

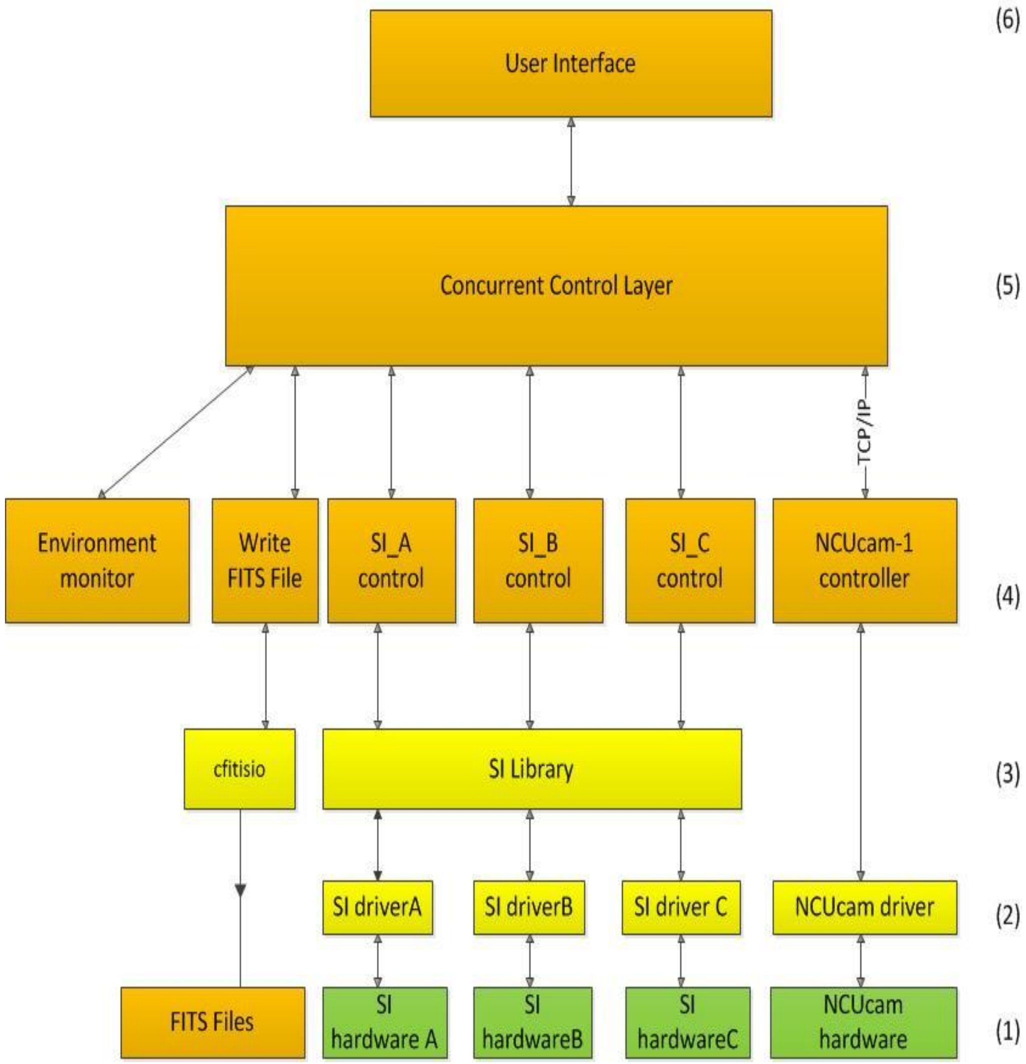

圖一:軟體設計架構圖介紹

三、目前進度

1. 以兩台電腦分別連接一台 SI 相機控制 shutter 開關

目前先以兩台 PC 分別控制一台 SI 相機做初步測試，一台 windows 系統控制 SI-155，一台為 linux 系統控制 SI-157，分別安裝符合不同 OS 的驅動程式及 library，windows 廠商以有提供完整驅動及 library，linux 部分為提供同一型號驅動但 library 是第三方 library，目前測試 library 結果是基本功能可以相通，尚須研究所有功能是否可用同一 library。以下為目前研究的進度報告:

- **Windows :**

為了達成控制三台 SI 相機的程式。首先，先以開發一台 SI 相機為基礎。第一台先完成初步功能後，再以此為基礎擴展為三台相機的控制程式。目前進度為 windows 下以 visual studio 2005 執行程式後介面可選擇一台 SI 相機(一次只能選一台相機，若一台電腦裝三台 SI 相機，則下拉選單會有三台可選擇)，並控制 shutter 開關，將拍攝圖片顯示於畫面中。如下圖二為 SI 相機控制程式畫面及拍攝圖片顯示於左半部，圖三為 SI- 155 相機 shutter 開啟畫面，程式將陸續增加新的功能；

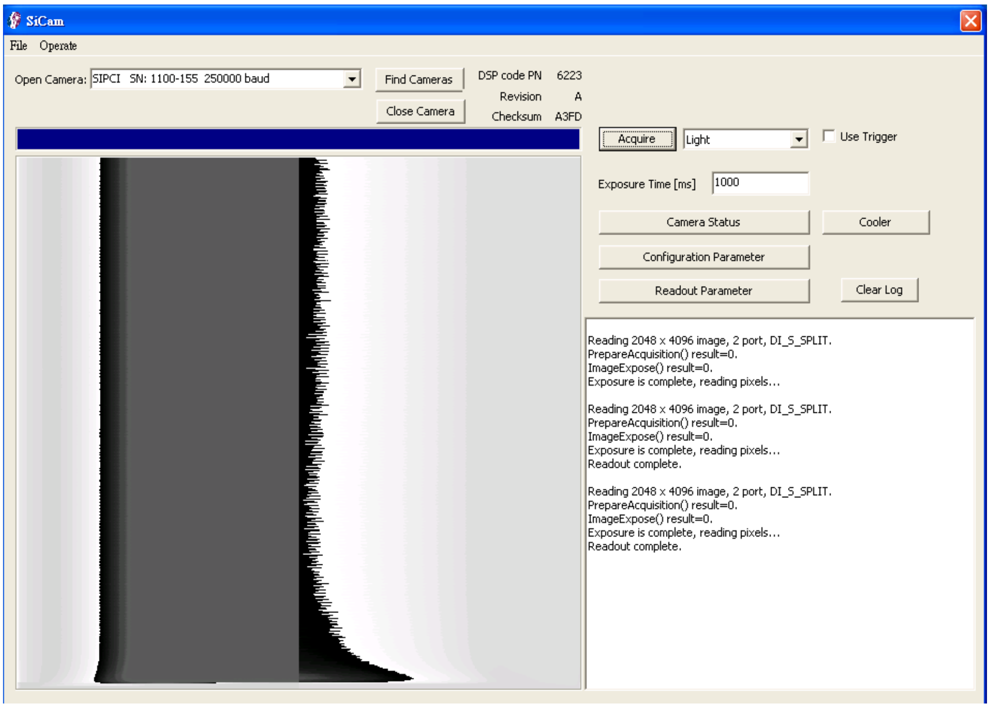

圖二: SI 相機控制程式畫面及拍攝圖片

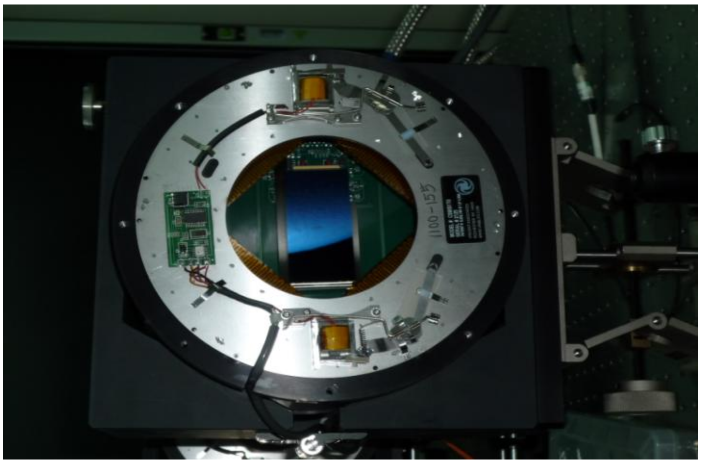

圖三: SI 155 相機 shutter 開啟畫面

● Linux :

另一 OS 版本為將 linux 程式執行後，以 command line 形式下指令使一台 SI -157 相機 shutter 開關。圖四為 SI- 157 相機 shutter 開啟畫面，相關功能研究撰寫中。

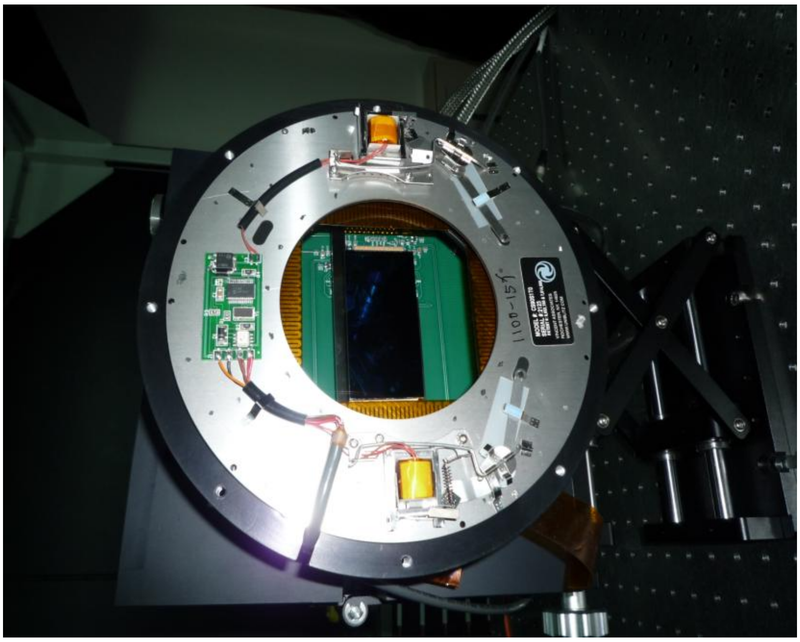

圖四: Linux 控制 SI-157 相機 shutter 開啟

2. AET UCAM 目前狀態

AET controller 是我們發展相機中的一部份，自加州 Lick 天文台一位老師購買而來，它是一個獨立部分，包含軟體及硬體。為了要從我們的程式控制這台相機，我們將在 AET 控制區塊裡實作 TCP 通訊方法。不只將 TCP 方法實作在此區塊，相機的功能也可以實作於此區塊裡，如同圖四中橘色區域。AET 介面是 GUI 介面，未來將透過我們實作的 UI 來控制它，以達到同步控制多台相機的機制。

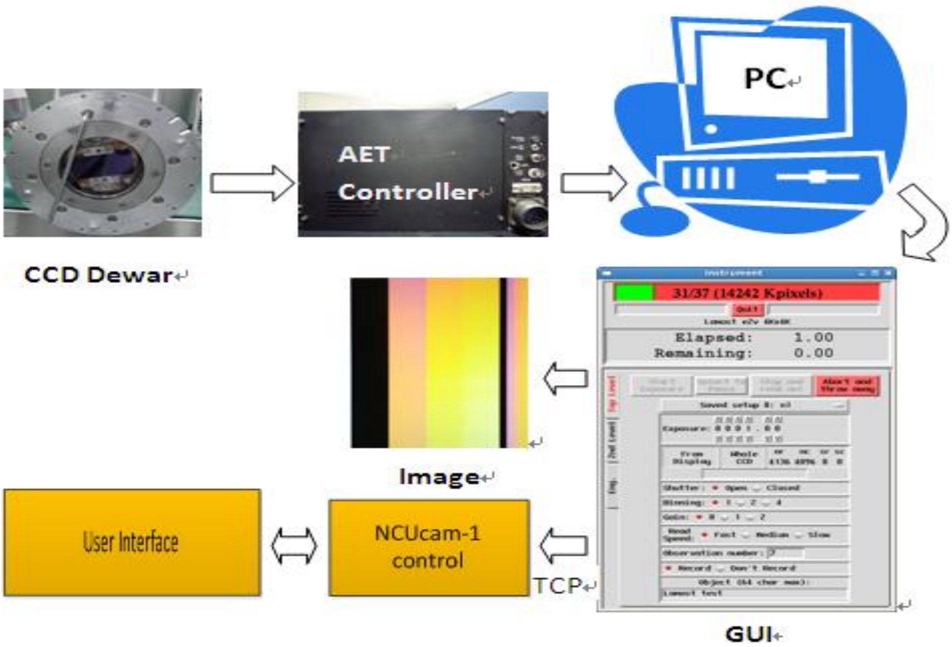

圖五: AET UCAM 硬體連接軟體架構及軟體介面；從 CCD Dewar 連接 AET Controller，再經由 USB 連接到 PC；GUI 為監控軟體畫面，使用者透過程式以 TCP/IP 通訊方式與 controller 做溝通。

3.Filter Wheel 程式介面及功能

Filter wheel 在 LOT(Lulin One-meter Telescope ，一米望遠鏡)觀測上為輔助作用，但每台相機都會搭配各自的 filte r(濾鏡片)來做觀測，讓特定波段光線通過。

我們設計了一個程式幫助天文觀測者在觀測上更為簡便，此程式為控制觀測濾鏡之轉換，可讓觀測者直接程式遠端遙控 filter wheel，坐在電腦前即可更換濾鏡片。目前主要功能如下：

1.開啟通訊埠

2.設定濾鏡放置初始位置

3.按下所需轉換位置

4.Filter wheel 轉動至定點隨即顯示目前狀態

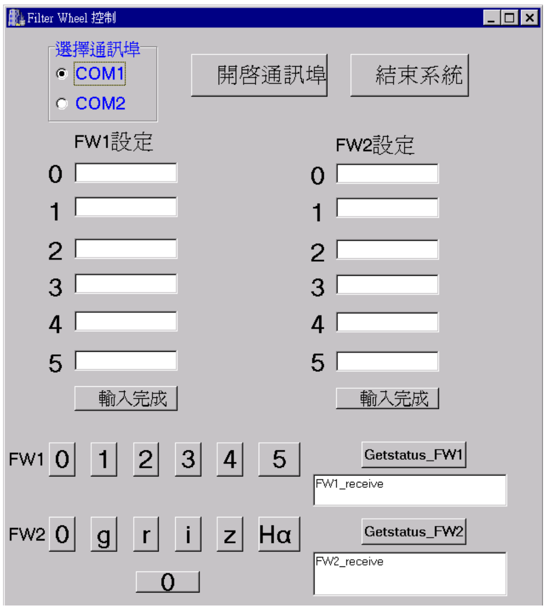

圖六: 初始執行畫面

圖七:開啟通訊埠後，設定初始位置，按輸入完成即修改至 FW1 各個 Button 上

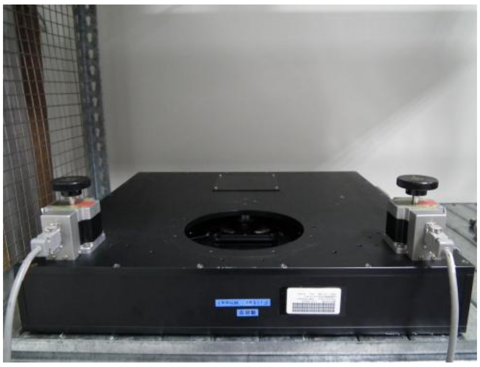

圖八: Filter wheel;

圖九: Filter wheel 控制面板

四、未來工作內容

1. 將一台 SI 相機初始功能設計完成，擴展設計成三台 SI 相機 shutter 開關。
2. 加入另一類相機 UCAM 的設計。
3. 目前設計方案為:考量使用網路設計架構，以一台(PC1)當主控端，一台(PC2)控制三台 SI，一台(PC3)控制 UCAM 共三台電腦。
4. 期望能將此控制軟體設計好，與團隊中的吳景煌設計的 Dewar 及陳澤銓設計的 filter wheel ，一同將整個系統運至美國，作整體系統的測試。

鹿林兩米天文望遠鏡四色同步分光儀器研製工作簡報

A brief of Lulin 2m telescope 4-color simultaneous imager

吳景煌，國立中央大學天文所兩米望遠鏡儀器團隊，28th/Feb/2011

一、 簡介：

本所為兩米望遠鏡設計了四色同步分光系統與成像系統。四色的波段分別是：552-689nm(r)、691-815nm(i)、815-915nm(z)以及 967-1024nm(y)，此部分由日商 Photocoding 公司承製。而其中的 552-689nm(r)、691-815nm(i)與 815-915nm(z)三個波段由美商 Spectral Instruments 公司承製。第四個波段 967-1024nm(y)，則由本所設計 dewar 與介面，而關鍵元件採用日商 Hamamatus 公司的 fully depleted CCD，因為該 CCD 具有較高的近紅外端 QE，其控制器則採用美商 Astro Electronics Technology(AET)公司的 ACS-164 UCAM 控制系統。

目前，除了四色同步分光系統要到 2011 年 4 月才能完成，其它部分都已經有了初步成果，本文將重點說明本儀器團隊在開發四色同步分光系統與成像系統的現況。

二、 目前進度：

1. **四色同步分光系統**：本系統的示意圖如下，目前已經完成設計與電腦光跡模擬，正在進行光學元件製作、鍍膜以及機械加工，預計 2011 年 4 月完成。

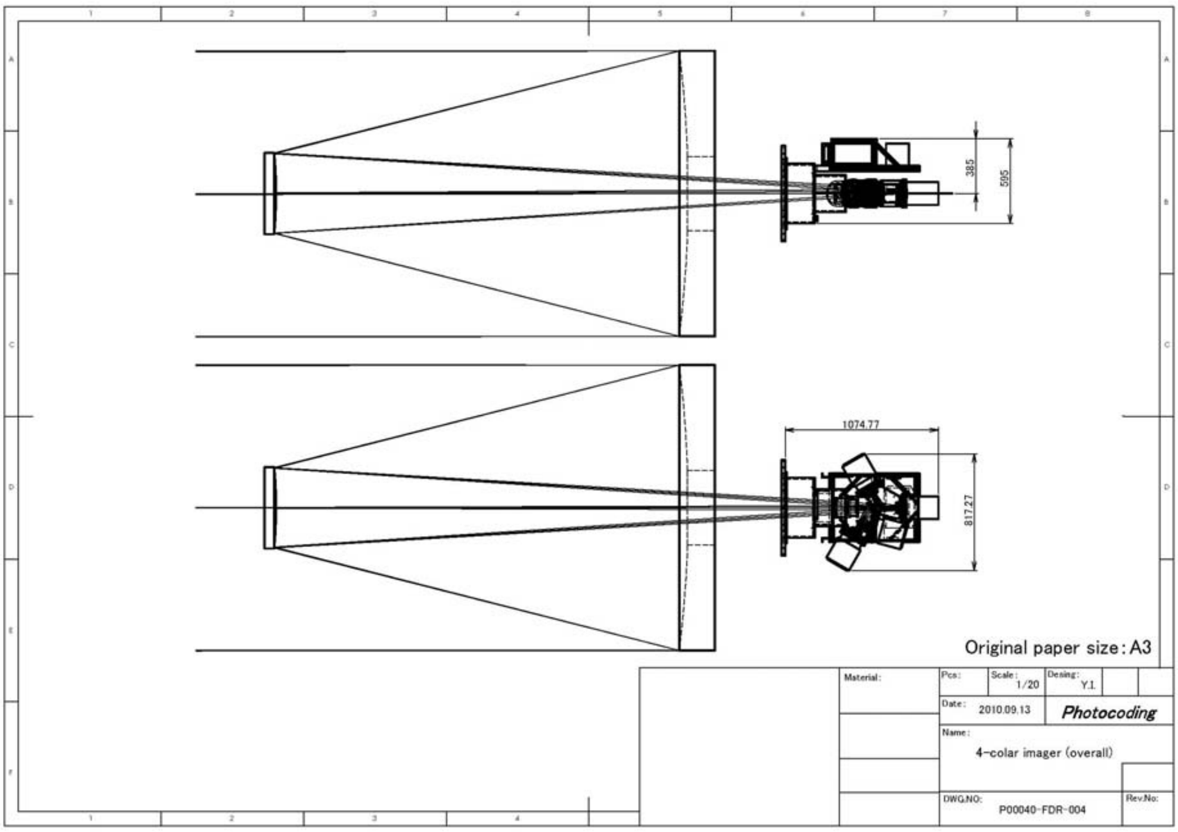

上圖左邊代表望遠鏡次鏡、主鏡與光路，右邊代表四色同步分光系統的上視與側視圖

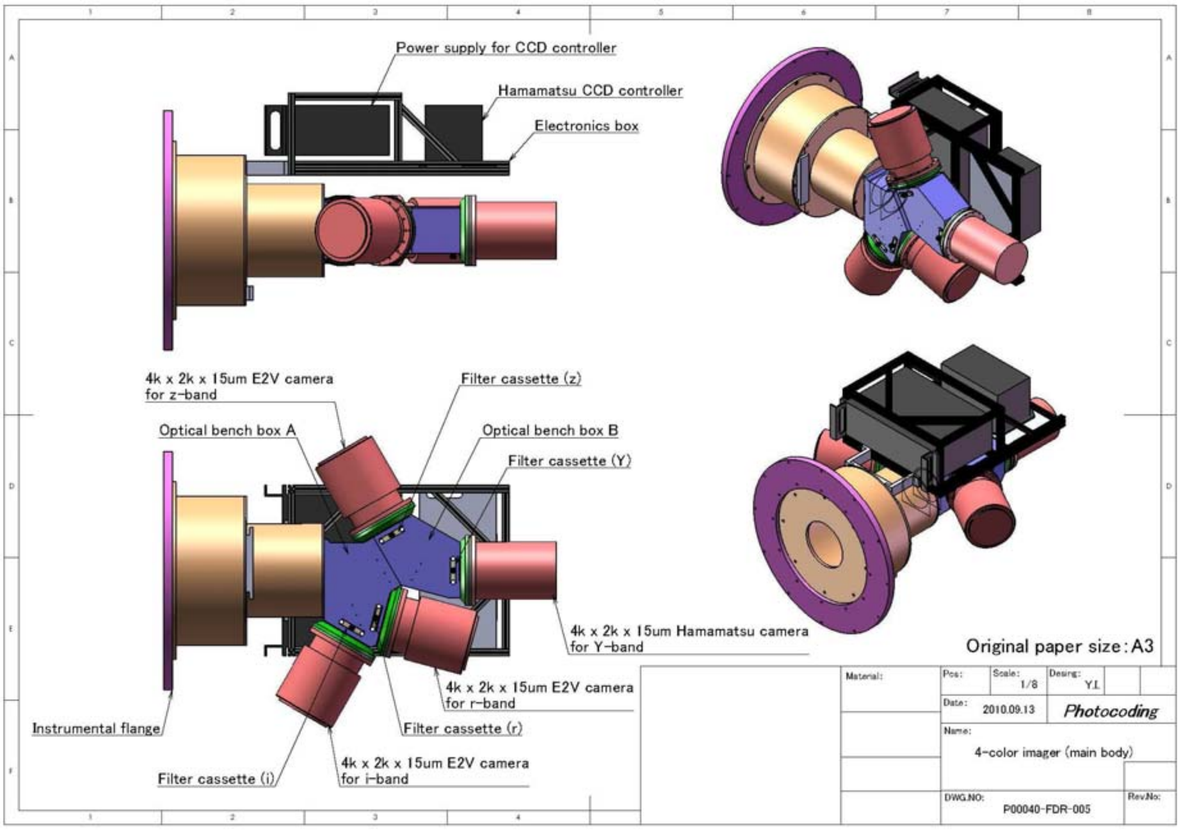

上圖將前述四色同步分光系統細部放大，並提供四個視角圖示

2. **r、i、z 波段成像系統**：由美商 Spectral Instruments 公司承製的成像系統，已經完成並進行一系列的測試與調校。本所自行開發濾鏡轉盤後，安裝在鹿林一米天文望遠鏡(LOT)，進行初步的觀測。

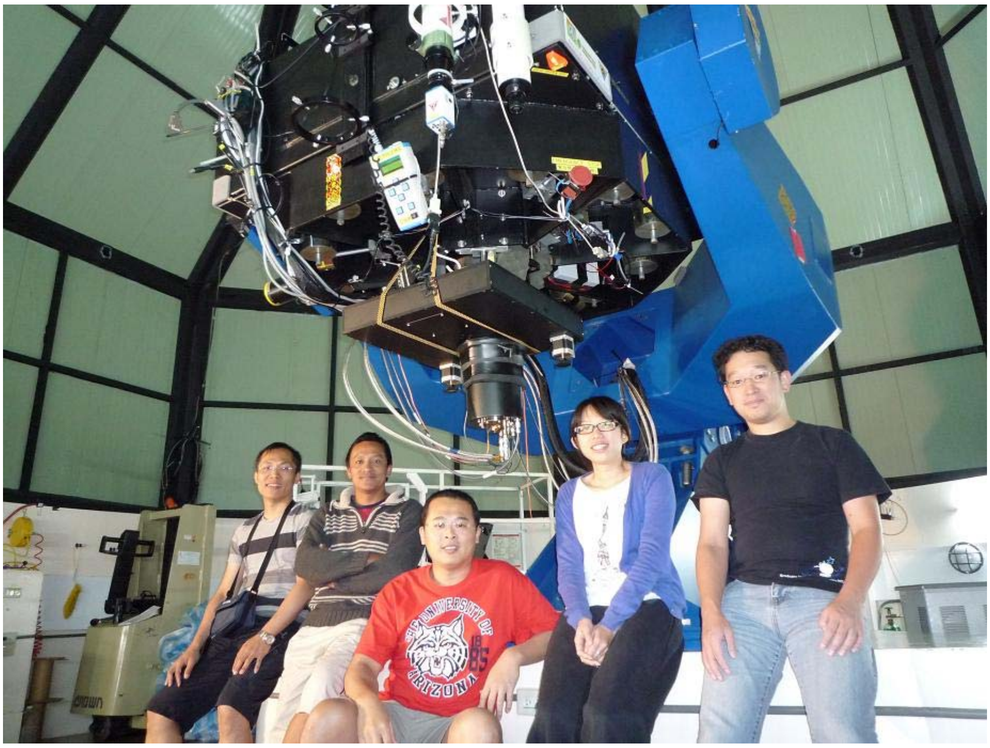

上圖是在鹿林第一次觀測的人力與設備合照

LOT / SI1100 First Light Image

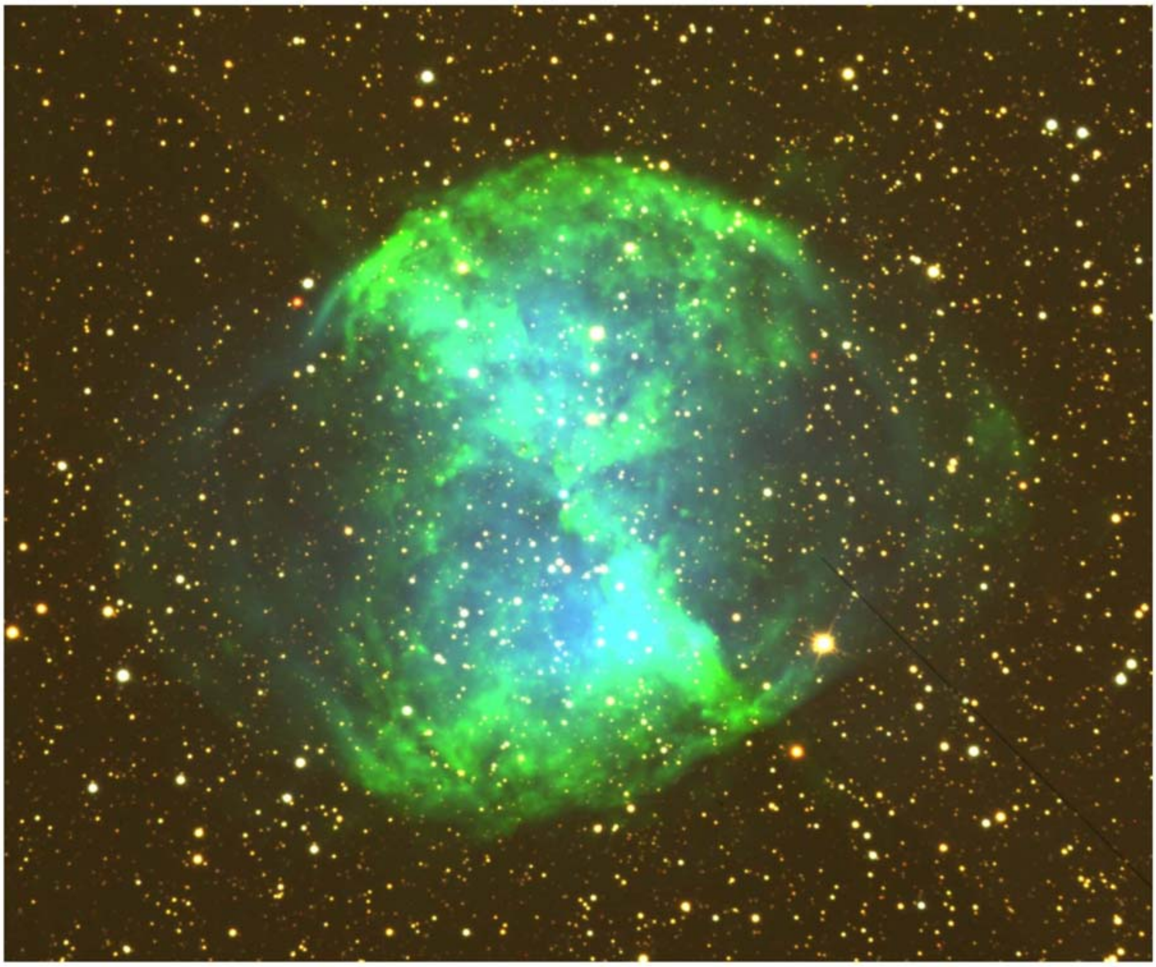

M27 (Dumbbell Nebula)

Lulin 1-m Telescope + SI 1100 Series Camera
SDSS g' (10 min), SDSS r' (10 min), SDSS i' (10 min)
10.0 arcmin × 8.3 arcmin
17:10:35 – 17:53:40 (UT) on 20/Jul/2010

Huang Ru-Huei, Chen Tse-Chuan, Wu Ching-Huang, Kinoshita Daisuke
Institute of Astronomy, National Central University, Taiwan

上圖是第一次觀測的成果

3. **y 波段成像系統**：本所第一次設計該用途 dewar，也是世界上目前唯一結合採用 Hamamatus 的 fully depleted CCD 與 Astro Electronics Technology(AET)的 ACS-164 UCAM 控制系統以及相關的界面。不但已經完成實驗室內的初步功能測試觀測，也證實這樣的組合有穩定的超低工作溫度(-110℃)、夠低的真空壓力(低於 10e-5 torr)與極低的整體雜訊(低於 6ev)，且具有相當實用的價值。

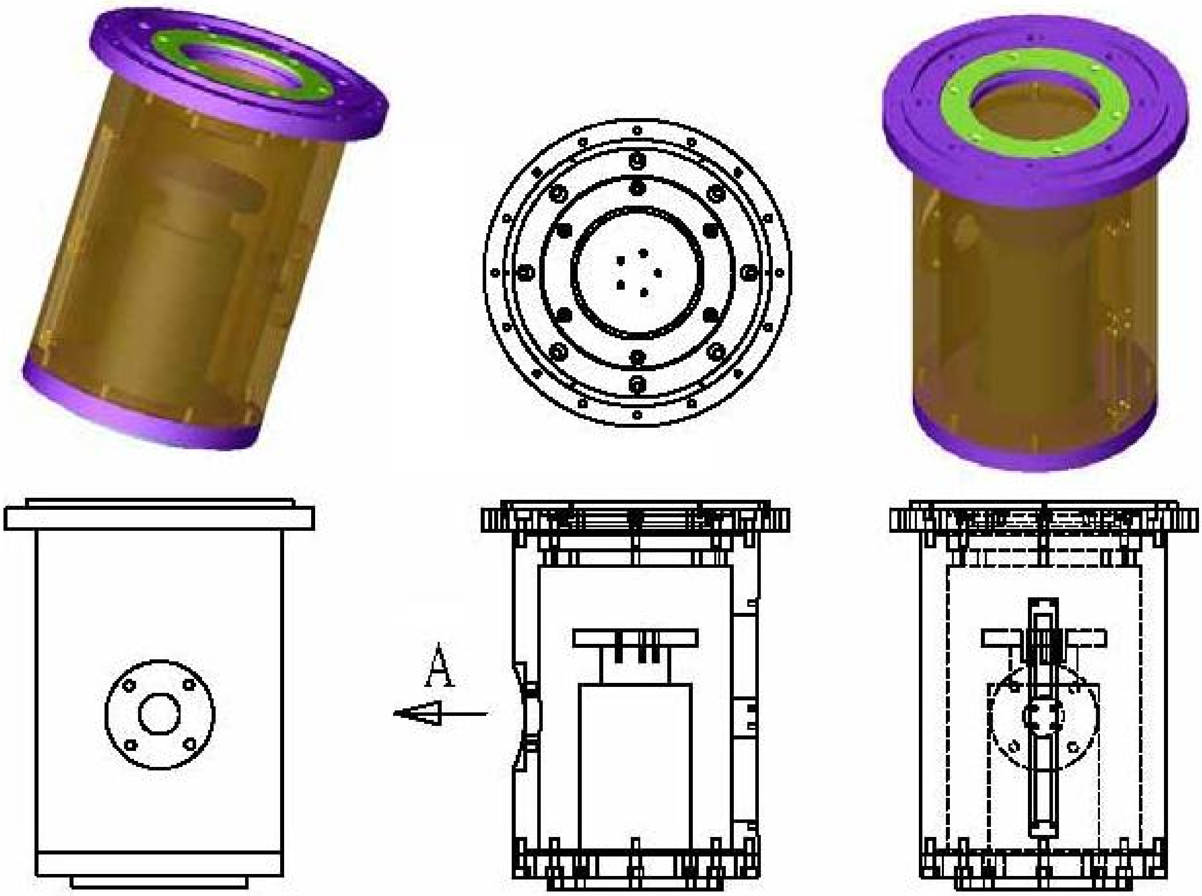

上圖是本所研發的 dewar 平面圖與立體透視圖

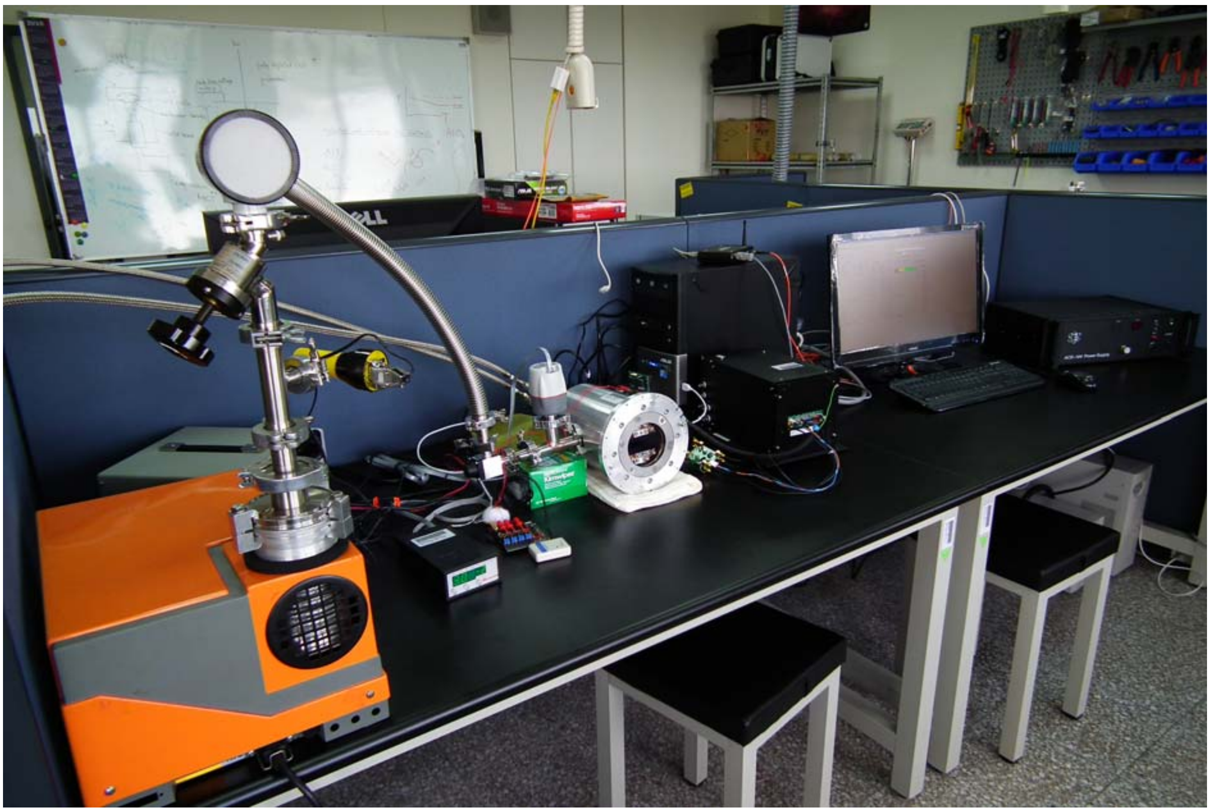

上圖是在實驗室內實際測試的狀況

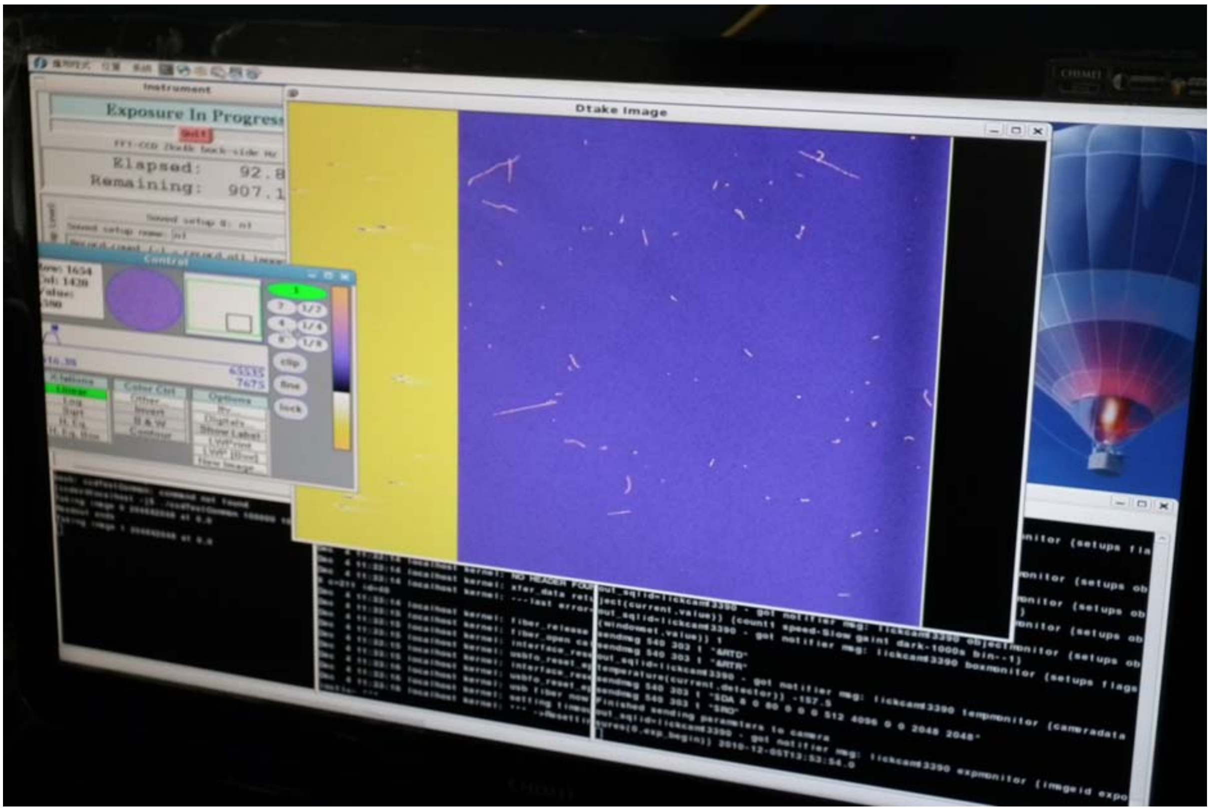

上圖正進行暗場測試，基本功能正常，系統雜訊夠低，因此能觀測到宇宙射線

三、　　未來進度：

1. r、i、z 波段成像系統：
   個別成像系統繼續進行觀測、測試，預計在 2011 年 7 月完成。

2. y 波段成像系統：
   Dewar 真空維持能力、溫度控制、紅外線 CCD 應用，以及各項參數設定與優化，預計在 2011 年 7 月完成。

3. 四色同步分光系統：
   預計 2011 年 4 月完成後，進行重量、結構、光路實驗，並與 r、i、z、y 波段成像系統進行完整組裝測試，預計在 2011 年 8 月完成。

國立中央大學天文研究所 2010 年年報之

鹿林兩米天文望遠鏡儀器研製計畫工作報告

2010 Annual Report of
Lulin 2 Meter Telescope Project for Developing Instruments

陳澤銓
(Duncan Chen)

一、 前言

儀器團隊 2010 年在儀器研製計畫上有著顯著的進展，包括儀器實驗室之軟硬體建置完成、三色相機(即 SI Cameras)到貨並完成部份鹿林觀測之測試、第四色相機(簡稱 NCUCam)之成功開發及完成初步測試、四波段同步光學系統即將於 2011 年第一季交貨、以及新進軟體工程師持續軟體開發工作..等。有別於 2009 年主要著重於實驗室的建置和儀器設備採購等準備工作，在這一年裡，我們將重心放在儀器開發的工作，並為接下來四色同步成像儀(4-Color Simultaneous Imager)的正式上線觀測做準備。

在 2010 年裡，我個人主要負責電控及機構件之設計製作、SI Cameras 的特性實驗、天文觀測、以及協助 NCUCam 的開發工作。以下，我將就這幾個主要的部份一一介紹和說明。

二、 電控和機構件設計

1. 濾鏡轉盤(Filter wheel)

在 2010 年 7 月份，我們申請了一個觀測計畫，用來測試剛到貨的 SI Camera，此 camera 是由美國 Spectral Instruments Inc.公司所製造生產，型號為 1100s 系列，其搭配 e2v CCD44-82 之科學等級 CCD chip，具有 2048 x 4096 的 pixel number，pixel size 則為 15-μm x 15-μm，因此 chip 本身為有別於傳統方型 CCD chip 的 60 mm x 30 mm 大小的尺寸。而為了此一特殊尺寸的 CCD，我們也特別訂購了 r’, i’, z’, y 各二片、尺寸為 80 mm x 50 mm 的 PS1-compatible filters，預備用來搭配四波段同步光學系統之用。

但由於 LOT 現行使用的 Filter wheel 為 ACE Dual Filter Wheel System，最大尺寸僅能容納 50 mm x 50 mm 大小的濾鏡，無法滿足 80 mm x 50 mm 的濾鏡尺寸，因此我設計了一個超大型濾鏡轉盤，用來放置最大可到 100 mm 見方的濾鏡，除了現階段供儀器團隊觀測使用外，將來也可放在鹿林天文台供觀測者使用，相信將會大大提升 LOT 的觀測效能。

1.1 設計概念

在我的設計構想上，除了面積上可容納最大 100 mm 見方的濾鏡外，還希望它可以同時放置多片不同波段的濾鏡，以省去經常更換及調校的時間。因此我設計了一個雙層、分別可放置 6 片濾鏡、一共 12 片裝的 Dual filter wheel。同時為了可相容多種不同尺寸及型式的濾鏡，目前製作了兩種不同尺寸的轉接治具，分別為 50 x 50 及 80 x 50 (單位：mm)，而因為上下空間有限且基於安全考量，我們在訂製濾鏡時，也必需嚴格限制其厚度(我們期望的厚度大約是在 9~10 mm 為佳)，圖一為 3D 示意圖。

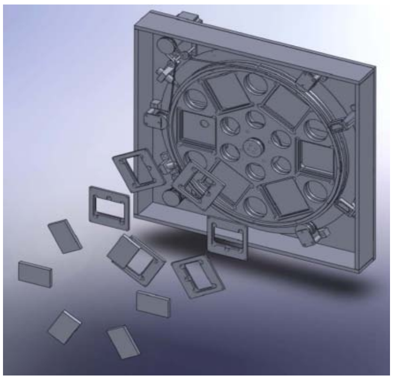

圖一 Filter wheel 的 3D 示意圖，由左下至右上三圈分別為：Filters, Adaptors, Filter wheel

1.2 尺寸與重量

外觀尺寸為 570 mm x 550 mm x 90 mm (圖二為尺寸圖)，以這樣的體積幾乎是現有 ACE 的五倍之多，而為了減輕整體重量，避免造成 LOT 的負擔，除了在材料上選用重量較輕的鋁合金外，對於沒有使用到的部份，也盡可能將其挖空，使得總重量得以控制在 30 kg 以內。

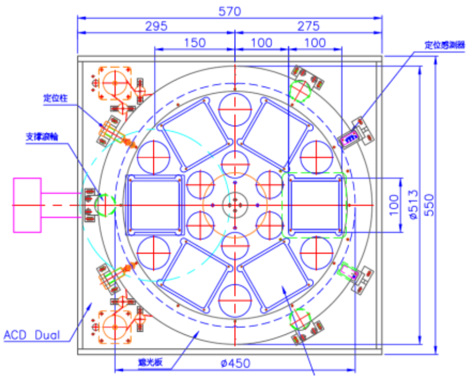

圖二 外觀尺寸圖

1.3 皮帶與驅動

在皮帶的選用上，採用了溝槽皮帶，利用皮帶本身的 V 型凹槽與轉盤外圍間的摩擦力來帶動轉盤的轉動。驅動部份，則採用上下各一顆的 ORIENTAL PK566 步進馬達(Stepping motor)來拖動溝槽皮帶的運動。

1.4 機械定位與光學定位

在這裡使用兩種定位方式，分別是機械定位與光學定位。前者為一彈簧式滾輪設計，上下各一個，安裝在轉盤的外圈並與轉盤有一定程度碰觸，配合轉盤上的凹槽設計，當轉盤轉至指定的位置時，利用滾輪卡進凹槽的機制，確保機構上到達指定位置而不致前後滑動(如圖三左)。後者則是在每一個濾鏡槽位旁鑿三個小孔，利用上下層各三顆並排之 LED 及光偵測器作為光學感測器(如圖三右)，例如『○ ○ ●』代表 Filter_1 (依此類推)，再回傳一信號至控制器，告訴使用者目前濾鏡所在位置。

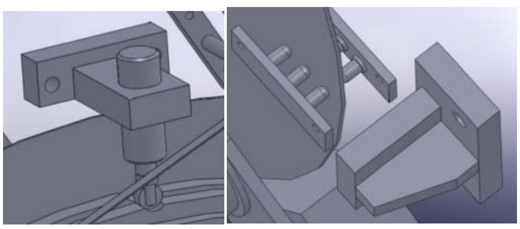

圖三 (左)彈簧式滾輪機械定為機制，(右)利用 LED 光學感測器做光學定位

1.5 特殊設計之 Filter holder

鹿林天文台所使用的濾鏡種類繁多，雖然尺寸都是 50 mm 見方，但卻有多種不同厚度，最薄為 2.9 mm、最厚則厚達 8 mm，如此大的厚度差距，勢必增加觀測助理更換濾鏡上的困難度，而且相當耗時，因此在 Filter wheel 的設計上必需考量到此一情況。為了解決厚度問題，我設計出一個簡單卻非常實用的方式，採用材質為工程塑膠之雙面彈簧壓框的設計方式(如圖四所示)。彈簧的目的是為了壓住(或是固定)濾鏡而又不至於傷到濾鏡脆弱的表面；雙面的設計，則是當欲安裝某一厚度的濾鏡時，可根據壓框兩面不同深淺度之凹槽，來決定使用哪一面(兩面皆可使用)；而且只用到四根 M4 螺絲來固定 Filter holder，甚至不必使用六角扳手或其他工具，1 分鐘之內便可安全又快速地換裝濾鏡。

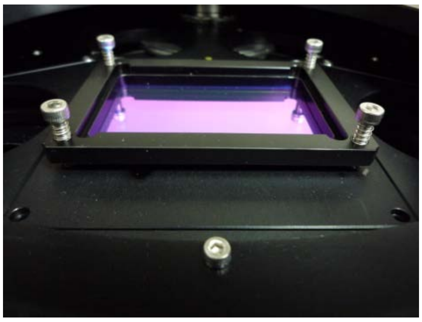

圖四 Filter holder 裝上濾鏡之實際使用情況

1.6 實測紀錄

整個 Filter wheel 約於 7 月初交貨驗收，緊接著馬上帶上鹿林並試裝於 LOT 成功，接下來在 7 月中下旬及 9 月中旬分別有兩次觀測都使用了這個 Filter wheel，經過這三次測試，不論承重、機械強度、使用性及方便性等，都有令人滿意的成果。唯整個 LOT 僅靠三顆 M8 螺絲與 Filter wheel 接合，當望遠鏡移動至較大角度時，強度上則會稍嫌不足之虞，但考量到 LOT 之原始設計問題，暫時不做變更，僅在 Filter wheel 下方以兩條彈性繩索使之與 LOT 固定，以防萬一(如圖五所示)。但若以觀測的結果來看，至少在光學性能上是不受影響的。

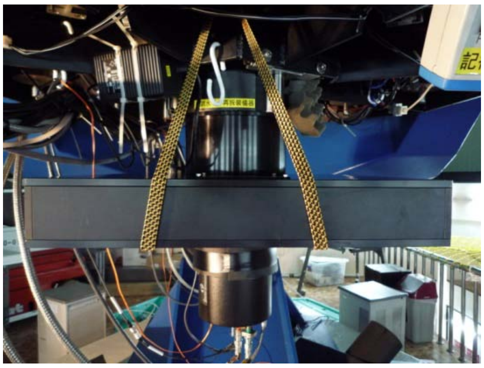

圖五 Filter wheel 安裝於 LOT 之實況

2. 機構件(1) – SI Camera holder

當 SI Cameras 在暗房裡進行相關的特性實驗時，有時候必需讓相機成水平橫躺、有時候則要使其在垂直方向作業，因此我分別設計了水平及直立的 Camera holder，如圖六所示。

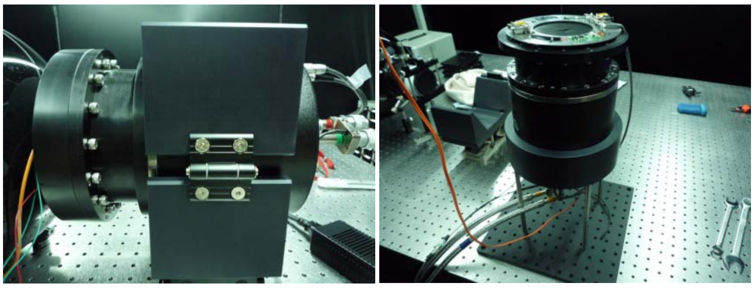

圖六 (左)水平式，(右)直立式

3. 機構件(2) – 光學桌儀器架

暗房裡的光學桌，其桌面尺寸為 240 cm x 120 cm，但若擺放儀器、電腦、相機等設備，再加上實驗光路之架設，桌面空間就會變得非常狹小甚至不足；考量暗房裡原本就不大的空間，我們捨棄常用且承重度較高的龍門式支架，改採由暗棚支架懸吊的儀器架(如圖七所示)。有了此儀器架，光學桌面就會多出至少一半的空間可供做其他用途。

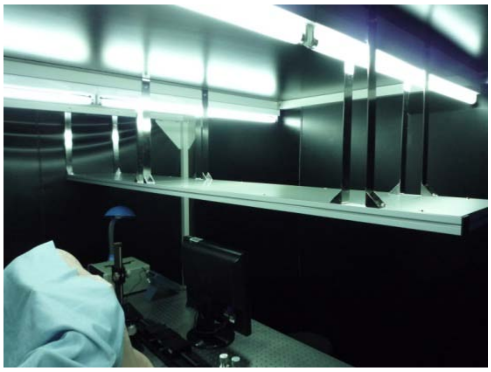

圖七 光學桌儀器架

4. 積分球(Integrating sphere)

SI Cameras 接下來將有一連串的特性量測實驗需要在暗房進行，包括**定義快門最短之開啟時間、增益和讀出雜訊之計算、線性度量測、CCD 滿阱位能量測..**等實驗，而這些實驗都需要一個穩定且均勻的平場(Flat field)，在實驗室最常用的平場方式則是積分球。我們使用一直徑為 300 mm 的透明壓克力球作為積分球的本體，先後噴以黑色(用以阻絕外部光線進入球體)及白色(作為球體內部的反射層塗料)的平光噴漆，並以相機口徑與球體半圓周約呈 1：3 的比例開鑿一個 90 mm 直徑的開口，作為積分球與相機接續的受光面，接著在沿著開口一圈的位置，嵌入 6 顆低功率的白光 LED 作為光源，此光源可藉由迴路中的可變電阻及電源供應器來調整其輸出亮度。圖八為積分球製作過程，唯其均勻度欠佳，因此接下來我們將試圖開發其他型式及材料的積分球，以獲得更好的量測效能。

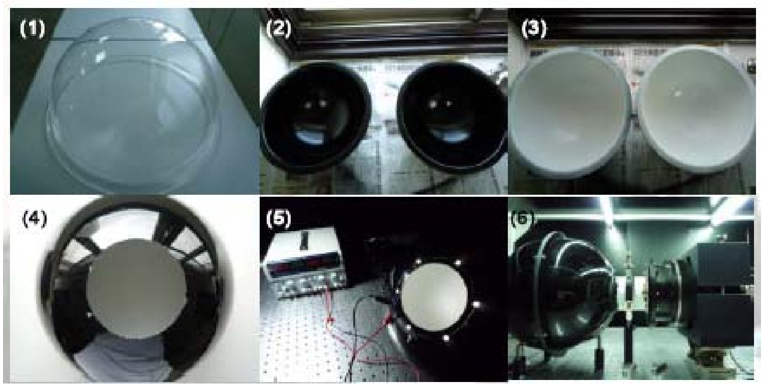

圖八 壓克力積分球製作過程

5. 機構件(3) – 積分球座

由於積分球為一圓形球體狀，在光學桌上固定不易，為了使其幾乎呈水平，並與相機能在同一光軸上，我設計了一個彎月型夾具(如圖九所示)，用來固定積分球。

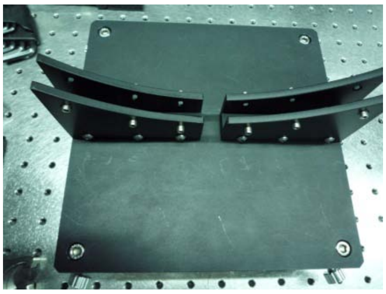

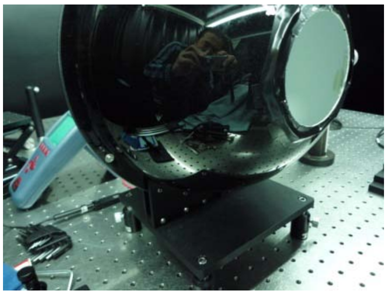

圖九 積分球座

三、 採購案進度報告

1. 天文光學濾鏡一批(案號：S599055)

此為 PS1-Comptible filters，共計採購 r', i', z', y 四個波段，每個波段各 2 片、一共 8 片的 filter，為直接向日本 Asahi Spectra 公司訂製，國內無代理商。此採購案使用的是 5500 經費，採購金額為 USD 17,060，於 2010 年 11 月初完成議價及簽約，交期為四個月，屆時將使用在四波段同步光學系統中。

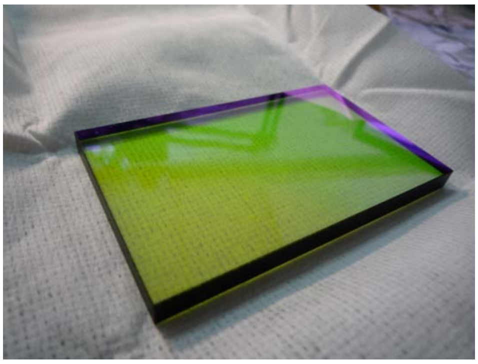

圖十 為配合 CCD chip 尺寸所訂製的 80 x 50 (mm)之 PS1-Compatible filters

2. 背照式紅外光感測器 2 個(案號：S99-8084)

此為用在儀器團隊自行開發之 y-band 第四色相機(稱 NCUCam)的 Fully depleted CCD chip，全世界目前僅日本 HAMAMATSU Photonics 公司有能力生產，其代理商為光菱電子。此採購案使用的是 97 設備費，採購金額為￥ 4,510,000，於 2010 年 12 月初完成議價及簽約，預計明年三月中交貨，並正式投入 NCUCam (如圖十一所示)之開發工作。

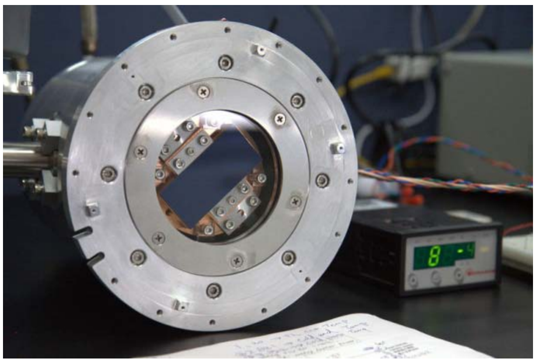

圖十 Fully depleted CCD (借自 ASIAA)與 NCUCam

3. AR Coated window

　　此玻璃是用在 NCUCam 的 Dewar 上作為窗鏡使用，而為了使其具有很好的穿透率，玻璃表面通常會鍍上抗反射層(Anti-reflection coating)。在這裡我們向裕群光電購入 4 片石英基板(Fused silica)，其中 2 片寄往日本 Photocoding 公司(即四波段同步光學系統之製造商)代為鍍膜，另外 2 片則擬委請校內之薄膜中心(TFTC)鍍膜。總金額約 NT 80,000 元。

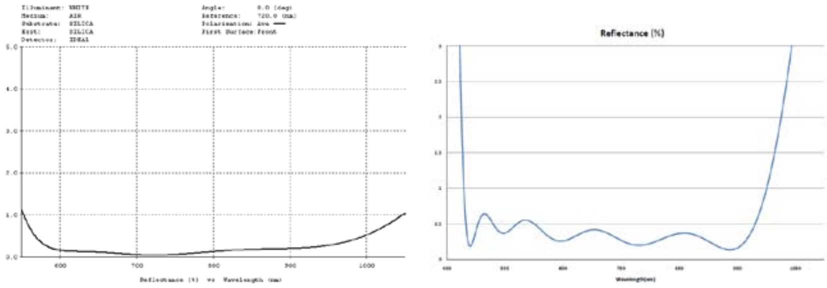

圖十一 (左)Photocoding 之反射率，(右)TFTC 之反射率

四、　未來一年之工作重點

1. SI Cameras 的特性量測

　　開發一具有良好穩定度及均勻性的積分球，以做為一個天文相機專用的測試平場，同時完成三顆 SI Cameras 的特性量測實驗。

2. 採購品項之驗收及測試

　　包括 PS1-Comptible filters、Fully depleted CCD chips 及 AR Coated window 等大額採購案到貨之驗收及測試工作的順利進行，一方面提昇計畫經費的執行率，更重要的是促使這些元件可以盡早投入第四色相機的開發工作之需。

3. 新設備及儀器之採購進行

　　預計將有包括 CaF_2 玻璃、第二版的 NCUCam、四波段同步光學系統所使用之治具、。磁碟陣列、Pumping cart，以及多種電子儀器、電腦、軟體…等，總金額超過新台幣 100 萬的採購需要進行。

4. NCUCam_2 之開發工作

　　我負責的是光學元件之訂製、相機特性量測及性能評估、天文觀測及資料分析，搭配吳景煌的 Dewar 開發及電路設計、沈霈姍的軟體開發，我們將改良第一版相機(NCUCam_1)的缺點，以期創造出性能更優越的第二版相機(NCUCam_2)。

5. 四色同步成像儀(4 Color Simultaneous Imager)之最終整合及測試

　　最終任務就是將各部元件一一準備好，包括四波段同步光學系統、SI Cameras (r’, i’, z’-band)、NCUCam (y-band)、UCAM CCD Controller、控制軟體等部份，確認其性能及動作皆正常，然後在實驗室進行模擬測試，進而在 2011 年第三季可以將整個系統運至國外天文台，以進行整體的性能測試及觀測，並順利結案。

鹿林天文台 2003-2010 觀測時數統計

林宏欽、蕭翔耀、林啓生

鹿林天文台自 2002 年 9 月開始有人員常駐，2003 年起 LOT 一米望遠鏡上線，始有觀測時數正式紀錄，可供瞭解鹿林長期的觀測條件。依 8 年來(2003-2010)的統計資料，鹿林天文台每年觀測時數約為 1500 小時。以月份來說，

- 10-12 月為最佳觀測季。
- 1-3 月為次佳觀測季。
- 4 月雨季開始，5-6 月受梅雨影響，天氣最差。
- 7-9 月受颱風及午後對流雲系影響，天氣好壞差很大。

詳細統計資料及統計圖如下，

表 1 每月觀測時數統計圖(2003-2010)

Month	2003	2004	2005	2006	2007	2008	2009*	2010	Average
1	78.75	125	163.25	129	127.32	179	234.52	206.9	155.47
2	142.5	145.98	94.75	149	128.55	118.25	165.7	100.6	130.67
3	147.5	163	143	126.05	116.4	138.5	146.75	181.3	145.31
4	126.5	110.5	144.75	86.8	53.75	85.25	71.8	75.8	94.39
5	129.75	106.25	136.25	59.5	106.6	98.25	167.4	86.05	111.26
6	24	133	45	39.3	54	37	81.75	26.5	55.07
7	222.5	48	167.75	91.57	128.88	88.4	76.6	99.85	115.44
8	137.75	142	76	111.65	56.6	118.95	6.8	98.3	93.51
9	142	116	129.25	60.05	69.55	59.8	0	109.95	85.83
10	149.25	219.75	210.25	150.6	172.63	191.38	175.6	139.8	176.16
11	166.5	214.5	216.25	71.75	160.55	152.55	175.8	163.65	165.19
12	271.5	232.45	129	132	261.09	211.17	169.8	169.65	197.08
Total	1738.5	1756.43	1655.5	1207.27	1435.92	1478.5	1472.52	1458.35	1525.37

* 2009 年因受 88 風災影響，自八月八日起至十月初約 2 個月期間，受停電影響以至於無法觀測。

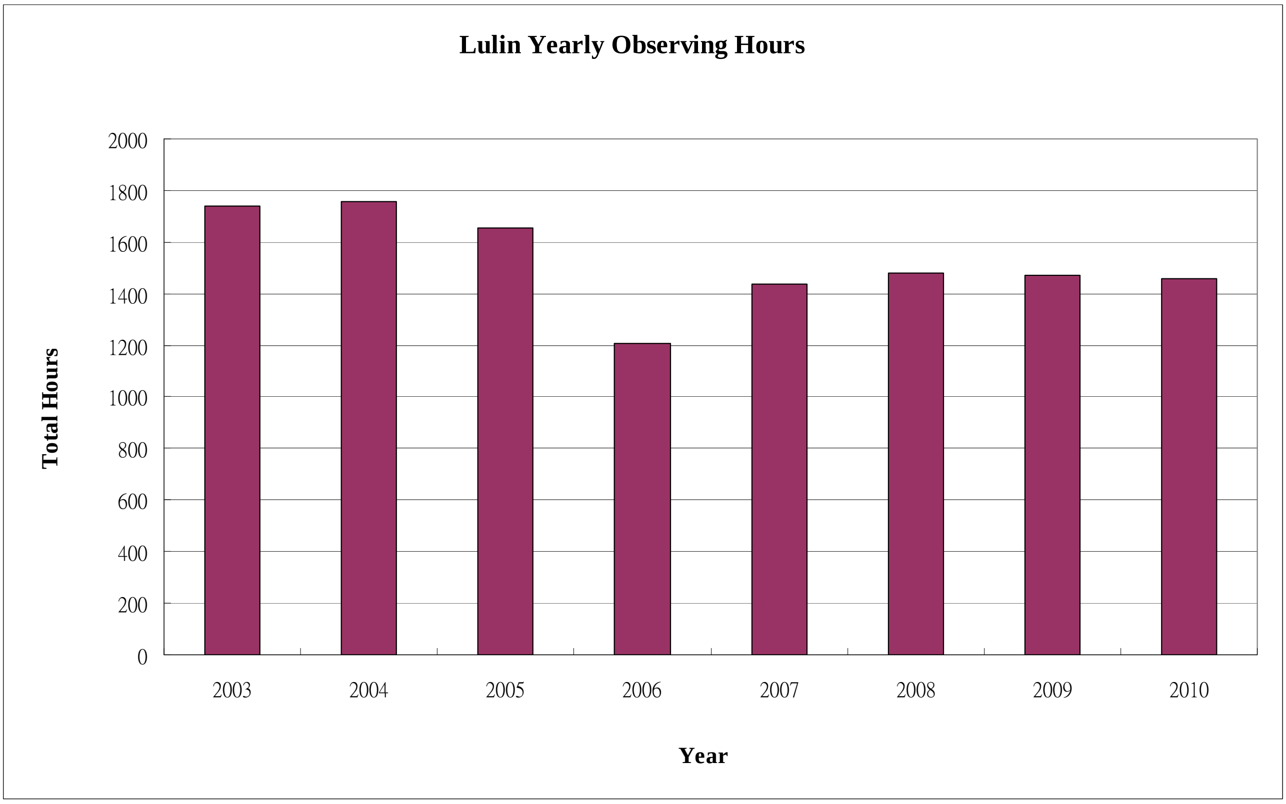

圖 1 鹿林天文台歷年觀測時數統計圖 (2003-2010)

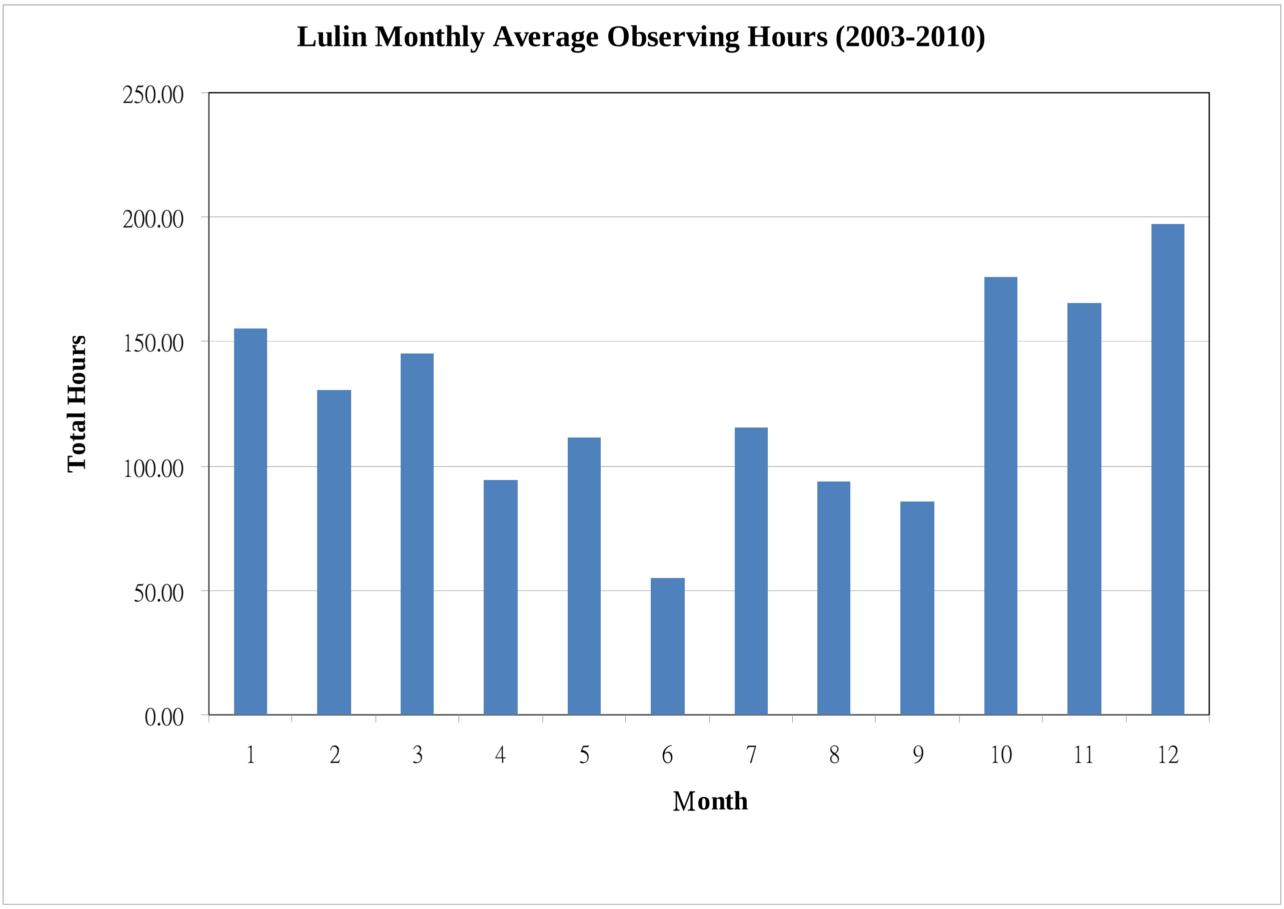

圖 2 鹿林天文台月平均觀測時數統計圖 (2003-2010)

相關報導

2010 展望秋季系列演講　怪力亂神　都怪外星人？

【記者蔡永彬／台北報導】

生物學家逐漸解開生命之謎，並指出適合生命存在的環境；天文學家則在太空中尋找這些環境。人類相信宇宙空間大、時間長，應該也有別的生物存在。如果有，在哪裡？如果沒有，為什麼？這些問題可能有答案嗎？

國家科學委員會主辦，台灣大學物理學系暨天文物理研究所承辦，聯合報、科學月刊、科學發展月刊、科學人雜誌、NEWS 98、Discovery 頻道協辦的「2010 展望秋季系列演講」。上周五第 4 場由國立中央大學天文研究所暨物理學系教授陳文屏主講「小心，外星人就在你身邊？－談生活中的怪力亂 神」。

給個理由　而非寧可信其有

「你相信外星人存在嗎？世界上有沒有鬼？細菌真的存在嗎？」陳文屏一開始就拋出很多問題，他強調，無論相不相信，都要有理由，而不是「寧可信其有」。比如說，每個人應該都沒看過自己的曾曾曾祖母，但應該不會懷疑祖先真的存在過。

根據已故美國天文學家 Edwin Hubble 發現的「哈伯定律」，宇宙正在膨脹。既然宇宙年齡有限（137 億年），意味著即使某件事情「有可能發生」，也不代表有生之年「一定會發生」。

陳文屏指出，我們雖然對很多事情不知道答案，但是不能把這些都推給外星人，因為目前沒有外星人存在的證據，也就是不該「用未知解釋未知」，許多怪力亂神的事情就打著權威人證、論文作為掩護。

例如 1835 年 8 月底，紐約太陽報頭條新聞宣稱英國天文學家 John Herschel 觀察月球，清楚看到「月球表面有生物」。報導整整一星期，從望遠鏡看到月球簡單表面特徵、月海、火山、畜獸，然後是月球人（蝙蝠人）彼此 談話，甚至有壯麗廟堂。事後證明，整個事件是記者 Richard Locke 為了諷刺當時流行的科學作者 Thomas Dick 所虛擬的故事。

月球人事件　原是虛擬故事

雖然人們已經不再相信「蝙蝠人」，但仍有人認為月球上的確有生物，即使人類登陸月球，加上許多太空任務證實月球上沒有生物也是一樣。陳文屏打趣問聽眾：「相不相信，只要報紙有登，第二天必定會有人砍雞頭，發誓前一天在街上的確看到綠色的外星人？」他認為，提出某項主張的人，必須負責舉證，尤其「非同小可 的主張得有非同小可的證據！」

他表示，就目前所知地球上的生命，碳元素和液態化學扮演重要角色，能源則來自恆星。因為這些環境產生生命的機率大，所以人類也以此為背景探索是否有外星生物，或嘗試接收其他文明可能發出的電波訊號。

外星智慧生物　證據力薄弱

陳文屏指出，查證外星人登陸地球或其他神秘、超自然的現象，需要像偵探辦案般找證據、推理，需要嚴謹、大規模（人力、物力）的研究。美國空軍從 1948 至 1969 調查 UFO，負責人 Edward Condon 在結案報告提出結論：「未來 1 萬年內應該沒有任何外星智慧生物將造訪地球。」他認為就目前而言的查證，「人」的因素太重，某些聲稱「極具說服 力」的證據，就算在一般法院打官司都嫌薄弱。

「有想像力沒什麼不好，關鍵在於不能只有想像力。」陳文屏說，科學態度與方法應想辦法證明自己正確，以嚴謹手段解決特定問題。

原文轉載自【2010-12-06/聯合報/D2 版/展望】

《人物側寫》 末日預言　激發天文熱情

【記者蔡永彬／台北報導】

「了解科學原理的美，不輸夜空的美。」中央大學天文研究所暨物理學系教授陳文屏認為，「天文」不只是「晚上不睡覺、看夜空」這麼浪漫，而是需要在研究上持續想像，並盡力實踐想法，進一步證明自己是正確的。

陳文屏在屏東縣的眷村長大，小時候碰過落雷就劈在他的腳踏車車輪前，也曾經看過火流星打在附近的牆上，「或許是這樣讓我想當天文學家吧！」他哈哈大笑說，「喔！還有一個原因啦！那時候流傳 1999 年是世界末日…」他回憶，當時「推背圖」、「燒餅歌」的預言不少，「我就認為未來天文學是顯學，因為要和外星人 打仗！」

「許多學生以為，選我的課就是看一學期『X 檔案』。」陳文屏在中大開的通識課名是「尋找外星生物」。他解釋，「尋找」就是外星 巡航，甚至是廣義地理學，還要了解歷史的來龍去脈，「外星生物」包含了天文學和生物學。他希望教給學生的不只是這樣，而是了解生命體甚至人類怎麼在太空中 生存。

以前台灣缺乏天文學的專門系所，所以陳文屏大學讀物理系，研究所再念天文，家人懷疑他「你怎麼越念越冷門啊？」不過父母還是讓陳文屏念自己想念的科系。
他鼓勵學子針對自己的興趣堅持下去，用嚴謹的手段解決碰到的問題，「或許不是萬能的，但是科學態度與方法很有用。」

原文轉載自【2010-12-06/聯合報/D2 版/展望】

太空探索／金星高層大氣發現硫源　爲地球暖化解套

生活中心／台北報導

中央研究院環境變遷研究中心副研究員梁茂昌博士參與的國際天文研究團隊，於 10 月 31 日在專業期刊「自然地球科學」(Nature Geoscience)發表論文，證實金星高層大氣中發現硫源，這項發現日後可望爲地球暖化問題，提供另項解套方法參考。
梁茂昌博士參與的研究團隊包括美國加州理工大學、密西根大學和法國的 LATMOS, CNRS/INSU/IPSL, Université de Versailles-Saint-Quentin、Universite´ Pierre et Marie Curie。
目前同 時合聘於國立中央大學天文研究所以及中研院天文及天文物理研究所的梁茂昌博士表示，對於解決全球暖化的問題，目前學術界公認最實惠且有效的方法之一是「地 球工程法」。這種工法是在平流層導入硫酸鹽，透過在平流層(即通稱的臭氧層)中經常性注入大量的硫酸鹽粒子可幫助地球降溫，但這項措施同時也會影響臭氧量 並使得臭氧洞的回復延後數十年。這種工法的效果如何，需要被檢驗。金星的大氣層中，硫含量超過地球大氣層 1000 倍以上，非常適合用來檢驗硫化物在光化學 上的限制，以及對氣候的影響爲何。
金星表面受到一層厚厚的硫酸液滴雲層完全的包覆，液滴層中含有約 15%的水。地球在地表高度 18 至 22 公里的範圍中，同樣也有一層天然的類似薄層。在兩顆行星上相同的是，當這些液滴形成時，二氧化硫（SO_2）都需要氧化爲三氧化硫（SO_3），過程中並 結合水（H_2O）形成硫酸（H_2SO_4），然後再與額外的水凝結，形成液滴雲層。
此次，透過地面觀測儀器以及「金星快車號」太空船，首次發現清晰證實金星在距離地表約 100 公里處的高層大氣具有一層二氧化硫（SO_2）。梁茂昌博士表示，「我們認爲，硫氧化物的來源，可能是光解作用中硫酸（H_2SO_4）釋放出的蒸氣溶膠。」
這新的理論完全改變先前舊假設，對金星大氣層上層的大氣化學模式提出新構想，並且對「氣溶膠微物理學」和「大氣環流」等迄今所知甚微的領域，具有指導性意義。「金星無疑是研究硫化物影響大氣化學的最佳大型天然實驗室。」梁茂昌博士說。
共同作者之一翁玉林教授目前爲美國加州理工大學行星科學系教授同時也是中研院院士。
「自然地球科學」月刊(Nature Geoscience)創立於 2008 年，隸屬於 Nature 出版集團，以刊登高品質的原創性學術研究爲主要訴求，內容涵蓋地球科學的所有範疇：大氣、海 洋、冰河及冰原、地球實體等。(文／引用自臺北天文館之網路天文館網站、中研院天文網)

原文轉載自【2010-11-19/NOWnews 今日新聞網】

16 年 15 億美元　丁肇中主導 NASA 尋太空反物質

【編譯張佑生／綜合報導】

歷經 16 年、花掉 15 億美元，該是華裔諾貝爾物理獎得主、台灣中研院院士丁肇中與美國太空總署（NASA）大顯身手的時刻了。
紐約時報 16 日以「宇宙黑暗之心的昂貴探索」（A Costly Quest for the Dark Heart of the Cosmos）爲題，介紹 NASA 與丁肇中合作的反物質太空磁譜儀（Alpha-Magnetic Spectrometer）的 AMS-02 計畫。
8 噸重的 AMS-02 實驗儀器將於 2011 年 2 月 27 日由太空梭送進國際太空站，要在太空中尋找暗物質、失落物質及反物質存在的證據，爲期 3 年。
計畫如果成功，NASA 回答宇宙由何組成的問題將邁進一大步，也可爲國際太空站和丁肇中（74 歲）輝煌的生涯畫下燦爛的句點。倘若失敗，從實驗計畫獲准後就斥爲錢坑的反對者，將更振振有詞。
丁肇中研究經費並非由 NASA 負擔，資助該研究的有全世界 16 個國家的 600 多位科學家，包括台灣中研院、中科院、中央大學、成功大學、中國、德國、義大利和俄國。
台灣的「國家太空中心」（NSPO）2002 至 2008 共計執行四次 AMS-02 計畫電子元件熱真空測試，包

括電腦及介面元件之驗證模組（QM）、飛行模組（FM）及備用模組（FS），以驗證電子元件之製造工藝以及熱分析模型的準確性。

丁肇中表示：「假使宇宙是從大爆炸來，因爲爆炸以前是真空，爆炸以後有物質，就應該要有同樣多的反物質，現在宇宙已經 150 億年了，所以我們這個實驗的目標之一，就是找反物質所組成的宇宙在什麼地方。」

1998 年，美國發現號太空梭就帶著丁肇中的 AMS 探測器升空，這是第一個在太空進行的高能物理實驗，十天的飛行，希望捕捉到特殊的粒子。但因爲儀器的磁 場強度不夠，發現到的粒子現象並不明顯。丁肇中於是決定製作一個巨大磁場的超導磁鐵，這些儀器必須能在國際太空站運作長達十年，還得耐得住外太空最低負 40 度、最高溫 90 度的劇烈溫差，而不能壞，困難度極高。

原文轉載自【2010-11-18/聯合報/A15 版/國際】

太空探索／衛星敗部復活　反成太陽風觀測利器

生活中心／台北報導

一對約一年前被判定失效的美國航太總署（NASA）衛星，現在敗部復活，即將進行一項嶄新的繞月任務。

這對衛星正式編號爲 THEMIS（西蜜斯任務）P1 和 P2，在 2007 年時，NASA 總共發射了由 5 架衛星組成的艦隊進入地球磁圈，研究地磁風暴的物理性質，臺灣地區的國家太空中心和中央大學太空所也有參與相關計畫。

THEMIS 是「Time History of Events and Macroscale Interactions during Substorms（副磁暴事件時間進程與大尺度交互作用）」的簡稱，而 P1 和 P2 是軌道在最外側的 2 架衛星。這個任務開始不久，就發現許多先前未知的現 象，如碰撞極光（colliding auroras）、太空磁震（magnetic spacequakes）、電漿子彈速擊（plasma bullets shooting up）以及地球背面的磁尾（magnetic tail）等。這些發現讓科學家解決了好幾個懸宕已久的北極光之謎。（註：以上名詞均爲暫譯）

然而由於這些衛星均以太陽能爲動力來源，原設計中，失去陽光而無法充電的時間可達 3 小時左右都沒問題；但隨著軌道演化，2009 年時 P1 和 P2 每天行經地球陰影的時間長達 8 小時左右，電力逐漸流失而導致衛星即將逐漸停擺。

由於這個任務本來進行得很順利，這兩架衛星就這樣停擺實在很可惜，因此任務科學家們絞盡腦汁想讓它們敗部復活。評估之後發現：衛星殘餘的電腦還足以讓它們航向月球！NASA 於 2009 年末同意這個敗部復活賽，P1 和 P2 因而開始遠離地球陰影的影響，向月球前進。

新契機要有新任務名稱，NASA 將新任務改名爲「ARTEMIS」，也就是希臘神話中的月亮女神之名「阿蒂米斯」，不過其實是 「Acceleration, Reconnection, Turbulence and Electrodynamics of the Moon's Interaction with the Sun（月球與太陽交互作用之加速、再連結、擾動和電磁動力）」的縮寫。

ARTEMIS 第一個大事紀發生於 2010 年 8 月 25 日，其中的 P1 抵達月球背面的 L2 拉格朗日點（Lagrange point），P2 隨後在 10 月 22 日進入月地之間的 L1 拉格朗日點。所謂的拉格朗日點就是地球和月球的重力平衡點。

這是人類首度探索地月系統的拉格朗日點，一般的太空船或衛星並不會在此停留。但這些拉格朗日點其實只在地球磁圈外一點點，因此可以好好地研究太陽風性質。 ARTEMIS 衛星上的感應器可感測抵達地球附近的太陽風粒子流或太陽風暴雲，可做爲太空氣象預測先鋒。從兩個相反的拉格朗日點進行觀測，可以前所未有的 大尺度來測量太陽風擾動狀況，對瞭解太陽風性質非常有幫助。

此外，ARTEMIS 還將探索月球的電漿尾流（plasma wake），也就是月球造成的太陽風擾動型態，就像是船前進時，在船尾形成的尾波一樣。換言之，這個地方簡直是研究電漿波動的寶庫，科學家們都在等著發現並研究各式各樣的電漿波動。

ARTEMIS 的另一個觀測目標是地球的磁尾（magnetotail）。地球磁場受到太陽風衝擊，面對太陽風一側被壓縮，但背對太陽風一側則向後延伸到 月球軌道以外之處，像條尾巴一樣。大約每逢滿月前後，ARTEMIS 便可隨著月亮穿越地球磁尾，此時便可趁機測量地球磁尾性質狀態，特別是磁力線重新連結（magnetic reconnection）事件，或甚至是磁暴期間被爆發加速的爆發漿團（plasmoids）襲擊月球的現象。無論哪一種現象，或許最後都可以應用在地 球探索中，將之轉換成地球可用的再生能源。

待在拉格朗日點約 6 個月之後，ARTEMIS 將會繼續向月球靠近，最初將維持距離月表約 100 公里的狀態，最後的距離則將遠少於此，因此可近距離直接觀察在沒有大氣層或磁場的保護下，太陽風對月表岩石所造成的風化侵蝕。這對未來的太陽系行星探索任務相當重要。

由於月球重力場並不規律，月球內部有許多質量聚集的質量瘤（mascon），會以未知的方式拉扯這些

衛星，造成它們的軌道逐漸改變。ARTEMIS 目前以 非常橢圓的軌道來盡可能規避這個問題，近月點約僅數十公里，但遠月點可達 18,000 公里左右，如此一來，接近月表的時間相當短暫，但遠離月球的時候還是 可以繼續觀察太陽風，累積觀測資料的時間可延長到數年之久。(文／引用自臺北天文館之網路天文館網站)

原文轉載自【2010-11-29/NOWnews 今日新聞網/生活新聞 】

「中壢」躍上國際　揚名宇宙

【記者徐乃義／中壢報導】

擁有七所大專院校的「中壢」，是中央大學所在地，更是客家族群的重鎮。爲彰顯「中壢」在台灣的特殊象徵意義，中央大學將編號 210035 小行星命名爲「中 壢」(Jungli)。24 日中大運動會開幕式，校長蔣偉寧頒贈小行星銘牌和模型給中壢市長魯明哲，在兩千多位師生見證下，讓「中壢」(Jungli) 躍 上國際，揚名宇宙。

中大天文研究所周翊所長表示，中壢小行星的發現，源自中大鹿林巡天計畫（Lulin Sky Survey，簡稱 LUSS），中壢小行星是 2006 年 7 月 18 日由中大鹿林天文台林宏欽與廣州中山大學葉泉志利用 40 公分望遠鏡所發現，經國際天文學聯合會 （IAU/CSBN）軌道確認和命名通過，今（2010）年 9 月 23 日正式名爲「中壢」(Jungli)。中壢小行星位於火星和木星之間的小行星帶，距離 地球最近的距離約 1.5 億公里，繞太陽一圈約 4.5 年。

周翊所長表示，要在浩瀚的宇宙中發現新天體，除專業，更需要恆心和毅力。人員工作日夜顛倒每天持續不斷的觀測，加上背後資料分析的縝密配合，才可能從茫茫星空大海中撈針，找到新的天體。

中央大學鹿林天文台位於玉山國家公園，是東亞最高、國際上重要的天文觀測台，1998 年設立後參與多項國際天文計畫，例如和美國夏威夷大學合作泛星計畫 （Pan-STARRS），大量搜尋在太空中運行並可能與地球碰撞的小行星或彗星，已找到第一顆對地球有潛在危險的小行星，引起國際各大媒體之關注。

原文轉載自【2010-11-25/大紀元時報/A6 版/台灣綜合】

小行星命名　「中壢」名揚國際

記者成漢/桃園報導

爲了彰顯「中壢」所在地的特殊象徵意義，中央大學鹿林天文台利用 40 公分望遠鏡新發現，經國際天文學聯合會(IAU/CSBN)通過，將小行星命名爲「中 壢」(Jungli)；昨日由中大校長蔣偉寧頒贈小行星銘牌和模型給中壢市長魯明哲，在兩千多位師生見證下，讓「中壢」(Jungli)躍上國際，揚名宇 宙。

中壢市長魯明哲爲感謝中大頒贈中壢小行星，特率領一級主管，繫上亮麗的客家領巾參與，並以祝福中壢「星星向榮」的紀念座回贈。魯明哲表示，中壢與中大同在一個生活圈，密不可分，中壢堪稱在外求學學子的「第二故鄉」，有著深厚的情感連結。

中央大學天文研究所周翊所長表示，中壢小行星是 2006 年 7 月 18 日由中大鹿林天文台林宏欽與大陸廣州中山大學葉泉志利用 40 公分望遠鏡所發現，經國際天文學聯合會(IAU/CSBN)軌道確認和命名通過，今年 9 月 23 日正式名爲「中壢」(Jungli)。

原文轉載自【2010-11-25/青年日報/13 版/桃竹苗地方通訊】

慶祝「中壢小行星」命名通過　兩千多位師生歡喜見證

【大紀元 2010 年 11 月 24 日訊】(大紀元記者徐乃義台灣中壢報導)擁有七所大專院校的「中壢」，是中央大學所在地，更是客家族群的重鎮。爲彰顯「中壢」在 台灣的特殊象徵意義，中央大學將編號 210035 小行星命名爲「中壢」(Jungli)。24 日中大運動會開幕式，校長蔣偉寧頒贈小行星銘牌和模型給中壢 市長魯明哲，在兩千多位師生見證下，讓「中壢」(Jungli)躍上國際，揚名宇宙。

蔣偉寧說，中大空氣清新、綠蔭扶疏，有「中壢後花園」之稱，一直是市民休憩好所在。中壢市公所協助中大前門、宵夜街之景觀改善工程，與中大互動密切。

蔣偉寧指出，中壢市是台灣族群最多元的城市之一，包括客家、閩南、外省、原住民和新住民等，客家人爲主要族群人口，以客家庄著名。中大設有全球首創之客家學院，長期以來致力於客家學術研究和

人才培育工作，彼此相得益彰。
中壢市長魯明哲爲感謝中大頒贈中壢小行星，率領一級主管，繫上亮麗的客家領巾參與，並以祝福中壢「星星向榮」的紀念座回贈。魯明哲表示，中壢與中大同在一個生活圈，密不可分，中壢堪稱在外求學學子的「第二故鄉」，有著深厚的情感連結。
中大天文研究所周翊所長表示，中壢小行星是 2006 年 7 月 18 日由中大鹿林天文台林宏欽與廣州中山大學葉泉志利用 40 公分望遠鏡所發現，經國際天文學聯合會(IAU/CSBN)軌道確認和命名通過，今年 9 月 23 日正式名爲「中壢」(Jungli)。
中壢小行星位於火星和木星之間的小行星帶，距離地球最近的距離約 1.5 億公里，繞太陽一圈約 4.5 年。2006 年最早發現時，位於魔羯座附近，目前則在人馬座附近。
中壢小行星的發現，源自中大鹿林巡天計畫（Lulin Sky Survey，簡稱 LUSS）。該計畫自 2006 年 3 月啓動以來，以 40 公分望遠鏡進行小天體巡天觀測。截至目前爲止，總計發現 800 多顆小行星、1 顆近地小行星 (2007 NL1)、1 顆彗星(C/ 2007N3 (LULIN))。其中鹿林彗星是台灣首次發現的彗星，爲去年(2009)全球最明亮的彗星，引起全球天文迷之關注。
周翊所長表示，要在浩瀚的宇宙中發現新天體，除專業，更需要恆心和毅力。每天太陽下山了，才是觀測人員工作的開始，日夜顛倒每天持續不斷的觀測，加上背後資料分析的縝密配合，才可能從茫茫星空大海中撈針，找到新的天體。
中央大學鹿林天文台位於玉山國家公園，是東亞最高、國際上重要的天文觀測點，自 1998 年設立，除發現小行星之外，更參與多項重要的國際天文計畫，例如和 美國夏威夷大學合作泛星計畫(Pan-STARRS)，大量搜尋及發現在太空中運行並可能與地球碰撞的小行星或彗星，已找到第一顆對地球有潛在危險的小行 星，引起國際各大媒體之關注。

原文轉載自【2010-11-24/大紀元時報首頁 > 新聞 > 台灣地方新聞 > 正文】

中壢小行星　中大贈中壢

【記者游文寶／中壢報導】

國立中央大學鹿林天文台 3 年多前發現一顆小行星，爲凸顯中大所在地行政區，決定命名爲「中壢」(Jungli)。中大校長蔣偉寧昨天將在中大運動會開幕式之前，將小行星銘牌及模型交給中壢市長魯明哲，讓中壢揚名國際。
魯明哲率領一級主管到場，每個人繫上客家領巾，同時回贈「星星向榮」紀念座。魯明哲說，中壢與中大爲共同生活圈，爲外地學子的「第二故鄉」，有深厚情感連結。
中央大學天文研究所周翊所長說，中壢小行星是 2006 年 7 月 18 日由中大鹿林天文台林宏欽與大陸廣州中山大學葉泉志利用 40 公分望遠鏡所發現，經國際天文學聯合會軌道確認和命名通過，今年 9 月 23 日正式名爲「中壢」 (Jungli)。
中壢小行星位於火星和木星間的小行星帶，距離地球最近的距離約 1.5 億公里，繞太陽一圈約 4.5 年。
蔣偉寧說，中大民國 51 年在台復校，原設址於苗栗，因校地太小，另覓校地，民國 57 年選定中壢這塊「福地」，42 年來穩健成長，如今名列世界 500 大、前 1%頂尖學府。
蔣偉寧說，中大綠樹成蔭，空氣清新，有「中壢後花園」之稱。中壢是台灣族群最多元的城市之一，也擁有 7 所大專院校，文風鼎盛。

原文轉載自【2010-11-25/聯合報/B1 版/桃園・運動】

中大發現小行星命名中壢　今頒贈儀式

【聯合報／記者游文寶 ／即時報導】

中壢市擁有 7 所大專院校，是國立中央大學所在地，爲彰顯「中壢」在台灣的特殊象徵意義，中央大學決定將鹿林天文台發現的編號 210035 小行星命名爲「中壢」（Jungli）。
今天中大舉辦運動會開幕式，校長蔣偉寧將小行星銘牌和模型頒給中壢市長魯明哲，在兩千多位師生見證下，讓「中壢」 (Jungli)躍上國際，揚名宇宙。

原文轉載自【2010-11-.24/即時新聞　地方新聞　聯合新聞網】

"台灣天文學家發現新的小行星威脅"

＜科技＞台灣天文學家發現新的小行星威脅

某些科學證據顯示萬物之間如此精密的自然運作可能是由大量的小行星和彗星撞擊地球所造成的。 另有證據推論恐龍也是因為這種撞擊而絕跡。 但是這會再次發生嗎?

小行星 2010ST3，目前距離地球 6400 公里，是一顆最新發現的星體，預計這顆星體將以距離地球少於 50 萬公里的距離經過地球。這是一顆最新發現的星 體，當時中央大學天文研究所的陳文屏教授帶領著 20 名科學家在夏威夷大學進行泛星計畫(全景巡天望遠鏡和快速回應系統)研究時發現的，因此這顆星體由他們 共同命名。 這個發現讓泛星計畫成為可以發現這種威脅的最敏銳天文望遠鏡。

雖然 50 萬公里是非常接近的距離，但是陳教授一點都不擔心。陳教授平靜地表示，「我們有許多預防人類被毀滅的方法。」 從足以粉碎這種威脅的強大雷射光束到把星體撞離軌道的太空船，人類擁有許多可以免於步上恐龍後塵的科技。

(Technology) Taiwanese Astronomers Discover New Asteroid Threat

There is some scientific evidence that the delicate balancing act that is nature and all life was made possible by massive asteroids and meteors that bombarded our planet. Still further evidence suggests that the dinosaurs were snuffed out into extinction by such a strike. Is this happening again?

Asteroid 2010ST3, currently 6.4 million kilometers from earth, is a newly discovered celestial body that is predicted to pass within half a million kilometers of our planet. It was first spotted, and thus named, by a group of 20 Taiwanese scientists, led by Professor Chen Wen-ping of The National Central Universitys Graduate Institute of Astronomy, working on the Pan-STARRS (Panoramic Survey Telescope & Rapid Response System) at the University of Hawaii. This discovery makes the Pan-STARRS the most sensitive telescope available to discover such threats.

Although 500,000 kilometers is considered an extremely close call, Professor Chen is not worried. "We have many ways of preventing human civilization from being wiped away," the Professor assuaged. From mighty laser beams that can fracture such a threat, to spaceships that can bump it from its path, mankind has the technology to avoid the fate of the dinosaurs.

原文轉載自【2010-10-07/FunDay】

金星高層大氣中有硫源　供地球暖化另項解套參考

記者曹逸雯／台北報導

中央研究院環境變遷研究中心副研究員梁茂昌博士參與的國際天文研究團隊(美國加州理工大學、密西根大學和法國的 LATMOS, CNRS/INSU/IPSL, Université de Versailles-Saint-Quentin、Universite´ Pierre et Marie Curie)，於 10 月 31 日在專業期刊「自然地球科學」(Nature Geoscience)發表論文，證實金星高層大氣中發現硫源，這項發現日後可望為地球暖化問題，提供另項解套方法參考。

梁茂昌表 示，對於解決全球暖化的問題，目前學術界公認最實惠且有效的方法之一是「地球工程法」。這種工法是在平流層導入硫酸鹽，透過在平流層(即通稱的臭氧層)中 經常性注入大量的硫酸鹽粒子可幫助地球降溫，但這項措施同時也會影響臭氧量並使得臭氧洞的回復延後數十年。這種工法的效果如何，需要被檢驗。金星的大氣層 中，硫含量超過地球大氣層 1 千倍以上，非常適合用來檢驗硫化物在光化學上的限制，以及對氣候的影響為何。

研究發現，金星表面受到一層 厚厚的硫酸液滴雲層完全的包覆，液滴層中含有約 15%的水。地球在地表高度 18-22 公里的範圍中，同樣也有一層天然的類似薄層。在兩顆行星上相同的是， 當這些液滴形成時，二氧化硫（SO2）都需要氧化為三氧化硫（SO3），過程中並結合水（H2O）形成硫酸（H2SO4），然後再與額外的水凝結，形成液 滴雲層。

此次透過地面觀測儀器以及「金星快車號」太空船，首次發現清晰證實金星在距離地表約 100 公里處的高層大氣具有一層二氧化硫 （SO2）。梁茂昌指出，「我們認為，硫氧化物的來源，可能是光解作用中硫酸（H2SO4）釋放出的蒸氣溶膠。」這新的理論完全改變先前舊假設，對金星大 氣層上層的大氣化學模式提出新構想，並且對「氣溶膠微物理學」和「大氣環流」等迄今所知甚微的領域，具有指導性意義，他表示，「金星無疑是研究硫化物影響 大氣化學的最佳大型天然實驗室。」

梁茂昌博士目前為中研院環境變遷研究中心副研究員暨中央大學合聘副教授和中研院天文及天文物理所合聘副研究員，而論文共同作者之一翁玉林教授目前為美國加州理工大學行星科學系教授，同時也是

中研院院士。
「自然地球科學」月刊(Nature Geoscience)創立於 2008 年，隸屬於 Nature 出版集團，以刊登高品質的原創性學術研究為主要訴求，內容涵蓋地球科學的所有範疇：大氣、海洋、冰河及冰原、地球實體等。

原文轉載自【2010-11-05/NOWnews 今日新聞網 /頭條新聞 】

太空探索／相距 700 公里　EPOXI 成功飛掠哈德利 2 號彗星

生活中心／台北報導

美國航太總署（NASA）EPOXI 任務於 11 月 4 日成功飛掠哈德利 2 號彗星（103P/Hartley 2），並開始回傳影像資料。EPOXI 任務負責人 Tim Larson 表示，能進距離看到這顆彗星的彗核，任務小組和科學家們近日來的一切辛苦都值得了！
一 如先前估計的，太空船最接近彗核時，距離大約為 700 公里。並在最接近後約 8 分鐘左右，太空船的高增益天線（high-gain antenna）便對準地球，以將資料回傳，由 NASA 位在加州的深空聯絡網（Deep Space Network）天線負責接收。大約 20 分鐘後，第一張接近彗核的影像便躍然出現在電腦螢幕上，將距離地球 3700 萬公里之遙的彗星真實面貌呈現在眾人面前。
上方是 EPOXI 上的 MRI 相機拍攝的接近哈德利 2 號彗星彗核的連續影像（從左上角開始，順時針方向，想看精彩圖片請進：http://www.nownews.com/2010/11/05/327-2661534.htm）， 太陽在右方。可以看到彗核外型像啞鈴、花生或海獺一樣，兩端的大小差不多、地質特徵比較粗糙，中間連接部分則比較窄但地表比較平滑，似乎覆蓋著比較細的塵 土；噴流則是從兩端似乎地質較粗糙的部分噴出，這是天文學家首度能將噴流現象與彗星表面特徵一起結合起來研究，尋找噴流發的機制。更多飛掠哈德利 2 號彗星的相關影像可參閱 http://epoxi.umd.edu/。
EPOXI 在接下來的 2 週逐漸遠離哈德利 2 號彗星的旅程中，仍會持續觀看彗星的變化。這些觀測資料夠科學家忙上好幾年了。而任務科學家們都個個摒息以待，不知道這顆彗星將帶給世人什麼樣的驚奇結果。
哈德利 2 號彗星是第 5 顆被太空船拜訪過的彗星。如上圖，其他幾顆包括：
哈雷彗星（1P/Halley）：1986 年，包括美國 ICE、前蘇聯 Vega 1 與 Vega 2、日本 Sakigake 與 Suisei、歐洲 ESA 的 Giotto 等都在哈雷彗星最近一次回歸時，飛掠哈雷進行觀測。
布洛利彗星（19P/Borrelly）：2001 年：美國 NASA 的 Deep Space 1 深空 1 號任務。
譚普 1 號彗星（9P/Tempel 1）：2005 年，Deep Impact 深擊任務。
威德 2 號彗星（81P/Wild 2）：2006 年，Stardust 星晨號任務。
哈德利 2 號彗星（103P/Hartley 2）：2010 年，Deep Impact 深擊任務延伸任務 EPOXI。
上述被探訪過的每顆彗星，大小尺寸和外型都不相同，但哈德利 2 號彗星的體積比深擊任務第一個目標─譚普 1 號彗星還小 100 倍左右，是到目前為止有太空船拜訪過的彗星中最小卻最活躍的。各項任務細節可參考 http://www.planetary.org/explore/topics/asteroids_and_comets/missions.html。
小行星和彗星是非常類似的天體，目前天文學家還在爭論這兩類天體究竟是否為同一類。日本隼太空船（Hayabusa）於 2007 年飛掠、甚至登陸糸川小行 星（Itokawa），並在 2010 年將所採集的樣本送回地球。由於外型與這次哈德利 2 號彗星的影像很類似，中央大學天文研究所阿部新助教授正在比較兩者 的差異，或許可以獲得意外的訊息。(文／引用自臺北天文館之網路天文館網站)

原文轉載自【2010-11-05/NOWnews 今日新聞網 /頭條新聞 】

中大發現小行星　命名慈濟

陳淑娟/整理

中央大學發現小行星並命名為「慈濟」，以表彰慈濟基金會對世人的貢獻，中央大學校長蔣偉寧（右）1 日將小行星在太陽系軌道銘板贈給證嚴法師（中）。 （中央社/慈濟基金會提供）
【中央網路報】

原文轉載自【2010-10-02/中央日報網路報-鏡頭看台灣】

「慈濟」小行星　台灣精神躍天際

【記者魏培淋花蓮報導】

中央大學發現編號 192208 小行星，今年七月通過國際天文學聯合會命名爲「慈濟」小行星。中央大學校長蔣偉寧，特地到花蓮靜思精舍，將「慈濟」小行星在太陽系軌道的銘板，獻給證嚴法師。這是台灣第一顆以宗教團體命名的小行星。

「慈濟（Tzu Chi）」小行星，2007 年 5 月 11 日由前中大天文所觀測助理施佳佑與當時大陸廣州中山大學學生葉泉志在鹿林天文台發現。爲彰顯慈濟對世人之貢獻，中央 大學將這顆行星命名爲「慈濟」，代表台灣精神的「慈濟」躍上天際，將其無私奉獻的精神恆久傳遞，在地球與宇宙同時發光發熱。2010 年 7 月 26 日經國際天 文學聯合會通過正式命名！

中大校長蔣偉寧、副校長暨天文所教授葉永烜、鹿林天文台長林宏欽等人到慈濟靜思精舍，拜會證嚴法師，獻上刻有 慈濟小行星在太陽系軌道的銘板。蔣偉寧表示，慈濟大愛沒有國界之分，慈濟小行星，讓慈濟在宇宙發光發熱，也讓代表台灣精神之一的「慈濟」躍上天際。他期待 未來中大能與慈濟緊密合作，透過科學，提供災前預防、災後救援等資訊，科學與人文結合，發揮更大的力量，幫助更多人。蔣偉寧讚歎，慈濟人就像是地球的守護 神！

證嚴法師表示，佛陀是宇宙大覺者，在兩千多年前就有宇宙觀。綜觀，天地萬物之間是習習相關，萬物離不開成住壞空，慈濟推動的環保， 將寶特瓶回收，再製成環保衣物，物歸源頭、重新再來。證嚴法師期待，每一位慈濟人需要盡心力，上知天文下知地理，天地之間沒有無關的事情，知天文才知怎麼 爲大地盡心力！

鹿林天文台台長林宏欽表示，當時發現這顆小行星有先將其進行臨時編號，在經過多年觀察確認小行星的軌道，去年經過國際永 久編號認證，今年7月26日經國際天文學聯合會通過，正式命名爲「Tzu Chi(慈濟)」。慈濟小行星爲太陽系中的移動天體，位於火星與木星之間的小行星帶。他指出，慈濟小行星繞太陽一圈約 5.62 年，與地球最近的距離約 3 億 公里。

星星恆久遠，一顆永流傳。慈濟慈善、醫療、教育與人文四大志業，福澤世界五大洲，締造人間傳奇。中央大學天文所鹿林天文台所發現的小行星，以「慈濟」命名之，期能天上、人間互相輝耀慈濟的貢獻。

原文轉載自【2010-10-05/民眾日報/14 版/花蓮新聞】

中央大學發現小行星　命名慈濟

（中央社記者劉嘉泰花蓮縣 1 日電）

中央大學和廣州中山大學 2007 年 5 月，在鹿林天文台觀測發現 1 顆小行星，今年 7 月獲得國際天文學聯合會通過後，正式被命名爲「慈濟」，表彰慈濟基金會的貢獻。

中央大學校長蔣偉寧今天專程到花蓮慈濟靜思精舍，把小行星「慈濟（TzuChi）」在太陽系軌道的銘板贈送給證嚴法師。他表示，這顆小行星命名爲「慈濟」，是爲了彰顯慈濟對世人的貢獻，希望代表台灣精神的「慈濟」躍向天際，把無私奉獻的精神恆久傳遞。

蔣偉寧表示，這顆小行星是前中央大學天文所觀測助理施佳佑和廣州中山大學學生葉泉志於 2007 年 5 月 11 日，在鹿林天文台觀測發現到；當時先進行臨時編號，經過多年觀察確認軌道後，去年通過國際永久編號認證。

陪同拜會證嚴法師的鹿林天文台長林宏欽指出，這顆小行星今年 7 月 26 日經國際天文學聯合會通過，並正式被命名爲「慈濟」。慈濟小行星是太陽系中的移動天體，位於火星與木星間的小行星帶，繞行太陽 1 圈約 5.62 年，與地球最近距離約 3 億公里。

證嚴法師表示，佛陀是宇宙大覺者，在 2000 多年前就有宇宙觀，綜觀天地萬物之間是息息相關，她期待每 1 名慈濟人需要盡心力，上知天文下知地理，天地間沒有無關的事情，知天文才知怎麼爲大地盡心力。

慈濟指出，「慈濟」小行星是台灣第 1 顆以宗教團體命名的小行星，慈濟的慈善、醫療、教育和人文 4 大志業福澤世界 5 大洲，希望慈濟無私奉獻的精神，能在地球和宇宙同時發光發熱。991001

原文轉載自【2010-10-01/中央社】

台灣首顆宗教團體命名小行星　慈濟躍上天際　中央大學銘板致意

記者湯平／花蓮報導

中央大學 發現編號 192208 小行星，今年七月通過國際天文學聯合會命名爲「慈濟」小行星。中央大學校長蔣偉寧昨日特別到花蓮慈濟靜思精舍，將「慈濟」小行星在太陽系軌道的銘板，獻給證嚴法師；這是台灣第一顆以宗教團體命名的小行星。

「慈濟（Tzu Chi）」小行星，二○○七年五月十一日由前中大天文所觀測助理施佳佑與當時大陸廣州中山大學學生葉泉志在鹿林天文台發現。爲彰顯慈濟對世人之貢獻，中央 大學將這顆行星命名爲慈濟，代表台灣精神的「慈濟」躍上天際，將其無私奉獻的精神恆久傳遞，在地球與宇宙同時發光發熱。今年七月二十六日經國際天文學聯合 會通過正式命名。

中大校長蔣偉寧、副校長暨天文所教授葉永烜、鹿林天文台長林宏欽等人昨天到慈濟靜思精舍，拜會證嚴法師，獻上刻有慈濟小行星在太陽系軌道的銘板。蔣偉寧表示，慈濟大愛沒有國界之分，慈濟小行星，讓慈濟在宇宙發光發熱。

鹿林天文台台長林宏欽表示，慈濟小行星爲太陽系中的移動天體，位於火星與木星之間的小行星帶。他指出，慈濟小行星繞太陽一圈約五點六二年，與地球最近的距離約 3 億公里。

原文轉載自【2010-10-02/青年日報/6 版/新視界】

中央大學發現小行星　命名慈濟

【花蓮訊】 2010/10/02

中央大學和廣州中山大學二○○七年五月，在鹿林天文台觀測發現一顆小行星，今年七月獲得國際天文學聯合會通過後，正式被命名爲「慈濟」，表彰慈濟基金會的貢獻。

中央大學校長蔣偉寧昨天專程到花蓮慈濟靜思精舍，把小行星「慈濟（TzuChi）」在太陽系軌道的銘板贈送給證嚴法師。

他表示，這顆小行星命名爲「慈濟」，是爲了彰顯慈濟對世人的貢獻，希望代表台灣精神的「慈濟」躍向天際，把無私奉獻的精神恆久傳遞。

原文轉載自【2010-10-02/台灣新生報/2 版/要聞】 相

小行星命名慈濟　中大校長獻銘版

陳信羽 鄧明怡 花蓮報導

中央大學鹿林巡天計畫團隊爲了感謝慈濟人在八八風災全力投入救災，在今年 7 月 26 日將一顆新發現的小行星命名登記爲「慈濟」。中央大學校長、副校長今天 (10/1)專程從桃園來到花蓮，在靜思精舍拜會證嚴上人，並獻上紀念銘板，感恩慈濟長期爲社會做出的貢獻，這也是台灣第一顆以宗教團體命名的小行星。

送上行星登記的銘板，這是由國際天文學聯合會通過命名所頒發的獎板，由中央大學副校長贈送給證嚴上人。

位於火星與木星之間的這顆小行星就是「慈濟星」，距離地球約 3 到 4 億公里，中央大學正式將小行星登記爲「慈濟」，除了感恩慈濟人長期在社會的付出與貢獻，更希望將天文的新發現回饋社會。

中央大學校長 蔣偉寧：「主要的考量，確實也感受到慈濟在證嚴上人的領導下，其實發揮大愛，對於大愛無國際，不分膚色。」

大愛無國界，哪裡有災難就可以看到慈濟人的身影。慈善與天文更是息息相關，當災難發生，透過衛星圖更可以準確掌握災情。

證嚴上人開示：「因爲希望他們(慈濟人)都要懂得天文，不知天文，就無法在地理上盡心力，大家都要懂得地理，爲什麼地球會受毀傷。」

長期投入天文研究的中央大學鹿林天文台花了一年多的時間觀察，才找出小行星的運行軌跡，能夠得到命名權，更是高興。

小行星永恆運行，就如同慈濟日不落的大愛精神，永遠守護地球。

原文轉載自【2010-10-01/大愛電視 DaAi TV】

人間菩提--寰宇中「慈濟星」

A Heart and Mind that Embraces the Cosmos
佛心覺性徹寰宇
慈濟行星殊勝義
節能減碳廣倡籲
惜護大地同一心

中央大學和廣州中山大學 2007 年 5 月在鹿林天文台觀測發現 1 顆小行星，今年 7 月獲得國際天文學聯合會通過後，正式被命名爲慈濟。證嚴上人說，宇宙之大， 行星繞著軌道運行，天地萬物都有奧妙的道理，期許大家上知天文下知地理，明瞭宇宙大覺者，也就佛陀的道理，才知怎麼去付出。

中央大學校長蔣偉寧贈送小行星慈濟在太陽系軌道的銘板，彰顯慈濟對世人的貢獻。慈濟星雖然與地球最近距離約有 3 億公里，但天地萬物息息相關，明白行星在軌道上規律運行的道理，就能瞭解宇宙大覺者教導人們的道理。

證嚴上人開示：「好好的依教奉行，佛陀所說的法，我們按照這樣的軌道去力行，總是也可以接近佛心，我們跟著佛陀的芳蹤步步向前，佛陀如何教我們就如何去接近，付出就對了。」

天上人間相互輝映，才能把愛散布到世界各角落。歡度 18 周年慶的慈濟加拿大分會，在今年台灣文化節的活動，推廣慈濟環保二十年的理念，也因多年來無所求的付出，讓當地人深受感動，溫哥華市政府特別頒定九月四號爲慈濟日。

證嚴上人開示：「地球上多少國家，常常都給慈濟日，那樣的來做，肯定慈濟人在他們的國度裡如何付出，這實在是都要感恩，林林總總，都是因爲有這麼多人用心、用愛付出，都是給我們的一個很大的鼓勵。」

落實佛陀的教育，盡自己的一分力量爲人類造福，期盼人人如星星月亮般，用光亮照亮黑暗，散發愛的光芒。

原文轉載自【2010-10-02/大愛電視 DaAi TV】

上人開示　大覺者體悟宇宙真理　慈悲度蒼生

林國新 劉泓志 花蓮報導

中央大學和廣州中山大學 2007 年 5 月在鹿林天文台觀測發現 1 顆小行星，今年 7 月獲得國際天文學聯合會通過後，正式被命名爲慈濟。證嚴上人說，宇宙之大， 行星繞著軌道運行，天地萬物都有奧妙的道理，期許大家上知天文下知地理，明瞭宇宙大覺者、也就佛陀的道理，才知怎麼去付出。

中央大學校長蔣偉寧贈送小行星慈濟，在太陽系軌道的銘板，彰顯慈濟對世人的貢獻。慈濟星雖然與地球最近距離約有 3 億公里，但天地萬物息息相關，明白行星在軌道上規律運行的道理，就能瞭解宇宙大覺者教導人們的道理。

證嚴上人開示：「好好的依教奉行，佛陀所說的法，我們按照這樣的軌道去力行，總是也可以接近佛心，我們跟著佛陀的芳蹤步步向前，佛陀如何教我們就如何去接近，付出就對了。」

天上人間相互輝映，才能把愛散布到世界各角落。歡度 18 周年慶的慈濟加拿大分會，在今年台灣文化節的活動，推廣慈濟環保二十年的理念，也因多年來無所求的付出，讓當地人深受感動，溫哥華市政府特別頒定九月四號爲慈濟日。

證嚴上人開示：「地球上多少國家，常常都給慈濟日，那樣的來做，肯定慈濟人在他們的國度裡如何付出，這實在是都要感恩，林林總總、都是因爲有這麼多人用心、用愛付出，都是給我們的一個很大的鼓勵。」

落實佛陀的教育，盡自己的一分力量爲人類造福，期盼人人如星星月亮般，用光亮照亮黑暗，散發愛的光芒。

原文轉載自【2010-10-02/大愛電視 DaAi TV】

小行星命名「慈濟」中大校長行星銘板贈證嚴

由中央大學所發現編號 192208 的小行星，今年七月通過國際天文學聯合會命名爲「慈濟」小行星。今天中央大學校長蔣偉寧，特地到花蓮慈濟靜思精舍，將「慈濟」小行星在太陽系軌道的（銘板），獻給證嚴法師。而這也是台灣第一顆以宗教團體命名的小行星。

「慈濟（Tzu Chi）」這個小行星，是 2007 年 5 月 11 號由前中大天文所觀測助理（施佳佑）與大陸廣州中山大學（葉泉志）在（鹿林天文台）所發現。他們爲彰顯慈濟對 世人的貢獻，中央大學將這顆行星

命名爲慈濟，代表台灣精神的「慈濟」躍向天際，希望將讓這份無私奉獻的精神恆久傳遞，在地球與宇宙同時發光發熱。而這個命 名已經在今年 7 月 26 號，經國際天文學聯合會通過正式命名。
 鹿林天文台台長（林宏欽）表示，慈濟小行星繞太陽一圈約 5.62 年，與地球最近的距離約 3 億公里。（圖片：慈濟基金會提供）

原文轉載自【2010-10-01/中廣新聞網】

中大發現小行星　以慈濟爲名

　　由中央大學天文所鹿林天文台發現的編號 192208 小行星，7 月 26 日由國際天文學聯合會通過命名爲「Tzu Chi（慈濟）」，這也是台灣人所發現的小行星中，第一顆以宗教團體命名者。昨天上午，中央大學特地到花蓮靜思精舍，將「慈濟」小行星在太陽系軌道的銘板 獻給證嚴法師。
 中央大學校長蔣偉寧說，慈濟讓愛沒有國界之分，因此將小行星命名爲「慈濟」，代表台灣精神躍上天際，在宇宙間發光發熱。（圖：慈濟基金會提供／文：記者蔡百靈）

原文轉載自【2010-10-02/自由時報/A18 版/生活新聞】

「慈濟」小行星　宇宙爭光

【記者熊迺群／花蓮報導】

 三年前中央大學觀測發現編號 192208 小行星，在感念慈濟對世人的貢獻下，特地以「慈濟」命名，經國際天文學聯合會通過，成爲台灣第一顆以宗教名義命名的小行星。中大校長蔣偉寧昨天上午，將小行星在太陽系軌道的銘板，獻給證嚴法師。
 「慈濟（Tzu Chi）」小行星，於 2007 年 5 月 11 日由前中大天文所觀測助理施佳佑與大陸廣州中山大學葉泉志在鹿林天文台發現，它是太陽系中的移動天體，位於火星與木星之間的小行星帶，繞太陽一圈約 5.62 年，與地球最近的距離約 3 億公里。
 中央大學覺得這分榮耀，象徵台灣精神的「慈濟」，爲讓無私奉獻的精神恆久傳遞，特地將小行星命名爲「慈濟」，並於 7 月 26 日經國際天文學聯合會通過正式命名。
 昨天上午，中大校長蔣偉寧、副校長暨天文所教授葉永烜、鹿林天文台長林宏欽等人到慈濟靜思精舍拜會證嚴法師，獻上刻有慈濟小行星在太陽系軌道的銘板。

原文轉載自【2010-10-02/聯合報/B1 版/宜花．運動】

慈濟小行星…紅到全宇宙

【洪祥和／花蓮報導】

　　中央大學在太陽系發現一顆新小行星，日前向國際天文學聯合會申請通過命名爲「慈濟」星，要讓外星人也知道慈濟的好。中央大學校長蔣偉寧昨天上午帶「慈濟」小行星在太陽系軌道的銘板，到花蓮慈濟靜思精舍，獻給證嚴法師，希望愛的光輝像星星般，永遠普照世人。
　　中大天文所觀測助理施佳佑與大陸廣州中山大學葉泉志在九十六年於鹿林天文台發現編號 192208 小行星，去年經過國際永久編號認證，今年經國際天文學聯合會通過，正式命名爲「慈濟」。
　　慈濟星位於火星與木星之間的小行星帶，繞太陽一圈約五．六二年，與地球最近的距離約三億公里。
　　一日上午，中大校長蔣偉寧、副校長葉永烜、鹿林天文台長林宏欽一行帶著刻有慈濟小行星在太陽系軌道的銘板到慈濟靜思精舍，獻給證嚴法師。
　　蔣偉寧表示，慈濟大愛沒有國界之分，慈濟小行星，讓慈濟在宇宙發光發熱。未來中大能與慈濟緊密合作，透過科學，提供災前預防、災後救援等資訊，科學與人文結合，發揮更大的力量，幫助更多人。
　　證嚴法師表示，佛陀是宇宙大覺者，在兩千多年前就有宇宙觀，期待每一位慈濟人需要盡心力，上知天文下知地理，天地之間沒有無關的事情，知天文才知怎麼爲大地盡心力。

原文轉載自【2010-10-02 中國時報/A8 版/生活新聞】 相關連結 /

2098 撞地球？　泛星計劃找到首顆潛在危險小行星

生活中心／台北報導

台灣參與的泛星計畫（Pan-STARRS, PS1）發現了第一顆對地球具有潛在威脅的小行星「2010 ST3」，開啓了清點危險天體的重要一步。科學家認爲，這顆小行星有很微小的機會在 2098 年撞擊到地球。

位於美國夏威夷的泛星望遠鏡找到了一顆軌道與地球接近的小行星，它將在 10 月中通過距離地球 640 萬公里。這個小行星直徑只有約 50 公尺，是在 9 月 16 日 所拍攝的影像發現，當時它距離地球約 3200 萬公里。這是泛星計劃所發現的第一顆潛在危險小行星(potentially hazardous object, PHO)，現在命名爲 2010 ST3。

「雖然這顆小行星不會立刻撞上地球，但是它的發現代表泛星計劃是目前搜尋潛 在危險小行星計劃當中，最爲靈敏的計劃。」負責小星行資料的夏威夷大學的泛星計劃科學家傑地基博士(Dr Robert Jedicke)說。他強調「我們發現這個天體的時候，它對於其他類似計劃來說太遠了，都還無法偵測到它。」

大部分體積比較大的潛在危險小行星都已經被編表，但是科學家相信仍有爲數眾多小於一、兩公里的小行星還沒有被發現。它們撞擊地球會造成區域性毀滅。像這樣的撞擊頻率大概幾千年就有一次。

像 2010 ST3 這樣的小行星通常在進入地球大氣層時會粉碎，但是爆炸震波仍然可以摧毀幾百平方公里的區域。「2010 ST3 將有很微小的機會在 2098 年撞擊到地球，所以非常需要監測」傑地基博士這麼說。

小行星中心主任史巴博士(Timothy Spahr) 說，「對於泛星計劃的這個發現，我感到高興。它證明擁有十億畫素跟精密移動天體偵測電腦系統的泛星計劃足以勝任其他巡天計劃所不能完成的任務。」位於美國 麻州劍橋的小行星中心，由國際天文聯合會建立於 1917 年，主要收集跟發佈小行星跟彗星的天體測量位置、確認它們的發現，以及給於臨時編號。

泛星計劃預期會發現並精確測量上萬顆小行星的軌道。對於未來 50 年內有機會接近地球的小行星都會標記「潛在危險」，而且謹慎地監測它們的軌道。美國太空總署相信如果有幾年的預警時間，能夠預知某小行星將撞擊地球，便可以發射太空船使其偏轉軌道，維護地球安全。

泛星計劃還有更廣大目標。泛星計劃目前只有一座望遠鏡，未來將完成四座，執行泛星 4 計劃，屆時將發現超過百萬顆小行星，同時研究其他更遠的天體，像是變星、超新星、以及橫跨半個宇宙的星系爆發等。

台灣聯大系統副校長、中央大學天文所葉永烜教授，同時也是台灣泛星計畫共同主持人說：「泛星計畫是革命性的天文觀測儀器，靈敏度與效率都很高，能夠快速搜巡天空。指認出可能威脅地球的天體乃是泛星計畫的首要任務，這次的發現只是開始，未來必定還有更多。」

「台灣團隊由天文與資訊工程專家合作，得以在這個極受國際學界矚目的計畫中做出貢獻。」台灣泛星計畫另位共同主持人、中央大學天文所陳文屏教授說。「對於 相同天區，泛星計畫每個月觀察數次，比較前後影像的差別，這樣一直循環，有如幫宇宙拍動畫，指認出發生位置或是亮度變化的天體。」

中央大學天文所博士生陳英同說，「我們不僅參與科學課題的探討，包括太陽系中的小型天體、銀河系當中的變星、星團，以及大尺度星系碰撞等。我們同時也協助整個系統的資料處理與分析，和其他國際團隊既合作又競爭。」

由泛星計劃望遠鏡所拍攝 2010 ST3（綠圈）在 9 月 16 日晚上的兩張影像，可以看到它與背景恆星及星系移動方向相反。經過軌道計算發現 2010 ST3 的軌道與地球軌道接近，屬於具有潛在威脅的小行星。(文／引用自臺北天文館之網路天文館網站)

原文轉載自【2010-09-30 /NOWnews 今日新聞網/生活新聞 】 相關連結 /

感念八八風災救援 小行星命名”慈濟”

陳彥珊 楊惟淳 桃園報導

鹿林巡天計劃團隊，命名的十一顆小行星中，其中有一顆就名爲"慈濟"，這顆小行星是在 2007 年的 5 月 11 日發現，今年天文團隊要進行命名時，因爲有感於 慈濟，在去年八八風災時，全力投入救災，對台灣有所貢獻，特別以此命名，表達感恩，而這也是台灣第一顆以宗教團體命名的小行星。

軌道圖上繞著太陽運轉的這顆小行星，就是慈濟，位置在火星與木星之間的小行星帶上，慈濟小行星，今年七月二十六日，經過國際天文學聯合會通過命名爲慈濟，也是台灣第一顆以宗教團體命名的小行星。

中大天文所所長 周翊：有些的團體，對於我們台灣的貢獻也非常大，像慈濟像雲門舞集，所以我們後來就開始尋找說，有哪一些的團體，能夠說對台灣有貢獻，能夠代表台灣精神 。

八八風災重創南台灣，慈濟人全體總動員投入救災，無私奉獻只盼家園重建。中央大學天文團隊，感動慈濟的付出，以慈濟小行星表達感恩。而爲了向災情最爲慘重的小林村表達哀悼之意，在同一天，今年的七月二十六日，也將另一個小行星，命名爲小林。

中大天文所教授 葉永烜：這些罹難的村民不幸罹難往生的村民，希望他們反而是永久的陪著我們，在天空上我們就能看到它。
以星象圖來說，慈濟小行星目前位於雙子座接近巨蟹座的位置，慈濟小行星　永恆運轉，就像慈濟堅持救苦難，無所求的精神。

原文轉載自【2010-09-30/大愛電視 DaAi TV】

危機環伺　2098 行星可能撞地球

〔鳳凰網記者陳庭笙台北報導〕

國際「泛星計畫」(Pan-STARRS)發現，一顆被命名爲「2010 ST3」的小行星，距離地球約三千兩百萬公里，在 2098 年有很微小的機率撞擊地球。
由美，台、英、德等國科學家共同參與的「泛星計畫」在 5 月中啓動，台灣團隊來自中央、台大、成功、清華 4 所大學和中央研究院，共約 30 人，由國科會資助營運。
泛星計畫的太空望遠鏡，由美國空軍建造，是目前探測太空星體，畫素最高的望遠鏡，現由夏威夷大學管理。葉永烜指出，計畫主要監測上萬顆直徑在一公里以下，未來五十年內有機會對地球造成區域性毀滅撞擊的小行星。
中央大學天文研究所葉永烜教授昨日表示，「2010 ST3」直徑約 50 公尺，假使進入地球大氣層，會燒光、粉碎，但爆炸震波仍可摧毀幾百平方公里區域。以直徑五十公尺的小行星而言，預估將在地表造成三百公 尺大坑洞。夏威夷大學「泛星計畫」科學家傑地基昨日發布訊息表示，「非常需要監測」。
葉永烜指出，依現有資料研判，這顆小行星撞擊地球機率微小，但「無法精準預估未來結果。」葉永烜說，如果有足夠的時間預知某小行星將撞擊地球，便可發射火箭使其偏轉軌道或改變速度，以保護地球。

原文轉載自【2010-09-28/鳳凰網鳳凰報導】

台灣團隊發現　2098 年彗星恐會撞地球

生活中心／綜合報導

電影《彗星撞地球》劇情將在生活中真實上演嗎？中央大學天文研究教授陳文屏表示，最近發現一顆直徑約 50 公尺、名爲 2010ST3 的小行星，目前正在地球附近，而且在 2098 年恐怕會撞擊地球。
由中央、清華、台大、成大以及中研院等團隊跨國參與的泛星計畫(Pan-STARRS)，發現第一顆對地球具潛在威脅的小行星，它的軌道距離地球只有 3200 萬公里。預計在今年 10 月時，會距離地球 640 萬公里，約地球與月亮的 17 倍距離。
陳文屏引述同爲泛星計畫成員的的夏威夷大學博士傑地基（Dr.Robert Jedicke）表示，2010ST3 將有很微小的機會，在 2098 年撞擊到地球，所以非常需要監測。陳文屏也說，這項發現已爲地球清除危險天體的任務展 開一大步，對於台灣的天文研究競爭力也有很大的幫助。
根據泛星計畫研究團隊分析，像 2010ST3 這類的小行星，雖然直徑不到 100 公尺，就算能進入地球的大氣層，也會在空中爆炸燃燒殆盡，但是爆炸震波仍可以摧上百平方公里的區域。雖然目前體積比較大的危險小行星都已被編表，但還有多 數直徑小於 1、2 公里的小行星沒被發現，它們撞擊地球的頻率，大概幾千前就有一次。

原文轉載自【2010-09-28/NOWnews 今日新聞網　/頭條新聞　】

彗星撞地球　二〇九八恐成真

（中央社記者許秩維台北二十七日電）

由中央大學天文研究所等單位參與的國際泛星計畫，發現一顆直徑約五〇公尺、名爲 2010ST3 的小行星就在地球附近，它的軌道有可能在二〇九八年撞擊地球。
中央大學天文研究所教授陳文屏今天表示，這是泛星計畫發現的第 1 顆對地球具潛在威脅的小行星，也爲地球清除危險天體的任務邁進一大步，台灣團隊在這個國際計畫中做出貢獻。
據中央大學提供的資料，泛星望遠鏡在十六日拍攝的影像中，發現 1 顆軌道與地球接近的小行星，雖

然直徑只有五〇公尺，但發現時距地球僅約三千二百萬公里。

陳文屏引述同爲泛星計畫的夏威夷大學博士傑地基（Dr. Robert Jedicke）表示，2010ST3 將有很微小的機會，在在二〇九八年撞擊到地球，所以非常需要監測。但科學家相信，仍有爲數眾多直徑小於一、二公里的 小行星，仍沒被發現，它們撞擊地球的頻率，大概幾千前就有一次

「泛星計畫」是在美國夏威夷架設泛星望遠鏡及數位相機，對天空掃描觀測的巡天任務，所拍影像可用來搜尋對地球有潛在威脅的小行星。參與泛星的團隊來自許多國家，台灣的中央大學、清大、台大、成大和中研院的科學家，都是團隊之一。

原文轉載自【2010-09-28/青年日報/6 版/新視界】

台灣研究：2098 年彗星恐會撞地球

【大紀元 09 月 29 日訊】

由台灣中央、清華、台大、成大以及中研院等團隊跨國參與的泛星計劃(Pan-STARRS)發現，一顆直徑約 50 公尺、名爲 2010ST3 的小行星，目前正在地球附近，而且在 2098 年恐怕會撞擊地球。

發現時這顆小行星的軌道距離地球只有 3200 萬公里。預計在今年 10 月，它距離地球僅 640 萬公里，約爲地球與月亮距離的 17 倍。

中央大學天文研究教授陳文屏表示，2010ST3 將有很微小的機會在 2098 年撞擊到地球。根據泛星計劃研究團隊的分析，2010ST3 這類小行星雖然直徑不到 100 公尺，就算能進入地球的大氣層，也會在空中爆炸燃燒殆盡，但是爆炸震波仍可以摧毀上百平方公里的區域。

陳教授表示，這項發現爲地球清除危險天體的任務展開一大步，對於台灣的天文研究競爭力也有很大的幫助。

泛星計劃（Panoramic Survey Telescope & RapidResponse System，簡稱 Pan-STARRS）是在美國夏威夷架設泛星望遠鏡及數位相機，對天空掃瞄觀測的巡天任務，所拍影像可用來搜尋對地球有潛在威脅的小行星。參與泛星的團隊來自許多國家，台灣的中央大學、清大、台大、成大和中研院的科學家，都是團隊之一。

原文轉載自【2010-09-29/大紀元時報首頁 > 新聞 > 科技新聞 > 正文】

2098 年　慧星撞地球？

中央社／台北二十七日電

由中央大學天文研究所等單位參與的國際泛星計畫，發現一顆直徑約五十公尺、名爲二〇一〇 ST3 的小行星就在地球附近，它的軌道有可能在二〇九八年撞擊地球。

中央大學天文研究所教授陳文屏今天表示，這是泛星計畫發現的第雨一顆對地球具潛在威脅的小行星，也爲地球清除危險天體的任務邁進一大步，台灣團隊在這個國際計畫中做出貢獻。

據中央大學提供的資料，泛星望遠鏡在十六日拍攝的影像中，發現一顆軌道與地球接近的小行星，雖然直徑只有五十公尺，但發現時距地球僅約三千二百萬公里。

陳文屏引述同爲泛星計畫的夏威夷大學博士傑地基表示，二〇一〇 ST3 將有很微小的機會，在二〇九八年撞擊到地球，所以非常需要監測。

據泛星計畫研究團隊分析，像二〇一〇 ST3 這樣的小行星通常在進入地球大氣層時會粉碎，但是爆炸震波仍可以摧毀幾百平方公里的區域。雖然大部分體積比較大的潛在危險小行星都已被編表，但科學家相信，仍有爲數眾多直徑小於一、二公里的小行星，仍沒被發現，它們撞擊地球的頻率，大概幾千前就有一次

陳文屏表示，目前美國正在建造第二台望遠鏡，未來可能會發展到四座。台灣會根據目前泛星執行的狀況和提供的學術價值來評估，作爲是否參加之後泛星計畫的依據。

泛星計畫（簡稱 Pan-STARRS）是在美國夏威夷架設泛星望遠鏡及數位相機，對天空掃描觀測的巡天任務，所拍影像可用來搜尋對地球有潛在威脅的小行星。參與泛星的團隊來自許多國家，台灣的中央大學、清大、台大、成大和中研院的科學家，都是團隊之一。

文轉載自【2010-09-28/中華日報/A3 版/焦點】

小行星 2098 年撞地球？科學家：具潛在威脅

【記者耿豫仙／台北報導】

中央大學天文研究所 27 日公布，該所參與的泛星計畫（Pan-STARRS, PS1）發現了第一顆對地球具有潛在威脅的小行星，夏威夷大學的泛星計畫科學家傑地基博士（Dr Robert Jedicke）說，「這顆行星有極微小的機會會在 2098 年撞擊到地球，所以非常需要監測」。

小行星被命名為 2010 ST3，雖然不會立刻撞上地球，但它的運行軌道也隨時受到外在大型的行星引力的牽引而變動，參與泛星計畫的中央大學天文研究所教授陳文屏表示，有如電影「慧星撞地球」的劇情，科學家會隨時監測，到確定行星運行方向直衝地球的前兩年，就會採取發射太空船撞擊等動作，使其偏離軌道。

傑地基博士說，像 2010 ST3 這樣的小行星通常在進入地球大氣層時會粉碎，但是爆炸震波仍然可以摧毀幾百平方公里的區域。大部分體積比較大的潛在危險小行星都已經被編表，但是科學家相信仍有為數眾多的小行星還沒有被發現，而它們撞擊地球會造成區域性毀滅。

泛星計畫對於未來 50 年內有機會接近地球的小行星都會標記「潛在危險」，而且會謹慎地監測它們的軌道。

原文轉載自【2010-09-28/大紀元時報/A2 版/國內要聞】

Taiwan scientists contribute to asteroid discovery 小行星撞地球威脅 台灣參與發現

Thu, Sep 30, 2010 - Page 15

A group of Taiwanese researchers working on a project in Hawaii have contributed to the discovery of an asteroid that could be potentially hazardous to Earth. This discovery is an important step in the cataloguing of hazardous celestial objects.

The Pan-STARRS (Panoramic Survey Telescope & Rapid Response System) at the University of Hawaii has named the asteroid 2010ST3. It’s only about 50m in diameter, and it travels at 20kps. When 2010ST3 was first spotted on Sept. 16, it was still around 32 million km away from Earth. More than 20 Taiwanese researchers are working on the project.

Professor Chen Wen-ping from National Central University’s Graduate Institute of Astronomy is the principal investigator for Pan-STARRS in Taiwan. He told the Taipei Times that although 2010ST3 will be 6.4 million km from Earth next month, many estimates predict that it will brush past our planet in 2098 at only 500,000km, which is considered close for celestial bodies.

Dr. Robert Jedicke, a Pan-STARRS scientist, said that although this particular object won’t hit Earth in the immediate future, its discovery shows that Pan-STARRS is now the most sensitive system dedicated to discovering potentially dangerous asteroids.

Asteroids normally disintegrate when they enter Earth’s atmosphere, but the blast waves they produce are capable of destroying areas of hundreds of square kilometers, and an asteroid of this size could make a hole about 300m wide.

Professor Chen said, “There’s a theory which says that an asteroid collision caused the extinction of the dinosaurs. However, we have many ways of preventing human civilization from being wiped away.”

According to Professor Chen, mankind could either send spaceships to intercept a potentially hazardous asteroid and push it away from its original orbit, or launch a rocket to propel it away. A powerful laser beam would work to destroy a comet because once it had been blasted by the beam, the particles would evaporate in space.

Most larger potentially hazardous asteroids have already been catalogued, but scientists believe that there are still many under one or two kilometers in diameter yet to be discovered. If such an object collided with Earth, it would cause serious regional destruction. Such collisions happen once every few thousand years.

(LIBERTY TIMES, TRANSLATION AND ADDITIONAL REPORTING BY TAIJING WU)

一群台灣研究員參與美國夏威夷的計畫，本月發現一顆對地球有潛在威脅的小行星，距離地球最近的時候是二零九八年，這項發現為清點危險天體的重要一步。

在美國夏威夷大學的泛星計畫將這顆小型星命名為 2010ST3，直徑只有約五十公尺，在太空的行進速度為每秒二十公里。當泛星計畫於九月十六日發現 2010ST3 時，它距離地球約三千兩百萬公里。這項計畫中有二十多位台灣研究員參與。

泛星計畫在台灣的主持人中央大學天文所陳文屏教授表示，雖然行星下個月將距離地球約六百四十萬公里，但是各種估算顯示，2010ST3 於二零九八年將距離地球約五十萬公里，這種距離對於天體運行相當近，幾乎是擦身而過。
該計畫科學家傑地基博士傳回的資料顯示，2010ST3 不會撞擊地球，但這項發現顯示泛星計畫，是目前搜尋潛在危險小行星計劃當中，居於最尖端的地位。
通常小行星在進入地球大氣層時會粉碎，但是爆炸震波仍然可摧毀幾百平方公里的區域。以直徑五十公尺的小行星而言，預估將在地表造成三百公尺大坑洞。
陳文屏教授說，「有一派理論表示，當時恐龍遭滅絕，起因可能就是地球遭行星撞擊。為了預防人類文明遭摧毀，我們有數種方式。」
根據陳教授，人們可用太空船推行星離開原本的軌道，讓它偏離與地球相撞的軌道，也可以發射火箭，讓火箭成為推動行星的引擎，將行星推開，甚至遇上彗星的話，也可以用強力的雷射光束照射，使彗星本體蒸發。
大部分體積較大的潛在危險小行星都已經被編表，但是科學家相信仍有為數眾多小於一、兩公里的小行星還沒有被發現，它們撞擊地球會造成區域性毀滅，撞擊頻率大概幾千年一次。

（自由時報記者湯佳玲，台北時報吳岱璟）

Published on Taipei Times :
http://www.taipeitimes.com/News/lang/archives/2010/09/30/2003484142

原文轉載自【2010-09-30/Taipei Times/15 版/BILINGUAL TIMES 雙語新聞】

2098年　將上演行星撞地球？

電影《彗星撞地球》有可能真的在現實發生嗎？由中央、清華、台大、成大以及中研院等團隊跨國參與的泛星計畫(Pan-STARRS)，日前發現一個直徑約 50 公尺的小行星(2010ST3)，對台灣可能造成威脅。目前該行星軌道距離地球 3200 萬公里，預計今年 10 月就會縮短距離為 640 萬公里，有微弱的 機會在 2098 年撞擊到地球。
研究團隊表示，2010ST3 直徑小，就算進入大氣層也會在空中爆炸燃燒，但爆炸震波可破壞上百平方公里的區域，目前仍在監測當中。

原文轉載自【2010-09-28/ 壹蘋果網絡】 相關連結

彗星撞地球　2098 恐上演

（中央社記者許秩維台北 27 日電）

由中央大學天文研究所等單位參與的國際泛星計畫，發現 1 顆直徑約 50 公尺、名為 2010ST3 的小行星就在地球附近，它的軌道有可能在 2098 年撞擊地球。
中央大學天文研究所教授陳文屏今天表示，這是泛星計畫發現的第 1 顆對地球具潛在威脅的小行星，也為地球清除危險天體的任務邁進一大步，台灣團隊在這個國際計畫中做出貢獻。
據中央大學提供的資料，泛星望遠鏡在 16 日拍攝的影像中，發現 1 顆軌道與地球接近的小行星，雖然直徑只有 50 公尺，但發現時距地球僅約 3200 萬公里。
陳文屏引述同為泛星計畫的夏威夷大學博士傑地基（Dr.Robert Jedicke）表示，2010ST3 將有很微小的機會，在 2098 年撞擊到地球，所以非常需要監測。
據泛星計畫研究團隊分析，像 2010ST3 這樣的小行星通常在進入地球大氣層時會粉碎，但是爆炸震波仍可以摧毀幾百平方公里的區域。雖然大部分體積比較大 的潛在危險小行星都已被編表，但科學家相信，仍有為數眾多直徑小於 1、2 公里的小行星，仍沒被發現，它們撞擊地球的頻率，大概幾千前就有一次
陳文屏表示，目前美國正在建造第 2 台望遠鏡，未來可能會發展到 4 座。台灣會根據目前泛星執行的狀況和提供的學術價值來評估，作為是否參加之後泛星計畫的依據。
泛星計畫（Panoramic Survey Telescope & RapidResponse System，簡稱 Pan-STARRS）是在美國夏威夷架設泛星望遠鏡及數位相機，對天空掃描觀測的巡天任務，所拍影像可用來搜尋對地球有潛在威脅的小行星。參與泛星的團隊來自許多國家，台灣的中央大學、清大、台大、成大和中研院的科學家，都是團

隊之一。

原文轉載自【2010-09-27/中央社】

2010 ST3 小行星飆速接近　彗星撞地球來真的? 泛星拉警報

【李宗祐／台北報導】

電影《彗星撞地球》情節可能真實發生！距離地球三千兩百萬公里的外太空，有顆直徑五十公尺的小行星，正以超過三萬公里的時速朝地球飆速接近。如果進入地球大氣層沒有爆炸粉碎，就會形成隕石直接撞擊地表，威力如同核子彈爆炸，若撞擊人口密集城市，會造成嚴重災難。

由美國主導，台灣、英、德等國科學家共同參與的「泛星計畫」昨日發布一項警訊，跨國科學團隊日前觀測發現有顆對地球具潛在威脅的危險小行星，有「很微小的機會」在二〇九八年撞擊地球。

中央大學天文研究所教授兼台灣聯合大學系統副校長葉永烜說，大部分體積較大（直徑大於一公里）的潛在危險小行星都已被發現命名，「泛星計畫」主要任務是找出為數眾多、直徑在一公里以下，可能對地球造成區域性毀滅撞擊的小行星，及時採取防衛措施。

這顆命名為「二〇一〇　ＳＴ３」的小行星是「泛星計畫」今年六月啓動巡天觀測任務後，發現的第一顆對地球具潛在威脅的危險小行星。它的剖面積接近十九座籃球場，十月中旬將從距離地球六四〇萬公里處（約地球與月球距離的十七倍）通過，不排除可能在二〇九八年撞擊地球。

葉永烜指出，依現有資料研判，這顆小行星撞擊地球的機率很微小，沒有立即的危險，但「我們現在沒把握可以精準預測未來到底會怎麼樣？」

夏威夷大學「泛星計畫」科學家傑地基昨日也跨國同步發布訊息，以「非常需要監測」形容這顆危險小行星可能的威脅。

原文轉載自【2010-09-28/中國時報/A5 版/生活新聞】

2098 小行星撞地球…擦邊不會 K 中啦！

【記者蔡永彬／台北報導】

美國夏威夷大學科學家傑狄克（Robert Jedicke）認為，一顆被命名為「2010 ST3」的小行星，將有「很微小的機會」在 2098 年撞擊地球。然而中央大學天文研究所教授陳文屏昨天表示，它屆時只是離地球「比較近」，不會撞上來。

傑狄克和陳文屏都參加一項跨國研究計畫「泛星」（Pan-STARRS），傑狄克負責小行星資料、陳文屏則是台灣參與泛星計畫的主持人。「2010 ST3」是該計畫最近發現第一顆對地球具有「潛在威脅」的小行星。

泛星計畫在 5 月中啓動，台灣參與人員來自中央、台灣、成功、清華 4 所大學和中央研究院，共約 30 人，由國科會資助參與營運。台灣團隊特別有興趣的課題是「太陽系中是否存在會動的天體」，並將這些天體軌道「列管」，估算這些「不速之客」是否會「K 中」地球。

陳文屏表示，地球和「2010 ST3」繞太陽轉的軌道、速度都不同，近期內兩者距離將在 10 月中達到最近，約 640 萬公里。他比喻，如果地球是一顆鹽粒大小，則地球到月球的距離大約是 1 公分，10 月中我們和「2010 ST3」的距離約是手掌比「6」時，姆指到小指長度。

事實上，大部分體積比較大、有潛在危險的小行 星都已被編表，但科學家相信還有很多小行星沒被發現。「2010 ST3」直徑約 50 公尺，假使進入地球大氣層，會燒光、粉碎，但爆炸震波仍可摧毀幾百平方公里區域。陳文屏說，這就像挨了一記掌風，「沒有打到卻內傷」，傑狄克認為它「非常需要監測」。

小行星靠近地球時會怎麼樣？該怎麼辦？陳文屏說「電影演得還滿對的」，兩者的引力會讓地球引發大潮，大氣也會被擾亂。他指出，如果行星很小，一般用飛彈或火箭把它的軌道撞歪；如果行星太大，可將火箭發射上去，變成行星的引擎，帶它離我們而去。

原文轉載自【2010-09-28/聯合報/A14 版/新鮮世】

2098 年小行星撞地球　我國參與發現

〔記者湯佳玲／台北報導〕

台灣中央大學等團隊參與的國際「泛星計畫」，發現了第一顆對地球具有潛在威脅的小行星，可能在二

〇九八年撞擊到地球，開啓了清點危險天體的重要一步。

距離地球三千兩百萬公里

位於美國夏威夷的泛星望遠鏡，找到了一顆軌道與地球接近的小行星，直徑只有約五十公尺，九月十六日時拍攝到的影像發現，距離地球約三千兩百萬公里，預計十月中將距離地球六百四十萬公里，此爲泛星計畫所發現的第一顆潛在危險小行星，命名爲 2010 ST3。

大部分體積較大的潛在危險小行星都已經被編表，但是科學家相信仍有爲數眾多小於一、兩公里的小行星還沒有被發現，它們撞擊地球會造成區域性毀滅，撞擊頻率大概幾千年一次。

預估造成三百公尺大坑洞

中央大學天文研究所葉永烜教授昨日表示，根據夏威夷大學的泛星計畫科學家傑地基博士傳回的資料顯示，2010 ST3 將有機會在二〇九八年撞擊到地球，所以非常需要監測。葉永烜說，小行星受到重力和太陽光照射的影響，以每秒二十公里的速度前進，通常在進入地球大氣 層時會粉碎，但是爆炸震波仍然可以摧毀幾百平方公里的區域，以直徑五十公尺的小行星而言，預估將在地表造成三百公尺大坑洞。

葉永烜表示，由於小行星很小，必須要到離地球很近的時候才看得到，泛星計畫就是精確計算測量上萬顆小行星的軌道，對於未來五十年內有機會接近地球的小行星都會標記 「潛在危險」，進而對小行星進行監測。葉永烜說，如果有足夠的預警時間預知某小行星將撞擊地球，便可以發射太空船使其偏轉軌道或改變速度，維護地球安全。

原文轉載自【2010-09-28/自由時報/A3 版/焦點新聞】

展望天際　有顆行星叫「雲門」!

【台灣醒報記者葉芷娟報導】

爲了表彰雲門舞集在藝術上的成就，中央大學鹿林天文台將 2007 年新發現編號 200025 的小行星，首次以台灣舞團命名，於今年初獲國際天文聯合會通過，正式命名爲「Cloud Gate」。

在最新出版的「2009 雲門舞集文教基金會年度報告」中，雲門繪製了一幅群星環繞太陽的天文圖，而其中一顆即是「200025Cloud Gate」。對已成立近 40 年的雲門來說，是無限的榮耀。

走過 2008 年排練場失火的意外，林懷民滿是感恩，甫獲德國伍爾斯堡藝術節頒贈舞動國際舞蹈大獎「終身成就獎」的他，在刊物中提及「藝術駐縣」、「藍天教 室」、「流浪者計劃」等回饋社會的活動，他認爲，能讓經歷失去家園、失去親人痛苦的學童跟著他們熱情地舞動雙手，才是最有意義的。

日前海外巡演還擁有總統夫人周美青相伴的雲門，2009 年共演出 144 個場次，平均每 2.5 天就演出一場。巡迴日本、匈牙利、荷蘭、德國、英國等九國，共計 39 場的海外演出，更曾創下宣傳海報還未付印，門票就已售罄的盛況。

今年 1 月雲門二度登上美國甘迺迪中心演出，不但票房開出紅盤，在《水月》70 分鐘的演出中，全場觀眾沉醉靜默，舞終時，更爆出如雷掌聲，全體起立歡呼 10 多分鐘，也引起《華盛頓郵報》以半版篇幅評介。

雲門在這本年度報告中，也特別以專頁介紹曾被歐美舞評盛讚爲「燈光界的繪畫大師」的張贊桃，以弔念這位一生奉獻給雲門的燈光設計師，得年 53 歲的他「一輩子只在一個地方工作」，爲雲門《流浪者之歌》、《水月》、《行草》等舞作的燈光設計。

原文轉載自【2010-08-11/台灣醒報】

「霓虹極光秀」　太陽風暴來襲

【蔡筱雯、張勵德／綜合報導】

猛烈的太陽風暴正吹向地球，天文學者本月 1 日觀測到太陽表面有個巨大的太陽黑子爆炸，還引發另場風暴，兩次爆發噴出大量的帶電粒子，估計將在昨晚至今天凌晨接近地球，學者表示部分地區民眾有機會觀賞到壯觀的極光現象。

美國「太陽動態觀測站」1 日拍攝到的「日冕物質噴發」現象，媒體形容激起的沖激波有如「太陽海嘯」，使得大量帶電粒子從 1.48 兆公里之外衝向地球，美國哈佛史密松天體物理中心天文學家戈布魯指出:「這是長期以來首次有太陽風暴朝地球方向吹來。」

影響飛航安全

美國航空總署（NASA）專家預測，帶電粒子抵達地球後將衝擊磁場，在兩極產生強烈的極光，過去

只有高緯度地區可以觀賞到極光，而這次受太陽風暴影響，美 國緬因州到密西根州之間的民眾可望看到這場大自然的「霓虹燈光秀」。極光的產生與太陽風暴有關。太陽風暴釋出的粒子接近地球時，會被推向地球磁場的南北 極，跟大氣層中的氧和氮分子碰撞，產生極光。

科學家曾在今年 6 月提出警告，預測太陽閃焰活動可能在 2013 年達到高峰，屆時猛烈的太陽 風暴可能嚴重干擾衛星、影響無線電通訊、甚至影響飛航安全或水電供應系統，造成嚴重災害，學者表示這次的太陽風暴還不算是大爆發，估計不會對衛星通訊造成 嚴重威脅，但可證明沉寂一段時間的太陽「逐漸甦醒了」。

中央大學天文研究所教授陳文屏昨說，地球有磁場保護，這些噴發出的帶電物質不會影響人體，但會影響太空中的太空站、衛星，及地面上的電力系統、通訊設備等，得事先關閉部分系統或切換到安全模式加以預防。

◎太陽風暴影響　示意圖

美學者指出，強大的太陽風暴恐致衛星通訊中斷，GPS 衛星導航失靈，無線電通訊中斷、飛航安全受影響，電力供應系統、甚至供水系統都可能癱瘓

資料來源：英國《每日郵報》

◎報你知

太陽風暴 搖晃磁層

太陽風暴是指太陽活動時所產生的激烈爆發活動，爆發時太陽表面會產生巨大的閃焰（solar flares），太陽黑子則會釋放大量帶電粒子，與地球磁場撞擊後會產生磁層搖晃，猛烈的磁層搖晃就是地磁風暴，可能會影響地球通訊、威脅人造衛星、破壞 臭氧層，極端狀況下還會造成電力中斷、羅盤指錯方向等狀況。

太陽活動的強度以太陽黑子的數目來測量，太陽黑子活動周期平均約為 11.1 年，黑子活動高峰期就是太陽風暴的活躍期，美國學者估計下次高峰期將出現在 2013 年。

原文轉載自【2010-08-04/蘋果日報/A18 版/蘋果國際】

台灣參與跨國研究「泛星計畫」日前啓動

【聯合報／記者蔡永彬／即時報導】

台灣參與的跨國研究計畫「泛星」(Pan-STARRS）日前正式啓動，望遠鏡「泛星一號」連接「全球最大數位相機」對著天空掃瞄、觀測，不僅可以搜尋對地球有潛在威脅的小行星，同時也探索宇宙中的黑暗物質、黑暗能量。

「泛星一號」位於毛依島的哈里阿喀喇火山頂，口徑 1.8 公尺，後面掛載和家用電冰箱一樣大的「14 億畫素」數位相機，成為最強大的「巡天望遠鏡」。台灣泛 星計畫主持人、中央大學天文所教授陳文屏指出，台灣團隊特別有興趣的課題是「太陽系中是否存在會動的天體」。如果發現某天體亮度、位置和昨天不同，就會下 載資料進行分析，並利用國內望遠鏡進一步觀測，估算這些「不速之客」是否會「K 中」地球。

原文轉載自【2010-06-16/即時新聞　全球觀察　聯合新聞網】

北縣客家文化園區　天文學家葉永烜開畫展

【聯合報／記者李承宇／即時報導】

台灣聯合大學系統副校長葉永烜，8 日到 6 月 13 日將在台北縣客家文化園區舉辦「江山萬里行之寶島台灣-葉永烜油畫創作個展」，展出以台灣寶島為主題的五十 幅畫作，以台灣的地理方向從北而南依序展出，讓參觀者在欣賞油畫創作個展同時，就好像與葉永烜共遊臺灣寶島，體驗寶島行。

葉永烜是一位天文與太空科學家，他的研究專長為彗星、行星大氣與行星環、太陽系與行星形成以及電漿物理等。葉永烜長期從事天文太空研究，但自幼喜愛繪畫，1987 年起開始自學油畫，內容包括歐美和台灣的風景、人物和花卉靜物等，嘗試以畫筆描繪出生活中的諸多感動。

原文轉載自【2010-05-06/訊息藝開罐　閱讀藝文　聯合新聞網】

天文學家　開油畫個展

【聯合報／記者蔡永彬／即時報導】

台灣聯合大學系統副校長、中央大學天文研究所與太空科學研究所教授葉永烜，最近增加了一個新頭銜「素人畫家」，今年 5 月 8 日至 6 月 13 日將在台北縣客家文化園區舉辦油畫創作個展，展出以臺灣寶島爲主題的 50 幅畫作。

畫作中有基隆、台北、桃園、新竹、嘉義、台南、後山風景，也有兩幅雲門舞者的舞姿，展場以台灣的地理方向從北而南依序展出，讓參觀者在欣賞油畫創作個展同時，就好像和他一起共遊寶島。

原文轉載自【2010-05/ 訊息藝開罐　閱讀藝文　聯合新聞網】

台灣聯合大學系統副校長　葉永烜寶島遊記　用畫的

【記者王長鼎／三峽報導】

國際知名太空科學家、台灣聯合大學系統副校長葉永烜應台北縣文化局之邀，昨天起至 6 月 13 日在三峽客家文化園區，舉辦「江山萬里行之台灣寶島」油畫創作個展，展出 50 幅油畫畫作，與民眾分享他的寶島遊記。

葉永烜是現任台灣聯合大學（中央、交通、清華、陽明等大學）系統副校長，也是國立中央大學天文研究所與太空科學研究所教授，論文刊載在美國 Nature 和 Science 期刊達 42 篇，爲全球華人最多者。

民國 89 年曾獲聯合國技術諮詢機構「國際宇航科學院」授予國際太空航行學院基礎科學組院士頭銜，去年更獲美國國家航空暨太空總署（NASA）頒發「特殊公共服務榮譽動章」，表彰他與美國太空總署在卡西尼探測土星的跨國合作計畫貢獻。

葉永烜從小就有繪畫天分，覺得外太空大部分是單調的黑色世界，僅有星雲和少量的星球呈現出瑰麗的色彩，在研究天文科學之餘，76 年重拾畫筆，展開油畫創作，成爲喜歡用色彩「寫」遊記的科學家。

原文轉載自【2010-05-09/聯合報/B2 版/北縣基隆綜合新聞】

太空探索／5-1 晚間的火流星　鹿林天文台秀出軌跡

生活中心／台北報導

根據多位民眾反映，於 5 月 1 日晚間 9 點多，看見西北方低空有一顆很亮的天體劃過天際，持續時間約 2 秒多，飛行速度比一般飛機還快許多，經國立中央大學鹿林天文台全天監視器錄影畫面揭露，可看出這顆「偶發流星」其中一端的軌跡。

根據中央大學天文所鹿林天文台提供的錄影畫面，圖中右下角(西北方)就是這個明亮的天體其中一端的軌跡，畫面中央偏上方則是春季大三角之一的 1 等星「牧夫 座大角星」，相較之下，顯現這是顆非常明亮的火流星。可惜沒有不同地點的觀測影像，不然就可以進行三角視差來測定流星發生的距離與高度。（想看大圖：請 進：http://www.nownews.com/2010/05/05/327-2599593.htm）

雖然近期有寶瓶座 Eta 流星雨，但寶瓶座要到凌晨 2 時左右才會升起，因此這個火流星顯然並非寶瓶座 Eta 流星雨的一份子，應是所謂的「偶發流星」。只是，這顆偶發流星究竟是太空中天然的小石塊造成的，還是某個太空垃圾造成的，就不得而知了。

中央大學天文所助理研究學者阿部新助博士(Dr. Shinsuke Abe)及鹿林天文台台長林宏欽先生正在推動所謂的「鹿林流星觀測網(Lulin Meteor System, LMS)」計畫，在鹿林天文台與桃園中壢的中大校區內，利用即時 CCD 加上廣角鏡頭進行全天流星動態監測，之後再用 UFO Capture 軟體來進行分析。

不過，5/1 晚間的事件，可能由於角度的關係，這套監測系統並未拍攝到火流星的畫面。由於所需設備非常簡單，目前已經引起許多業餘同好的響應，未來或許會 成爲一個遍及臺灣各地的流星監測網，如果您有心加入這個流星監測網，可洽阿部新助博士或林宏欽台長。(文／引用自臺北天文館網路天文館網站)

原文轉載自【2010-05-05/NOWnews【重點新聞】】

有顆星叫雲門　舞台躍上天際

【汪宜儒／台北報導】

雲門舞集不光只在國內外的舞台上舞躍，更會在天上閃耀！中央大學鹿林天文台發現編號 200025 的小行星，通過國際天文聯合會的小行星命名委員會審議，正式命名爲「雲門」（Cloud Gate），這是第一顆以華人地區藝術團隊命名的小行星。

以華人藝術團隊命名　全球第一

「雲門」由中央大學鹿林天文台觀測員林啓生與葉良志發現於二〇〇七年七月廿五日，它與太陽最近的距離約是四 • 四億公里、最遠約五億公里，大小估計是五公 里，亮度介於十九至廿等星之間，軌道位置則處於火星與木星之間。鹿林天文台台長林宏欽表示，今年的五到六月間，正是「雲門」小行星距地球最近的時候。「但 因亮度小、距離遠，一般民眾無法直接以肉眼或望遠鏡觀測，僅能透過拍攝的方式來觀察這顆小行星。」

中央大學大天文所所長周翊表示，在研究觀察的時候，「從發現、持續觀察紀錄、確認軌道，到肯定那不是已被發現的小行星或只是個人造衛星，到最後提出命名申請，通常需要數年的時間。」另外，命名也有原則限制，「不能和商業、政治等利益有關，每兩個月至多只能命名兩個。」

鹿林天文台台長林宏欽指出，已命名的小行星目前共有一萬五千多顆，其中不乏以樂團、明星爲名的案例，像是維也納愛樂管絃樂團、音樂家貝多芬、聲樂家帕華洛帝及作家馬克吐溫等，還有影藝名人包括林青霞，乃至電影導演史蒂芬史匹柏，目前都是天上運行不歇的小行星。

而鹿林天文台自一九九九年設立至今，發現過八百多顆小行星，雲門小行星是第十顆被中央大學命名的小行星，也是他們首度以藝術團隊來命名。

副校長李誠表示，「中央大學希望朝向結合理工與文化藝術的方向，而林懷民的雲門舞集是世界舞台上最能代表台灣創意與軟實力的代表。」過去，中央大學爲他們 發現的小行星命名，曾多次採用台灣的地名與人名，像是南投、嘉義、鹿林，也曾採用企業家溫世仁、鄭崇華、天文學家沈君山命名。

林懷民感謝中大肯定　盼被仰望

雲門舞集創辦人林懷民說：「從古至今，人們習慣仰望天空去寄託希望，獲取安慰，今天雲門能被命名，是給我們的肯定，也提醒了雲門要走得更廣、眼界要更遠，希望雲門更值得被大家仰望。」

林懷民肯定鹿林天文台多年來持續觀測台灣天空的努力，「那是需要怎樣鍥而不捨的守候啊！這次的事件，也提醒了我自己，我們是否已埋頭苦幹了太久，都忘了抬起頭看天空呢？」

原文轉載自【2010-04-30/中國時報/A14 版/文化新聞】

第一顆以世界一流台灣舞團命名之小行星

【大紀元 5 月 4 日訊】

(大紀元記者徐乃義台灣中壢報導)中大鹿林天文台所發現的編號 200025 小行星，最近經國際天文聯合會（IAU）之小行星命名委員會審議通過，正式命名 爲「Cloud Gate」，代表台灣的「雲門」躍向星際，同時在世界與太空發光。此乃台灣本土望遠鏡所發現，並首次以台灣舞團爲名，林懷民創辦雲門之成就，再一次獲得國 際社會之肯定。

中央大學天文所所長周翊指出，雲門小行星繞太陽一周約 5.6 年，最接近太陽時約 4.4 億公里，離太陽最遠時約 5 億公里。發現時位置在水瓶座，目前位於獅子座，大小估計約 5 公里。今年五、六月份，即可透過鹿林天文台一米望遠鏡觀看到它的身影。

中央大學副校長李誠說，「不論是雲門現代舞或是中大天文研究，都發揮了無限的創意與軟實力，在這個世界的舞台上，台灣不僅沒有缺席，更在此兩個領域上，扮演了舉足輕重的角色」。

林懷民與雲門閃耀星空

林懷民先生於 1973 年以《呂氏春秋》記載之中國最古老的舞蹈「雲門」爲名，創辦了「雲門舞集」，帶動台灣現代表演藝術的發展，這是台灣第一個職業舞團，也是所有華語社會的第一個當代舞團。

中央大學也有一群受到林懷民老師感召的學生，去年成軍的現代舞社獻上一支創作舞碼 unfinish，向林懷民老師及雲門致敬。這支舞由該校地科系學生許庭 瑄編舞，她說「人與人之間的相遇總是需要緣分和偶然的交集，儘管是千分之一抑或萬分之一。而在某個不經意的契機下，奇蹟發生了」。

2008 年 10 月，雲門舞集 2 首度在中大開設「與雲門共舞」課程，從初選 4、500 人篩選至 120 位同學，分成 12 組進行小組授課。兩周的集訓期間，雲門舞者帶給學生的不只有他們對舞蹈的熱愛，更讓學生知道如何激發自己的想像力，如何擺動肢體表達內心想法。

林懷民出生於嘉義，鹿林天文台一半地址也在嘉義縣境。林懷民創辦「雲門舞集」，帶動台灣現代表演藝術的發展；鹿林天文台也帶動台灣天文研究與天文教育的發展。

中央大學天文所所長周翊表示，該校鹿林天文台利用有限的經費，在 2006 年 3 月開始啓動的「鹿林

巡天計畫（Lulin Sky Survey, LUSS）」，有計畫性觀測小行星，總計發現約 800 多顆小行星、1 顆近地小行星及 1 顆彗星，對於小型望遠鏡的觀測而言，可以說是成效卓著。

鹿林天文台的觀測工作都是應用小型望遠鏡和台灣觀測條件的優勢。因爲小型望遠鏡的運作及時間分配，比兩米以上的大型望遠鏡更具彈性，而且台灣緯度接近赤 道，經度上則與夏威夷相隔千里，因此可以一方面集中注意力在南方天空目標，一方面對於瞬間發生的天文現象，更佔了 5-6 小時的便宜。

鹿林天文台站長林宏欽說，鹿林巡天計畫與國外經費充裕的五大巡天計畫相比，只能算是「小蝦米對大鯨魚」，但憑著永不放棄的精神，也能展現亮麗的成果。

原文轉載自【2010-05-04/大紀元時報首頁 > 新聞 > 台灣地方新聞 > 正文】

雲門上浩瀚宇宙　爲小行星之名

【 駐 國立台灣藝術大學 記者 連珮如 報導 】

在眾多星海中將有一顆名爲「雲門」的小行星誕生，這個在 2007 年被發現的行星是台灣首次以藝文團體爲行星命名，象徵台灣的「雲門」躍向星際，同時在世界各地發光發亮。

編號 200025 的小行星命名爲「雲門」(Cloud Gate)，透過中央大學鹿林天文台經過國際天文聯合會小行星命名委員會審議通過，肯定雲門創辦人林懷民的成就。鹿林天文台至今已發現近千顆小行星，曾以 玉山，還有台達電創辦人鄭崇華、前清大校長沈君山命名過小行星，希望透過小行星的命名，彰顯台灣具代表性的人事物。

中央大學副校長李誠說，談到台灣最具特色的表演團體，許多人會立刻想到雲門舞集林懷民創立「雲門」，突破中華舊有文化，走向全球，雲門 2 也和中央大學合作開課，把現代舞從台灣發揚到國際帶向宇宙。

雲門舞集創辦人林懷民表示，得知小行星將以「雲門」命名，像小學生領到獎狀一樣興奮，他認爲人類自古就以浩瀚星空爲情感寄託對象，充滿希望。對於未來也會持續努力看得更高、更遠、更寬廣，讓「雲門」成就值得爲眾人仰望。

位於獅子座，介於火星與木星之間的雲門小行星，大小約直徑 5 公里。中央大學天文所所長周翊指出，在今年五、六月，民眾可透過鹿林天文台一米望遠鏡觀看到雲門小行星。

原文轉載自【2010-04-29/1111 大學網】/news.asp?id=29091）

太空探索／雲門小行星　首顆以世界一流的台灣舞團命名

生活中心／台北報導

林懷民先生領導的雲門舞集，以當代手法闡釋亞洲文化獨特卓越，被譽爲「世界一流舞團」，透過雲門，東方與西方和諧交融，燦然生輝，爲了彰顯雲門舞集在台灣 特殊的象徵意義，中央大學將編號第 200025 號小行星命名爲「雲門(Cloud Gate)」，此提議已通過國際天文聯合會(IAU)小行星命名委員會的同意。

中央大學鹿林天文台自 2002 年開始鹿林巡天計畫(LUSS)迄今，已發現近千顆小行星，並有多顆取得正式編號，擁有命名權，近年來陸續以有意義的臺灣地區人物或地名等爲這些小行星命名。

爲了彰顯雲門舞集在臺灣特殊的象徵意義，中央大學特別將編號第 200025 號小行星命名爲「雲門(Cloud Gate)」，此提議已通過國際天文聯合會(IAU)小行星命名委員會的同意，讓代表臺灣的雲門躍向國際，讓「雲門」同時在地面與太空揚名全球！

雲門小行星由中央大學天文研究所的鹿林天文台助理林啓生先生於 2007 年 7 月 25 日觀測到，並經由中國廣東中山大學葉泉志先生分析而找出，故當時小行星的 暫時編號爲 2007 OK10，後來又確認與 2002 TK296 小行星爲同一顆，確認真的是新的小行星之後，則給予永久編號爲第 200025 號小行星。

後續觀測分析得知這顆小行星直徑約 5 公里，位在火星與木星之間的主小行星帶中，距離太陽平均爲 3.15AU，繞太陽一周約 5.59 年，軌道傾角只有 5.77 度，幾乎位在黃道上。由於亮度不高，僅約 19-20 等左右，因此僅能利用口徑較大的望遠鏡才能觀測到。

中央大學之前已命名的小行星包括：(145523)Lulin (鹿林)、(145534)Jhongda (中大)、(168126)Chengbruce (鄭崇華)、(202605)Shenchunshan (沈君山)、(145545)Wensayling (溫世仁)、(216261)Mapihsia (馬碧霞)、(185216)Gueiren (歸仁)、(175586)Tsou (鄒族)、(147918)Chiayi (嘉義)、(160493)Nantou (南投)、(185546)Yushan (玉山)和(210580)Kaohsiung (高雄)。名稱前的數字就是這顆小行

星的永久編號。(文／引用自臺北天文館網路天文館網站)

原文轉載自【2010-05-03/NOWnews【生活新聞】】

雲門化身小行星　閃耀天際

楊惠芳／臺北報導

全球第一顆以臺灣舞團命名的小行星昨天誕生，中央大學副校長李誠宣布，新發現的編號二○○○二五小行星，已經獲得國際天文聯合會審議通過，以雲門（Cloud Gate）為名，使雲門舞集不只在國際發光，也在浩瀚星空中閃耀，更是科技與人文融合的佳話。

雲門舞集創辦人林懷民表示，這是一份特別的禮物及榮耀，也是對雲門的肯定及鼓舞，鞭策雲門要更努力、更用心，值得大家仰望。

雲門小行星在今年五六月份最接近地球，透過鹿林天文臺的望遠鏡，就能觀察到它的身影。小行星發現者林啓生，邀請林懷民到時候上山觀星，說不定能夠激發靈感，創作新舞碼。

原文轉載自【2010-04-30/國語日報/2 版/文教新聞】

肯定台灣藝術力　小行星命名「雲門」

作者：羅智華

在滿天星斗中，將有一顆名為「雲門」的小行星！中央大學鹿林天文台 表示，決定以「「Cloud Gate（雲門）」命名這顆新發現的小行星，象徵台灣的「雲門」躍向星際，同時也在世界與太空發光。中大表示，這顆小行星是透過台灣本土望遠鏡所發現，且 首次以台灣舞團為名。

編號 200025 小行星，是中大的天文所職員林啓生與大陸天文研究生葉泉志在 2007 年 7 月 25 日發現，最近經國際天文聯合會（IAU）的小行星命名委員會審議通過，正式命名為「Cloud Gate」，肯定林懷民創辦雲門的成就。

中大副校長葉永烜表示，小行星發現者擁有對命名權，鹿林天文台藉著小行星的命名，表彰具有代表性的台灣人事物。葉永烜說，只要談到台灣最具特色的表演團 體，許多人會立刻想到雲門舞集，尤其是雲門舞團 2 也在 2008 年 10 月到中大開設「與雲門共舞」課程，受到學生歡迎，顯見雲門精神在中央校園中，扮演重要 的一環。

原文轉載自【2010-04-30/人間福報/13 版/遇見科學】

雲門小行星　林懷民：盼放下你我開步走

中評社台北 4 月 30 日電（記者　鄒巧韻）

得知“雲門”（Cloud Gate）成為世界上第一顆以台灣舞團命名的小行星，雲門舞集創辦人林懷民感激由衷。他說，這是給雲門的肯定與鼓勵，雲門會更努力成為大家所仰望的對象；這個與宇宙的有趣連結，帶給我們更寬廣的視野，他也期望台灣內部放下你我的分別走出去。

由台灣中央大學鹿林天文台所發現的編號 200025 小行星，經國際天文聯合會（IAU）之小行星命名委員會審議通過，正式命名為“Cloud Gate”（雲門），為全球第一顆以台灣舞團為名的小行星。中央大學昨日下午舉辦“慶祝雲門小行星”命名記者會。

中央大學副校長李誠表示，感謝雲門給中大的禮物，2008 年雲門舞集 2 首度在中大開設“與雲門共舞”課程，讓中大的理工與人文結合，教導學生追求更精緻的文化生活；雲門的成就不單是突破中華傳統文化，更走向全球、走向全宇宙。

國際知名天文專家、中央大學天文所教授葉永烜也說，成功以雲門命名小行星，對台灣來說意義重大，在世界舞台上也相當具有指標性；雲門的創辦精神，克服困難、達成夢想，相當具有教育意義。

原文轉載自【2010-04-30/中國評論新聞首頁 ->> 臺灣時政】

躍上星空　小行星以「雲門」為名

(陳映竹報導)

　雲門不只在國際發光，也在浩瀚星空閃耀。中央大學鹿林天文台今天宣布，以雲門的英文名稱「「Cloud Gate」命名新發現的小行星，這顆小行星是首次以台灣舞團為名。雲門舞集創辦人林懷民十分興奮，認為這是一份特別的榮耀，林懷民也好奇，鹿林天文台內， 只有三、四個研究員，卻能發現這麼多星星，實在讓人敬佩。
要談到台灣最具特色的表演團體，許多人會立刻想到雲門舞集，雲門 2 也和中央大學合作開設課程，受到學生歡迎。中央大學新發現編號 200025 小行星就以「雲門」為名。
雲門舞集創辦人林懷民表示，這是一份特別的禮物，讓雲門把眼光拉的更寬遠，自古以來，人類就在仰望星空獲得安慰、寄託希望，雲門將更努力，值得大家仰望、帶給大家安慰。
林懷民說，過去他從農人、工人、年輕人獲得很多創作靈感，但從還沒有想過是什麼樣鍥而不捨的精神，讓這些研究員夜復一夜探索星空？林懷民也自我解嘲，對天文，「我攏不知啦！詩歌的星星我倒是知道。」
雲門小行星在今年五、六月份，透過鹿林天文台一米望遠鏡就能觀察到身影，小行星發現者林啓生也邀請林懷民，到時候上山觀星，說不定能激發靈感，創作新舞碼。

原文轉載自【2010-04-29/中廣新聞網】

「雲門小行星」第一顆以台灣舞團命名

浩瀚星空中，有一顆小行星叫「雲門」，這是中央大學鹿林天文台發現的小行星當中，第一顆以台灣舞團命名的小行星，希望表彰雲門舞集將台灣帶上國際舞台，讓雲門不只在國際，也在星空閃耀。
　中央大學鹿林天文台在 2007 年 7 月 25 號發現的這顆小行星，直徑 5 公里，介於火星與木星之間，距離地球約 5 億公里，繞太陽一周約需要 5.6 年，最近經國 際天文學聯合會通過，正式命名為「雲門」。中央大學天文所所長周翊說，今年 5、6 月透過鹿林天文台一米望遠鏡就可以看到它的身影。
雲門舞集創辦人林懷民表示，這顆小行星以雲門命名，是極大的鼓勵及肯定，未來雲門會更努力，展現更好的表現。鹿林天文台從 91 年到現在已發現近千顆小行星， 過去曾以玉山，還有台達電創辦人鄭崇華、前清大校長沈君山命名過小行星，希望透過小行星的命名，表彰具有代表性的台灣人事物。
(2010/4/29 下午 05:58:34　徐詠絮)

原文轉載自【2010-04-29/國立教育廣播電台－【文教新聞】】

雲門躍上天際　化身小行星

（中央社記者鄭景雯台北 29 日電）

中央大學鹿林天文台經過國際天文聯合會小行星命名委員會審議通過，把編號 200025 小行星命名為「雲門」，這是台灣首次以藝文團體為行星名稱，以肯定雲門創辦人林懷民的成就。
雲門小行星於 2007 年 7 月 25 日由林啓生與葉泉志在鹿林天文台發現，位置介於火星和木星之間，目前位於獅子座，大小估計約直徑 5 公里。中央大學天文所所長周翊指出，今年 5、6 月，可透過鹿林天文台一米望遠鏡觀看到雲門小行星的身影。
林懷民表示，得知小行星以「雲門」命名，對他而言，彷彿回到小時候領獎一樣興奮。他說，他對於天文完全沒有研究，但認為自古以來人們就在仰望天空，未來也會持續努力，希望「雲門」能當 1 個值得眾人仰望的舞團。
中央大學副校長李誠說，林懷民創立「雲門」，突破中華文化傳統，把現代舞從台灣發揚到國際，如今中央大學藉由小行星命名，再將雲門從國際舞台帶向宇宙。
發現雲門小行星的林啓生，從 1978 年就投入天文觀測的研究，他的工作時間與一般人相反，經常是到了太陽下山後才開始工作，林懷民對於林啓生的觀星工作感到好奇，認為在寂靜的夜晚林啓生應該很孤單，但當眾星出現在眼前時，卻又能和這些星星交談，非常浪漫。
林懷民與林啓生也相約在 6 月到鹿林天文台觀看雲門小行星，期盼能激發「雲門」下一個創作。990429

原文轉載自【2010-04-29 /中央社即時新聞 CNA-NEWS.COM】

藝術之光　小行星命名雲門

中央社／台北二十九日電

中央大學鹿林天文台經過國際天文聯合會小行星命名委員會審議通過，把編號 200025 小行星命名爲「雲門」，這是台灣首次以藝文團體爲行星名稱，以肯定雲門創辦人林懷民的成就。

雲門小行星於二零零七年七月廿五日由林啓生與葉泉志在鹿林天文台發現，位置介於火星和木星之間，目前位於獅子座，大小估計約直徑五公里。中央大學天文所所長周翊指出，今年五、六月，可透過鹿林天文台一米望遠鏡觀看到雲門小行星的身影。

林懷民表示，得知小行星以「雲門」命名，對他而言，彷彿回到小時候領獎一樣興奮。

中央大學副校長李誠說，林懷民創立「雲門」，突破中華文化傳統，把現代舞從台灣發揚到國際，如今中央大學藉由小行星命名，再將雲門從國際舞台帶向宇宙。

林懷民與林啓生也相約在六月到鹿林天文台觀看雲門小行星，期盼能激發「雲門」下一個創作。

原文轉載自【2010-04-30/中華日報/A4 版/綜合】

小行星命名雲門　林懷民分享榮耀

【楊景婷／台北報導】

由中央大學鹿林天文台發現的編號 200025 小行星，經國際天文聯合會認可，正式命名爲「Cloud Gate（雲門）」，「雲門舞集」創辦人林懷民昨開心說：「希望雲門將來的成就，也能值得人們仰望。」

3 年前被發現

「雲門」小行星在 2007 年 7 月 25 日被發現，也是全球首次以台灣藝文團體當名稱的天體，林懷民昨說：「現在的人埋頭苦幹太多，不如抬頭看星星吧，仰望星空可以尋求慰藉。」他也表示希望找一天上天文台，親眼看看這顆「雲門」星。

據悉，發現者原打算以「林懷民」爲名，在他堅持下才改爲「雲門」。

小行星是目前唯一可以由發現者命名，並得到世界公認的天體，至少 4 次在回歸中心被觀測到，並測出運行軌道後，才能獲認可。所有小行星命名，須經國際小行星中心和小行星命名委員會審議通過，才能公諸於世。

原文轉載自【2010-04-30/蘋果日報/C8 版/娛樂名人】 相關連結 /

雲門小行星　表彰林懷民

【記者邱瓊平／台北報導】

浩瀚星海中，將有一顆「雲門」小行星！中央大學鹿林天文台今天宣布，決定以「「Cloud Gate(雲門)」命名新發現的小行星，象徵台灣的「雲門」躍向星際，同時也在世界與太空發光。中大表示，這顆小行星是透過台灣本土望遠鏡所發現，且首次以台灣舞團爲名。

編號 200025 小行星，是中大的天文所職員林啓生與大陸天文研究生葉泉志在 2007 年 7 月 25 日發現，最近經國際天文聯合會（IAU）的小行星命名委員會審議通過，正式命名爲「Cloud Gate」，肯定林懷民創辦雲門的成就。

中大副校長葉永烜表示，小行星發現者擁有對命名權，鹿林天文台藉著小行星的命名，表彰具有代表性的台灣人事物。例如中大曾以台灣第一高峰玉山、台達電創辦人鄭崇華，與前清大校長沈君山命名小行星。

葉永烜說，只要談到台灣最具特色的表演團體，許多人會立刻想到雲門舞集，尤其是雲門舞團 2 也在 2008 年 10 月到中大開設「與雲門共舞」課程，受到學生歡迎，顯見雲門精神在中央校園中，扮演重要的一環。

中大天文所所長周翊指出，鹿林天文台利用有限的經費，從 2006 年 3 月開始啓動的「鹿林巡天計畫」，有計畫性觀測小行星，總計發現約 800 多顆小行星，其中有 30 顆已取得永久命名，成爲亞洲發現小行星最活躍的地方。

原文轉載自【2010-04-29/聯合晚報/A10 版/生活】

台灣之光　雲門小行星舞向天際

中央大學鹿林天文台 4 年前發現編號 200025 小行星，為彰顯雲門在台灣的特殊意義，昨宣佈命名為「Cloud Gate」，讓浩瀚星海中，多了一顆名為「雲門」的小行星。

雲門創辦人林懷民感動地說:「好像小學時第一次領獎的興奮，非常特別，把台灣帶到更大的世界去！」雲門小行星是由鹿林天文台的林啓生與葉泉志觀測發現，亮度約為 20 星等、距離地球約有 3 億公里遠。雖然肉眼完全無法觀測、用天文望遠鏡也得透過拍照，但卻充滿象徵意義。

目前星空中不但有「雲門」，還有「蘇東坡」，就連「金庸」、「嫦娥」、「林青霞」、「徐克」等小行星也都有。　（圖文：記者陳怡靜）

原文轉載自【2010-04-30/自由時報/A9 版/生活新聞】

雲門小行星　讓林懷民 High

【記者李威儀／台北報導】

為表彰雲門舞集的文化成就，中央大學昨天將編號二○○○二五小行星命名為「Cloud Gate」，這是台灣首次以藝術團體命名的小行星。

雲門舞集藝術總監林懷民昨天致詞時表示，能有小行星以「雲門」命名，感覺就像小時候領獎一樣興奮，「這樹立了一個我們必須完成的方向，我們得看得更遠更高。」他說，很高興台灣藝術團體受到自己人肯定，「我們社會需要互相鼓勵，不要只是廝殺、分你我。」

中大天文所所長周翊指出，雲門小行星介於火星和木星之間，距離地球約五億公里，繞太陽一圈要五年多。一般人肉眼無法看到，得用特殊望遠鏡拍照才能辨出。鹿林天文台台長林宏欽說，目前還有近三十顆已發現行星尚未命名。

原文轉載自【2010-04-30/聯合報/A10 版/話題】

中大命名　雲門小行星　宇宙發光

【記者何定照、李承宇／台北報導】

浩瀚星空中，將有顆叫「雲門」的小行星！中央大學今舉辦記者會，將編號二○○○二五小行星命名為「Cloud Gate」表彰雲門舞集將台灣帶上國際舞台的特殊地位，讓雲門在宇宙熠熠生輝。這是台灣首顆以藝術團體命名的小行星。

這顆直徑五公里的小行星是九十六年七月廿五日由鹿林天文台觀測員林啓生和廣州中山大學學生葉泉志發現。雲門小行星位於小行星帶上，距離地球約五億公里，繞太陽一周約需要五點五年。

中大八十七年設立鹿林天文台，從九十一年至今已發現近千顆小行星，並有多顆取得正式編號，擁有命名權。中大真正有計畫觀測小行星是從九十五年啓動的「鹿林巡天計畫」，中大天文所和美國夏威夷大學合作的泛星計畫，目的就是大量搜尋、發現小行星或彗星。

鹿林天文台發現過一顆彗星，命名為鹿林；並正式命名十一顆小行星，有地名的「嘉義」及人名的「溫世仁」等。

原文轉載自【2010-04-29/聯合報/A10 版/話題】

玉山塔塔加觀星　一睹星月爭輝

【記者廖平風／南投報導】

台灣最佳觀星地點之一的玉山國家公園塔塔加鞍部，位於海拔 2,610 公尺，處玉山山脈與阿里山山脈交界處。在阿里山鄒族原住民的語言中，塔塔加是「開闊、平坦的草原區」的意思。夜晚滿天繁星，遠離塵囂，又完全無光害的高山草原，可讓人仰望無際星空，留連忘返。

玉山國家公園管理處表示，管理處與中央大學合辦 99 年度「星月爭輝」觀星活動，即將開鑼。塔塔加的夜晚，星辰清晰明亮，是觀星的最佳地點，每年都吸引許多天文愛好者前來。希望藉由觀星活動，帶領民眾認識與親近遼闊無垠的天體世界。

在零光害的夜空下，銀河是很耀眼的。管理處帶領民眾辨識星座，從銀河中最明顯的星座開始。春季星空的主角是大家耳熟能詳的北斗七星和春季大三角。觀星入門基本裝備有一個星座盤和一個小手電

筒，有雙筒望遠鏡當然更好。
活動還邀請中央大學天文研究所專業講師臨場解說，不管是初學者，或者是觀星族，來一趟「星月爭輝」之旅，透過中央大學天文研究所專業解說，會有意想不到的收獲。
玉管處指出，正逢春季園區內新中橫公路沿線繁花似錦，滿山綠野可見森氏杜鵑繽紛的紅白花朵，還有許多小花也含苞待放，而像鈴鐺般的白色小花「馬醉木」，是 迷人的有毒植物。同時，台灣山胡桃、台灣櫸木和二葉松，也正萌生新芽，將帶給遊客一波波驚豔。活動詳情可洽：塔塔加遊客中心 049-2702200。

原文轉載自【2010-04-07/大紀元時報/A7 版/文教新聞】

塔塔加每月辦觀星

玉山國家公園管理處塔塔加遊客中心邀請中央大學天文研究所專業講師，將於 4 月 17 日、5 月 15 日、6 月 12 日、7 月 10 日、8 月 14 日、9 月 11 日、10 月 9 日、11 月 6 日、12 月 4 日，晚上 7 至 9 時舉辦觀星活動，歡迎有興趣民眾參加，洽詢電話：（049）2702200。

原文轉載自【2010-04-03/聯合報/B2 版/彰投綜合新聞】

極光出現多寡　取決太陽黑子活躍度

作者：羅智華

有趣的是，隨著太空科學的發展，科學家也逐漸觀察到原來「太陽黑子」的活躍程度與「極光次數」有著密不可分的關係！
黃崇源說，當太陽黑子較活躍的時候，會導致太陽發射出較大量的高能帶電粒子（如質子、電子等）；當這些粒子從太陽表面四面八方發射出來時，就有部分粒子會受地球磁場的牽引「跑」來地球南北極，因而衍生極光的出現。
他表示，太陽黑子是太陽表面比較陰暗的地方，看起來就像是太陽表面出現了斑點，古代將太陽稱爲「金烏」，究其原因其實是因爲古代人看到金黃色的太陽表面出現斑點，誤以爲太陽裡住了一隻烏鴉，所以取其名爲「金烏」。
「對不少天文迷來說，能親眼目睹極光是他們一生的最大夢想」林琦峰表示，儘管大家都想看看極光的廬山真面目，但卻不是一年四季都能如願以償。
以台灣天文迷爲例，由於北半球極區的夏天會呈現永晝狀態，因此若是夏季前往北極看極光，可能會敗興而歸，而若要前往南半球看極光，則要避開冬季才不會撲了空。
由於太陽黑子的活躍程度會影響極光的出現次數，加上太陽黑子每十一年會出現一次活躍期，依照時間來估算，林琦峰表示，下次的太陽黑子活躍期會出現在二〇一一年或二〇一二年左右，換言之這也會是極光最常出現的時刻，因此若想一窺其貌的天文迷不妨把握這難得機會。

《科學小辭典》太陽黑子是什麼？

作者：羅智華

太陽黑子是太陽表面的黑斑點，是太陽磁場的一種表徵，在磁場愈強的地方，壓力愈大，但帶有正負電荷的離子氣體密度卻反而愈稀薄，而該處的溫度也會愈低。對 黑子的科學研究始於 17 世紀初的伽利略，他用望遠鏡長期觀察太陽表面，發現太陽表面出現黑斑，而這也是後人所稱的黑子。

原文轉載自【2010-03-19/人間福報/13 版/遇見科學】

美麗極光　非地球獨有　木星也曾現芳蹤

◎記者羅智華專題報導

「期待著一個幸運和一個衝擊，多麼奇妙的際遇；翻越過前面山頂和層層白雲，綠光在那裡⋯ ⋯」歌手孫燕姿這首節奏輕快的歌曲《綠光》，不但引起許多年輕族群的共鳴，也唱出你我對美麗極光的無限想像。
縱然不是每個人都有緣前往南北極親眼目睹耀眼的「極光（aurora）」倩影，但相信不少人都曾在照片

裡或電視上看過它的美麗姿態。然而，儘管多數人都知曉極光模樣，卻不見得清楚極光究竟是什麼光？

在太空科技未蓬勃發展的古早年代，因遙測工具不發達而讓極光成因眾說紛紜，甚至因此衍生出不少耐人尋味的極光傳說。有人認爲極光的產生是因地球以外的太空 中燃起了熊熊大火，因爲南北極靠近地球兩端，所以可以看到火光；還有人認爲極光是太陽照射在北極海或冰山時所反射出的耀眼光芒，各種不同版本的想像揣測， 一直要到太空觀測工具日益進步，才釐清迷思。

事實上，人類親眼目睹極光的出現已有上千年歷史了，台北市立天文科學教育館解說員林琦峰指 出，「極光」顧名思義指的就是發生於地表高緯度極圈上空的光，可依區域不同而有北極光（northern light）與南極光（southern light）。中國古代就曾出現過對極光現象的描述，像是《漢書・天文志》中就寫下一段被後人推測爲極光敘述的文字「漢惠帝孝惠二年，天開東北，廣十餘 丈，長二十餘丈。」由此可知極光歷史之悠久，只是當時的老祖先並不明白他們眼中所看到的奇特現象原來就是極光。

而進一步分析極光的出現 成因，中央大學天文研究所教授黃崇源表示，極光是一種太陽與地球產生交互作用的大氣現象，其背後的科學原理是因爲太陽表面發射的高能帶電粒子，到達地球時 會受到地球磁場的影響而隨著地球磁力線繞向地球兩端的南、北極，並與極區的空氣分子碰撞後、激發出各種波長的可見光，而這個可見光就稱爲「極光」。

但，很多人或許會感到好奇，爲什麼一樣都叫極光，但卻有紅、藍、綠等多種炫目耀眼的不同顏色呢？

林琦峰解釋，極光會出現不同顏色，主要是因爲從太陽發射出的高能帶電粒子與地球大氣層高層不同的氣體分子或原子相互碰撞，因而從中激發出不一樣顏色的光 芒。他舉例，例如高能帶電粒子與地球大氣層高層中的氮分子相互碰撞時，會使得氮分子吸收帶電粒子的能量激發出紅色、紫色、藍色的光芒；而綠色與深紅色極光 則是氧原子與高能帶電粒子相互碰撞的結果。因此下次若有機會親眼目睹極光本尊，不妨從極光顏色來判斷這些帶電粒子究竟是跟那些分子的氣體「碰」在一塊呢！

不過，你若以爲美麗極光是地球人「獨享」的禮物，那可就大錯特錯囉！黃崇源表示，其實過去也有天文科學家透過觀測工具「窺見」其他星體曾出現過極光芳蹤， 像是西元 1994 年，彗星撞到木星時，天文專家就曾透過望遠鏡在木星的南北極看到極光的出現，由此可見極光並非是地球獨有的產物。

原文轉載自【2010-03-19/人間福報/13 版/遇見科學】

泛星計畫
核塌縮超新星與其前身星之研究

文/ 陳婷琬
審稿/ 陳英同

前言

「宇宙，人類最後的疆界」，在美國知名科幻影集《星艦奇航記—銀河飛龍》（Star Trek－The Next Generation）中，星艦企業號上面載著已經發展出可以在星系中旅行的下一代人類，為了探索未知、發現新事物的夢想，人類不惜賭上性命。而這股好奇心與無盡的追尋，自古皆然，想知道我們從哪裡來？想知道我們未來會去哪裡？想知道一切的起源。而解開這亙古之謎的鑰匙，就在我們頂上的穹蒼。

從臺灣超新星巡天到泛星計畫

我們可以把宇宙想成是一個非常巨大的動物園，動物園裡面有大象、獅子…等，除了體型有大有小，生活習性也非常不一樣：像是臺灣獼猴喜歡在白天活動，而眼鏡猴則喜歡在夜間出沒。對於不同習性的動物，飼養員會予以不同的食物與生活環境，當遊客想要在日間觀看夜行性動物的生態時，可以到設計成顛倒作息的夜行館。但是對天文學家而言，我們無法改變天體的規律，所以，對於不同的天體，我們必須以不同的方法進行觀測，並拼湊出其本質。

對瞭解「超新星」（supernova）的本質研究來說，我們利用巡天觀測，以及單一目標後續深入觀測兩種不同方法來進行。在國立中央大學葉永烜教授的主持下，利用中央大學鹿林一米望遠鏡，針對一千多個南天區域的鄰近螺旋星系，定期進行監測，並利用影像對減的方式，將超新星候選者挑選出來。一旦找到候選者，經確認過後即通報國際天文聯合會（IAU），讓更多天文學家對這顆超新星進行後續的觀測，以光譜辨別出超新星之類型，以及光度變化情況，來瞭解超新星的本身特性與其周圍環境。從2004年到2008年，臺灣超新星巡天計畫共成功通報了十五顆超新星。不過，有鑑於新一代大型巡天計畫－泛星計畫（Pan-STARRS）上線，歷時五年的臺灣超新星巡天計畫宣告結束，將人力轉投至泛星計畫。(請參見臺北星空第39期，陳英同與筆者所介紹之「臺灣超新星巡天計畫」)

參觀動物園要記得買門票，泛星計畫的可見光學望遠鏡，就是讓我們走進宇宙動物園的一組珍貴套票，售價全部約一億美金。在這麼龐大的資金需求下，單一研究機構不太可能可以單獨勝任，所以跨國合作更顯其必要性。除了美國空軍的資助，目前參與泛星計

畫的國家，有臺灣、美國、德國、英國…等，共十多個研究單位。泛星計畫的原型望遠鏡（Pan-STARRS1）已經於2010年5月上線運作，為一座口徑1.8公尺的超廣角望遠鏡，搭配14億像素的CCD照相機，總共要建立4座這樣的望遠鏡。不僅可以監測全天達3/4的區域，極限星等約22.5，對於特殊天區還可得到深度曝光至24星等的影像，並以每4到7天的頻率，重複觀測夏威夷可見天區，對於尋找位置或是亮度有變化的天體，堪稱一大利器。在天空中位置會改變的星體，像是小行星、古柏帶天體…等，尤以對地球威脅最大的近地小行星，更是泛星計畫的首要科學目標，(詳細內容請參閱臺北星空第42期，周翊教授所著之「望向大宇宙（一）/Pan-STARRS—泛星計畫」一文)。至於超新星則屬於亮度會改變的天體，在短期內重複搜尋同一天區的策略下，讓我們有機會偵測到超新星的極早期光變，並準確測量峰值的亮度，藉以得到完整的光度（能量）變化曲線。

泛星計畫之 超新星與前身星研究

在泛星計畫眾多的科學目標中，關於巨質量恆星與超新星前身星的研究，原本規劃有：低紅移（距離較近）核塌縮超新星巡天、核塌縮超新星之前身星與所在環境、鄰近星系的藍超巨星普查、與Ia型超新星之前身星這四大主題。前兩者由英國Belfast女王大學Smartt教授主導，而後兩者則由美國夏威夷大學的Bresolin教授與美國哈佛大學的Wood-Vasey教授所主導；臺灣中央大學與中央研究院的研究人員亦參與其中。筆者有機會於2008年到北愛爾蘭跟Smartt教授的團隊合作學習一個月，因此本文將專注於探討前面兩個主題。

低紅移核塌縮超新星巡天

所謂的低紅移指的是紅移值小於0.04，在這個距離以內所包含的體積範圍，因為較暗的核塌縮超新星－II-P型的絕對亮度約為-15星等，加上考慮消光的影響，因此設定此一範圍，讓泛星計畫能發現在這個有限體積範圍內所有的超新星。為了獲得全面性資料，泛星計畫在巡天上有著前所未有的優勢。多數的超新星巡天計畫，像是臺灣超新星巡天計畫、美國LOSS（Lick Observatory SN Search）計畫…等，選擇的巡天目標均為選定的特殊星系（集中在高恆星形成率的星系），他們通常含有高金屬豐度與高表面亮度的特性，因此，所發現的核塌縮超新星大都在金屬豐富的區域；對於低表面亮度的星系或是矮星系，則甚少對其監測。泛星計畫排除了選擇效應，並非針對目標星系逐一進行監測，而是全天區的巡天，並利用影像對減的方式，找到位置不會改變，但亮度改變的候選者，將其位置座標與資料庫中星系的座標進行比對，如果剛好在星系範圍內，則很有可能是超新星、活躍星系核、變星等天體，再經由後續觀測決定是否為超新星。

泛星計畫排除了選擇效應的影響，可以在紅移值小於0.04的距離範圍內，建立一個史上最完

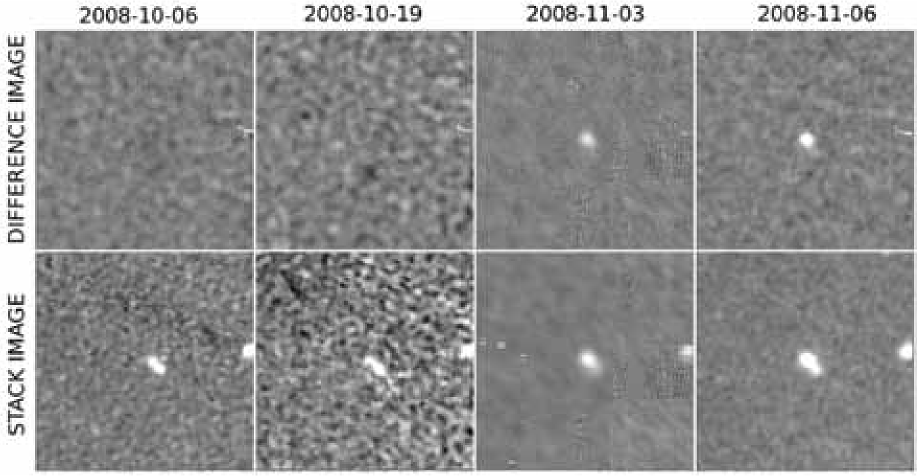

（圖一）泛星計畫發現的第一顆超新星－SN 2008id，圖中最上方為觀測日期，上排為對減後的影像，下排為疊加數張相同天區的影像。可以清楚地看到，在十月的對減影像中，並沒有新的天體出現，但是在11月3日的對減影像中，則明顯看出有新的天體作為超新星候選者，並經後續觀測確定其為Ia型超新星。圖片來源：http://pan-starrs.ifa.hawaii.edu/public/project-status/supernova_discovery.html

整的超新星樣本資料庫；當然如果對於更亮的超新星，我們可以看的更遠，但會受到星等的觀測限制而無法做全面性的統計。Young等人於2008年的論文中預期，在紅移值小於0.6的距離範圍內，泛星計畫的原型望遠鏡每年可以找到24000顆超新星。因為找到超新星的數量龐大，因此後續的觀測更顯重要，臺灣有很好的地理位置，可以在泛星計畫發現超新星後，馬上接續觀測，研究超新星早期的光度變化；唯所發現的超新星，大部分皆暗於20星等，需要大口徑的望遠鏡進行觀測，我們知道口徑大一倍，能減少四倍的曝光時間，因此二米以上口徑等級望遠鏡興建，刻不容緩，需要全民的支持才能順利將鹿林二米望遠鏡完工，並發揮其最大的科研價值。

尋找超新星的前身星

當我們在動物園裡面看到黃色毛茸茸的小雞，很難想像牠會長成咖啡色羽毛，頭頂與下巴垂著紅色肉冠的公雞。不過，如果我們知道一隻動物在幼時長什麼模樣，就可以知道牠將來長大後會變成什麼樣子的話，對我們有非常大的幫助，至少，你不會想養一隻雞叫你起床時卻不小心養到了鴨。對天文學家而言也是這樣，當我們看到有一個天體爆發，就很想知道是什麼東西爆炸了？它的「小時候」會是什麼樣子？培養它長大的「環境」對其有什麼影響？當我們知道，在爆炸前它是什麼樣的天體與周圍物質的狀態，我們就可以推測，它之後會是以什麼樣的形式結束其一生。

就超新星爆發機制上來說，我們可以將其分為兩大類：由巨質量恒星演化到末期爆發的現象，稱為核塌縮超新星（core-collapse supernova）；另外一種由白矮星－白矮星或是白矮星－紅巨星的雙星系統產生的爆發，則稱為熱核型超新星（thermonuclear supernova）。根據Smartt在2009年發表的論文，闡述了能夠產生核塌縮超新星爆發的星球，其初始質量的下限為8 ± 1倍太陽質量，這個數據來自於直接觀測到II-P型超新星之前身星的質量下限，與理論模型中白矮星的質量上限。

我們是怎樣觀測超新星的前身星的呢？答案是等超新星爆炸以後，再去對照爆發前的星系影像，找到相同位置的恆星，即懷疑它就是前身星。舉例來說（圖二），在Mattila等人於2008年論文，尋找II-P型超新星2008bk的前身星，利用不同波段的星等資料，我們可以畫出光譜能量分佈圖（spectral energy distribution），再配合恆星演化的模型，得到前身星是一顆紅超巨星，質量是8.5±1倍太陽質量。

然而，尋找前身星是有難度的：人類自1885年發現銀河系外第一顆超新星開始，到2010年8月，找到超過5541顆超新星，但是確定找到前身星的數量卻低於30顆（<0.5%）。原因是我們需要高解析度的影像，才能分辨出一顆顆位於其他星系的恆星，近十多年，拜哈柏太空望遠鏡與地表大型光學望遠鏡的高解析度影像之賜，才讓我們有機會得以窺見鄰近（小於20Mpc）星系中，超新星前身星的蹤影。不過，並不是所有的超新星，都找得到爆發前該星場的高解析度影像（圖三）；或是曝光深度不夠，無法獲得前身星的星等資訊。因此，建立

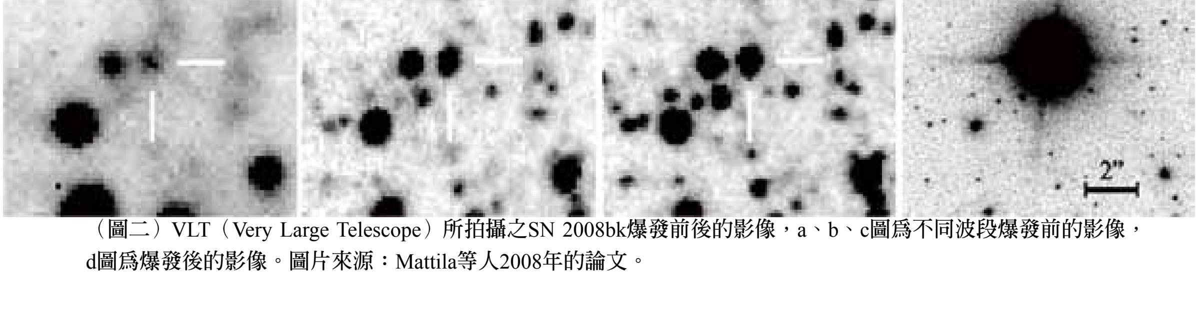

（圖二）VLT（Very Large Telescope）所拍攝之SN 2008bk爆發前後的影像，a、b、c圖爲不同波段爆發前的影像，d圖爲爆發後的影像。圖片來源：Mattila等人2008年的論文。

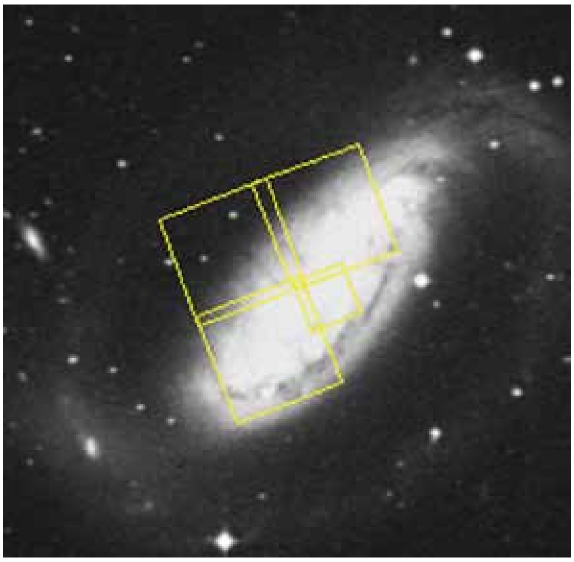

（圖三）星系NGC1808的影像，黃色框爲哈柏太空望遠鏡上面Wide Field Planetary Camera 2的視場大小，爲5.345 平方角分。若超新星爆發在黃色框以外的範圍，我們就找不到爆發前的影像可以比對。泛星計畫的超廣角望遠鏡則可提供7平方度的視場大小，可輕鬆覆蓋住整個星系的範圍，使我們不會遺漏在此星系爆發的超新星前身星。
圖片來源：http://www-int.stsciedu/~mutchler/n1808/

一個廣視野、高解析度、與深度的星系影像資料庫，是一件很重要的工作。泛星計畫中，有個非常重要的子計畫：Deep Medium Survey，此子計畫是對幾個選定的天區加重複觀測，並且將巡天的影像疊加，得到長時間曝光的全天影像，藉以完成此全面性的星系影像資料庫。可惜大氣視相度不如預期，因此可能只有在少數極近的星系才有機會分辨出單一星球。

超新星類型與前身星的本質

上文中所提到的Ia型超新星或是II-P型超新星是指什麼呢？這是超新星另外一種常見的光譜分類方式（圖四）：由超新星在最大亮度時期附近的譜線（吸收線或發射線）特徵為依據，沒有氫譜線特徵者稱做I型超新星，有氫譜線者為II型超新星（Minkowski，1939、1940年）。I型超新星依照矽6150Å的譜線再細分，有矽線者為Ia型超新星，沒有矽線者又可再細分有氦線者為Ib型，無氦線者為Ic型（Filippenko，1997年）。在這邊要注意的是，除了Ia型超新星是熱核型超新星之外，其餘的類別，則皆為核塌縮超新星。至於II型超新星，可以依據其從最大光度下降時的光變曲線細分為二：其一在光度下降時出現一段平緩期（plateau），此種稱為II-P型，另外一種光度直線（linear）下降，稱為II-L型（Barbon等人，1973年）。此外，根據光譜特徵，有窄（narrow）的氫發射譜線，稱為IIn型超新星（Schlegel，1990年）。

以上只是粗略的分法，當我們對每一顆超新星研究的更加徹底，越發現每顆超新星都有其不同之處，像是爆發在大麥哲倫星系中的超新星1987A，因其明顯的氫譜線特徵被歸類在II型，但是其光度變化卻無法被歸類在II-P型或II-L型（da Silva，1990年）。近期的研究（Smith等人，2007年）有一些極亮（ultrabright）II型超新星，像是SN 2006gy，其積分亮度可以達到10^{51}耳格/秒，是一般核塌縮超新星的100倍。

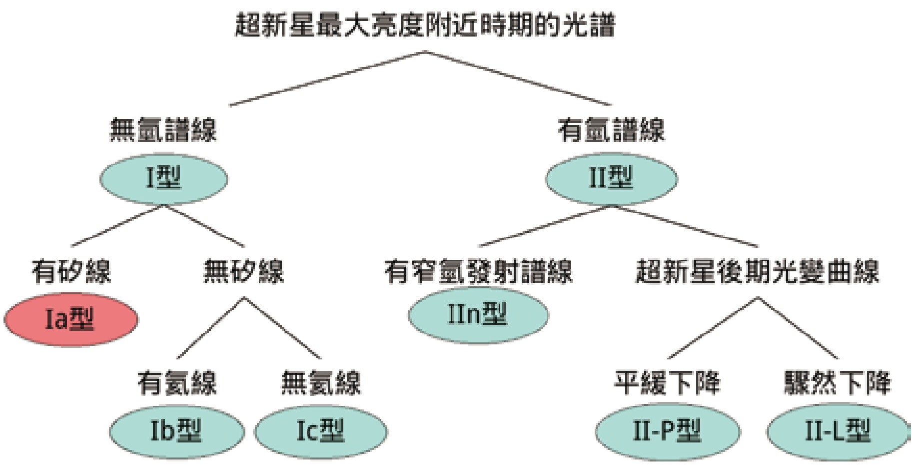

（圖四）超新星的分類示意圖

Gal-Yam等人在2007年發表的論文中，將不同質量的前身星與不同類型的超新星做了一張關係圖，筆者借取相同概念將之重新製圖（圖五）。左邊前身星的部分，質量有越往下越大的趨勢，右邊是不同類型超新星，顯

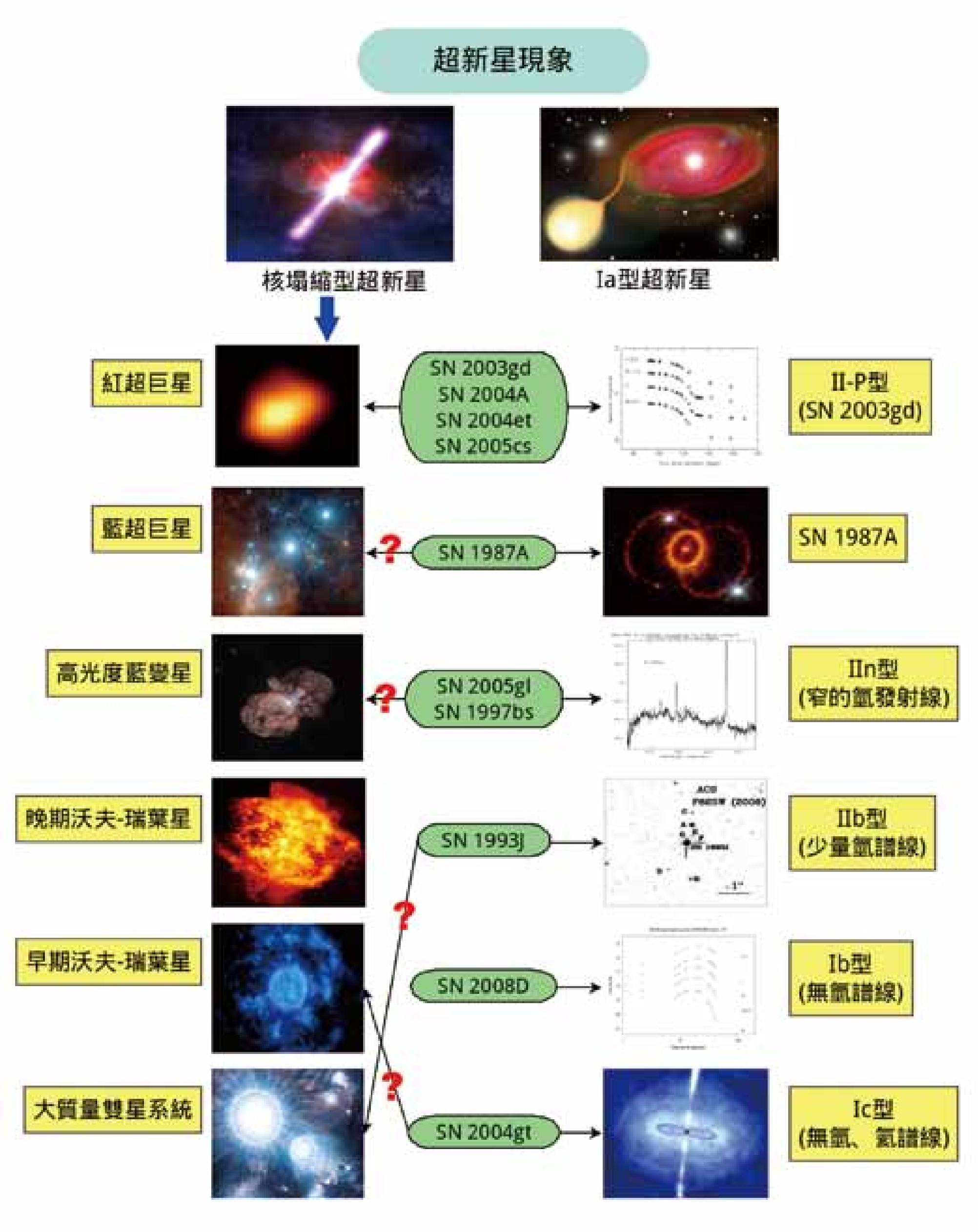

（圖五）超新星前身星與不同超新星類型的關係圖。圖片概念於Gal-Yam等人於2007年的論文，經筆者重新彙整，各小張圖片來源整理於文後。

示不同的前身星會造成不同類型的超新星爆發。其中比較肯定的結果，II-P型超新星的前身星為質量在8到15倍太陽質量的紅超巨星。超新星1987A則可被歸類在II型超新星，但是它的光度較暗且下降緩慢；它的前身星為藍超巨星，是人類第一次偵測到來自太陽以外的微中子，證實了超新星爆炸能產生大量微中子的理論。

請讀者要注意的是，其餘超新星類型的前身星本質，目前還沒有那麼確定。IIn型超新星，目前相信在其前身星－藍超巨星的周圍，有濃密的物質圍繞，這些物質可能是藉由大量恆星風與高光度藍變星（luminous blue variable）噴發，從藍超巨星表面所拋出去的，詳情可參閱本期臺北星空中，黃立晴著作的「IIn型超新星的觀測」一文。至於Ib與Ic型超新星，其前身星可能為20倍太陽質量以上的沃夫－瑞葉星（Wolf–Rayet stars），兩者差別在於強烈的恆星風將外層大氣吹離，吹掉氫氣殼的為Ib型，連內層氦氣殼也吹掉的為Ic型（Filippenko，2005年）。另外一種非單星系統的前身星，像是超新星1993J，則被認為是位於巨質量雙星系統中的紅超巨星爆發，其大部分的氫殼層被鄰近的伴星吸走，因此光譜特徵呈現II到Ib型超新星之間的過渡型（Maund等人，2004年）。

在累積到越來越多觀測證據與搭配上理論模型的發展，對於前身星的本質，我們有更多與以往不同的看法。像是Smartt等人在2009年發表的論文中認為，似乎多數的Ib/c型超新星，是由中等質量的交互作用雙星所引起的，而更高能量的寬譜線（broad-lined）Ic型超新星，其前身星很可能才是大質量的沃夫－瑞葉星。超新星前身星的本質在近年中時有辯論，不僅挑戰既有的恆星演化模型，也帶給我們更多的未解之謎。期待泛星計畫可以提供更多的觀測證據，像是找到「失敗的」（failed）超新星，這些超過20倍太陽質量以上的巨質量恆星，演化到末期核心可能會塌縮成黑洞，但是其爆發的殘餘物質並沒有被偵測到。研究這些超新星的前身星，是我們用來瞭解巨質量恆星演化到最終狀態－黑洞的最根本關鍵。

泛星計畫的初步成果

在泛星計畫原型望遠鏡（Pan-STARRS1）發現第一顆超新星2008id之後，至今發現了75顆超新星，其中有一些有趣的成果：

SN 2009kf－Botticella等人在2010年的論文提到，這是一顆非常明亮的II-P型超新星。Pan-STARRS1在超新星亮度達到峰值以前就發現到它，因此我們得到相當完整的光度變化曲線（圖六）。圖中的黑色實心圓點為SN 2009kf在V波段的絕對星等，跟另外兩顆II-P型超新星：SN 1992am以及SN 1992H的光度變化曲線做比較，可以發現在超新星爆發後約七十天的光度平緩期，其V波段的絕對星等達到-18.4，比II-P型的平均亮度-17還亮超過一個星等。而紅色實心三角形，則為SN 2009kf在R波段的絕對星等，也是非常明亮，推測其爆發能量比普通的II-P型超新星高5至10倍，或是其前身星半徑非常巨大，因此，就算其距離我們非常遙遠，紅移值高達約2.5，我們還是可以觀測到它。

SN 2010aq－Gezari等人於2010年送出的論文中提到，Pan-STARRS1與星系演化探測器（Galaxy Evolution Explorer, GALEX）在超新星2010aq爆發的第一天內就偵測到它，因此對於超新星的「shock breakout」現象，提供了一個很好的研究機會。所謂shock breakout理論，是由Colgate於1974年所提出，起源於超新星的前身星內層往內塌縮產生的震波反彈，向外撞擊到外層大氣（恆星表面），震波前沿的高溫會產生高能的伽瑪射線與X射線的輻射。換句話說，shock breakout就是超新星爆炸的瞬間所發生的現象。得到這個階段的光度變化曲線（圖七），我們可以藉由理論模型的擬合，推測超新星爆炸後一天的黑體輻射溫度為31, 000 ± 6, 000K，以及前身星－紅超巨星的大小為700 ± 200太陽半徑。

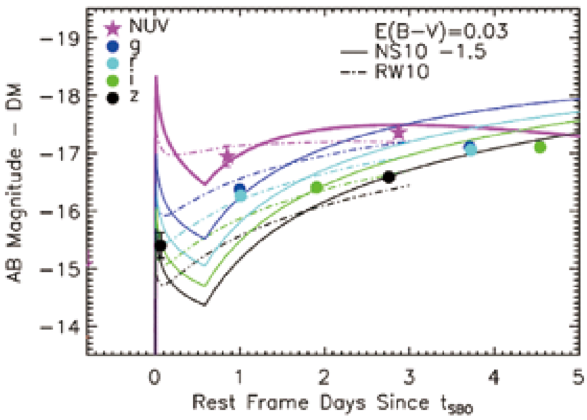

圖七）SN 2010aq的早期光度變化曲線與模型的擬合。橫軸爲超新星shock breakout之後的天數；粉紅色星狀符號爲GALEX所得到的近紫外波段星等，其他各色實心圓點爲Pan-STARRS1在g、r、i、z波段得到的星等，實線與虛線則各自代表不同的模型。圖片來源：Gezari等人，2010。

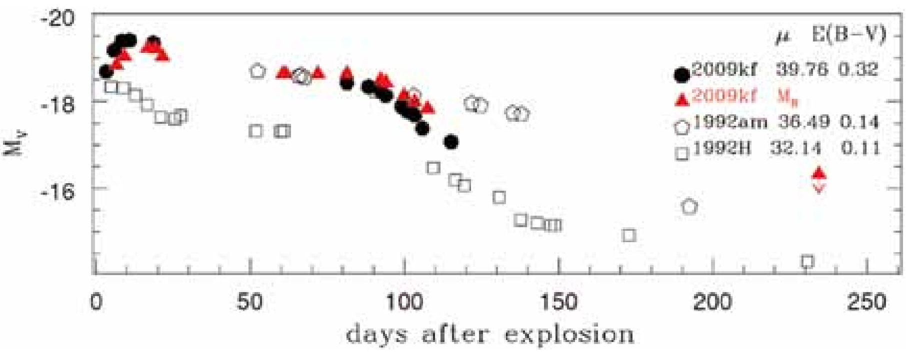

（圖六）SN 2009kf與其他兩顆II-P型超新星的光度變化曲線比較圖，絕對星等的數值已經做過本銀河系及宿主星系的消光修正。圖片來源：Botticella等人，2010。

未來展望

解密核塌縮超新星與長伽瑪射線爆之關連

伽瑪射線爆（gamma ray burst）是來自天空中某一區域的伽瑪射線突然增強的現象，依照它的爆發持續時間，以2秒鐘為界，分為長伽瑪射線爆（long-duration gamma ray burst）與短伽瑪射線爆（short-duration gamma ray burst）兩種。Woosley於1993年提出伽瑪射線爆的來源與旋轉的恆星級黑洞吸積盤有關，並在1999年與Macfadyen更進一步指出，這些黑洞來自於特殊的巨質量恆星塌縮，它們必須為已撥去外層氫殼的沃夫－瑞葉星，其核心質量要大到能塌縮產生黑洞，並且快速的轉動，產生吸積盤與筆直的相對論性噴流。這類型超新星的爆炸能量（10^{52}耳格/秒），高於一般核塌縮超新星的10倍，Paczy’nski於1998年稱呼其為「超級超新星」（hypernova），也就是寬譜線Ic型超新星。Stanek等人於2003年提出，Ic型超新星與長伽瑪射線爆的來源有關。但並非所有超級超新星爆炸都有伽瑪射線爆的現象（Mazzali等人，2005年），根據Modjaz等人於2008的論文，這些有伽瑪射線爆現象的超級超新星，偏向在低金屬豐度的星系中產生，因此泛星計畫可以提供我們更多在此種星系環境下產生的超新星樣本，幫助我們解開長伽瑪射線爆的來源之謎。

各類型超新星的相對產生機率

根據Smartt等人於2009年發表的論文，統計自1998到2008年之間，在約28Mpc體積範圍內所發現的超新星，如表一。由核塌縮超新星的相對產生機率，我們可以發現，II-P型超新星佔核塌縮超新星的一半以上，至於II-L與IIn型的超新星則是比較稀少的。我們習慣用Ib/c型與II型超新星的比例來描述前身星的星族特性，例如在近似太陽金屬豐度的星族，Ib/c比II約為0.4±0.1，跟此篇論文統計出來的數值類似；而金屬豐度越低的星族，這個比例越低。但是這個統計是有偏差的，因為我們無法發現被銀河系的塵埃遮蔽掉的超新星，以及爆發時跟太陽視線方向相同的超新星；另外就是前述傳統超新星巡天的選擇效應，沒有對低表面亮度的星系進行監測，或是沒有發現亮度微暗的超新星。因此，需要藉由泛星計畫提供本地超新星的全面性的資料，準確的訂出各類型超新星相對的產生機率，讓我們對前身星的特性有更正確的了解。

後語

泛星計畫對於偵測超新星…等天文瞬變（transient）現象，提供了大量的樣本，不僅讓我們了解鄰近超新星的特性與前身星的本質，挑戰我們既有的恆星演化模型之理論，更帶給我們許多研究未知的爆發現象的機會。聽完宇宙動物園的其中一個展示區的初步導覽，在這個沒有生命被禁錮的廣闊虛空中，不知道各位是否對這無盡的追尋有一點點的輪廓？讓我們一起期許，泛星計畫在屬於它自己的《銀河飛龍》中的旅程，跟星艦企業號有著一樣的任務：「繼續探索這全然未知的新世界，尋找新生命和新文明，勇敢地航向前人所未至的領域。」

超新星類型	數量	相對比例(百分比)	核塌縮超新星相對比例(百分比)
II-P	54	39.1	58.7
II-L	2.5	1.8	2.7
IIn	3.5	2.5	3.8
IIb	5	3.6	5.4
Ib	9	6.5	9.8
Ic	18	13.0	19.6
Ia	37	26.8	–
LBVs	7	5.1	–
未分類	2	1.4	–
總計	138	100	100
核塌縮超新星總計	92	66	100

（表一）近10.5年所發現的鄰近超新星，不同類型的相對產生機率，最後一欄排除掉熱核型超新星（Ia型）與高光度藍變星（LBV），爲核塌縮超新星的相對產生機率。資料來源：Smartt等人，2009年。

圖表來源

圖片一 http://pan-starrs.ifa.hawaii.edu/public/project-status/supernova_discovery.html

圖片二 Mattila, S. et al., 2008, ApJ, 688, 91

圖片三 http://www-int.stsci.edu/~mutchler/n1808/

圖片四 陳婷琬，2008，碩士論文

圖片五：各小圖片來自於…

核塌縮超新星 http://www.newscientist.com/article/dn12778

紅超巨星 http://www.astronet.ru/db/xware/msg/1210845

藍超巨星 http://antwrp.gsfc.nasa.gov/apod/ap051013.html

高光度藍變星 http://hubblesite.org/newscenter/archive/releases/1996/23

晚期沃夫－瑞葉星 http://hubblesite.org/gallery/album/nebula/pr1998038a/

早期沃夫－瑞葉星 http://en.wikipedia.org/wiki/File:Wolf-rayet.jpg

大質量雙星系統 http://www.stsci.edu/~inr/thisweek1/2008/thisweek280.html

Ia型超新星 http://www.lbl.gov/Science-Articles/Archive/sabl/2007/Nov/darkenergy2.html

II-P型Hendry, M. A. et al., 2005, MNRAS, 359, 906

SN 1987A http://astroprofspage.com/archives/744

IIn型 http://www.cfa.harvard.edu/supernova/spectra/sn97bs.gif

IIb型 Van Dyk, Schuyler D. et al., 2002, 114, 1322

Ib型 陳婷琬，2008，碩士論文

Ic型 http://www.astronomy-education.com/index.php?page=2&year=2009&category=0

圖片六 Botticella, M. T. et al., 2010, ApJ, 717, 52

圖片七 Gezari, S. et al., 2010, ApJ, 720, 77

表一 Smartt, S. J. et al., 2009, MNRAS, 395, 1409

參考文獻

泛星計畫網頁：http://pan-starrs.ifa.hawaii.edu/public/

黃崇源等人，2009，物理雙月刊，卅一卷三期，246

Young, D. R. et al., 2008, A&A, 489, 359

Smartt, S. J., 2009, ARA&A, 47, 63

Mattila, S. et al., 2008, ApJ, 688, 91

Minkowski, R., 1939, ApJ, 89, 156

Minkowski R., 1940, PASP, 52, 206

Filippenko, A. V., 1997, ARA&A, 35, 309

Barbon, R. et al., 1973, A&A, 29, 57

Schlegel, E. M., 1990, MNRAS, 244, 269

da Silva, L. A. L., 1990, RMxAA, 21, 471

Smith, N. et al., 2007, ApJ, 671, 17

Gal-Yam, A. et al., 2007, ApJ, 656, 372

Filippenko, A. V., 2005, ASPCS, 332, 34

Maund, J. R. et al., 2004, Natur, 427, 129

Botticella, M. T. et al., 2010, ApJ, 717, 52

Gezari, S. et al., 2010, ApJ, 720, 77

Stanek, K. Z. et al., 2003, ApJ, 591, 17

Woosley, S. E., 1993, ApJ, 405, 273

Macfadyen A. I. & Woosley, S. E., 1999, ApJ, 524, 262

Paczyn’ski B., 1998, ApJ, 494, 45

Mazzali, P. A. et al, 2005, ASPCS, 342, 366

Modjaz, M. et al., 2008, AJ, 135, 1136

Smartt, S. J. et al., 2009, MNRAS, 395, 1409

陳婷琬：國立中央大學天文研究所碩士

陳英同：國立中央大學天文研究所博士候選人

IIn型超新星的觀測

文/ 黃立晴

什麼是超新星？

當天空中出現一顆以往看不見的星星，我們叫他新星，如果這顆新星的亮度增加非常多，幾乎像一個星系一樣明亮時，我們便稱作超新星。超新星是來自死亡的巨質量恆星（大於八個太陽質量）爆發或是白矮星質量超過負荷時放出大量能量成為明亮的超新星。

密近雙星中的白矮星吸積伴星物質達到錢氏質量上限（Chandrasakhar limit）時爆發會產生Ia型超新星，另外來自巨質量恆星爆發的超新星則分屬I型及II型。目前區分超新星的方法是根據超新星的光變方式或是光譜特徵，由於是用觀測特徵作為分類的依據，所以無法明確地區分超新星的形成機制。

超新星的光度變化大致可分為最大亮度時期前光度上升的階段、達最大亮度之後光度下降的過程以及後期微弱的光度三個階段。最大亮度時期前大約會有一週至數十天的時間光度不斷的上升，而當超新星光度到了最大亮度時期後光度則開始下降，下降的方式與超新星的周圍環境、核心質量以及輻射能量來源有密切的關係，例如超新星是否被環星物質包覆或是四周星際物質濃密與否、衝擊波衝撞環星物質將其激發等都是影響的因素。後期也可能因為有伽瑪射線爆而使光度再次提高及下降。

超新星的光譜有許多不同的特徵，最大亮度時期時的光譜也是超新星分類的依據之一，光譜中的譜線可以反應前身星的組成物質以及超新星的四周環境，我們也可以由光譜譜線的寬度推算超新星爆發的擴張速度，還可以利用譜線的位移計算超新星和其所在星系與我們的距離。

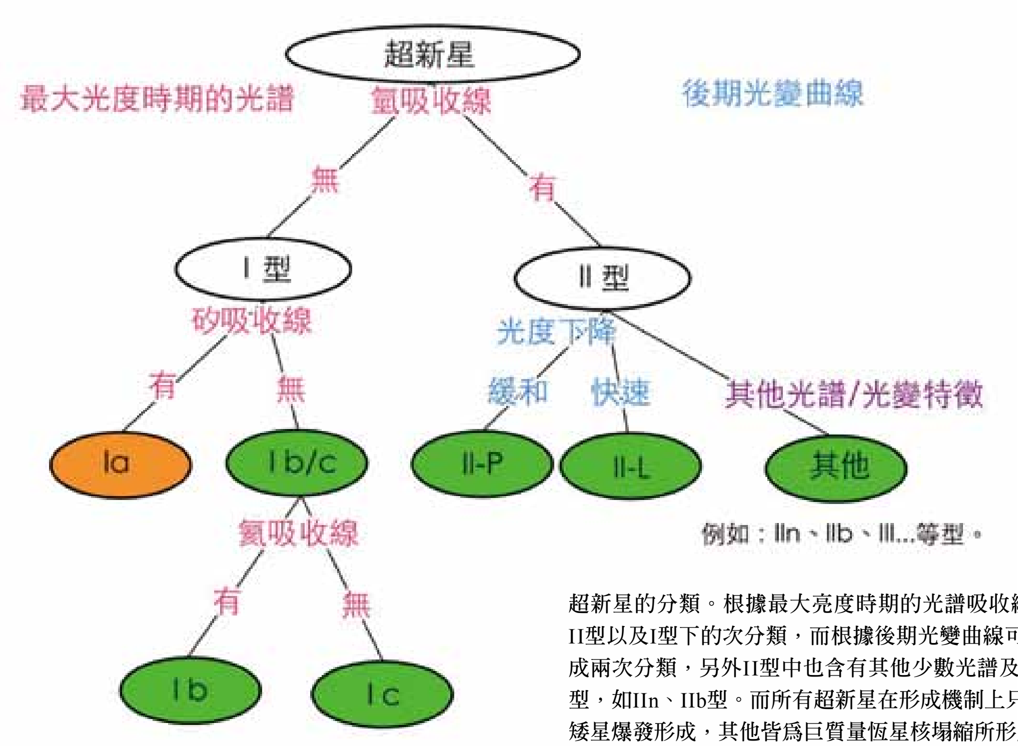

超新星的分類。根據最大亮度時期的光譜吸收線可分出I型、II型以及I型下的次分類，而根據後期光變曲線可以將II型略分成兩次分類，另外II型中也含有其他少數光譜及光變特徵的類型，如IIn、IIb型。而所有超新星在形成機制上只有Ia型是由白矮星爆發形成，其他皆爲巨質量恆星核塌縮所形成。

IIn型超新星

IIn型超新星也是一種由巨質量恆星核塌縮所形成的超新星，其特點是早期光譜中的寬發射線上帶有強烈的巴耳麥窄發射線（narrow Balmer emission），取narrow的第一個字母「n」為此次分類的名字。這類型超新星光譜中有顯著強烈的Hα窄發射線，從其譜線半寬全高可推出其擴張速度約為每秒1000公里，屬非常窄的發射譜線，同時亦可能伴隨Hβ、FeII、OIII或HeI的發射線。

一般認為，窄發射線的來源是超新星爆發時的噴流與周圍又熱又濃密（每立方公分含10^7個以上的粒子）的環星物質交互作用所產生，並非來自超新星的高速噴流，速度只有每秒數百公里的震前環星物質（Pre-shock CSM）亦是氫發射線的來源之一，但造成的譜線寬度則較寬。大量的環星物質則來自前身星的恆星風吹出的物質，由於必須將恆星風吹出的物質保留在超新星附近，因此在超新星爆發前數十年間的恆星風風速不能太快，或是前身星必須吹出非常大量的物質，恆星風造成的前身星質量流失率約為每年$10^{-4}M_{\odot}$，而非常明亮的IIn型超新星則需要每年$10^{-1}M_{\odot}$以上的流失率，例如eta-Carinae(海山二)或其他高光度藍變星（LBVs）可以有每年$0.01M_{\odot}$~$1M_{\odot}$的質量流失率。

濃密的環星物質對於噴流也有減速的效果，當噴流撞上環星物質產生震波，原本的大量動量及動能則轉變為X光或可見光釋出 ，大大提高了超新星的輻射光度。而噴流被環星物質反彈的部份往回撞到噴流又會產生逆向震波，逆向震波則是一個相較於正向震波擴張速度為慢的殼層。

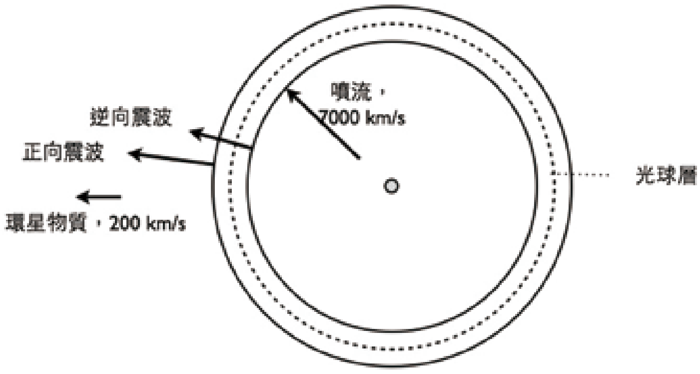

圖二、IIn型超新星模型。高速的噴流與緩慢擴張的環星物質交互作用產生Hα的窄發射線。

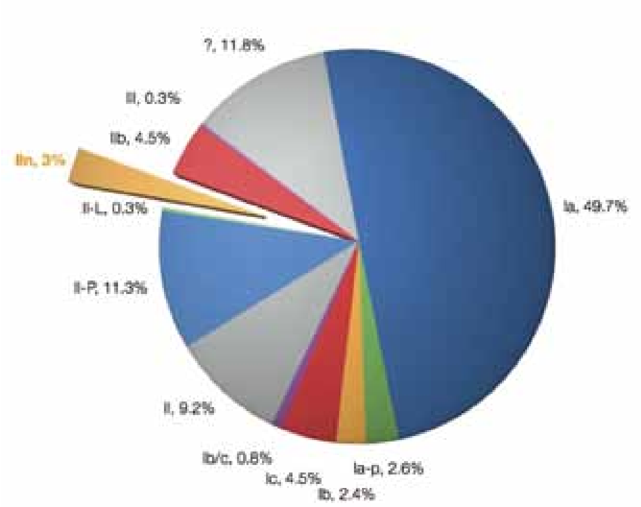

圖三、2009年超新星類型數量統計。

IIn型超新星為較稀少的類型之一，以2008年及2009年的統計為例，2008年總共發現兩百四十五顆超新星，其中IIn型只有十四顆，約佔5%，而最常見的Ia型超新星則有一百二十一顆，約佔49%。2009年則在三百八十二顆超新星中有十一顆IIn星超新星，約佔3%。

觀測目標

我們在2009年上半年觀測兩個IIn型超新星SN 2008ip及SN 2009au，以下將分別對其做更詳細的介紹。

SN 2008ip

SN 2008ip在2008年12月31日為Takao Kobayashi所發現，位於Sb星系NGC 4846。（z=0.015124）中，其天球座標為R.A.=12h57m50.20s，Dec.=+36 22’33.5”，發現時的亮度為15.7等。

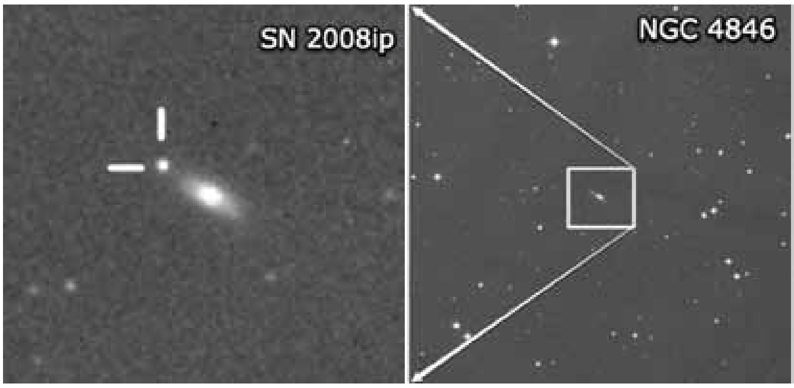

圖四、發現超新星SN 2008ip時的影像。
（修改自http://www.rochesterastronomy.org/SN 2008/n4846s1.jpg）

SN 2009au

SN 2009au於2009年3月11日由CHASE (The CHilean Automatic Supernova sEarch)發現，位於Sc星系ESO 443-21（z=0.009404）中，其天球座標為R.A.=12h59m46.00s，Dec.= -29 36’ 07.5”，發現時的亮度為16.4等。

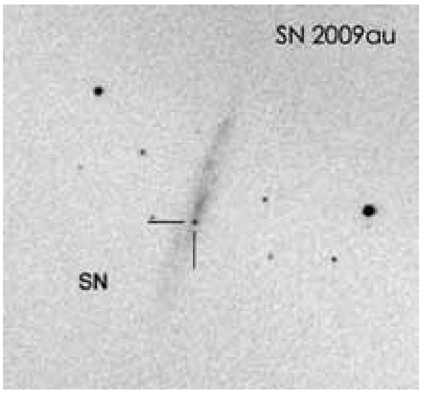

圖五、發現超新星SN 2009au時的影像。
（修改自 http://www.das.uchile.cl/proyectoCHASE/sne_2009/carta_sne_2009au.jpg）

觀測儀器

我們利用鹿林天文台的SLT及LOT望遠鏡和CTIO的SMARTS 1.3m望遠鏡來對這兩個超新星做一百日以上的後續觀測。

鹿林天文台位於嘉義縣阿里山鄉及南投縣信義鄉交界的鹿林前山山頭，海拔2862公尺。我們利用這裡的SLT及LOT望遠鏡搭配B、V、R、I四種濾鏡進行觀測。而CTIO位於智利聖地牙哥北方五百公里的Tololo山，海拔2200公尺，其中SMARTS共有四部望遠鏡，口徑分別為1.5公尺、1.3公尺、1.0公尺以及0.9公尺，而我們使用1.3公尺口徑的望遠鏡搭配B、V、R、I四種濾鏡進行觀測。

觀測策略

當有人發現超新星後會向IAUC通報，經過確認後我們就可以在List of Recent Supernovae網站上看到已發現的超新星列表，這個網站提供許多超新星的基本資料，包括位置、發現時間、發現時的亮度，甚至是超新星的類型，我們可以從中挑選適合的觀測目標。由於我們希望能做一百天以上的觀測記錄，因此這段時間內超新星所在的天區不可以超出可觀測範圍外，也就是開始觀測時超新星的R. A.座標值不可以太接近太陽位置，以免這個天區在未滿一百天時就轉到太陽的另一邊導致無法進行觀測。另外一個限制是望遠鏡的集光能力，加上超新星的亮度會日益減弱，因此我們不能選擇亮度在一開始就太暗的超新星作為目標，理想的目標是16星等以下的明亮超新星。而超新星位置也是考量的因素之一，如果超新星投影的結果離星系核心太近，測光時容易將過多的星系的光列入，影響測光的準確性，因此以投影在星系盤面或旋臂上的超新星作為觀測目標會是較佳的選擇。

ToO

由於超新星爆發是無法預測的現象，因此我們不能在提出一季的觀測時間申請前預知要使用的時間，加上超新星的後續觀測需要長期間地隔幾天就觀測一次，但每次觀測並不需要用到整晚的時間，因此我們申請ToO（Target of Opportunity）觀測，在適合的超新星出現時聯繫天文台，請天文台協助觀測工作，接下來每五至七天觀測一次以取得長期且連續的光度資訊。

測光

當我們取得觀測影像並將雜訊處理完畢後便開始進行測光的工作，測光可以分為孔徑測光和點彌散函數測光。孔徑測光是直接圈選星點的範圍，將這個範圍內的讀數全數視為來自星點的流量。但是超新星通常落在星系裡頭，這樣的測法會把其他屬於星系的流量當作超新星計算，使測光的結果太亮，因此我們可以使用去擬合星點流量分布（高斯分布）的點彌散函數測光法進行測光，將不屬於超新星的流量排除在外以得到更準確的測光結果。

利用點彌散函數測光可以得到「儀器星等」，但這並不是實際的星等值，因為CCD接收到的流量會因為觀測當時的大氣厚度（因仰角而改變）、天氣狀況等因素影響。因此我們需要一份國際公認的星表，裡面所列的目標都有詳細的各波段星等資料，我們在觀測超新星時同時觀測一些星表裡的星星，便可以當作校正儀器星等用的依據。

觀測結果

我們對SN 2008ip及SN 2009au的觀測影像做測光，將所得的視星等繪成光變曲線，亦可利用我們與星系的距離算出其絕對星等，再繪出絕對星等的光變曲線。

SN 2008ip的最大亮度時期約在MJD(Modified Julian Date, 修正儒略日)=54837.2。我們可以從SN 2008ip的光變曲線看到我們開始觀測時已經過了超新星的最大亮度時期，因此我們看見的是光度下降的區間。在一開始的六十天內，光度減弱速率約為每日0.025等，而B波段下降的速率較其他波段稍快，接下來的八十天中光度下降速率減緩，約為每日0.005等，直到最後四十天才又快速下降，並且，在MJD=54880時的光變曲線有不連續的現象。

SN2009au也是在光度達最大亮度時期後才開始觀測，光變曲線下降的速率比較一致，約為每日0.01等，但B波段光度下降較快速，約為每日0.043等。

比較SN 2008ip以及SN 2009au，SN 2009au較為明亮，光度下降的速率較快。由於這幾顆超新星皆錯過光度最大亮度時期的觀測時機，且超新星的年齡是以超新星發現當日作為第零日而非超新星爆

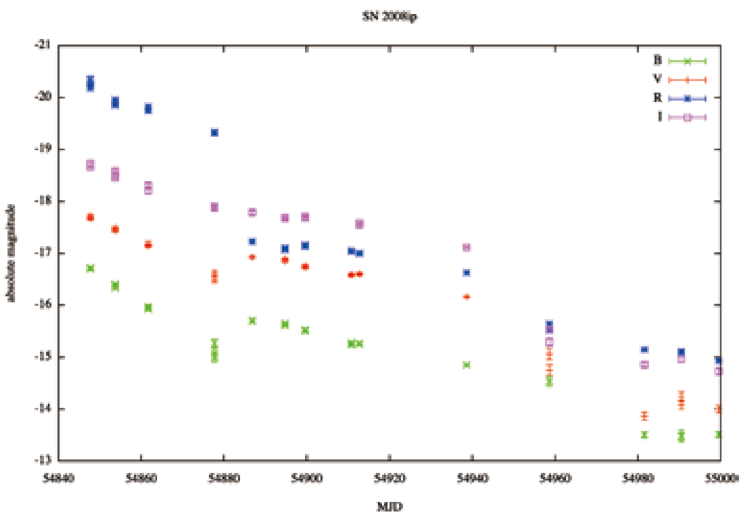

圖六、SN 2008ip各波段的光變曲線（絕對星等）。（SLT and LOT）

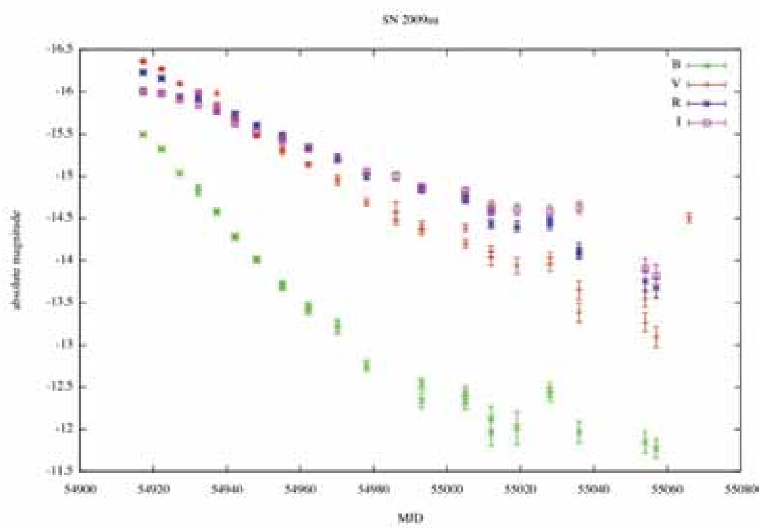

圖七、SN 2009au各波段的光變曲線（絕對星等）。（SMARTS 1.3m teloscope）

發當日，實際上應該要有十日或十日以上的平移，才能真正比較每顆超新星在相同年齡時的特徵，但我們仍能從目前所得到的數據比較超新星的光度大小以及光度變化的速度。比較SN 2008ip、SN 2009au以及其他IIn型超新星，SN 2008ip及SN 2009au的光度明顯較其他超新星黯淡，且光度下降速率也較快。

比較SN 2008ip、SN 2009au以及SN 1998S的B-V、V-R、R-I色曲線，三者趨勢相似，B-V值皆在七十至八十日左右達到最高，並在之後緩緩下降，而V-R及R-I皆為逐漸上升。比較IIn型超新星與Ia型超新星的B-V色曲線，IIn型超新星B-V的最大值發生在第八十至一百天左右，而Ia型超新星的最大值則發生在光度最大亮度時期後的十至二十天左右。

Ia型超新星的光變曲線有固定形狀且最大光度為定值，因此可作為標準燭光，但IIn型超新星的光變曲線並沒有固定形狀，最大光度也不一致，因此不能做為標準燭光。相較於其他IIn型超新星，我們所觀測的SN 2008ip和SN 2009au光度皆下降得比較快，且光度也較暗，可推測SN 2008ip和SN 2009au的前身星質量應該小於另外三顆IIn型超新星（SN 1988Z、SN 1995G以及SN 2006tf）。而光變曲線中B波段光度下降的速度也較其他波段快，表示超新星周圍有塵埃的存在，放出偏紅外的光。我們可以利用B-V、V-R及R-I

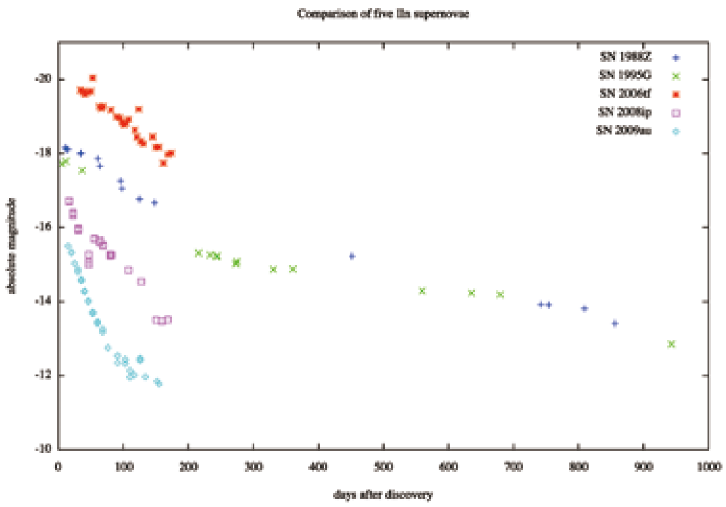

圖八、SN 1988Z、SN 1995G、SN 2006tf、SN 2008ip以及SN 2009au的絕對星等比較。

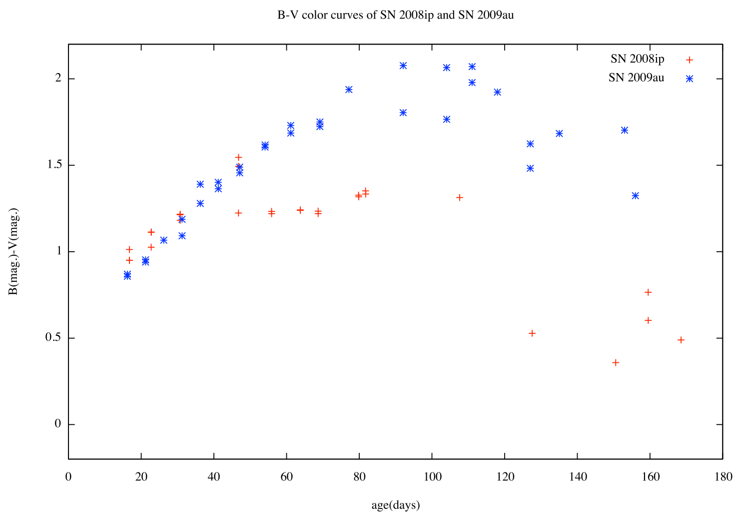

圖九、SN 2008ip及SN 2009au 的 B-V color curves。（SLT、LOT以及SMARTS 1.3m telescope）

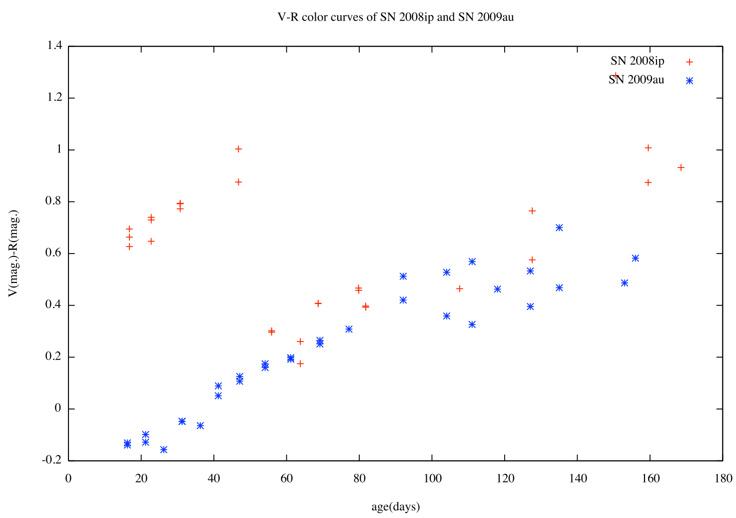

圖十、SN 2008ip及SN 2009au的 V-R color curves。（SLT、LOT以及SMARTS 1.3m telescope）

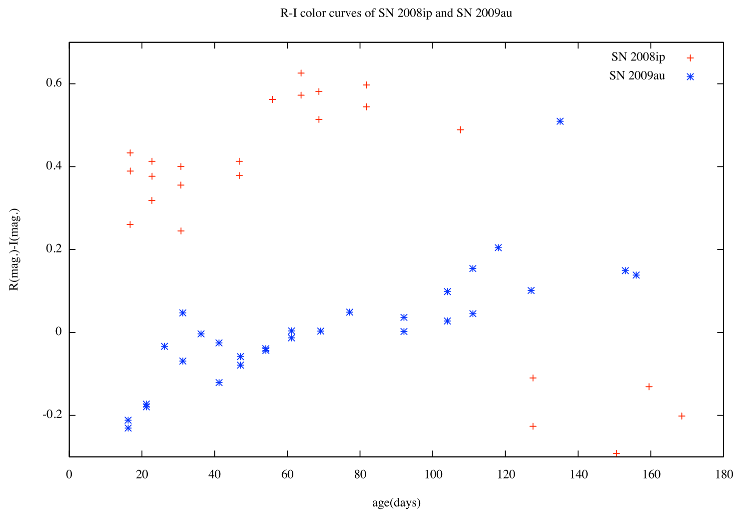

←圖十一、SN 2008ip及SN 2009au的R-I color curves。（SLT、LOT以及SMARTS 1.3m telescope）

↓圖十二、SN 1988Z的B-V、V-R及R-I的顏色變化。Fassia et al. 2000）

↓↓圖十三、Ia型超新星的B-V顏色變化。（Wang et al. 2005）

等數值作為比較一天體顏色的方法。以B-V為例，這代表B波段的星等值減去V波段星等，由於星等值越小則亮度越高，因此當B-V值越高則代表此天體在V波段較B波段亮越多，也就是此天體的顏色越藍的意思。比較三個IIn型超新星SN 1988Z、、SN 2008ip及SN 2009au的B-V、V-R及R-I色曲線，B-V的值皆在第八十日左右達到最高，表示在此之前超新星的顏色是逐漸偏紅，直到第八十日左右趨勢才轉為逐漸偏藍。而V-R和R-I的曲線則顯示超新星的顏色越來越紅。比較Ia型和IIn型的B-V色曲線，B-V值皆為先上升再下降，表示一開始的光由於有周圍的環星物質以及超新星產生的塵埃造成的偏紅現象，待超新星的噴流逐漸將環星物質推開後我們方可看到內部較為炙熱的核心，後期的顏色才轉為偏藍。Ia型的轉折點發生在光度最大亮度時期後十天至二十天左右，而IIn型則發生在八十至一百天左右。

黃立晴:國立中央大學天文研究所碩士班研究生

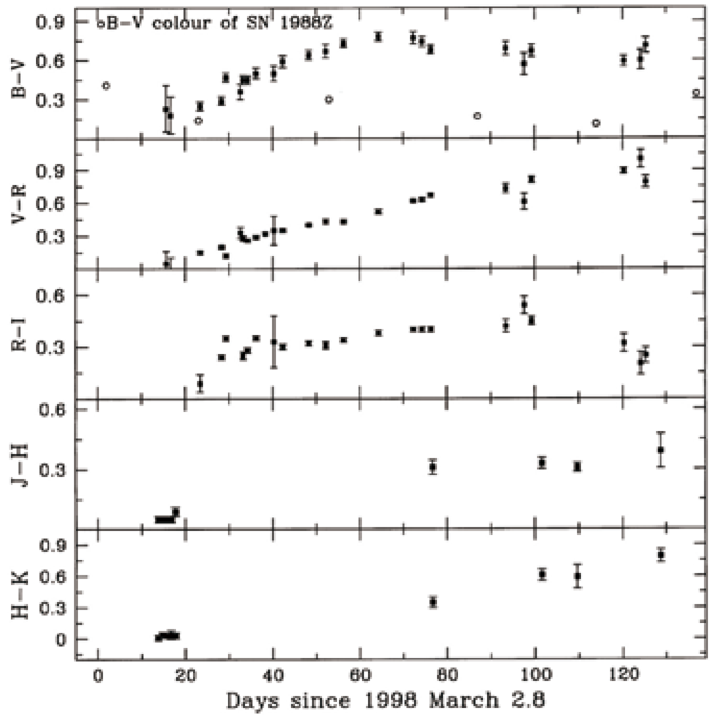

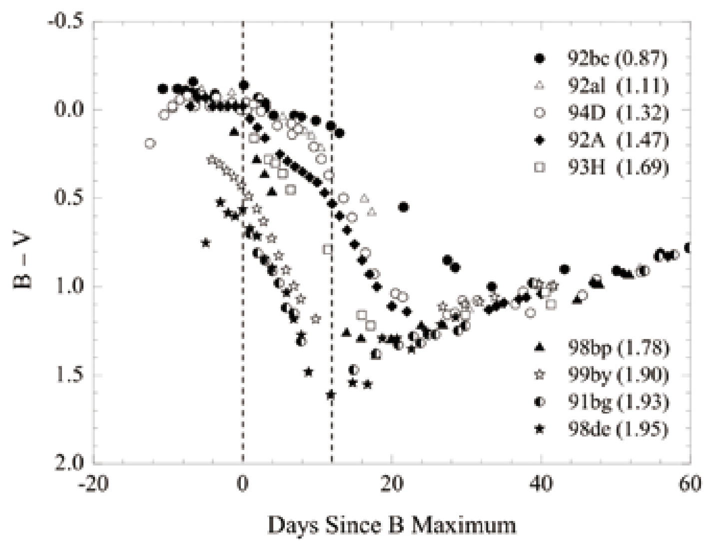

一個冬陽和煦的午後，我們到板橋拜訪鄒志剛教授。聽鄒老師娓娓談起在國外的求學、工作時，親炙受教於一些當代大師的典故軼事，如數家珍發人深省；當老師談到正在進行的研究課題時，神采飛揚熱情洋溢，讓我們見到科學家、學者的典型。這一趟聆聽老師口述歷史的過程，如飲醇醪如沐春風。

天文界的老頑童

經歷非凡、樂在研究

文/ 葛必揚

攝影 蔡和熹

退而不休

我2004年從中央大學退休，在文化大學兼一學期課，講授天文學漫談，屬於通識課程性質，學生來自各個學系，將近100人，很熱鬧。上課內容提到關於宇宙中心的問題，宇宙沒有中心，處處是中心，是中心即非中心；有一回我就舉金剛經的經文為例，說：「老佛爺如是說，『微塵衆，即非微塵衆，是名微塵衆。』」我問學生老佛爺指的是誰，前排一位女同學竟然答曰：慈禧太后。真是令我笑煞又復感嘆。

大陸國家天文臺艾國祥教授知道我退休了，而且身體還很硬朗，就極力邀請我到國家天文臺訪問。因此2005年我就到北京交流參訪；另外也與南京大學彭秋和教授合作，主要在星系物理方面，如星球在星系盤上的運動、星系盤厚度等，也做關於微中子天文物裡方面的東西。總之，範圍比較廣泛。事實上，我在退休前10年就已經與大陸方面的學者們進行密切的學術交流活動，透過國科會與陸委會等機關的鼎力協助，先後邀請彭老師3度來過臺灣在中央大學天文所研究訪問；也邀請過南京大學天文系的陸埮與戴子高等高能物理專家來中大天文所交流合作。

少小離鄉

我是瀋陽人，出生那年滿州國剛成立。15歲到北京，一年後來到臺灣，在臺北建國中學讀3年高中，高一的英文老師就是齊邦媛，她前些年從臺大退休，是齊鐵老的女兒。當年國民政府北伐，統治華北地區的東北王張作霖因為沒有答應日本人遊說，脫離中國獨立，而被炸死在皇姑屯。據說，當時少帥張學良受齊鐵聲、吳鐵城的勸說，東北易幟，中國統一。

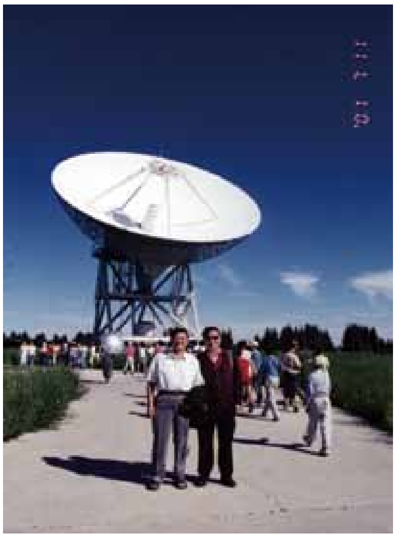

鄒教授與彭秋和教授攝於新疆烏魯木齊電波望遠鏡前。

鄒教授與南京大學天文系的陸埮教授（左二）與戴子高教授（右一）等高能物理專家。

中央大學漠河日全食觀測訪問團（1993年）

高中畢業後，在臺大機械系讀了兩年，1955年到美國留學，先後在俄亥俄大學（Ohio State Univ.）及哥倫比亞大學（Columbia Univ.）讀書，於1973年紐約大學（New York Univ.）物理系完成學業。在美國讀書工作，一待就是19年多，然後才回臺灣來。

1993年在東北邊境的漠河有日全食。應艾國祥院士的邀請，我也參加孫維新教授帶領的觀測訪問團，回程時在瀋陽停留，但幼年時的屋舍都已經拆除，山河依舊景象全非了。

負笈他邦

1955年到美國後，先落腳在俄亥俄州立大學工程物理系中的核物理組，插班讀三年級；這個系不是應用物理系（applied physics），而是工程物理系（engineering physics），這是Ohio大學的特色；系下面分好幾個組。因為當時國事多秋，我心想報國，所以學原子核物理。啓蒙老師是Mills先生，他與楊振寧以「楊－米爾斯規範場理論（Yang-Mills theory）」名聞天下。Mills老師是楊振寧教授在普林斯頓高等研究院的博士後，長我10歲上下，患有氣喘，可惜多年前過世，不然很有可能獲得諾貝爾獎。楊老師因為與Mills老師合作研究，所以常到Ohio來；在李楊獲得諾貝爾物理獎（楊振寧與李政道於1957年獲獎）的前幾個月，我因為擔任中國學生會會長，也請楊老師到俄亥俄州立大學的中國同學會演講。當時他講的就是弱作用在微觀尺度的不對稱，還舉了宏觀世界的對稱情形，如左手右手、在英國與美國開車該靠左或靠右的例子，至今還有印象。

系上還有幾位有名的教授，俄亥俄州立大學一向以分子物理見長，系主任Nilson教授就是當時美國分子物理的權威之一，他常提起他的同學吳大猷，還推薦吳老師寫的關於分子物理的書讓我讀。教量子力學的老師是Landé，當時已經70多歲，原子物理中有關電子的合成的角動量Landé –g factior，就是他的重要貢獻。

Landé教授說過許多故事，其中一個今天我轉述出來，希望給年輕人一些啓發。Landé是海森堡（Werner Heisenberg）的學長，他們的老師是發現X射線的倫琴，海森堡的博士論文是廣義相對論方面應用的題目，博士口試時，倫琴問了海森堡一個光學的問題，即所謂「鑑別度（resulting power）」是什麼意思？海森堡當時答不出來，因此回去補修幾何光學與波動光學方面的知識，結果引發了量子力學中不朽的「不確定原理（uncertainty principle）」。Landé說，由此看來考試也有它的功效，激發出了物理的里程碑。

我也聽過一次海森堡本人的演講，講有關非線性場論的內容，神采奕奕；不過我當時對其內容似懂非懂。

天文初邂逅

我Ohio state碩士畢業後，就到紐約進哥倫比亞大學物理系。有一回，李政道老師請我們幾個哥大的學生到到學校附近的一家名為新月（New Moon）的中國餐館；飯桌上，我請教李老師的博士論文做的是什麼題目，他說是關於白矮星能量傳輸的東西，指導老師就是Chandrasekhar。這是我第一次接觸天文的題目。他說當年Chandrasekhar，找到白矮星的質量上限以後，原本打算用這個題目作為博士論文，雖然 Dirac贊成，但是 Eddington 反對，因此只好另選題目重起爐灶；二次大戰如火如荼進行之際，愛因斯坦、Chandrasekhar和Fermi都先後到了美國。其後Chandrasekhar就把這個題目給了李政道，所以就成了李老師的博士論文，做出來後，當年還得了獎。

李老師接著就解釋什麼是白矮星，接著問我白矮星的密度有多大，我回答很大，李老師立刻糾正我，說做物理的人，要具體說出大小，不能只含混說很大，所謂很大到底有多大呢？我答不上來，因為當時我並不知道太陽的質量、月球的半徑等數據。

遍訪名家

在1964年間我離開學校到阿拉巴馬州一家製造戰鬥機的Northrop Space Laboratories公司工作。當時這家公司向美國的國科會申請到一筆研究經費，訪談諮商傑出的天文太空方面專家，徵詢登陸月球的可能性。我的主管是哥大先期的同學，於是兩人就四處聯繫、走南訪北，因此有緣見了多位那個年代大師級的人物。

其中包括創立太陽風理論模型的Parker，其實當時我們要訪問的對象是芝加哥大學的Chandrasekhar，錢氏在電話中斷言，在登月途中關於太陽風的預測是不太不可能，不願受訪；但我們還是去了芝加哥，Chandrasekhar安排他的助手（associate）與我們見面，就是Parker。

鄒教授與紐約大學Richardson教授在花蓮合照（1988/12/18）


鄒教授與業師Canuto教授及印度的Chitre教授在國際會議上合影（1994/08/23）

另外我們也還訪問了Van Allen（地球范愛倫帶的發現者），當時他是愛荷華大學的系主任，這位老先生非常親切仁慈，與他交談真有如沐春風的感覺。還有其他好幾位，也都是一時俊彥。

這場訪問計畫，讓我從美國西岸又回到東岸，回到哥大。

再回校園

回到紐約我見了美國太空總署哥達德太空研究院紐約分部（Goddard Institute for Space Studies in New York）的主任Jastrow，他也是哥大的教授，在甘乃迪時代曾經獲選為美國10大傑出青年；他建議我回學校完成學業。並介紹我認識他的得力助手丘宏義教授，丘教授又推薦我跟隨丘的博士後研究員Canuto，Canuto老師因此就成了我的博士指導教授，他比我還小三歲，是義大利佛羅倫斯大學的博士。剛開始的一段時間，我是跟

Canuto的太太學習處理超強磁場下β decay 的計算細節，她也是物理學家，我對相對論性量子電動力學的認識與基礎，因此增強，受益匪淺。最後我在紐約大學物理系完成學業，在NYU的論文指導是多體問題專家 Robert Richardson。

當時波霎（pulasr）剛被發現沒多久。波霎的標準模型是高速自轉並具有強大磁場的中子星，磁力線是dipole magnetic field；因為波霎自轉所以有角速度，因而產生感應電場，這個感應電場會垂直於磁力線的方向，所以沿磁力線方向就沒有電場，帶電粒子在磁力線方向就不受力，運動方式就是等速運動或靜止；但我們希望粒子在磁力線方向也有加速運動，因為這樣波霎才會輻射出電磁輻射。

如何讓磁力線方向也有電場，最經典的模型就屬Ruderman的 inner gap模型，這個模型認為在中子星表面不遠的地方，有個真空的空隙，空隙內有電場，此電場在磁力線方向有分量，電子和正子在inner gap中受該電場加速，沿磁力線轉彎運動時又加速，因此引發中子星在低頻的電波波段與高能波段的電磁輻射。

丘宏義教授的老師Salpeter每兩個星期就來一趟紐約；他與Bethe曾合寫過一本量子力學經典名著："Quantum Mechanics of One- and Two-Electron Atoms"。有一回他對我們說波霎中的康普頓散射相當重要，也就是在磁場中康普頓散射的情形。Canuto要我處理這個計算。我用古典電動力學的方法，計算出強大磁場下的電子散射標準模型，屬於古典低能量非相對論性的情形；這個結果現在被應用的很廣泛。

1990年代丘宏義老師退休回臺灣時，建議我繼續研究星系空間在磁場效應下，光子入射碰撞電子的情形，基本上也就是逆康普頓散射（inverse Compton scattering），於是我加入當光子連續碰撞多個電子的情形，並且是熱電子（thermo electrons）的條件。因為一般都以黑體輻射去修飾宇宙背景輻射，而加入逆康普頓散射與磁場效應的考量後，應該更可以凸顯這個修飾的結果，這也是這個研究的重點。近幾年這個題目又熱絡了起來。我也把20年前作的一些結果加以整理，交給彭秋和老師的學生仝浩同學做後續處理。

教學與研究

畢業後離開美國回到臺灣，進了中央大學，當時中大尚未完全復校，沒有那麼多院系，學校名稱還稱為中央大學理學院，院長是李新民先生。我先到地球物理研究所，也由於前院長戴運軌先生的輾轉介紹，在文化大學兼教了幾年課。後來中央大學物理系向教育部申請成立研究所，為了要與國內其他大學的研究所有特色區隔，因此往天文方面推展，我與郭富雄教授就轉到物理系任教。從此就在物理系及天文所一直待到退休。

在中大時期曾多次出國參加國際天文學會（IAU）會議。早些年前，我國出席IAU的代表經常都只有沈君山教授一人，而大陸更是無人出席。1985年IAU在日本京都舉行亞洲太平洋區的會議，當時有消息指出大陸方面也將首次派出多人與會。為了維持會籍，因此找我出席發表一篇論文。團的成員除了沈老師當領隊外，還有圓山天文臺的蔡章獻臺長，以及吳心恒教授。當時向

鄒教授與諾貝爾得主波霎發現者Hewish及孫維新教授合照

鄒教授與沈君山院長、劉品彩教授及闕志鴻教授（由左至右）於玉山合照。

政府申請出國開會的費用，教育部表示案件係臨時申請，無法補助；所幸國科會自然處的處長劉兆玄支持，經費才有著落而圓滿成行。

這篇論文是把密度波理論應用到太陽雲氣團的情形。會有這個論文產生，繫鈴人是袁旂教授。袁教授1984年第一次回臺灣，起初計畫與沈君山教授合寫一部書，但沈教授過於忙碌抽不出空；國科會方面又要求必須有國內教授合作的研究計畫，才能補助袁老師成行，因此找上我具名邀請，促成了我結識袁旂，也開啟我接觸到密度波研究的課題。袁老師後來做非線性的密度波問題頗有心得，而密度波的後續研究還一直在發展。

1985年京都開會時，兩岸還沒有開始交流，當時是我初次見到大陸代表，我本著「君子以文會友，以友輔仁」的精神與大陸同仁交流。當年我這句話，直到現在他們還常提起。有了這第一次經驗，後來與大陸人士的接觸和交流便日益頻繁而具有研究成果。

樂在研究

從2006年開始，連續3年我在大陸的國家天文臺開課，講授星系動力學，學生約20多人，分別來自科學院、北大、清華，還有其他地方。後來這門課就由北大教授范祖惠接手。她與清華的樓宇慶教授都是這個領域的專家，他們對密度波放大很有研究，我感興趣的則是考慮密度波加入磁場的影響；他們解決了一個以前我沒有完成的課題，就是密度波震盪放大模型在盤中加入磁場的情形。

密度波理論是林家翹先生與他的學生徐遐生首先提出的，不過當時麻省理工學院的Toomre批評這個理論，認為在星系中螺旋密度波轉過幾圈後就消散了，因此提出線性振盪放大的修正模型，後來Mark借用量子力學中的WKB計算方法和理論，成功的證明密度波本身也能放大，但放大的效果卻不如Toomre的擺盪放大論的顯著。Jean Mark本人修長帥氣如玉樹臨風，廣東人，約20年前曾短暫來臺訪問，也一度被中大研究所考慮延聘為所長，後來未果。


鄒教授與夫人攝於臺北板橋寓所，右後方爲鄒教授油畫作品。

去年（2009）年5月，承蒙國家天文臺的韓金林教授邀請，在他所領導的團組訪問。也與北大退休的喬國俊教授交流並以文會友，研究具有超強磁場的波霎方面的課題，直到10月回臺。在這5個月中，朝夕與年輕學者與同學們切磋琢磨，給我帶來極大的鼓舞，真有返老還童之感。

去年夏天，大陸韓金林教授主持一個關於波霎的研討會。針對磁星的問題也有一番討論。所謂「磁星」（Magnetar），簡單的說就是指一顆星的磁場強度遠大於10的12次方，乃至達到15、16次方，這顆星就稱為磁星。在這種超強磁場條件下，帶電粒子的運動，要用相對論性量子電動力學來計算；因為在沿著磁力線方向與垂直於磁力線方向的電子氣體壓力是不一樣的，所以磁星可能不穩定。但康乃爾的教授賴東，還有哥大的教授Thompson等學者則認為磁星是穩定的。回憶卅多年前在美求學的最後階段，撰寫博士論文時正值波霎星的發現，因而引起學界對強磁場中的物理學的濃厚興趣。如今由於磁星的理論和觀測日益蓬勃發展，很多我年輕時涉獵過的問題現在又推進到更上一層樓的新境界。去年五月以來我在國家天文臺訪問，有機會再見到諸多天文界馳名國際的學者如Ostriker等人，真有時光反轉回到從前的朦朧喜悅。我由衷的期盼能為兩岸天文學的交流發展盡心盡力，發揮餘溫，以期達到「青山依舊在，幾度夕陽紅」的夢想。

葛必揚: 任職於臺北市立天文科學教育館

中央大學鹿林天文台二米望遠鏡簡介

文 / 黃崇源

百　年　大　夢

在台灣高山建造一座大型光學望遠鏡，一直是台灣天文學界長久以來的期待。最早可追溯到日據時代的一戶直藏(1878-1920)於西元一九一二年所規劃的小塔山天文台。可惜，後來他因故離職，小塔山天文台構想也就無法實現。但當時他所提出的小塔山天文台規劃報告及設計圖現仍由南投中興新村的國史館台灣文獻館收藏。西元一九四三年，另一位日本人窪川一雄開始在玉山上頂興建新高山天文臺，但興建到一半後，卻因戰爭及窪川一雄的病逝而使整個天文台的興建計畫因而中斷。

一九九零年代，台灣重新發展現代天文研究。在台灣高山建造一座二米級的光學望遠鏡的構想也再次在台灣天文十年規畫的討論中被提出。但當時許多人評估二米望遠鏡在國際上已沒有競爭力，而台灣的氣候潮濕多雨，高山通常地型險峻，開發超過二米級的望遠鏡，並不太合適，因此沒有繼續推動。一直到本世紀，中央大學因執行由教育部與國科會支持的「追求卓越」計畫，而開發建設鹿林天台，且買了一個舊的一米望遠鏡，才有鹿林天文台一米望遠鏡，成為目前台灣最大的光學望遠鏡。

過去數十年，全球天文界的望遠鏡的口徑愈蓋愈大，以求能有更大的集光力而能來探索更遙遠的宇宙。因此十米級的望遠鏡成為目前“主流”的研究型望遠鏡。不過在二十世紀末，一些天文學的發展，讓人開始重視特定用途的小口徑望遠鏡的優點，特別是在瞬變天文學的領域。例如在珈瑪射線爆，超新星，太陽系小天體的研究。這些領域需求的是能對突發天文現象做快速反應及長期監測的望遠鏡。過去數年中大天文利用鹿林一米望鏡在瞬變天文學領域做了許多研究，且在三年前加入夏威夷大學合作的泛星計畫。泛星計畫為使用一點八米口徑望遠鏡的快速巡天計畫。因為地理位置的關係，鹿林天文台是世界上第一個能追蹤泛星計畫中各種瞬變資料的天文台。若能充分利用泛星計畫的觀測結果，作為各種新發現的追蹤及後續觀察，將能產出大量的第一手重要科學結果。因此在鹿林天文台建構一台與泛星計畫望遠鏡口徑相似的兩米望遠鏡，來做為泛星計畫新發現的追蹤及後續觀察將有非常好的研究利基。又正好有教育部五年五百億的補助，因此有了鹿林二米望遠鏡計畫的產生。

黃崇源、陳文屏、周翊
中央大學天文所
E-mail：hwangcy@astro.ncu.edu.tw

鹿林二米望遠鏡

鹿林二米望遠鏡計畫是要在鹿林天文台建造一座東南亞位置最高的二米級望遠鏡。鹿林天文台位在玉山國家公園邊界，嘉義及南投縣交界處，海拔約 2860 公尺。選定在鹿林前山蓋二米望遠鏡是因該處觀測條件良好，每年可觀測天數超過二百天。且該處已有一米望遠鏡及其它不少的望遠鏡及儀器設備，各種水電設施完備，各種軟硬體的後勤支援比較完整。整個計畫可粗分為四大部份，包括望遠鏡的建造，天文台主結構及運輸，天文台圓頂，及觀測和相關儀器設備。

本計畫雖受到大力支持，但在開始建造天文台時，我們卻遇到一個前所未料的難題。因為國土復育及永續發展等理由，台灣的高山，近年都被劃為國土保安用地，除了某些些明訂的項目外，禁止各種的開發或建設。雖說全世界所有最重視環境保護的國家，他們的天文台也一定蓋在高山上。但台灣的法規中，雖有一些類似天文台量體的項目，如衛星接收站等允許在高山開發，但天文台卻不是允許建設的項目。這

使我們在天文台建構的時程上受到很大的延誤。不過幸好經過很多人的努力，特別是立法院王金平院長的幫忙，終於透過增定法規，將此問題解決。

鹿林二米望遠鏡的規格

鹿林二米望遠鏡是由日商西村製作所承包製造。該公司歷史悠久，負責人的父親早年也曾承造過圓山天文台的望遠鏡。二米望遠鏡的光學系統是採用Ritchey-Chretien (簡稱RC)的光學設計。RC系統是由兩個雙曲面鏡組合而成，是屬於蓋賽格林 (Cassegrain)光學系統的一種變型。與蓋賽格林系統的主要不同在於蓋賽格林系統的主鏡是拋物面鏡。RC系統的特點在於沒有球形像差和較少的彗形像差，且鏡筒的設計可以較短，且有較大的像場。現代的專業望遠鏡常採用RC設計。二米望遠鏡的焦長設計爲F/8，與目前的鹿林一米望遠鏡一樣，其好處是彼此的儀器容易互換。影像品質則要求實測哈特曼常數小於0.35角秒，在仰角30度以上，80%星光能量集中於直徑0.4角秒內。另外主焦平面具有一度的可用視場，光軸 0.25度範圍內爲無漸暈(unvignetted)視場，且在不需修改光學設計可加裝奈氏 (Nasmyth)焦點，以備未來增加儀器所需。圖一是鹿林二米望遠鏡的樣式圖。

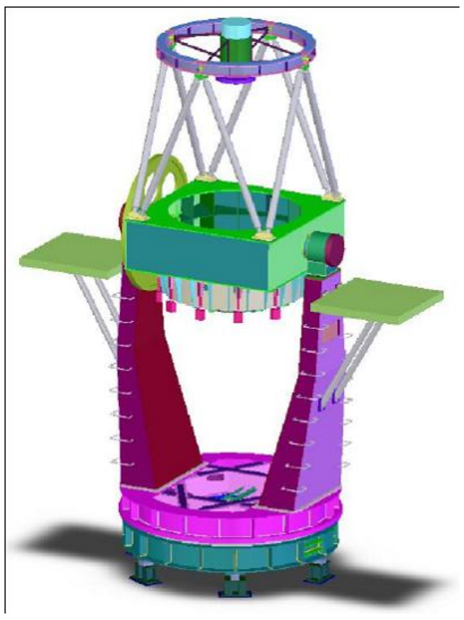

圖一、鹿林二米望遠鏡的樣式圖。

二米望遠鏡的鏡片是由蘇俄 Lytkarino Optical Glass Factory (LZOS) 所製造。鏡材採用的是超低熱膨脹的陶瓷玻璃 Astrositall®。這種鏡材是一種矽晶結構及玻璃結構混合材質，其在望遠鏡的工作溫度下，有非常低的熱澎漲係數。在-60 to 60 °C 間，其線性熱膨脹係數爲 $0\pm1.5\times10^{-7}$ °C^{-1}，而熱膨脹係數的均勻度≤０.２$\times10^{-7}$ °C^{-1}。另外鏡片的表面精度小於觀測波長的十五分之一。具有真空鍍鋁的反射膜及保護膜（SiO），在 400nm-700nm 波長範圍內反射率應達 85%以上。圖二爲 2008 年 6 月鹿林二米主鏡在蘇俄 LZOS 磨製的情形，圖三是 2008 年 10 月 10 日主鏡磨製完成後的干涉儀測試結果。

圖二、二米主鏡在蘇俄 LZOS 工廠磨製的情形。

圖三、二米主鏡的干涉儀測試結果。

由於電腦的發達，現代的望遠鏡通常採用"經緯台"基座，二米望遠鏡也是。望遠鏡的指向精度要求為 2 角秒，而移動時的速度要能達到每秒 4 度。經緯台相對於赤道儀台的優點，在於大幅簡化望遠鏡的機械結構與重量。但在追蹤星體時，赤道儀只要轉動赤經軸。而經緯儀台在追蹤星體時，則必須同時驅動水平與垂直軸，所以其控制系統必須能夠對不同的星體和座標，給予不同的驅動指令。但以現代的電腦技術，這些都可以很容易克服。

鹿林二米望遠鏡的主要科學目標

世界上已有許多十米級的光學望遠鏡，因此當我們要建造二米級的望遠鏡時，一個很明顯的問題便是，除了教學外，我們如何以一個這樣小型的望遠鏡，在科學研究上來與世界其它大型的望遠鏡競爭？因此開始建造望遠鏡前，我們便設定一個可行且有競爭力的目標。

鹿林天文台的二米望鏡的主要科學目標，是要觀測及追蹤將來「泛星計畫」(Pan-STARRS; the Panoramic Survey Telescope And Rapid Response System)所發現的瞬變星體。泛星計畫是由美國國務院提出，透過美國空軍委託夏威夷大學在夏威夷建置望遠鏡，用來搜尋太空中任何可能撞擊地球的天體，以便及早做好因應對策。此計畫由美國夏威夷大學建構獨特的廣角觀測系統，由四座 1.8 公尺望遠鏡組成，各自配備最新型，具備 14 億個像元之 CCD 偵測相機，視野達 7 平方度。泛星計畫每晚將可巡天約 6000 平方度，深度達 24 星等，每月可全天空巡天數次。關於泛星計畫，本刊另有專篇介紹。

除了對於星系、恆星，以及太陽系天體史無前例的深度曝光與天空廣度覆蓋以外，泛星計畫特別適合探測「變化」(包括亮度與位置變化）的天體。泛星計畫的首要目標在標認出可能撞擊地球的小行星，其後果攸關人類文明的延續。同時泛星計畫也將產生極大資料量，涵蓋天空深度、廣度以及時間覆蓋面，這些資料將對觀測天文學產生革命性影響，包括古柏帶天體、變星、系外行星、超新星，以及珈瑪射線源的研究。但泛星計畫的巡天觀測時間間隔約為一週，所以極需要和其他天文台聯線，針對一些變化時間尺度短暫的天體做密集測量。因為地理位置的關係，鹿林天文台是世界上第一個能追蹤泛星計畫中各種瞬變資料的天文台。若能充分利用泛星計畫的觀測結果，作為各種新發現的追蹤及後續觀察，鹿林二米望遠鏡將能產出大量的第一手重要科學結果，同時也對泛星計畫的科學成果有決定性的影響。

雖然鹿林的二米望遠鏡在口徑上與 1.8 米的泛星望遠鏡的鏡頭大小類似，因此在集光力上是可相提並論的。但泛星望遠鏡搭配有最先進的 Orthogonal Transfer Charge Coupled Device (OTCCD) 能大幅降低大氣擾動對影像的影響，在影像解析度為 0.6 角秒的半高寬的情形下，還能辨別 0.07 角秒的影像位置。而且其測光的準確度也可達到 0.01 星等。以鹿林天文台的條件，我們並無法達到這樣的影像解析度。但因為二米的的主要科學目標是要對那些會變化（包括亮度與位置變化）的天體做後續追蹤觀察。因此如何提高二米望遠鏡的"快速反應"的效率，以便能做泛星資料的後續觀測及做適當的比較，是非常的重要。而要達到這些設定的觀測目的，我們特地為兩米望遠鏡設計同步多波段照相機。

同步分光多波段照像偵測儀

為了達成二米望遠鏡設定的科學目標，我們也需要適當的偵測儀器來完成。而這儀器要達到的目標包括要能快速及準確的測量天體的顏色及亮度變化，而且要與泛星計畫具有類似的濾鏡及光度系統。一個可能的選擇便是一個同步分光多波段照像偵測儀。它能"同時"測量星體在不同波段亮度。

同步分光多波段照像偵測儀設計上的概念是利用雙色分光鏡把入射的光譜分成兩個波段。圖四顯示雙色分光鏡可以讓在一定波長以上的光線全部穿透，而短於此特定波長的光線會被全部反射。兩個分光鏡的組合，便可將入射的光線分成三個波段。例如，如果

我們有兩個二片分光鏡的分光波段為 700 and 850 nm,我們便可得到 SDSS 的 r'，i'，和 z'的三種濾光波段。如果用三個雙色分光鏡便可得到四個濾波波段。這些波段會設計成與泛星計畫的波段一致。目前我們預定設計一組具有 r'，i'，z'，和 y 四波段的同步照相機，圖五是同步分光四波段照相機的設計概念圖。

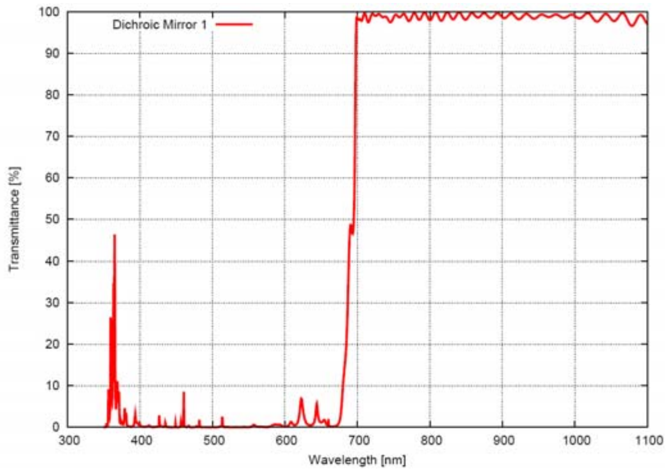

圖四、雙色分光鏡的穿透率。

由於每個波段都需要有一個 CCD 的偵測儀，因此二米望遠鏡至少需要四個 CCDs。而為了要能充分發揮二米望遠鏡的功能，CCD 的效能便非常重要。目前所選擇的 CCD 是所謂的空乏層型 CCD (Deep Depleted CCDs 和 Fully Depleted CCDs)。一般的 CCD 厚度約 15μm，而這些 CCD 厚度可達 200-300μm。因具有較厚的高電阻抗的 Si 層，因此能吸收較多的紅光，而在長波段可以有較高的量子效率，且比較不會產生干涉形態。一般的 CCD 在 900nm 附近的量子效率僅有約 25%，而這些空乏層型的 CCD 則可提高到約 75%。目前規劃的 CCD 視場約 13.2 角分×6.6 角分，CCD 大小為 4k×2k 像素。每一個像素大小約 15μm，像素張角大小約 0.19 角秒。

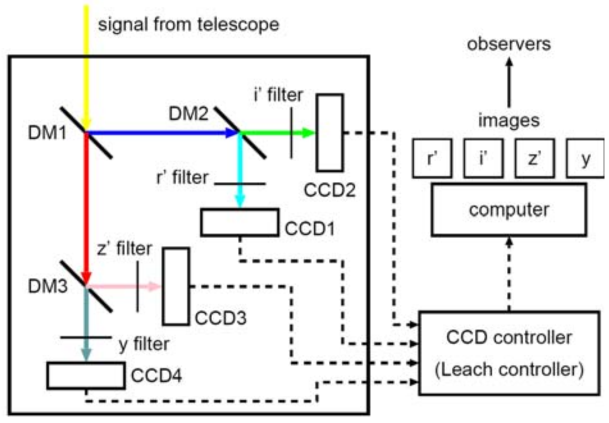

圖五、同步分光四色照相機的設計概念圖。

Deep Depleted CCDs和Fully Depleted CCDs主要量子效率的差別是在於長波長區域。但目前全世界上只有日本的 Hamamatsu Photonics 有生產 Fully Depletion CCDs。因為Deep Depleted CCDs在使用經驗及儀器控制方面比較完備。因此我們決定在r'，i'，和z'三波段使用Deep Depleted CCDs，而僅y波段部份才使用Fully Depletion CCDs。

使用同步分光照相儀的優點在於可以讓二米望遠鏡有更高的觀測效率。使用同步四色分光偵測儀就如同同時使用四部兩米望遠鏡來觀測同一個物體。在效益上則約等於有了 3.3 部的二米望遠鏡。而且因為是同步觀測，所以在天體顏色的測量上，較不受天氣影響，更容易較正。另外因為使用 Fully Depleted CCD 使得即使是像二米這種小型的望遠鏡，也可將觀測擴展到幾乎是近紅外線的訊號。

附 屬 設 備

二米望遠鏡的鏡片表面是鍍鋁，需要定時的重鍍及維護以維持良好反射率。但因鹿林天文台的運輸困難，望遠鏡建造安裝完成後，將無法將鏡片運下山鍍膜，且國內目前並無如此巨大的鍍膜設備。因此我們計畫在天文台建造一套鍍膜設備，以便維持望遠鏡的長久觀測品質。鍍膜設備將在國內設計及製造。目前我們預計將採用濺鍍或蒸鍍式的設計，除要求能真空鍍鋁外，若有必要也能改鍍金，預留未來二米望遠鏡改成近紅外線望遠鏡的空間。此一設備完成後，將是

國內最大的鍍膜設備。除了可從事二米望遠鏡的鍍膜外，也可以提供國內其它研究單位的大型儀器鍍膜所需。

但重新鍍膜完全後的鏡片，要如何確保其保有原始設計品質要求呢？為此我們與中大光電所合作開發非球面天文望遠鏡監控技術，研究開發軸向掃瞄式干涉儀系統作為二米望遠鏡的監控及量測方法，並可對我們鍍膜的均勻性與可靠度進行分析。而為了同步培養國內天文儀器的研發能力。我們也在天文所內成立一間天文光學儀器實驗室。除作為多波段可見光照相機元件的各式校正及測試之用外，也做為訓練及培養儀器研發人員之用。我們期待二米望遠鏡的發展，除了天文學上的重要性外，對提昇國內天文相關儀器的研究及開發也能有很大的正面幫助。

徜徉數字間的玩童

文/ 趙瑞青

除了那可愛的笑容外，獨特的口音也是高老師特色之一。老師笑說，來台灣這麼久了，口音還是一樣這麼明顯，當初因為喜歡鄧麗君的歌曲，而學會了國語。工作的關係，在因緣際會下來到了臺灣，而現在也在這裡落地生根。

攝影：李澤林　　地點：中央大學科四館辦公室

陰錯陽差的研究之路

當時香港還是英國殖民地，所以和英國的教育體制相同，大學三年就可以畢業了，香港大學物理系畢業後，幾個同學問我要不要到國外試試看，因當時申請學校費用很貴，於是只申請了幾間學校碰碰運氣。如果能夠申請到獎學金，就過去念。當時的資訊並不是這麼的發達，加上自己也沒有很用功去查一下資料，原本是想申請芝加哥大學，沒多久收到一間大學回信說要給我獎學金，我很高興，以為是芝加哥大學，結果是University of Illinois at Chicago, UIC（伊利諾大學芝加哥分校），申請錯了。後來西北大學也給獎學金，於是去了西北大學。我喜歡做理論，在西北大學找了一位年輕的老師，主要做白矮星的研究，但因老師初任教職，因此建議我找其他老師多看一下，我找了其他的老師，還是都沒有興趣，於是再回去找他，他說既然你那麼喜歡做理論天文物理，那我介紹你去亞利桑納大學（University of Arizona），我有一些朋友，你可以去那邊試試看。於是我在西北大學一年多一點拿了個碩士，就轉到亞利桑納大學。當初沒跟到的那位老師，後來在學術上很有成就，最近也到台灣服務，他就是Ron Taam老師。

理論計算中找到樂趣

因為香港的光害嚴重，天氣狀況並不好，要看到星星是蠻難的。再加上香港中小學的教育，對天文這一塊，並不是這麼的注重，不像台灣發展的這麼好。因此最早的時候，就只是在書上看到介紹一些星星、星座…等等，再加上身體不好，不太方便往外面走。直到大學的時候，參加一些營隊，到香港一些比較沒有人住的島嶼，才第一次看到美麗的星空，才開始認識一些星座。到了美國，在研究所的旁邊，有一個星象館，裡面有一個小小的望遠鏡，有時候會去幫忙招待夜間開放，偶而也會看一下星空，但整體來說，對於觀測的部份可說是一竅不通。

我喜歡算東西，如果這個東西可以被我算出來，就會覺得非常有成就感，就是最滿足的時候，但往往是算不出來居多。念完書後，還是想做研究，覺得這個部分還蠻有趣的。在國外的時候比較辛苦，想到找工作，說實話就是見一步走一步，先找一個博士後，完了再找另外一個。壓力一定會有，但因為還是單身，所以就算是隨便亂走也可以。如果有家庭、有小孩，我覺得會很辛苦，壓力是完全不一樣的。當然如果顧慮太多的話，其實也不適合做研究。

做天文這一門就是哪裡有工作，就去哪裡，除非真的很厲害、很頂尖，否則能夠選擇的機會其實是不太大。我老闆不太管學生，他喜歡自己做自己的，我可能受他的影響，我一直認為，老闆最大的功用呀，就是要幫學生找工作，尤其是國外的部份。老師的訊息比較多，認識的人也比較廣，不過，我現在好像也還沒有做得很好。

博士畢業後分別在美國及德國各當了兩年的博士後，博士後結束，開始找工作時，確定香港短時間內不會發展天文，剛好在我來臺灣的前兩年，中央大學物理系想要發展天文，再加上在德國的時候，碰到葉永烜老師，他一直說臺灣很好，臺灣的學生是很厲害的，回去應該會有很大的發展。也就因此來到了臺灣。

原動力足以驅動一切

喜歡天文的同學，可以想想未來是否想繼續走研究的這條路。如果是，我建議能夠在念書的時候參加大的計畫，因為這樣的計畫通常都會有一套完整的規劃，會有自己的一套規範或方法，跟著人家走總是容易一些的。而且以未來找工作的角度來看，大的計畫因為接觸的面比較多，將來也一定會有一些後續的發展，需要的人力也會比較多。但如果覺得跟著大的計畫走，自己能夠真正掌控的部份不多，好像不是自己生出來的東西，那當然就建議自己做自己的。

並不是每個學生將來都要當科學家，每個學生進來天文所，我們並不是都要培養成天文學家。以我的角度，我會選擇不要管，讓同學們自己發展。大家念書的目的不太一樣，如果只是想要拿一個學位，就把它當成是一種訓練，學習如何完成碩士的過程，所以我倒覺得並不一定要做那些最前沿或熱門的東西。

就研究天文方面，整體來說，還是念物理會比較適合、比較接近。其實不管是那個階段，只要你有一個目標，或對一個東西感興趣，就是你的原動力，念起來會比較容易。因為是為了想要了解或解決某一些東西，而不是我念完了，卻不知道未來要用這個來做什麼。

天文就是一種好奇心，真的要說應用，好像比較少，天文的應用技術或許可以延伸到生活上，可是我覺得這也只是副產品。如果有一天同學會想到，我要念天文，那就表示整個社會或國家已經有這樣的能力，願意提供經費，讓大家可以在不同領域上去發展做研究。要不然我畢業就要找工作，要賺錢，哪來多餘的時間或精力去想這些事情。大學、研究所這個過程可以浪漫一下嘛，當做是一種學習，一種訓練。

我剛到西北大學的時候，一些念經濟的朋友常問我，為什麼要念天文？你應該要學一些對人類有用、有幫助的學科，後來我真的很認真去想這個問題的答案，但是到現在我還是沒有辦法回答。一個人的能力和精力要放在什麼地方，才算對這個社會有影響、有貢獻？當時我對天文感興趣，我覺得我這樣做對自己很好，最起碼對社會來說就少了一個麻煩。每一個人的才能不一樣，你說要放在什麼地方對社會最有用，只要盡好自己的責任，我想這就是對社會最好的貢獻。

研究方向

目前我主要的研究計畫有兩個大的方向，一個是關於分子雲，另一個是關於暗物質。目前一般相信分子雲裡會形成星團，後來星團解體形成瀰漫天際的場星。但我們懷疑是否真的會經過星團這個階段，才變成場星。或者說，在雲氣裡面，星團是什麼？或許它只是一些星偶然而短暫的聚在一處而已，並不是在自引力平衡態。另目前大多認為，分子雲是受到宇宙射線的影響，使

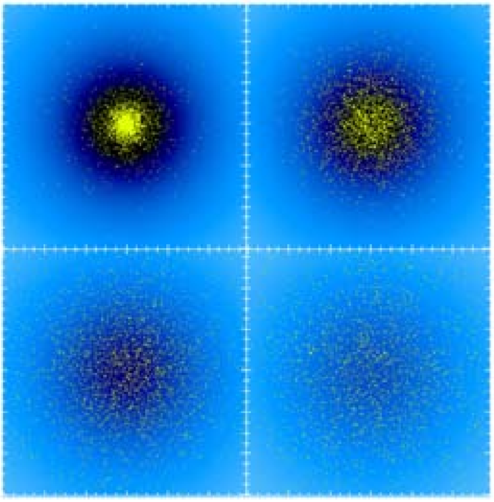

圖1. 隨著原生分子雲因恒星風或超新星爆炸而消散，原本聚集在一起的星團也逐漸擴散，甚至於從此解離而不再受到彼此的重力束縛。圖中黃點爲星團的成員星，藍色的深與淺代表雲氣的濃與稀。左上圖是雲氣開始消散，而右下圖則是雲氣已消散殆盡了。

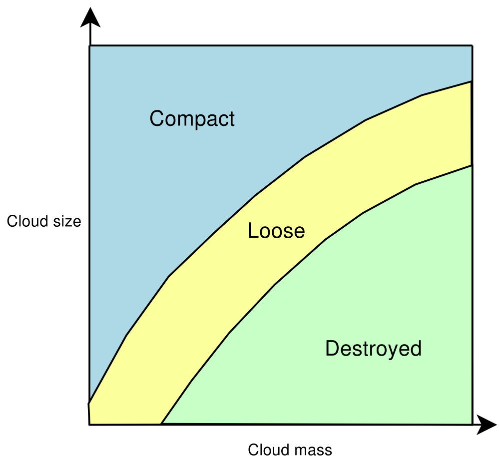

圖2. 原生分子雲的質量和大小影響著星團的命運。在雲氣消散之後，星團可能被摧毀(Destroyed)，也可能保存下來(Compact)，而一部份則是變得比較鬆散(Loose)。總的來說，原生雲氣質量越大越集中，則星團越難存活下來。

得它能保持一定的溫度，我也希望能從這個方向多了解一點。(圖 1、圖 2)

有關暗物質的一些問題，儘管暗物質從未被直接地觀察到，大多數的科學家還是都認為有暗物質的存在。暗物質主要分為兩類，一類就像是一般的物質，由質子、中子組成，只是我們看不到，譬如說不會發光的星或塵；另一種暗物質以本質來說，並不是構成一般物質的粒子，而是由高能物理理論裡面所衍生出來的一些粒子。

【暗物質 (dark matter)】

美國航空暨太空總署(NASA)在2003年2月11日召開記者會，宣告最新測得的宇宙參數，其中關於宇宙物質的成分，認為只有4%的質量是由一般的物質，也就是指質子、中子以及由它們構成的各種物體；24%是暗物質，即是無法看到的，卻又能察覺得到它們存在的東西；以及72%是相當奇異的暗能量。

【分子雲 (Molecular cloud)】

從六十年代開始，天文學家對一種密度更高、由氣體和塵埃複合而成的暗星雲很感興趣。從中發現了很多星際分子(Interstellar molecules)，我們也直接地稱之為分子雲。這種星際雲的密度，為每立方厘米萬餘顆分子，有些甚至更高。一團分子雲的總質量，可達太陽的百萬倍，並且橫跨三百光年的星際空間。理論上，當這些星際分子雲氣受擾動後，會藉著自己的重力逐漸收縮成多個較濃密雲塊，然後演變成恆星。（右圖：分子雲-NGC 6914）

反射星雲NGC 6914是一個活躍的恆星誕生地。黑暗的地方是濃密的分子雲把背景的星掩蓋，而分子雲也正爲恆星誕生提供原料。（圖片來源:http://pic.stardusts.net/sources/200609/20060902_Sep-Image2005-CFHT-Coelum.jpg)

【MOND (Modified Newtonian Dynamics) 修正牛頓力學】

長期以來，科學家們在對星系的運動觀測中發現，如果星系僅由我們可以觀測到的常規物質組成，其運動不能用牛頓引力理論來解釋。於是科學家們提出星系是由我們可以觀測到的常規物質和我們觀測不到的暗物質組成，而且星系的大部份質量來自暗物質。

在1983，莫德採．米爾格若母(Mordecai Milgrom)提出「修正牛頓力學(Modified Newtonian Dynamics, MOND)」，試圖修改牛頓力學理論，認為像星系外圍這樣的區域，根本不需要加進暗物質這樣的東西，只要修正力學定律，便可以解釋星系自轉速率（未隨距離而降低）的現象。

科學家為了解釋大結構，尤其是背景輻射，經過計算的結果，物質大概占整個宇宙能量的百分之二十幾，其中只有六分之一是一般的物質，其他的就是一些奇奇怪怪，我們不知道的東西，也就是目前所說的暗物質，目前相信大結構是暗物質加上暗能量造出來的結果。

而我們目前的想法是，我們認為並不需要所謂暗物質這種東西。我們用一種「修正牛頓力學」（MOdified Newtonian Dynamics，MOND）的理論，也就是把牛頓力學第二定律稍微修正，可以用來解釋漩渦星系的自轉速度問題。也可以用MOND來解釋重力透鏡現象，我們看到的質量就是所有的質量，不需要暗物質(圖3、圖4)。假如這樣的想法也能解釋背景輻射，及大結構的話，或許我們能夠提供另一種解釋的方法，另一個選擇。

在牛頓力學方程中，一邊是力，另一邊是加速度，我們發現如果要產生一些觀測到的加速度，質量好像不夠多，所以現在大部分的科學家解釋，這是因為宇宙中存在一些看不到的物質。但我們解釋的角度是，物質已經全部都被看到，而是加速度的大小需要修正。在牛頓引力理論和力學方程中有三個地方可以檢驗，一個是平方反比定律對不對，一個是質量對不對，另一個則是加速度是否符合。以目前來講，大家都覺得是質量的部份出了問題，但我們認為需要修正的是加速度的部份。

選擇可以不只一種

其實我覺得天文應該是從觀測出發，但是我走的這條路卻是反過來的，歸根到底，我還是以做物理的心情比較多一點，我希望能弄懂一些東西，而不是需要跟真實的這個世界配的很完美才行。科學中很多東西，都可以從不同的面向、不同的角度去思考，誰都說不準，什麼才是正確的，包括我做MOND的這個東西，是非主流，目前很難說服人家說沒有暗物質，我們現在只是提供另外一種想法與選擇，讓解釋的方向能夠更多元。

趙瑞青：任職於臺北市立天文科學教育館

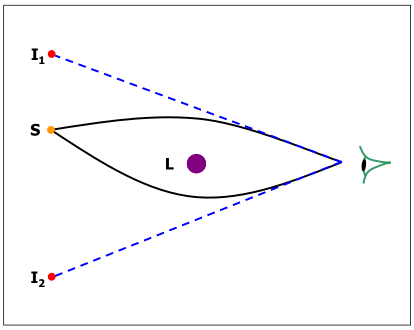

↑ 圖3.重力透鏡效應的示意圖。當光線從遠方的星體(S)出發經過另一個天體(L)時，光線會被其引力偏折。這天體稱爲重力透鏡，而光線越靠近透鏡偏折越嚴重。對觀察者來說，光線是直線前進的，因此會誤以爲S星體產生了多重影像(I_1, I_2)。

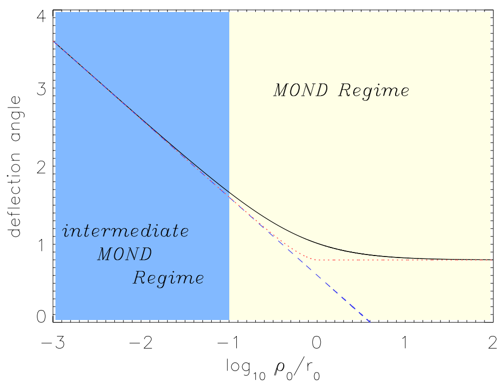

← 圖4. 在不同的引力理論裡，光的偏折角與光線最靠近重力透鏡的距離之關係會不一樣。折線是廣義相對論的結果，實線則爲一種相對論性修正牛頓力學(relativistic MOND)的結果。當最靠近距離很小的時候，兩個理論的結果相若。當最靠近距離增加時，廣義相對論預測偏折角會趨向零，但相對論性修正牛頓力學則預測偏折角會趨向常數。(紅色虛線是另一個MOND模型的結果)

Astronomical photo gallery

美星映象館

2009年2月24日鹿林彗星最接近地球時，離土星角度僅有約2度！(林啓生 攝)

Comet of Cooperation—鹿林彗星

文/ 林宏欽

2009年「全球天文年」，鹿林彗星恰巧恭逢其盛，受到全世界的關注！自一年半前發現以來，鹿林彗星距離地球從8.5億公里接近到6100萬公里，星等從19等增亮到5等，從一個微暗幽暝的小光點逐漸成長為帶著奇特彗尾的綠色彗星，亮度增加了40萬倍，在媒體推波助瀾下，彷彿一夕之間大家都知道了「鹿林」的存在，知道這是顆台灣發現的彗星！

鹿林彗星是在2007年7月11日由鹿林巡天計畫(Lulin Sky Survey, LUSS)的林啓生(中央大學天文所)與葉泉志(中國大陸廣州中山大學)，使用鹿林天文台41公分望遠鏡共同發現的。因發現之初是以小行星上報，而被別人證實為彗星，遂以共同合作發現的天文台命名為「鹿林（Lulin）」。依其為非週期彗星、2007年7月上半個月發現的第3顆新彗星的特性，編號為C/2007 N3。鹿林彗星不但是台灣本土所發現的第一顆彗星，也是唯一海峽兩岸合作發現的彗星，國際上都稱呼她”Comet of Cooperation”。

剛發現時候的鹿林彗星只是一個小光點，後來才慢慢長出短短的彗髮，呈現橢球狀，隨著接近太陽，逐漸變大變亮，尾巴慢慢長出來了。鹿林彗星因含有大量氰(CN)及分子碳(C_2)氣體，顏色十分鮮綠。但和一般拖著長長尾巴飛掠夜空的彗星不同，

鹿林彗星有著明亮的塵埃尾和比較黯淡的離子尾，像是翅膀一樣分佈在彗核兩側，形成少見的反向彗尾景觀，而且持續了很長的時間！塵埃尾因反射太陽光而呈現黃色，離子尾則一直朝向太陽的反方向；鹿林彗星的運行方向和地球相反，隨著軌道變動，兩者錯身(彗星最接近地球)之後，兩尾居然合而為一！但這其實是地球對彗星的視角改變所致，不是真的兩條尾巴合為一體！

鹿林彗星不僅出現了少見的反向彗尾，而且其離子尾有明顯纏繞的結構，甚至出現斷尾的現象！這是因為離子尾受太陽風及太陽磁場影響，由帶電粒子形成的離子尾受太陽風磁場拉扯，隨著太陽風磁場變化，彗星的物質大量散佈到太空中，以及地球看彗星的視角不同，彗尾一直是呈現千姿百態、變化多端，甚至複雜的分叉開花現象

彗星軌道可分為拋物線、橢圓或雙曲線，只有具有橢圓軌道的彗星才會繞太陽運行週期性地出現。鹿林彗星的軌道非常接近拋物線(離心率=1.000188…)，此一軌道特性顯示它是來自太陽系外圍歐特雲(Oort cloud)區的彗星，且很可能是第一次繞行到太陽系內部，因為我們目前能觀察到的只有其極長軌道中接近太陽的一小部分，當她遠離內太陽系時還會受很多其他的天體引力影響，所以無法確切地知道她是否可能回歸。像鹿林彗星這種週期(遠)超過200年且即使下次通過近日點人類也不知道還存不存在，則歸類為非週期彗星(前面加 C/)，預測鹿林彗星是第一次也將是最後一次造訪太陽系和地球！

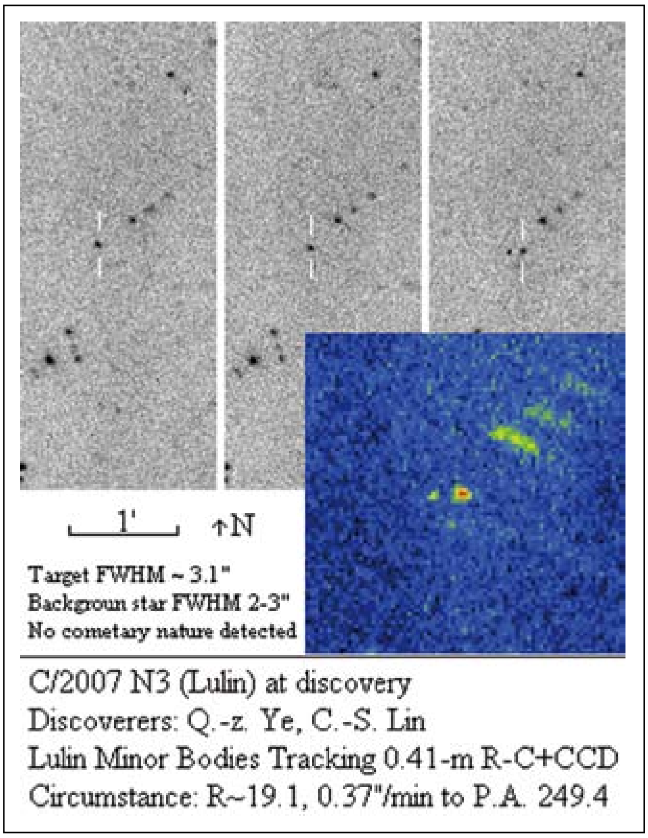

↑鹿林彗星發現時的原始影像，由上方連續三圖可看到彗星相對於背景恆星的移動，經假色處理的彩圖中並沒有發現明顯的彗星特徵(彗髮)。
(資料來源：http://yeiht.y234.cn)

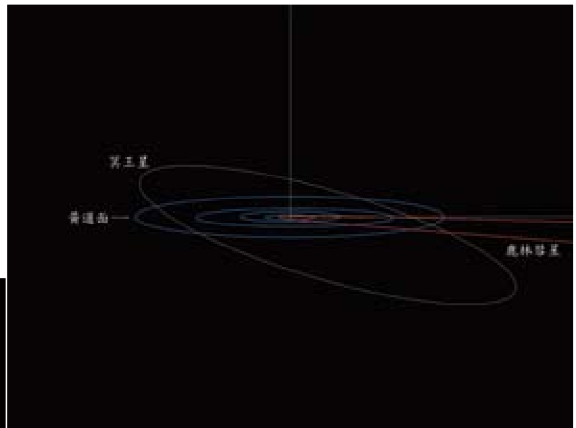

←鹿林彗星運行的軌道和黃道面夾角只差1.6度，和地球幾乎是在同一軌道面上運行！

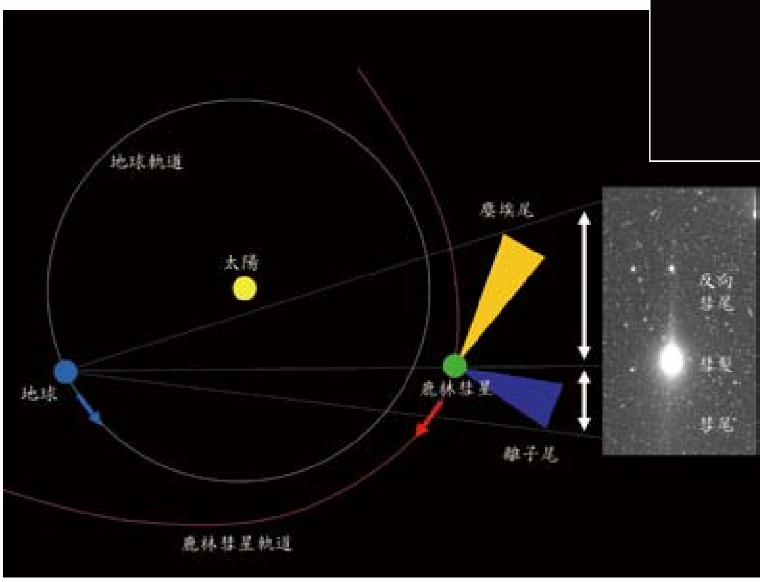

←由於鹿林彗星運行的軌道幾乎和黃道面一致（夾角只差1.6度），所以兩條尾巴都在黃道面上。彗星運行的方向和地球相反，塵埃尾拖曳在彗星行進方向的後方，而被太陽風吹出的離子尾則指向太陽的反方向，因地球與彗星相對位置的關係，所以兩條彗尾就出現在兩個完全相反方向，換句話說鹿林彗星等於是躺著，而頭朝向我們，兩條彗尾就好像兩隻張開的手臂，所以我們就會看到頭(彗髮)和一左一右兩條手臂(彗尾和反向彗尾)。

雖然鹿林彗星已經算是蠻亮的彗星（比起同時期其他彗星亮100倍以上），號稱肉眼可見，但所謂5等指的是彗星總和星等，也就是將整個彗星加起來的亮度，實際上彗核的亮度還要再暗一些，加上尾巴不明顯，要用眼睛看到並不容易！都市地區光害嚴重，即使再大的望遠鏡也看不出個什麼所以然！一定得要好天氣到天空條件很好沒有光害的地方(如高山)看才行！此外眼睛看到的只是一小團綠綠的模糊光點，必須使用雙筒鏡或小望遠鏡方能真正感受到她美麗的身影！

值得一提的是NASA也用Swift衛星觀測了鹿林彗星，這是天文學家第一次同時在紫外及X光波段同步對彗星進行觀測！在鹿林彗星接近地球的這段期間，全世界從地面天文台到太空中衛星對鹿林彗星進行了大量的觀測，這將有助於我們更進一步對於彗星的瞭解

參考資料

1. 天文年鑑2009, 台北立天文科學教育館
2. 彗星, 維基百科
3. Comet Lulin on the Way Out, Alan MacRobert, http://www.skyandtelescope.com/observing/highlights/35992534.html
4. http://www.spaceweather.com/comets/gallery_lulin.htm
5. 每日一天文圖(成大物理分站) Astronomy Picture of the Day
6. http://www.tam.gov.tw
7. http://www.nasa.gov/mission_pages/swift/bursts/lulin.html

林宏欽：國立中央大學鹿林天文臺臺長

資料彙整/ 洪景川

同焦距下之鹿林彗星大小及變化比較
吳昆臻(臺北天文館) 攝影

《共同資料》： 赤道儀：高橋EM10赤道儀
影像處理：DeepSkyStacker、Photoshop
相機：Nikon D50(clear)

← 時間：2009年2月17日 0:02~0:12 曝光：10分*2幅；總曝光20分
器材：Nikon 300mm f/4.5@4.5; Tamron 300mm f/2.8@4.0
地點：南投縣新中橫石山停車場

↙ 時間：2009年2月22日 0:41~1:52
曝光：5分*8幅；總曝光40分
器材：Tamron 300mm f/2.8@4.0 地點：臺中縣武陵農場富野渡假村停車場

↓ 時間：2009年3月19日 21:55~22:58
曝光：10分*6幅；總曝光60分
器材：Nikon 300mm f/4.5@4.5 + Nikon D50
地點：南投縣合歡山鳶峰停車場

另類臺灣之光 鹿林彗星

文、攝影/ 林啓生

時間：20090225 00h27m23s
曝光：180s
器材：NJKON 180mmED F2.8->F4
CANON 450D相機
感光度1600

壹 、前言

自從1985年12月6日晚上11點多使用普通的雙筒望遠鏡生平第一次觀測到彗星（哈雷彗星）以來，若是把所謂的「拍攝彗星」納入廣義的天文觀測範疇內，到現今也觀測過至少30顆以上的彗星了。在早先的年代，新彗星都是肉眼搜索發現的，不像近來幾乎都是巡天望遠鏡的天下。 我曾在1996年3月中旬拍攝百武彗星時期，在大雪山林道14公里附近找了一個人煙罕至大約1100公尺高的秘密基地，想說有空時也可以利用黃昏下班後到此處找找新彗星，說不定我就是那一個幸運兒 !! 遺憾的是身在人間雜事太多，到如今這個念頭一直沒有付諸執行，然而我卻在11年後於工作中成了那位幸運兒，有幸與大陸同好合作發現了鹿林彗星。

貳、 鹿林巡天介紹

鹿林巡天計劃是在2006年3月初展開，它的英文全名是Lulin Sky Survey，簡稱LUSS，這個計劃是以發現太陽系的小天體為目的。

說起LUSS，主要的推手是林宏欽台長。在2006年初林台長結識大陸的葉泉志同學。從Skype的交談中，得知葉同學可以提供鹿林的天氣預報並且他從其它大巡天資料庫中學會了找尋新小行星的技術，但卻沒有自己的望遠鏡拍攝找星，而鹿林天文台的40公分望遠鏡那時沒什麼研究生申請使用，於是兩方有了合作巡天的共識，才有了鹿林巡天計劃。

截至2009年7月，鹿林巡天計劃的成績不凡，總共發現新的小行星超過800顆，其中已經被命名的有10多顆 、 彗星一顆 、近地小行星一顆，73P彗星分裂的小團塊數顆。 這其中以小行星的成就最亮眼，在台灣這邊 ,「中大」是台灣第一顆被命名的小行星， 「嘉義」是台灣第一個被命名的縣市，「鄒族」是台灣第一個被命名的原住民民族，此外還有溫世仁、鄭崇華和沉君山等。

參、鹿林彗星發現紀實

以下是簡略的發現紀實

•2007年7月12日清晨，天空放晴，我即打開SLT的天窗， 並根據葉泉志傳來所規劃天區，進行巡天拍攝的任務，當玉山上空的曙光出現了，就把圓頂天窗關上望遠鏡歸位就到宿舍睡覺。想不到這竟然成為台灣天文界使用本土望遠鏡打破鴉蛋，發現第一顆彗星的夜晚。

•然後某天，鹿林天文台林宏欽台長傳來一份震撼性的電郵，

Hi all, We probably discover a new comet
Best, HcLin

•當初葉泉志將這個剛發現的移動天體是以小行星上報到MPC，後來在2007年7月14日經由美國的天文學家James Young以桌山天文台61公分望遠鏡觀測證實具有彗星特徵，從一顆小行星搖身一變為一顆彗星。

•2007年7月17日天文快報IAUC第8857號正式公告命名為「鹿林」彗星。 8857號原文如下

COMET C/2007 N 3 (LULIN)

An apparently asteroidal object discovered by Quanzhi Ye, a student at Sun Yat-sen University (Guangzhou, China), on images acquired by Chi Sheng Lin (Institute of Astronomy, National Central University, Jung-Li, Taiwan) with the 0.41-m f/8.8 Ritchey-Chretien reflector in the course of the Lulin Sky Survey (discovery observation tabulated below), has been found to show marginal cometary appearance by J. Young, who reports that CCD images taken with the Table Mountain 0.61-m reflector on July 17.4 UT in 1" seeing shows a small coma of diameter 2"-3" of total mag 18.8 surrounding a bright central core.

2007 UT	R.A. (2000)	Decl.	Mag.
July 11.77867	22 33 35.14	- 8 46 38.8	18.9

The available astrometry, preliminary parabolic orbital elements (T = 2009 Jan. 7.354 TT, q = 1.18775 AU, i = 178.380 deg, Peri. = 137.379 deg, Node = 338.515 deg, equinox 2000.0), and an ephemeris appear on MPEC 2007-O05.

肆 、這團髒雪球叫做鹿林彗星

有人說，鹿林彗星是台灣命名的彗星，這是錯誤的，其實這不是由台灣命名，而是國際天文聯合會小行星中心(MPC)「給」的名字。

如一般所知，新彗星命名方式是以發現者的姓氏來命名，而它怎麼會叫做「鹿林彗星」呢？

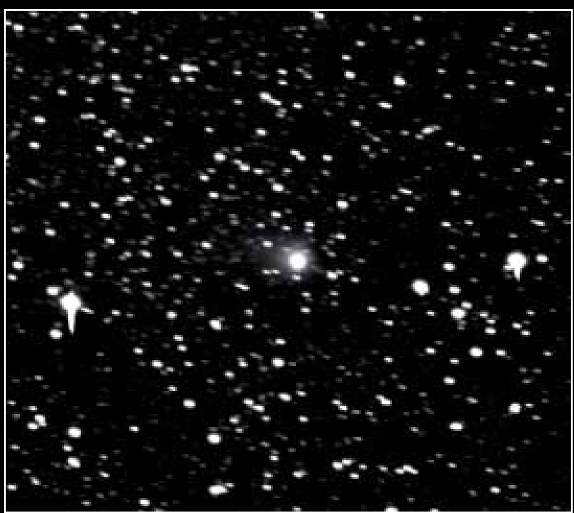

時間：20080811

時間：20090110 05h52m19s 曝光：181s
器材：高橋16公分F3.3反射鏡
CANON 450D相機 感光度400

那個「林」字不剛好是我的姓氏嗎？真的嗎　？告訴你那只是巧合罷了。

當初被認證為彗星時的確是有人建議小行星中心說彗星名字是否命名為葉-林或林-葉彗星，但後來給的卻是鹿林彗星。我沒跟小行星中心打過交道，但據我所推測及香港楊光宇同好也這樣認為，當初是以小行星上報到MPC，後來才被證實為具有彗星特徵，大概就依照某種規則辦理，所以他們才用天文台的名字命名。如果當初一發現這個新天體時就是以彗星性質上報到MPC，應該就會以兩位共同發現者的姓氏為名稱。前述以天文台或巡天名稱命名的情形，在其它大型巡天望遠鏡也曾經有過例子。

伍、記者小姐的問題

2009年2月下旬鹿林彗星正熱時，採訪我的記者最喜歡問兩件事，1.你是怎麼第一時間發現鹿林彗星？2.發現當時的心情如何？

記者小姐用人間慣有的想法—在拍下照片後就會馬上看出照片中有壯觀的彗星狀天體…等等。 其實照片是後來經過處理後才看出有這麼一顆很暗很暗的移動光點，當時彗星亮度只有18.9等 !!!! 更何況還是在過幾天後才被認證為彗星，所以我根本是排在第N時間才知道發現了新彗星，那來的第一時間 !!

中樂透彩頭獎會不會高興？那是一定會的，說到發現新彗星我也是很高興的；不過記者小姐又想當然爾地認為我的心情一定是很興奮到可以跳個2公尺高才是。 其實我的心情只有51分的欣喜、也沒有想跳起來的激動，剩下的49分就分享給其他人，不過為了配合採訪的演出，我還是說我的心情有70分的高興。

陸、追逐彗星的日子

2009年2月下旬鹿林彗星成為新聞媒體注目的焦點，那時段是一般朋友最容易觀看到它的日子，但對天文圈來說，彗星早在2008年夏天就可以用10多公分的望遠鏡拍到它的蹤跡，不過它離太陽還遠，光度還暗，拍不出壯觀的影像來。我曾在此段期間內試著拍它，但卻一直沒有將影像找出來檢查到底有否拍到。

在2008年10月底，鹿林彗星亮度已經到達8~9之間，同時他慢慢要跟太陽同起同落，我把握在此時拍下了它，以迎接12月下旬之後真正觀測攝影期的到來。

2008年11月到12月中，這一陣子都無法觀測到彗星，因為它在太陽的後方，要到12月下旬才會出現在快天亮前的東南方低空。

冬至時，林宏欽首先在清晨的微光中將彗

時間：20090122 04h26m40s　曝光：301s
器材：高橋16公分F3.3反射鏡
CANON 450D相機　感光度1600

時間：20090123 05h22m51s　曝光：301s
器材：高橋16公分F3.3反射鏡
CANON 450D相機　感光度1600

星拍了下來；元旦期間有多位天文同好聚在塔塔加守候著它，那時塔塔加的停車場東邊有山擋住彗星，所以追星族就在深夜3點前後, 開車到石山停車場，如預期地守到了那帶綠色的模糊光團。 我可不想讓他們專美於前，在1月2日深夜2點多開車到大雪山林道17公里，苦等彗星爬過山頭，才在4點半左右拍到它。這時的彗星有著白霧般的彗頭，彗尾不明顯。

快到近日點1月10日的前幾天，月亮逐漸影響到觀測與拍攝彗星，加上彗星緩步向西移，東升仍遲，可拍攝時間不多。 近日點期間，雖然明月當頭，我仍然找到它的蹤影並拍下幾張紀念性的倩影；過了近日點之後的日子那只有一聲「慘」, 大月亮嚴重影響攝影，雖然彗星很亮了，但所拍出的影像卻一點也不可愛，沒什麼好看的。

鹿林彗星最早被發現時，預估最大亮度約6等，近地點日期是2月27日；在亮度方面後來又有預估到4.5等的情況。 有些人士綜觀12月中以來的表現，可能因為他們的觀測環境不好或缺乏觀測彗星的經驗，加上所看到的鹿林彗星一直沒有想像中的精彩，就推測說到時彗星最亮只有6等或更暗!! 我聽到這個說法是有點在意的，畢竟這傢伙跟我有密切關係，所以我一直期望彗星能如最佳預期的亮度，因此我總會在睡覺時加持它，希望彗星能表現更亮點。

農曆春節前幾天，彗星又再度來到適宜拍攝的好日子，此時彗星雖已過近日點，不過它因為逐漸接近地球而顯得更亮更大。拍攝到的影像中，有著短短向西的離子尾，塵埃尾也有但是不很明顯。

過完年禁不住誘惑又跑上山拍攝，彗星已經提早東升，但是塔塔加停車場東邊的山讓彗星遲遲地到4點才翻過黑山頭，在拍出的影像中，彗星包裹著綠色的氣體，使它有別於一般的彗星。

時間：20090207 22h48m36s 曝光：120s
器材：高橋16公分F3.3反射鏡
CANON 450D相機 感光度1600

時間：20090206 04h33m22s 曝光：181s
器材：高橋16公分F3.3反射鏡
CANON 450D相機 感光度1600

時間：20090217 04h43m20s 曝光：181s
器材：高橋16公分F3.3反射鏡
CANON 450D相機 感光度1600

2月4日起連續碰到3個晴天而且彗星剛好從天秤座的α雙星旁通過，讓彗星變得更有看頭。從所拍的影像中可見，彗頭往東西兩端各有一條彗尾，西邊帶點噴射狀的是離子尾，往東邊的是塵埃尾。就一般人的認知來說，彗星尾巴不是都應該在同一邊嗎？真是一顆奇怪的掃把星!!（編者注：因視覺與物理上的機制，彗星會有反尾的現象，使塵埃尾指向太陽。）

2月9日大月亮不僅影響彗星觀測，還發生了半影月食，不過在明亮月光下，我還是使用望遠鏡看到了彗星。半影月食過了之後，月亮又再度嚴重影響彗星的拍攝與觀測。

2月16~17日，在鹿林彗星觀測相關的網路上，我看到已經有發燒級的國外同好高興地宣佈他用肉眼直接看到了彗星，但那幾天我就是看不到。唉，如果是在20年前，沒有老花眼的話，我一定也可以輕易地用肉眼看到。用肉眼看到代表什麼呢？代表彗星至少比6.0等還要亮了 !!!

2月17日中央大學舉行鹿林彗星的記者會，一時之間鹿林彗星的消息就轟動起來了，有記者打電話到山上採訪我，問得最多還是如何發現以及發現當時的心情如何之類，也有問到未來觀測情況等等。

2月18日公共電視台下課花路米的製作團隊上到鹿林天文臺錄影，主題就是鹿林彗星，我就順理成章入鏡成為主角，除了介紹鹿林彗星之外還介紹了鹿林天文台。 這一兩天天氣還是不太好，不過20日凌晨3點多天文台的自動氣象站顯示天氣放晴了，我就到室外看看天氣狀況，並抬頭看一下彗星所在的星域，耶！那淡淡的一團不就是彗星嗎 ？為了確認起見，我拿出雙筒望遠鏡再確認了一次，真的喔，我真的用肉眼看到了我自己發現的彗星了!!

21日起，我懷疑自己成為台灣最忙的一個人， 幾乎每天晚上都有辦理觀測彗星或相關的活動，有時配合電視台採訪，經常要接記者電話，老是要問我發現當時的心情如何等等的？這幾天我真的很忙很忙，這兒要交待一下歷史如下：

22日下午到蘭潭國小錄影，除了跟鹿林彗星有關的訪問之外，讓我很驚奇一個國小竟然有小小的攝影棚，晚上10點看天氣不錯就殺上石卓休息站在路邊拍彗星。 這晚上的鹿林彗星又有一次明顯的離子尾噴發情況，剛好被我紀錄下來後半段的過程。

23日下午回到台南老家的大潭國小辦理彗星觀測活動，活動結束之後再開著老爺車衝上阿里山，在公田產業道路一處懸崖路邊架器材拍照。

24日中午醒來，就直接殺回台中準備晚上的觀測活動，結果在路上就有電話打來說台中有幾

時間：20090223 01h56m13s 曝光：180s
器材：NJKON 180mmED F2.8->F4
CANON 450D相機 感光度1600

時間：20090225 01h40m20s 曝光：180s
器材：NJKON 28mm F2.8->F4
CANON 450D相機 感光度1600

組電視台要採訪我。我跟記者們碰面後就帶到我家中秀秀昨晚拍的彗星照片，經過一番訪談之後還要求我載器材到都會公園架起來，讓他們拍攝我用望遠鏡觀星的模樣，不過因為我還有太多事要處理，婉拒了。

晚上在都會公園的觀測彗星活動因為天氣不好，只能就地用電腦給前來捧場的朋友上個彗星的課程，等活動結束後，彗星才露出臉來！之後，收拾器材我直奔大雪山，在19公里處遇到了多位從台北下來的同好，他們為了今生只有一次的鹿林彗星這樣地辛苦應該是值得的。

25日中午醒來又直奔新竹，跟新竹實驗中小學的小朋友殺到了桃山。 星星在9點多露臉，我們觀測了土星以及主角彗星，同時還教他們每人拍下彗星的倩影，我還跟山莊主人介紹了他們布農族祖先怎麼在山上帶著獵狗去打獵的傳奇故事，他聽了還心有戚戚焉呢！

26日晚上沒有安排活動，不過我還是載著器材到大雪山200林道35公里跟星星工廠廠長一起拍照，今晚的鹿林彗星最有風情又漂亮，不過因為衝的關係，離子尾跑到彗頭後方而難以拍到。

27日晚上在潭陽國小辦理彗星課程及觀測活動，因為這陣子冷暖氣團交會導致平地天空濛濛的，所以觀測效果不好，有點令人失望。 活動後有幾位老師跟我又跑到大雪山19公里基地觀測拍照，但後來有薄雲干擾，導致早早地收場下山。

28日又大忙起來，中午先下台南大內南瀛天文園區說說鹿林彗星的故事，然後再騎電單車到塔塔加停車場參加活

時間：20090226 21h54m47s 曝光：120s
器材：高橋16公分F3.3反射鏡
CANON 450D相機 感光度1600

時間：20090301 22h37m17s 曝光：180s
器材：高橋16公分F3.3反射鏡
CANON 450D相機 感光度1600

時間：20090417 20h49m21s 曝光：301s
器材：高橋16公分F3.3反射鏡
CANON 450D相機 感光度800

時間：20090317 21h25m41s 曝光：301s
器材：高橋16公分F3.3反射鏡
CANON 450D相機 感光度800

動。 今晚有許多天文同好在此聚集拍攝彗星，並同聲舉杯暢飲紅酒，為我舉辦慶祝發現了鹿林彗星的酒會；後來前行政院長謝長廷先生出現，跟我們一起觀看鹿林彗星。原來這幾天高雄市天氣不怎麼好，所以特地到高山來看看傳說中帶著尾巴的台灣之光，當然他如願以償看到了鹿林彗星。

預報說鋒面即將來臨，所以我3月1日晚上又來到了大雪山19公里基地拍彗星，彗星仍然明亮輕易可見。3月2日天氣終於不好，這一陣子連續10個晚上追逐彗星的我，打破了1996年6月連續6個晚上追逐Hale-Bopp彗星的紀錄，彗星的觀測就暫告一段落。

3月6日彗星經過M44星團，天氣不好無緣一見；3月10日左右大月亮，觀測效果不好；3月14日我去廣州，跟廣州同好找了好久，就是找不到彗星，但有拍下影像，彗星看來很暗，莫非它急速變暗？

3月16日天氣變好，我還是繼續追蹤它，7×50的尋星鏡還是很容易抓到它。拍到的影像，彗星模樣依舊，帶著明顯的塵埃尾，倒是亮度暗了很多。

再過一個月，使用7×50的尋星鏡已經找不到它的蹤跡，得要靠攝影才能將它從茫茫星海中揪出來，此時彗星的身裁更加地瘦小，但還拖著短短的尾巴。

5月1日，才過半個月而已，彗星亮度下降非常多，同時受月光影響，從拍得的影像中看來簡直跟小星星沒兩樣，只帶點星雲狀尾巴；5月16日天晴繼續奮鬥，彗星還帶點淡淡的尾巴，5月19日是最後一次拍它的日子，代表著完整句點。

柒、結語

你可能是20到30多歲的年紀，錯過了當年響叮噹的哈雷彗星，也不知道1996年的百武大彗星，更錯過了今次的鹿林彗星！天上只有鹿林彗星和哈雷彗星嗎 ？不是的，天空中隨時有幾十顆彗星，只是都不能亮到肉眼可見罷了。

什麼時候大彗星會再度光臨地球呢？快則幾個月慢則數年之後，當大彗星出現時，你一定要捨得走到高山走到鄉村，抬頭仰望那拖著長長尾巴的大彗星，感受宇宙的奧妙。

時間：20090516 19h44m56s 曝光：150s
器材：高橋16公分F3.3反射鏡
CANON 450D相機 感光度800

林啟生：國立中央大學鹿林天文臺專任助理

台灣之光(一)：鹿林彗星

林 啟 生

一．鹿林巡天介紹

中央大學天文研究所鹿林天文台在 2006 年 3 月開始鹿林巡天的計劃，簡稱 LUSS，這個計劃是以發現太陽系小天體為目的．成員包括天文台的林宏欽台長和觀測員林啟生、楊庭彰、張敏悌、施佳佑以及蕭翔耀等人以及廣州的大學生葉泉志同學．器材方面則使用直徑 40 公分的高精度 RC 型反射望遠鏡配合超高感度的冷卻 CCD 相機搭載在追蹤精度很高的中型赤道儀上做整體的攝影任務．

操作方式是由葉同學選定拍攝天區，並交付給鹿林天文台值班觀測助理執行拍攝任務，拍攝好之後的照片並經 FTP 下載到廣州，由葉同學使用電腦分析出移動天體，再經確認之後，將已經早就發現和今次新發現的移動天體上報到國際小行星中心，而這些首次被拍到的移動天體就成為鹿林巡天計劃之下所發現的太陽系天體．

截至 2009 年 3 月，也就是計劃滿三周年的今天，鹿林巡天計劃的成績不凡，總共發現新的小行星將近 800 顆，其中已經被命名的有 10 多顆 、 彗星一顆 、近地小行星一顆，73P 彗星分裂的小團塊數顆．這其中以小行星的成就最亮眼，而「中大」是台灣第一顆被命名的小行星，「嘉義」是台灣第一個被命名的縣市，「鄒族」是台灣第一個被命名的原住民民族．有關鹿林巡天的成績請參見中央大學天文所網頁．

二． 鹿林彗星發現紀實

鹿林彗星是台灣本土望遠鏡發現的第一顆彗星．

- 2007 年 7 月 11 日晚上 7 點晚餐後天氣還是烏雲密佈，看來是一個很典型的夏季午後多雲的天氣，那天是我在值班，飯後我就進入觀測室等待天空放晴．直到子夜時分烏雲退散了，溼度也降了下來，即打開 slt 的天窗，並根據葉泉志傳來的規劃天區進行巡天拍攝的任務．當玉山上空的曙光出現了，也一如往常地把圓頂天窗關上望遠鏡泊好就到宿舍睡覺．這一夜只是一個很普通很普通的夜晚，卻是台灣天文界使用本土望遠鏡發現第一顆彗星的夜晚．
- 一天，鹿林天文台台長林宏欽傳來一份震撼性的電郵，

Hi all, We probably discover a new comet Best, HcLin

- 最初葉泉志將這個剛發現的移動天體以 NEO 報到 MPC(http://www.cfa.harvard.edu/iau/mpc.html) 以及出現在 The NEO Confirmation Page 上(http://www.cfa.harvard.edu/iau/NEO/ToConfirm.html)．之後就會有全世界各地的有心人士繼續追蹤該天體； 並在 2007 年 7 月 14 日經由美國的天文學家 James Young 以 Table Mountain 天文台 61 公分望遠鏡觀測證實具有彗星特徵，從一顆小行星搖身一變為一顆彗星．
- 彗星剛發現時，距離地球大約 9 億公里，位在寶瓶座內的黃道附近，亮度約 19 等．
- 自 7 月 12 日起鹿林天文台的天氣就一直不好，而在這個發現之後，直到 7 月 18 日晚上鹿林天文台才有個短暫的 1 小時晴天；而當時中大天文所的研究生陳婷琬就把握這個短暫時間放棄了她原先的觀測目標，用 1 公尺 LOT 鏡拍攝了多幅鹿林彗星的影像．
- 2007 年 7 月 17 日天文快報 IAUC 第 8857 期正式公告命名為「鹿林」彗星 .8857 號原文如下

COMET C/2007 N 3 (LULIN)

An apparently asteroidal object discovered by Quanzhi Ye, a student at Sun Yat-sen University (Guangzhou, China), on images acquired by Chi Sheng Lin (Institute of Astronomy, National Central University, Jung-Li, Taiwan) with the 0.41-m f/8.8 Ritchey-Chretien reflector in the course of the Lulin Sky Survey (discovery observation tabulated below), has been found to show marginal cometary appearance by J. Young, who reports that CCD images taken with the Table Mountain 0.61-m reflector on July 17.4 UT in 1" seeing shows a small coma of diameter 2"-3" of total mag 18.8 surrounding a bright central core.

2007 UT	R.A. (2000)	Decl.	Mag.
July 11.77867	22 33 35.14	- 8 46 38.8	18.9

The available astrometry, preliminary parabolic orbital elements (T = 2009 Jan. 7.354 TT, q = 1.18775 AU, i = 178.380 deg, Peri. = 137.379 deg, Node = 338.515 deg, equinox 2000.0), and an ephemeris
appear on MPEC 2007-O05. (資料出自 IAUCs 8857 號)

三．鹿林彗星的重要事項

1. 回歸周期

當鹿林彗星剛剛被發現後，初步的軌道顯示它的離心率在1左右，並沒辦法定的很精細．這是因為在它繞行太陽的軌道中，天文學家在短短幾天中只觀測到極長軌道中很小很小的一段而已．到了2008年年底，小行星中心給的數值是e=0.999987，表明它的周期是2850萬年，更後來公布的資料是e=0.999991，周期是5000萬年左右，但根據NASA的JPL最新資料，e= 1.000201000134273，這個數據顯示它是一顆軌道屬於雙曲線的非周期彗星．不管離心率到底要採用那一組數字，都表明它的家鄉是在太陽系外圍的歐特雲區(Oort cloud)，我們就只能看它這麼一次而已．

2. 軌道面特性

鹿林彗星的軌道面和地球繞太陽的黃道面交叉角度小，有如一台筆記型電腦的螢幕與鍵盤快合起來的模樣，不同於1996年的百武及1997年的HALL-BOPP及2007年1月的McNaught等彗星，後者與黃道面都有著比較近於90度的交叉角度．因為鹿林彗星的軌道面特性之故，所以它在今年1到3月適合觀察的期間內，在天空的路徑都是貼近在黃道旁．

此外鹿林彗星的運行軌道標示著它跟著名的哈雷彗星一樣，用句通俗的話就是逆向開車．眾所皆知，太陽系的8大行星與大多數的小天體都以同一個方向繞行太陽，有如在單行道上同向駕駛的方式，但鹿林彗星卻是向我們迎面而來，是一個比較少見的彗星軌道．

3. 重要的節點

鹿林彗星已經慢慢遠離地球及太陽，要回到非常遙遠的故鄉．在它運行到太陽系內層時，最靠近太陽的時候是1月10日，那時離太陽還有1億8000多萬公里，還位在地球軌道外側，不巧這時地球還在差不多一樣遠的一方，不能看見它最壯觀的一面；等它繞過近日點之後，要遠離太陽了，地球才在2月24日卡位到離它最近的地方，這時只距離6000多萬公里，大約有著4~5等左右的亮度，雖然不算完美，但這個亮度已經是彗星中少見的了．

此外還有一個有趣的節點，那就是鹿林彗星在2月26日到達類似行星衝的位置．簡單的說衝就是太陽-地球-行星呈一直線的狀態．鹿林彗星衝有兩個層面可探討，其一就是讓彗星幾乎整夜可見，因此在子夜12點都可以毫無困難地在頭頂的天空觀測到它，這個現象與一般人印象中彗星大都出現在黃昏西方低空或天亮前東方低空有相當的落差．其次彗星的離子尾都是以彗頭為準背對著太陽，鹿林彗星衝使得那一陣子我們看不到它的離子尾，因為離子尾跑到大大彗頭的後方去了；塵埃尾反而因為前些日子通過近日點急轉彎甩尾的動作加上地球以及彗星軌道特性等關係，罕見的成為朝向太陽的逆向彗尾，在觀測上實屬少見的彗星．

四．簡要的鹿林彗星觀測與拍攝日記

在 2 月下旬鹿林彗星成為新聞媒體注目的焦點，的確沒錯，那時段是一般朋友最容易觀看到它的日子，但對天文圈來說，鹿林彗星早在2008年夏天就可以被天文同好以10多公分的天文望遠鏡拍到它的蹤跡，不過那時它離太陽還遠，光度還是暗，拍不出壯觀的影像來．

2008 年 11 月到 12 月中，尤其是 12 月中旬，彗星離 1 月 10 日過近日點的日子已經很近了，不過那一陣子都無法觀測到彗星，因為它在太陽的視線後方，要到 12 月下旬才會出現在快天亮前的東南方低空．

元旦假期深夜 2 點多我開車到大雪山林道 17 公里，苦等彗星爬過山頭才在 4 點半左右拍到它．這時的彗星有著白霧般的彗頭，彗尾不明顯．

接下來的日子月亮逐漸影響到觀測與拍攝彗星，農曆過年前彗星早已過近日點，不過它因為逐漸接近地球而顯的更亮更大．拍攝到的影像中，有著短短向西的離子尾，塵埃尾也有但是不很明顯．

過完年禁不住誘惑又跑上山拍攝，彗星已經提早東升，拍出的影像中，彗星包裹著綠色的氣體，使它有別於一般的彗星．

在 2 月 5 日的影像中，彗頭往東西兩端各有一條彗尾，西邊帶點噴射狀的是離子尾，往東邊是塵埃尾．就一般常識來說，彗星尾巴不是都應該在同一邊嗎?真是一顆奇怪的掃把星!!

2 月 9 日大月亮不僅影響彗星觀測，還發生了半影月食，不過在明亮月光下，我還是使用望遠鏡看到了彗星．

2 月 16~17 日，鹿林彗星觀測相關的網路上，經有發燒級的同好高興地宣佈他用肉眼直接看到了彗星，但我就是還看不到．用肉眼看到代表什麼呢?代表彗星至少比 6.0 等還要亮了!!!

之後好幾天天氣都不太好，20 日凌晨自動氣象站顯示天氣好了，我到室外看看天氣狀況，抬頭看一下，那個淡淡一團不就是彗星嗎？用了雙筒望遠鏡再確認了一次，真的耶，我真的用肉眼看到了我自己發現的彗星了!! 它已經亮到成為肉眼彗星．

21 日開始我成為台灣最忙的一個飛人，有時配合電視台錄影，經常要接記者電話，老是要問我發現當時的心情如何等等的？這幾天我真的很忙很忙：前一天在台南辦活動後一天在台中辦，再隔天晚上馬上出現在新竹的山上帶活動；每天山下活動一結束，就馬上開著25 歲的老爺車即刻上山拍那顆我的彗星，天亮就睡在車上，締造了我一連 8 個晚上連拍彗星的紀錄；直到 3 月 2 日壞天氣終於來臨，追著我的彗星的日子就暫時告一段落．

在這段瘋狂追彗星的日子裏，於每天所拍的影像中，曾拍到了彗星離子尾噴發的現象；離子尾逐漸變成看不著；往東指逆向的塵埃尾愈來愈明顯，愈來愈亮愈來愈長的過程以及彗星經過明亮的土星旁的倩影等等；每天晚上看著天空中那一團矇朧光芒-我的彗星，就別有一番不同的滋味在心頭．

2 月 28 日晚上一群天文同好選在玉山國家公園塔塔加地區的停車場為我辦理了一次鹿林彗星慶祝酒會，那天是有那麼一點感動的．

五．結語

當你展閱此文的此刻，對一般人來說，鹿林彗星已經走了，他們再也看不到它的蹤影了；但是對天文學家來說，鹿林彗星仍然是一顆明亮的彗星，天文同好還可以一直拍到 5 月份為止．

觀看一張印刷的彗星照片，你不會有多少感動的，說很感動那是騙了自己，而你一定錯過了肉眼可見---尤其是台灣自行發現的鹿林彗星．別嘆息，明亮的大彗星也許很快就要出現在天空中，那時你一定要撥出時間到山上去看看什麼是拖著 90 度尾巴的大彗星．

【註】感謝康軒文教提供，並同步發表於康軒自然通訊五月號！

台灣之光(二)：小行星發現記

蔡　元　生(本會監事)

本團隊發現的第一顆永久編號小行星出爐，由測量成員袁鳳芳測量發現到的 2009 FX18 由 MPC 公布為第 215080 號小行星，這是我們團隊向鹿林山申請的觀測時間中發現的小行星，也是第一顆得到永久編號的，意義重大，但別問我們要命名什麼，那是機密...

２００８年底向鹿林山天文台申請了ＳＬＴ４０望遠鏡的觀測時間，經過審核在２００９的第一季２～６月我得到了兩次觀測時間，內容是小行星與超新星等天體搜尋，依照ＳＬＴ４０的特性，如天氣好每張曝光１２０秒可攝得２１等天體，每區域依３Ｘ３的相機視場拍攝３個ＰＡＳＳ。每區域共拍攝２７張影像，含導入 及導入點校正與下載每張約１４０秒，每區域約８０分鐘完成，每晚約可觀測６～９個區域。每張約占天空４０ｘ４０arcmin，每區域４平方度，每晚約可觀測２４～３６平方度，效率雖然不高但成果並不差。

第一次觀測時段為０３／１６～０３／３１共１６天，前三晚雖然晴天但透明度差，拍攝星等不高約１９等，適應期加上大月光影響前三晚毫無所獲，０３／１９～０３／２２連續的晴天，加上拍攝位置選的不錯（避開大型巡天望遠鏡掃過的位置如ＮＥＡＴ，ＬＩＮＥＡＲ等，請參考 http://scully.harvard.edu/~cgi/SkyCoverage.html），四晚下來總共發現超過６０顆未知小行星，但之後的連續陰天使得追蹤到２～３晚數據的只有２～３０顆，因此錯失很多發現權，陸續接到小行星中心的確認信件，目前已有１３顆是屬於我們發現的，還在增加當中。

如果以四～五晚觀測發現１３小行星來說效率是相當高了，鹿林每年可有２００個晴夜，發現數量一定不少，我們之所以能有如此的效率，全賴於人工檢察自動比對後的遺漏，如果沒有人工比對應該只能發現１／１０以下的數目，如何在這競爭激烈的環境下發現先的天體，唯有花更多的人力與精力，當然這不是我一個人的功勞，我的團隊加我至少有四位能做天體測量的人，兩位以上能製作拍攝計畫，加上鹿林的兩位操作員輪班，在這種天衣無縫的合作下才能有此成績。

◎ 天體測量成員介紹 ◎

陳韜---蘇州盤門風景區解說員,發現 C2008 C1(陳-高彗星),發現 SOHO 彗星 10 顆,發現 NEAT 小行星 210 顆(世界排名第五).

金彰偉---韓商企業的主管,發現 NEAT 小行星 321 顆(世界排名第四),與新疆高興老師聯合獨立發現新星 **N Cyg 2008**

袁鳳芳---廣東華南農業大學光資訊科學與技術系大四學生熟悉天體測量.

目前戰績：

臨時編號	發現者	ＯＰＰ	永久編號	命名
K09F18X =2004 CG69	**YFF**	**4**	**215080**	?
2009FS44=2006KE100	CT	4	?	?
K09F18Z	CT	4	?	?
K09F30C	YFF	4	?	?
K09F19A	JZW	3		
K09F05L	TYS	1		
K09F29S	CT	1		
K09F30B	YFF	1		
K09F30A	YFF	0		
K09F29V	CT	0		
2007 WX5 = 2009 FM5	TYS	3		
2002 EV135 = 2009 FN5	YFF	4		
2006 PR20 = 2009 FY18	YFF	2		

※４次衝日點觀測到兩晚以上數據者可有永久編號，即可以命名。

【下圖】蔡元生所發現的 215080 號小行星 **ò**